University of Oxford

Modelling Secondary Cancer Risk From Photon And Proton Therapy In Medulloblastoma

By Abdossalam Mohammed A Madkhali, MBBS, MSc
Linacre College

Supervised by: Dr Mike Partridge (2012-2016), Dr Claire Timlin (2012-2015),

Prof Katherine Vallis, Prof Frank Van den Heuvel, and Dr Mark Hill (2017-2018)



A thesis submitted for the Degree of Doctor of Philosophy
TT 2018

Dedicated to:

My late mother

ROQAYAH S. BAGHDADI

1944 ~ 2007

through whose lasting memory,

I prevail.

&

To my dear father

MOHAMMED A. MADKHALI

a most generous man,

through whose resilience & love,

I persevere.

&

To the women in my life

that are sources of happiness,

strength, & encouragement.

Acknowledgements

I would like to thank my supervisors, *Dr Mike Partridge* and *Dr Claire Timlin*, for their immense and continuous support, and their rigorous scientific supervision. Their encouragement, their confidence in me, and their dedication enabled me to grow academically, and professionally, and helped me to take on research challenges with calm and clarity. I would also like to thank the supervision team of *Prof Katherine Vallis, Dr Mark Hill*, and *Prof Frank Van den Heuvel* for guiding me through the corrections and the needed steps to complete this work (not once, but twice!).

I would also like to thank *Dr Daniel Warren*, whom I had the great pleasure of working with for years, and was always helpful in pointing out to directions for possible solutions for technical problems. I also thank the collaborators in the Mayo Clinic organization in the United States, Haukeland University Hospital in Norway, and Rigshospitalet in Denmark, *Dr Jim Loken* for the time and effort he invested in this project, and *Monsieur Conor E W Manders, Esq*, one of the finest gentlemen I ever had the pleasure and privilege of knowing, for providing much-needed aid in reading through this work, along with *Ms Elaine Chew* & *Mr Kiron Neale*. I extend my gratitude to *Dr Sam Warren*, *Dr Tracy Undewood*, *Dr Mariane Aznar*, and *Dr Christiana Kartsonaki* for her invaluable input.

My sincerest thanks go to Oxford and Linacre friends, notable "*The Strada Fund*", "*#Fezcom*" & *"#PresCom"*, who made the ride much more endurable, much more fun, and infinitely enriching. A special heartfelt thank you to *Ms Evgenia Ivanova*, *Ms Diana Maddison*, *Ms (soon to be Dr) Amanda Shriwise*, and *Ms Ashley Tsai* for their unconditional support, and continuous belief in my work and myself. In addition, I would like to thank the administratives at Saudi Arabian Cultural Bureau in London, and the staff at King Saud University's Human Resources Department, namely: *Mr Sultan AlKhathlan*, *Mr Jama'an AlGhamdi*, and *Director of HR, Mr Faisal AlHarbi* for their unwavering support.

Finally, I would like to thank my father and my loving family, with whose prayer, generosity, and love from afar I was able to steer steadfast through this project. My eternal gratitude to my most missed "*424 & Co*" friends and the many other friends who kept my morale high during challenging times, and stayed by my side through the best of times and darkest of hours.

This work was made possible by the encouragement, help, and support of the following individuals and organisations:

جامعة الملك سعود

أ.د. مساعد بن محمد السلمان
عميد كلية الطب الأسبق—جامعة الملك سعود

أ.د. مبارك بن فهاد آل فاران
أ.د. فهد بن عبدالله الزامل
أ.د. خالد بن علي فودة نيل
عمداء كلية الطب—جامعة الملك سعود

أ. د. صالح بن محسن الحازمي
أستاذ الكيمياء الحيوية

د. عبدالله بن عمير العمير
أستاذ مشارك و استشاري طب الأطفال

د. إياد بن فوزي السعيد
أستاذ مشارك و استشاري العلاج بالاشعة و مؤسس وحدة العلاج بالاشعة بالمستشفيات الجامعية

أ.د. عبدالله بن صالح الدهمش
أستاذ التشريح

د. فيصل بن عبد الله السيف
أستاذ مشارك و استشاري جراحة الكبد و البنكرياس

أ. فيصل بن سعود الحربي
مدير إدارة تنمية الموارد البشرية

أ. سلطان بن رشيد الخثلان
وحدة الابتعاث

أ. جمعان بن عبدالله الغامدي
سكرتير اللجنة الدائمة للابتعاث و التدريب

سعادة الملحق الثقافي بسفارة خادم الحرمين الشريفين في لندن

424 و زملاؤهم

محمد و بندر و خالد أبناء مبارك بن حنيف الدوسري و عائلتهم الكريمة

باسم بن سامي الكريع

علي بن عبدالخالق الغامدي

فهد بن عبد العزيز اللحيدان

يوسف بن توفيق خوجة

عبدالعزيز بن عبدالله المحمود

سعد بن محمد آل طلحاب

طارق بن مضيان المضيان

نواف بن عبدالله الشهوان

محمد بن حمود المشيقح

عبدالله بن محمد البداح

سعد بن محمد السعوي

و الشكر الموصول لكل من سأل و تابع و شجع و غمرني بالثقة و الرعاية.

شكر خاص لمن قدم تسهيلات مالية أو دعماً نقدياً خلال فترة العمل على هذه الرسالة:

مصرف الإنماء	الشيخ/محمد بن عبده مدخلي	فيصل بن برهان حجازي
علي بن عبدالخالق الغامدي	محمد و بندر أبناء مبارك بن حنيف الدوسري	فهد بن عبدالعزيز اللحيدان
محمد بن عطاالله المشعلي	تميم بن محمد الغنام	نواف بن عبدالله الشهوان
عزة بنت محمد مدخلي	خالد بن محمد مدخلي	حسام بن محمد مدخلي
طارق بن محمد مدخلي	سحر بنت محمد مدخلي	الليث بن أحمد مدخلي

This work was made possible by the encouragement, help, and support of the following individuals:

The Lloyds Family (Keith and Marjie & Kim and Sara)

The Fristensky Family & George Guszcza

Evgenia Ivanova

Amanda Shriwise

Linda Geaves

Diana Maddison

George Taylor (King George)

Adriana Bianco

Rachel Poor

Ashley Tsai

Julianne Viola

Jenna Milani

Jordan Mansell

Thomas Krulle

Emine Yeter

Kian Mintz-Woo & Ariane van den Hof

Adelin Travers

Andrew Faull

Morwari Zafar

Justin Young-Chan Choi

Donata Wollensak

Sophie Hall

Alex Lucas

Stefani Ruper

Kelly Casey

Kiron Neale

Marcos Calo Medina

Dragana Savic

Ina Jasini

Alix de Zitter

Hannah Mosley

Cath Cunningham

Konstantin Sietzy

Jessica Luise Sorge

Francisco Girbal Eiras

Kimberly Schoemaker

Mick Gantley

Ndjodi Ndeunyema

Jaeyoung Lee

Annette Wagner

Maria Cury

Rosa Krogh

Angelika Abendsommer

Julian Nowag

Alex Doukas & Courtenay Lewis

Roy Amin

Agnes Zwolfer

Mara Schmidt-Klie

Guillaume Croisant

Kate Rehberg

Natasza Piasecka

Anne-Marie Baan

Gemma Clucas

Nico Kist

Lars Hanssen

Daniel DeBrincat

The Linacre Ball Committee: 2017 & 2018

The Linacre CR Executives: 2012-13, 2015, 2017-2018

The Refurb Squad, Linacre College

Global South Coalition Write-Up Squadron:
Milton Barbosa da Silva Jr & Carlos Rios

Alison Reid, Simon Barker, Jackie Favarin, and the Linacre College Principal, administration, and staff.

Abstract

More than half of cancer patients receive radiotherapy for radical or palliative purposes. Increasing survival rates in cancer patients makes it important to study long-term side effects, especially secondary cancers. Medulloblastoma (MB), a posterior fossa tumour, predominantly a childhood disease, is an example of a clinical scenario where proton therapy could have significant advantages. It is therefore used as an exemplar in this thesis to investigate the relationship between malignant induction probability (MIP) and secondary cancer risk in 3D conformal photon therapy (3DCRT) and actively scanned proton therapy by using MATLAB-based code, models, relevant parameters and input values from voxel-by-voxel dose maps.

In this thesis, work started by modelling MIP for different treatment plans to assess the relative MIP values. MIP for different modalities was investigated whilst explicitly incorporating the uncertainty in the model parameters in the modelling process. Results showed that proton therapy is less likely to induce malignancy when compared to 3DCRT (p-value < 0.05). To be able to compare our results with published absolute secondary cancer risk estimates and across patients, model parameters were calibrated and benchmarked, and absolute risk values were calculated. This thesis also addresses, in part, some of the other uncertainties that affect secondary cancer modelling. The effect of spatial dose averaging on predicting MIP was studied by modelling risk using mean, and voxel-by-voxel dose. The effect of changes in radiobiological effectiveness (RBE) on modelling MIP was also studied.

This work showed that independent of the model chosen, and independent of the uncertainty in parameters, proton therapy is less likely to induce malignancy and cause secondary cancer than 3DCRT in patients with medulloblastoma. It was also shown that models used could be benchmarked and calibrated against published models, enabling the calculation of clinically realistic absolute secondary cancer risk estimates. The use of mean dose was shown to introduce a systematic error in regions of high dose inhomogeneity in comparison to the voxel-by-voxel method, making use of the high resolution voxel-by-voxel MIP calculation a necessary step in decreasing uncertainty in modelling outcomes. The work also demonstrated that using an RBE of 1.1 could lead to errors in the range of 5%, leading to potentially higher NTCP or lower local control, which is in agreement with what published literature suggests.

Table of Contents

Acknowledgments ii

Abstract v

List of tables xii

List of figures xiii

List of abbreviations and symbols xviii

1 Chapter 1: Introduction and Background 1

1.1 Introduction 1

1.2 Secondary malignancy: 2

1.3 Existing literature of secondary cancer 7

1.3.1 Breast cancer cohorts 10

1.3.2 Medulloblastoma cohorts 11

1.3.3 Prostate cancer cohorts 12

1.4 Modelling secondary cancer risk: different approaches 12

1.5 Uncertainties in modelling secondary cancer 13

1.6 Medulloblastoma 17

1.6.1 Presentation 17

1.6.2 Classification 21

1.6.3 Treatment of medulloblastoma 22

1.6.4 Outcome and prognosis 24

1.6.5 Adult medulloblastoma 24

1.7 The role of radiotherapy in treatment of medulloblastoma 25

1.7.1 Differences between photon and proton therapy 28

1.8 Proton beam delivery 32

1.8.1 Proton beam 33

1.8.2 Spread-out Bragg Peak 34

1.9 Scope of this work 37

2 Chapter 2: Theory 39

2.1 Modelling Malignant Induction Probability 39

2.1.1 Models and Dose-response Curves 40

2.1.2 MIP models used 41

2.1.3 Dose-response curves for MIP models 44

2.2 Testing the sensitivity of MIP models towards the uncertainty of parameters 48

2.2.1 Sensitivity testing over pre-set parameter space 48

2.2.2 Parameters sensitivity testing using randomly-generated parameter modifiers values 48

2.3 Benchmarking and calibration with BEIR VII report 49

3 Chapter 3: Methods and materials 50

3.1 Modelling MIP after proton and photon therapy 50

3.1.1 Treatment plans details 50

3.1.2 Preparation of plans for MIP modelling 52

3.1.3 Step-wise analysis of the MATLAB code 53

3.1.4 Parameters and parameters assignment 54

3.2 Sensitivity of MIP models to uncertainty in parameters 56

3.2.1 Sensitivity testing over pre-set parameter modifier space 56

3.2.2 Sensitivity testing of parameters over randomly generated modifiers space 57

3.3 Calibration and benchmarking 60

3.3.1 Estimation of the Linear Coefficient value for the LNT model for calibration with the BEIR VII Report 60

3.3.2 Modelling and Calibration 64

3.3.3 Validation 65

3.4 The effect of spatial dose averaging on predicting malignant induction probability and secondary cancer risk 68

3.5 Effect of radiobiological effectiveness on modelling malignant induction probability and dose calculation 69

3.5.1 Effect of radiobiological effectiveness on modelling malignant induction probability 70

3.5.2 Effect of radiobiological effectiveness on dose calculation 71

3.6 Statistical analysis 72

4 Chapter 4: Results 73

4.1 Modelling of MIP after Proton and Photon Therapy 73

4.1.1 Whole Body MIP 73

4.1.2 Organ-specific MIP 77

4.2 Sensitivity of MIP models to uncertainty in parameters 80

4.2.1 Sensitivity testing over pre-set parameter modifier space 81

4.2.2 Sensitivity testing of parameters over randomly generated modifiers space 88

4.2.3 Assessment on of uncertainty in MIP and $MIP_{Relative}$ values 98

4.3 Calibration and benchmarking 103

4.3.1 Comparison with Life Span Study 103

4.3.2 Calibration and benchmarking to BEIR VII report 104

4.4 The effect of spatial dose averaging on prediction of malignant induction probability and secondary cancer risk 111

4.4.1 Whole body 111

4.4.2 Organ Specific MIP 116

4.5 Effect of radiobiological effectiveness on modelling malignant induction probability and dose calculation 121

4.5.1 Modelling MIP for medulloblastoma cases 121

4.5.2 RBE modelling using Wedenberg model 124

5 Chapter 5: Discussion and Conclusions 126

5.1 Modelling of MIP after Proton and Photon Therapy 130

5.2 Sensitivity of MIP models to uncertainty in parameters 134

5.3 Calibration and benchmarking 136

5.4 The effect of spatial dose averaging on predicting malignant induction probability and secondary cancer risk 138

5.5 The effect of radiobiological effectiveness on modelling malignant induction probability and dose calculation 141

5.6 General discussion, relation to existing work, future direction, and conclusion 145

Appendices 153

Bibliography 174

List of tables

Table 1: Range of modifying factors for the parameters α, β, γ, δ, and λ used. 58

Table 2: EAR (per 10000 Person-Year, PY) for uniform single exposures at age of 37 years, and attained age of 46 years using LIN model. Numbers are compared with the plots in Figure 12. 66

Table 3: Standard deviation of normalised MIP for the treatment plans of Patients 1 and 2, and for $MIP_{Relative}$ 98

Table 4: F-Test for variance for data from uncertainty testing performed according to 3.2.2 and illustrated in 4.2.2. 102

Table 5: MIP for a single uniform exposure of 1Gy using non-calibrated parameters for all three models, using the adult patient (Patient 1) plan contours, compared with the ERR from LSS. 103

List of figures

Figure 1: T2 MRI image of a medulloblastoma. 19

Figure 2: "Classification of patients by risk" (from Massimino *et al*, 2016). 20

Figure 3: The calculated path dose curve of a 140 MeV proton beam in tissue and single proton 28

Figure 4: Dose map (sagittal section) of a female adult patient (Patient 1) with medulloblastoma. 32

Figure 5: Schematic presentation of components in passively scattered proton system (from DeLaney and Kooy, 2008). 34

Figure 6: Spread Out Bragg Peak (SOBP) covering a tumour of 2.8 cm in depth, using 5 different Bragg Peaks (DeLaney and Kooy, 2008). 35

Figure 7: Panel a: RBE as a function of depth within the SOBP. Panel b: the dose-averaged linear energy transfer (LET_d) determined from the weighted sum of range-shifted Monte Carlo-modelled raw Bragg peaks. Panel c: the physical dose profile of the SOBP, along with the measured and Monte Carlo-calculated raw Bragg peaks (From Wouters *et al*, 1996). 36

Figure 8: RBE values are plotted as a function of the estimated α/β values for the target cells or tissues. (From Gerweck *et al*, 1999). 37

Figure 9: Dose-response curves for the LQ (a), LIN (b) and LNT (c) models for single exposure. 46

Figure 10: Dose-response curves for the LQ (a), LIN (b) and LNT (c) models for fractionated radiation exposures of 1.8 Gy per fraction. 47

Figure 11: Frequency distribution of parameters modifying factors used in the sensitivity testing in this section:(a) α, (b) β, (c) γ, (d) δ, and (e) λ. 59

Figure 12: Plot (Schneider and Walsh, 2008) of cancer incidence per 10,000 persons per year as a function of organ equivalent dose (OED) of the atomic bomb survivors (as squares) and the Hodgkin's patients (as a diamond). 67
Figure 13: a-c The absolute and relative MIP values for the photon and proton treatment plans (12 patients) for each model. 76
Figure 14: MIP and $MIP_{Relative}$ for thyroid, for (a) LQ, (b) LIN, and (c) LNT models. 78
Figure 15: MIP and $MIP_{Relative}$ for the lung, for (a) LQ, (b) LIN, and (c) LNT models. 79
Figure 16: Whole body MIP and Relative MIP of adult patient (Patient 1- top panels) and teenage patient (Patient 2 – bottom panels) using single parameter variation approach for α. 83
Figure 17: Whole body MIP and Relative MIP of adult patient (Patient 1- top panels) and teenage patient (Patient 2 – bottom panels) using single parameter variation approach for β 84
Figure 18: Whole body MIP and Relative MIP of adult patient (Patient 1- top panels) and teenage patient (Patient 2 – bottom panels) using single parameter variation approach for γ 85
Figure 19: Whole body MIP and Relative MIP of adult patient (Patient 1- top panels) and teenage patient (Patient 2 – bottom panels) using single parameter variation approach for δ. 86
Figure 20: Whole body MIP and Relative MIP of adult patient (Patient 1- top panels) and teenage patient (Patient 2 – bottom panels) using single parameter variation approach for μ. 87

Figure 21: Frequency distribution of MIP_{Photon} and MIP_{Proton} for the adult patient (Patient 1) using LQ model, as well as distribution of $MIP_{Relative}$ 90
Figure 22: Frequency distribution of MIP_{Photon} and MIP_{Proton} for the teenage patient (Patient 2) using LQ model, as well as distribution of $MIP_{Relative}$. 91
Figure 23: Frequency distribution of MIP_{Photon} and MIP_{Proton} for the adult patient (Patient 1) using LIN model, as well as distribution of $MIP_{Relative}$ 93
Figure 24: Frequency distribution of MIP_{Photon} and MIP_{Proton} for the teenage patient (Patient 2) using LIN model, as well as distribution of $MIP_{Relative}$. 94
Figure 25: Frequency distribution of MIP_{Photon} and MIP_{Proton} for the adult patient (Patient 1) using LNT model, as well as d distribution of $MIP_{Relative}$. . 96
Figure 26: Frequency distribution of MIPPhoton and MIPProton for teenage patient (Patient 2) using LNT model (n=400, rms = 0.25), as well as distribution of $MIP_{Relative}$ 97
Figure 27: LAR after 0.1 Gy single exposure before calibration of λ, using the LNT model compared to the BEIR VII report values.. 105
Figure 28: LAR for 0.1 Gy uniform single exposure, using LNT model (after calibration of λ.) and LAR from the BEIR VII report. 105
Figure 29: LAR after 0.1 Gy single exposure compared to the BEIR VII report values, before calibration of λ, using LIN model. 106
Figure 30: LAR for 0.1 Gy uniform single exposure, using LIN model, after calibration of λ, and LAR from BEIR VII report. 106
Figure 31: LAR after 0.1 Gy single exposure compared to the BEIR VII report values, before calibration of the model parameters of LQ model. 107
Figure 32: LAR for 0.1 Gy uniform single exposure, using LQ model, after calibration of LQ model parameters, and LAR from BEIR VII report..... 107

Figure 33: EAR and LAR for the adult (Patient 1) treatment plans (PH: photon plan, PR: proton plan) using LQ model, with varying age at exposure settings, using the calibrated model parameters..... 108
Figure 34: EAR and LAR for the adult (Patient 1) treatment plans (PH: photon plan, PR: proton plan) using LIN model, with varying age at exposure settings, using the calibrated model parameters..... 109
Figure 35: EAR and LAR for the adult (Patient 1) treatment plans (PH: photon plan, PR: proton plan) using LNT model, with varying age at exposure, using calibrated model parameter. 109
Figure 36: EAR for patients 3-12 radiotherapy plans calculated using LQ model with calibrated parameters. 110
Figure 37: EAR for patients 3-12 radiotherapy plans calculated using LIN model with calibrated parameters. 111
Figure 38: Whole body MIP for the 3DCRT plans using LQ model, calculated using mean dose and VbV dose maps..... 112
Figure 39: Whole body MIP for the Proton plans using LQ model, calculated using mean dose and VbV dose maps..... 113
Figure 40: $MIP_{Relative}$ using LQ model for mean dose and VbV dose maps. ... 113
Figure 41: Whole body MIP for the 3DCRT plans using LIN model, calculated using mean dose and VbV dose maps..... 114
Figure 42: Whole body MIP for the Proton plans using LIN model, calculated using mean dose and VbV dose maps..... 114
Figure 43: $MIP_{Relative}$ using LIN model for mean dose and VbV dose maps. . 115
Figure 44: Organ-specific MIP for a number of selected organs from the 3DCRT plans of Patient 1 (PT 1), calculated using LQ model, and Patient 2 (PT

2) calculated using the LIN model with mean dose (MIP MD) and VbV dose maps (MIP VbV) for each organ..... 117
Figure 45: MIP for lung for the 3DCRT plans of the 12 patients, calculated using mean dose (MIP MD) and VbV dose maps (MIP VbV) for the LQ model (a), and LIN model (b). 119
Figure 46: MIP for thyroid for the 3DCRT plans of the 12 patients, calculated using mean dose (MIP MD) and VbV dose maps (MIP VbV) for the LQ model (a), and LIN model (b) 120
Figure 47: Whole body MIP for the patients calculated using RBE of 1.1 ($RBE_{1.1}$) or RBE_{MinMax} for the LQ model (a), LIN (b), and LNT (c)..... 122
Figure 48: Mean dose (a) and maximum dose (b) for selected organs with using RBE of 1.1 and RBE using MinMax model..... 123
Figure 49: RBE calculated with the Wedenberg model using different $(\alpha/\beta)_{Photon}$ values. 125

List of abbreviations and symbols

3DCRT	3D conformal radiotherapy
PH	Photon plan (3DCRT)
PR	Proton plan
BED	Biologically effective dose
BEIR	VII Biological Effects of Ionizing Radiation
C	Cells per voxel
CERR	Computational Environment for Radiotherapy Research.
Cm	Number of malignant cells
C_{org}	Number of cells per organ
CSI	Cranio-spinal irradiation
d	Dose per fraction
D	Total dose (nd)
D_i	Dose at voxel i
DICOM	Digital Imaging and Communications in Medicine
EAR	Excess absolute risk
ERR	Excess relative risk
Gy	Gray

GyE	Gray equivalent
IMRT	Intensity modulated radiotherapy
L	Risk-free period in calculating EAR and LAR
LAR	Lifetime attributable risk
LET	Linear energy transfer
LIN	Linear malignant induction model
LNT	Linear-no-threshold malignant induction model
LQ	Linear-quadratic malignant induction model
LSS	Life Span Study of Atomic Bomb Survivors
MB	Medulloblastoma
MIP	Malignancy induction probability
MIP_{Photon}	MIP of photon therapy (3DCRT) plan
MIP_{Proton}	MIP of proton therapy plan
$MIP_{Relative}$	Ratio of MIP MIP_{Photon} to MIP_{Proton}
MIP_{LQ}	MIP modelled using LQ model
MIP_{LIN}	MIP modelled using LIN model
MIP_{LNT}	MIP modelled using LNT model
MIP_{MD}	MIP modelled using mean dose

MIP_{VbV}	MIP modelled using voxel-by-voxel dose maps
n	Number of fractions
N	Number of voxels
NTCP	Normal tissue complication probability
OED	Organ equivalent dose
OER	Oxygen-enhancement ratio
P_m	Probability that a given cell is malignant
PY	Person-Year
q	Constant used in the $RBE_{Wedenberg}$ model
RBE	Radiobiological effectiveness
RBE_{Max}	Maximum RBE value used to calculate RBE with MinMax model
RBE_{Min}	Minimum RBE value used to calculate RBE with MinMax model
RBE_{MinMax}	RBE calculated using the MinMax model
$RBE_{Wedenberg}$	RBE calculated using the Wedenberg model
rms	Root-mean-square
RR	Relative risk
s	Sex-dependent variable used in calculating EAR
S(a)/S(e)	Survival probability to age a, conditional on survival to age e

SCR	Secondary cancer risk
SF	Surviving fraction of cells given radiation
SOBP	Spread-out Bragg peak
V	Total structure volume
VbV	Voxel-by-voxel
V_i	Volume elements with homogeneous dose
VMAT	Volumetric modulated arc therapy
WBRT	Whole brain radiotherapy
α	Linear radiosensitivity parameter
β	Quadratic radiosensitivity parameter when used with LIN and LQ MIP models
$\boldsymbol{\beta}$	Initial slope of the incidence curve when used with the OED model
γ	Linear radiosensitivity parameter
γ_e and γ_a	Constants related to the age at exposure used in calculating EAR
δ	Quadratic radiosensitivity parameter
λ	Linear coefficient of malignant induction used in LIN & LNT model

μ	Population specific risk modification factor, a function of age at exposure and age attained and sex
ρ	Cellular density (cells/cm^3)
*.mat	MATLAB-compatible file format

1 Chapter 1: Introduction and Background

1.1 Introduction

More than half of all cancer patients receive radiation therapy, either for radical or palliative indications, as part of their treatment (Delaney *et al*, 2005, Schneider U, 2011). With advances in chemotherapy and radiation therapy, survival rates and life expectancy for some cancer patients, especially paediatric oncology patients, have significantly improved (Dhall G, 2009, Koeller *et al*, 2003, Mariotto *et al*, 2009, Packer *et al*, 2011, Parry *et al*, 2011, Robison and Hudson, 2014). With this improvement in survival, the impact of long-term side effects of radiation therapy can become a source of clinical concern, especially given the well-established carcinogenic effects of radiation exposure (Cahan *et al*, 1948), and with the risk and associated mechanisms have been extensively reviewed by a range of international bodies over the years (BEIR VII Report, 2006, ICRP Publication 103, 2007, UNSCEAR, 2012).

Based on the physical characteristics of charged particle therapy with its finite range and increasing dose with depth, the resulting dose distribution can be beneficial when compared with photons (see section 1.7.1). This is due to a reduction in the exposures of normal tissues to radiation, with a decrease in the probability and severity of normal tissue complications, as well as in the malignant induction probability (MIP) and secondary cancer risk (SCR).

The main purpose of the current study was to evaluate the differences, if any, in the induction of secondary malignancies by photon in comparison to proton therapy. Medulloblastoma was used as a relevant clinical model since it occurs in children who will be at risk of second malignancy over their remaining life, and because a large volume of normal tissue is usually exposed to radiation during the course of treatment. Through the use of mathematical modelling, the MIP for each treatment modality was calculated to determine whether any differences would provide further support for the use of proton therapy in this group of patients. A major focus of this work was to systematically study the uncertainties in MIP modelling, quantifying how, if modelling is implemented, these uncertainties affect clinical decision-making and minimising them when possible.

1.2 Secondary malignancy:

Second cancer is defined as a histologically-distinct confirmed cancer found after treatment of the initial cancer. Neither metastases nor local recurrences are included in this definition and are not the focus of this work. In the United States, 6-10% of all new cancers diagnosed every year are second cancers (Bhatia and Sklar, 2002). Some of these second malignancies are spontaneous; others are treatment-related.

For a better understanding of the problem of second malignancy that arises as a result of previous radiation therapy, it is essential to review the associated risk factors to better understand mechanisms of development of second cancers, and potentially consider preventive strategies (Chargari *et al*, 2016). Known risk factors for the development of secondary cancer include

age at diagnosis of the primary cancer, sex, and the type of treatment for the primary (initial) cancer (Neglia *et al*, 1991, Neglia *et al*, 2001, Bhatia and Sklar, 2002). The younger sections of the population are thought to be more susceptible to the development of secondary cancers. Contributing factors may be: an increased sensitivity of their tissues to the effects of radiation, the high rate of proliferation of their cells, genetic susceptibility, along with a higher prevalence of genetic syndromes that may be correlated with some pro-mutagenic entities, resulting in a dose-related increase in the risk of developing a secondary cancer after receiving radiotherapy (O'Malley *et al*, 1997, UNSCEAR, 2013, Manolio *et al*, 2009). The long follow-up period of paediatric and young adult cancer survivors allows time for second cancers to develop, and to be diagnosed (Neglia *et al*, 2001, Preston *et al*, 2007, de Bruin *et al*, 2009, Friedman *et al*, 2010). The effect of age on secondary cancer risk is supported by evidence from the Japanese atomic bomb survivors Life Span Study (LSS), as set out in LSS report 14 (Ozasa *et al*, 2012). LSS demonstrates that the risk of developing a secondary cancer is higher when exposure occurs at a younger age.

Some studies have also shown that females are at higher risk of developing secondary cancer than males (24.8% vs 19.3% after 25 years) (Dores *et al*, 2002). The higher risk for females could be attributed to the risk of secondary breast cancer, and to some extent, lung cancer (BEIR VII Report, 2006). An increased risk of breast cancer in females has been documented in several populations that received radiotherapy at young age (Boice JD, 2001). For young women treated with mantle-field radiation for Hodgkin's disease,

premature ovarian failure related to pelvic irradiation and/or MOPP chemotherapy might be expected to attenuate the elevated, radiation-related breast cancer risk. The effect of hormone replacement therapy in this group is unclear (Hankock *et al*, 1993). The apparent higher risk of developing secondary cancer resulting from radiation exposure in women is an important observation to be taken into consideration when prioritising patients' access to proton therapy treatment. This has clinical implications: for example, 40% of breast cancer occurs in women younger than 60 years old (CRUK, 2015), many of whom will survive for a protracted period following treatment, during which they will be at risk of developing secondary cancer.

Chemotherapy may be a contributing factor to the risk of developing secondary malignancy (Tucker *et al*, 1987, Dores *et al*, 2002, Travis *et al*, 2005, Dores *et al,* 2014). In Hodgkin's disease, radiotherapy is believed to be the main cause of secondary cancers as there was no significant difference in risk between patients receiving chemo-radiotherapy and patients receiving radiation therapy alone (van Leeuwen *et al*, 2005), and risk was found to be much lower for chemotherapy alone than after combined modalities (chemotherapy and radiotherapy) (Swerdlow *et al*, 2011) . The role of chemotherapy in inducing secondary cancer is important and recognised for certain agents, like alkylating agents (Swerdlow *et al*, 2011, Swerdlow *et al*, 2000, Birdwill *et al*, 1997, Pera *et al*, 1989, Sasajima *et al* 1977). However, a consideration of this phenomenon is outside the scope of this thesis, which concentrates solely on radiation effects.

In studying secondary cancer risk, the location of the secondary cancer is important in understanding the development of secondary malignancy. Some solid secondary cancers arise in the radiotherapy treatment field, areas of relatively high dose. Others develop at field margins, areas of intermediate or low radiation dose, while others still may arise in locations distant from the primary (initial) tumour (Brenner *et al*, 2000, Diallo *et al*, 2009, Hauri *et al*, 2016). The spatial pattern of secondary cancer occurrence may help define the dose-response model and guide future clinical practice, discouraging or encouraging modalities like IMRT (Intensity modulated radiotherapy) for example. IMRT leads to improved dose distribution, conforming to the tumour and minimising dose to organs at risk. However, in IMRT, a large volume of the treatment field receives a low dose creating a dose bath. This does not necessarily lead to normal tissue complications, but could result in increased cancer risk, as this is a stochastic effect. That is, it is the type of effect that can occur after any dose, in contrast to deterministic effects, which only takes place if a certain dose threshold is exceeded. IMRT is a relatively recent technology that provides solutions to certain problems concerning the delivery of conformal radiation therapy to tumours. For example, IMRT has enabled physicians to deliver doses that could not possibly be given with older techniques due to the existence of dose-limiting organs at risk. On the other hand, because IMRT uses several beams to deliver treatment, a relatively large volume may receive a low integral dose. Other technologies include gating and 4D radiotherapy, where moving targets are only irradiated when they lie within a certain, pre-set field, so dose to the tumour volume is maximised and dose to normal tissues is decreased.

Secondary cancers can be associated with the location of the initial disease: for example, secondary thyroid cancer may arise after radiotherapy to the head and neck, or secondary bladder or rectal cancer after radiotherapy for prostate cancer. In other cases, however, secondary cancer may develop in organs well outside the treatment field which is possibly related to scattered radiation, like secondary lung cancers arising in prostate cancer patients (de Vathaire *et al*, 1999, Sklar *et al*, 2000, Brenner *et al*, 2000, Abdel-Wahab *et al*, 2008, Hauptmann *et al*, 2015, Hauptmann *et al*, 2016).

The latency period between the initial radiation therapy and the secondary cancer differs depending on the type of tissues irradiated. Leukaemia may be diagnosed within 5-7 years after radiation therapy, while some solid secondary cancers typically arise ten or more years after the initial treatment. Breast cancer, for example, may take up to 20 years to develop (Bhatia *et al*, 1996, Rubino *et al*, 2005, Travis *et al*, 2003, van Leeuwen *et al*, 2003). This protracted latency period highlights the importance of long follow-up studies of cancer survivors. Brenner and Shuryak and others (Brenner & Shuryak, 2011, Chargari *et al*, 2016) demonstrated that the follow up of patients for up to 10 years following treatment is insufficient to assess Lifetime Cancer risks. As secondary solid tumours tend to take a long time to arise and become clinically detectable, studies have been carried out looking into patients who have received radiotherapy with different equipment, techniques, and quality assurance protocols. Modelling historical data (where there is sufficient follow-up) is challenging, since the exact details of the 3D-dose delivered are often not available. This, together with the change in

treatment techniques over time, means that predicting MIP for patients treated today carries uncertainty (Murray *et al*, 2013).

1.3 Existing literature of secondary cancer

The literature concerning the carcinogenic effects of radiation exposure is extensive and spans many years (Cahan *et al*, 1948, Li *et al*, 1975). The study of secondary cancer after radiotherapy has been conducted in different cohorts of patients. Among the best-studied groups are Hodgkin's disease patients and breast cancer patients, with less complete information for patients with other cancers, such as with cervical cancer (Boice *et al*, 1985, Boice *et al*, 1988, Rodriguez *et al*, 2014).

The available studies agree on the general conclusion that radiotherapy is associated with an increased risk of secondary cancer (Bartkowiak *et al*, 2012). Some of the main differences between the studies are the quantification of risk, the generated dose-response curves, and the variables associated with the models used.

Hodgkin's disease patients' data are a relatively good source of information to generate secondary cancer dose-response curves. This is because the survival rate of patients is high, and the radiation dose they receive to a relatively large volume can be in the order of 20 and 35 Gy, and a number of critical organs are often exposed to a dose that could be of interest. The long-term side effects of radiotherapy for Hodgkin's disease, including lung disease, cardiac pathology as well as secondary cancers, make this group of cancer patients a particularly rich source of data to generate dose-response curves for those side effects. Modern-day treatment techniques have

successfully led to a reduction in irradiated volumes in certain scenarios, making radiotherapy potentially less morbid, being less likely to cause long-term side effect (Hall and Wuu, 2003). However, historical data are helpful for the understanding of secondary cancer risk, even when treatment techniques have become outdated.

In one study (Dores *et al*, 2002), data from 32,591 Hodgkin's disease patients (1,111 25-year survivors) were included in 16 population-based cancer registries in North America and Europe (1935 to 1994) 726 second solid tumours were reported. Cancers of the lung, digestive tract, and female breast accounted for the largest number of subsequent malignancies. 25 years after Hodgkin's disease diagnosis, the risk of developing a secondary solid tumour was 21.9% overall, 19.3% for males (95% CI: 17.5%-21.1%) and 24.8% for females (95%CI: 22.4% -27.2%, observed/expected = 1.8, absolute excess risk = 60 / 10,000 Person-Year). The relative risk of secondary solid cancer decreased with increasing age at initial diagnosis. However, patients aged 51 to 60 years at initial diagnosis (making up about 10% of the study population, and older than ~75% of it) experienced the highest cancer burden. A significant increase in the risks of second cancers was observed in all age groups. After a progressive rise in relative risk and absolute risk of all solid tumours over time up to 25 years, although significantly elevated risks for some cancers persists, there was then an apparent decrease in risk. This downturn in relative risk at 25 years might be expected, due to the increase in background risk with advancing age in the general population (Dores *et al*, 2002).

Another study (Morton *et al*, 2013) focused on secondary cancer of the stomach after treatment for Hodgkin's disease established a dose-dependent increased in risk of stomach cancer for those who received sub-diaphragmatic radiotherapy. Patients with Hodgkin's disease who received sub-diaphragmatic radiation therapy had dose-dependent risk increase of stomach cancer, with noticeable risks for patients who also received chemotherapy containing high-dose procarbazine, which is an oral alkylating anticancer agent. For patients being considered for treatment, disadvantages and benefits of exposure to both procarbazine and sub-diaphragmatic radiation therapy should be weighed carefully. For patients treated previously, GI symptoms should be evaluated promptly (Morton *et al*, 2013). An earlier study that focused on lung cancer after treatment of Hodgkin's disease drew similar conclusions (Gilbert *at al*, 2003). It showed that estimated excess relative risk (ERR) per Gy was 0.15 (95% CI: 0.06-0.39), and there was nearly complete linearity even with lung doses for the majority of Hodgkin's patients treated with radiotherapy exceeding 30 Gy. ERR/Gy was not affected by time since exposure, age at exposure, or attained age. Grantzau *et al* showed similar results concerning the development of lung cancer after treatment for breast cancer. 2358 second cancers had occurred during the follow-up of the cohort. For radiotherapy-associated sites hazard ratio (HR) for women who received radiotherapy was 1.34 (95% CI 1.11–1.61) with significantly increased HRs for the time window of 10–14 years and equal to or greater than 15 years after treatment (HR 1.55; 95% CI 1.08–2.24 and HR 1.79; 95% CI 1.14–2.81, respectively). Non-radiotherapy-associated sites showed no increased risk (HR 1.04; 95% CI 0.94–1.1).

Grantzau *et al* estimated the attributable risk related to radiation therapy for the radiotherapy-associated sites to translate into 5 radiation-induced secondary cancer in every 1000 women treated with radiotherapy (1 in 200) (Grantzau *et al*, 2013).

Berrington de Gonzalez and colleagues conducted a review that included 28 eligible studies with 3,434 second cancer patients across 11 types of second solid cancer. The authors found that there was little evidence that the dose-response curve was non-linear in the direction of a down-turn in risk, even at organ doses of ≥60Gy (Berrington de Gonzalez *et al*, 2013). Although the risk was found generally to relate linearly with dose, the magnitude of risk was different from one study to another, and varied between different cancer sites. For example, ERR/Gy for breast cancer was 0.13-0.27 (Travis *et al*, 2003, Guibout *et al*, 2005, Inskip *et al*, 2009), while for lung cancer it was 0.15-0.20 (Inskip et al, 1994, Gilbert et al, 2003).

1.3.1 Breast cancer cohorts

In addition to their often long survival, breast cancer patients are selected for studies of radiation late side effects because of the dose received to the heart, the age range at which treatment is given and the ability to compare right and left side endpoints in the same patients, giving an internal control in the case of radiation-induced heart disease. In a study by Inskip *et al*, which focused on lung cancer after treatment to breast cancer, ERR/Gy was found to be 0.2 for the affected lung. Relative risk was found to be 1.8 (95% CI: 0.8-3.8) for 10-year survivors, and RR increased with the time following treatment for the initial cancer (breast cancer) (Inskip *et al*, 1994). In a paper

published in 2017, meta-analyses of over 40,000 breast cancer patients yielded lung cancer incidence 10 years after radiotherapy RR of 2.10 (95% CI, 1.48 - 2.98), and an ERR/Gy of 0.11 whole-lung dose (95% CI, 0.05 - 0.20) (Taylor *et al*, 2017). Rubino *et al* looked at risk of soft tissue and bone sarcoma after breast cancer treatment, and ERR/Gy was found to be 0.05 (Rubino *at al,* 2005).

1.3.2 Medulloblastoma cohorts

Given that medulloblastoma patients are usually young at diagnosis, and that 5-year survival rates are can be 85%, a consideration of late side effects is important. A major obstacle in the study of secondary cancers in medulloblastoma is the small number of cases available for analysis, a result of the low incidence rate of medulloblastoma, which in the United States is 1.5 per million population, and 6 per million for children aged 0-9 years (Goldstein *et al*, 1997, Smoll *et al*, 2012). In a population-based study by Goldstein and colleagues, a 5.4-fold excess of second cancers was found (95% CI: 3.3-8.4). The second cancers occurred 8 months to 432 months (median = 73 months) after initial diagnosis (Goldstein *et al*, 1997).

1.3.3 Prostate cancer cohorts

The main difference between the prostate cancer cohorts and the previous cohorts is the average age of the patients. The interest in prostate cancer from the second cancer perspective is the large patient population, the treatment delivered to the prostate, and the dose received by the rectum. However, the high average age at the time of treatment makes extended follow-up of this group challenging. Brenner *et al* (Brenner *et al*, 2000) analysed data of patients with prostate cancer treated with radiotherapy, and patients treated without radiotherapy. Radiotherapy for prostate cancer was associated with a small, statistically significant increase (6%, 95% CI: 1–11%) in the risk of solid tumours when compared with patients treated with surgery (with no radiotherapy). The most important contributors to the increased risk in the group that received radiotherapy were rectal cancer, bladder cancer, and lung cancer, in addition to sarcomas within the treatment field (Brenner *et al*, 2000).

1.4 Modelling secondary cancer risk: different approaches

Several different attempts have been made to quantify the risk of secondary cancer after radiotherapy, with researchers in the field using a range of approaches and methodologies. Epidemiologists have looked at data as a whole and tried to simplify the relationship between the dose and the response. Although this approach can establish a proven relationship, it almost entirely overlooks the potential mechanisms that lie beneath and drive the dose-response curve. Modellers, on the other hand, typically start with a simple mechanistic hypothesis and add complexity and additional

parameters to their models when necessary to better describe their data. However, there are uncertainties associated with the various hypotheses and assumptions requiring the models to be validated and benchmarked against experimental and clinical data. This differences in approach are illustrated in a paper by Berrington de Gonzalez *et al* (Berrington de Gonzalez *et al*, 2013), who attempted to carefully build dose-response curves, following the epidemiology paradigms. However, in this process, many details were lost by using mean dose, for example, as a proxy for the dose characteristics of the structures studied. But the uncertainties faced by Berrington de Gonzalez et al and others epidemiologists are similar to those faced by researchers who conducted work trying to model secondary cancer risk, including the work presented in the following chapters of this thesis.

1.5 Uncertainties in modelling secondary cancer

Modelling is an attempt to predict outcome using mathematical models that describe the behaviour of the system in question under certain conditions. Models require input parameters, and values for those parameters. In the case of secondary cancer, the system being investigated is the patient (human body) and the conditions under investigation are aspects of the radiation therapy, such as dose. Parameters that may be relevant are sex, age, and tissue type, in addition to the other input parameters that modify and partially influence the shape of the dose-response curve.

In modelling secondary cancer risk, the greatest source of uncertainty probably remains the choice of the model itself; the nature of the patient's response to radiotherapy. Part of the difficulty lies in the relative scarcity of

data, or the sub-optimal quality of the available data, or both. The scarcity of high quality data can be partially attributed to the type of studies that are needed to screen for and diagnose secondary cancers. A long follow up time is needed, well beyond the traditional 3-5 years usually used in survivorship studies in cancer patients. Some argue that even 10 years of follow up is insufficient as it would only show a fraction of the secondary cancer cases that will develop over the lifetime of the patient (Brenner & Shuryak, 2011). Further secondary cancer occurrence does not necessarily relate linearly with age attained, so extrapolation from such data is not straightforward. The ideal subjects, those who make the best candidates for secondary cancer studies, are young patients who are expected to live beyond 5-10 years. Patients with aggressive types of cancers are unlikely to live long enough to develop a secondary cancer. Similarly, patients in their late seventies with curable malignancies, for example, would not be the best candidates for such studies as their life expectancy may not be long enough to allow meaningful conclusions to be drawn. Nevertheless, understanding secondary cancer risk in all age groups is important. In such studies, the role of chemotherapy must be duly noted, as some chemotherapies are known to increase risk of secondary cancer.

Even when a population of adequate size is studied for a long period of follow up, the quality of radiotherapy data available for analysis may be suboptimal. For example, the patients studied may have received an outdated treatment regimen, and/or the radiotherapy plans were generated using non-digital means. In some cases, digital form of radiotherapy plans may not be

available, necessitating reconstruction of the plans on phantoms or 'standardised' patient CT scans. This will inevitably eliminate many of the patient-specific dosemetric and anatomical details, and has the effect of narrowing the spectrum of variation between organ doses. On the other hand post-hoc reconstruction of plans may provide a better approach than use of mean doses. Reconstruction methods are more likely to produce more relevant risk estimates in the absence of patient-specific dose maps, and reduce the uncertainty in using broad dose indices only (Ligot *et al*, 1998, Yoon *et al*, 2010). The dose-volume histogram (DVH) is a good indicator of dose distribution in some cases and is an established metric for dose-related studies, especially those concerning the normal tissue complication probability (NTCP). However, the reliance on DVHs as a surrogate for 3D dose to organs masks some details of the treatment plans. In secondary cancer modelling, using DVHs blocks out details related to precise localisation of dose (e.g. intra-organ dose distribution) which can be very important in understanding the response of organs to radiation therapy. Studies of secondary cancer risk should optimally be based on digital DICOM radiation therapy files, where all treatment plan details can be accessed to assure the highest possible resolution of data and most accurate generation of dose-response curves, as details of anatomy and dose are available.

One further problem is that different types of cancer, and even different stages of the same type of cancer, are treated using different radiation therapy protocols, resulting in a complex interplay between risk of second cancers, details of the treatment delivery, and patient heterogeneity (Daşu *et*

al, 2011, Inskip *et al*, 2016). The implications of this can be very profound as projecting from one cohort of patients to another may not be reasonable, depending on the endpoint being studied. As long as organs receive similar doses delivered using comparable techniques, the comparison may be sound. This highlights why high resolution dose maps are important for studies of secondary cancer, as understating and analysing the high resolution dose distribution maps allows valid comparisons between different groups of patients.

Throughout this work, exercises are carried out to address some of the uncertainties inherent in modelling MIP and secondary cancer risk. Adherence to a single model is avoided when possible: rather multiple models are used to assess potential differences in relative MIP. Differences between the shapes of dose-response curves and the effect of those differences on relative MIP are studied.

To investigate the effect of uncertainty in input parameters, work was carried out to quantify the sensitivity of models towards those parameters. The variation of parameters' values, whether from a pre-set value of parameter or from randomly generated parameter spaces should establish if relative MIP will stay the same or not.

As DVHs and mean doses are often used to calculate long-term side effects, comparing of secondary cancer risk between different models would aid in establishing the nature of trends of differences between MIP values using mean dose and using high resolution dose maps. As discussed earlier, the use of high resolution dose maps will be invaluable in understanding long-term

side effects, namely secondary cancer as mean dose data and DVH data obscure a certain level of details.

When working with proton therapy, a conversion between proton therapy and photon therapy prescription doses must be used. Differences in radiobiological effectiveness (RBE) due to tissue-specific factors between photon and proton treatments will be discussed.

1.6 Medulloblastoma

Medulloblastoma is among the most common central nervous system malignancies in the paediatric age group (Martínez León MI, 2011). In the United Kingdom, medulloblastoma is the brain and central nervous system cancer with the second highest incidence after astrocytoma in the age group 0-14 years (Cancer Research UK, 2011, National Registry of Childhood Tumours/Childhood Cancer Research Group, 2011).

While in children it accounts for 20-30% of CNS cancers, in adults it is a rare pathology, with an incidence of around 0.5 per million (Giordana *et al*, 1999, Frost *et al*, 1995).

1.6.1 Presentation

According to the Central Brain Tumor Registry of the United States, medulloblastoma occurs in a bimodal fashion with peak incidences between 3 and 4 years and 8 and 9 years of age. 10–15% of medulloblastoma cases are diagnosed in infants. Boys have a higher incidence than girls (CBTRUS, 2004-2005). Patients with medulloblastoma frequently present with signs of increased intracranial pressure related to obstructive hydrocephalus due to

tumour growth and compression of the fourth ventricle. Early morning headache with vomiting, irritability, and lethargy can be preceding signs. Because many paediatric medulloblastoma tumours arise in the cerebellar midline, axial instability is often observed, which manifests as an unsteady gait. Vomiting, headache, ataxia, and nausea are predominant symptoms (Halperin *et al*, 1996). There is an inverse relationship between the duration of symptoms and the stage of medulloblastoma (Halperin *et al*, 2001). The occurrence of these symptoms and signs should prompt a performance of a full history and clinical examination, with a thorough neurological examination, to look for relevant neurological deficits. In an emergency setting, while CT scan is usually the first line of imaging used due to its wide availability, in medulloblastoma it is only informative (provides radiological finding suggestive of medulloblastoma) in 30-55% of cases (Tsuchida *et al*, 1984). Typical features of medulloblastoma that can be found on MRI scans include a heterogeneous hypointense mass on T1-weighted imaging. On T2-weighted sequences, medulloblastoma is intermediate between grey and white matter (Figure 1). With contrast, enhancement is usually heterogeneous. Drop metastases (spinal metastases) found in up to 40% of the patients, are mostly noted in the thoracic and lumbosacral areas. They are best seen on post-contrast T1-weighted images (Kumar *et al* 2001, Buhring *et al*, 2002, Malheiros *et al*, 2003, Massimino *et al*, 2016).



Figure 1: T2 MRI image of a medulloblastoma. The presentation of the tumour (arrow) in the radiological exams, depends on the histological type. (Case courtesy of A. Prof Frank Gaillard, Radiopaedia.org, rID: 7912).

A lumbar puncture is performed (with extreme caution) to assess the cerebrospinal fluid and test it for the presence of any cells indicative of spinal spread of medulloblastoma, especially in the cases were MRI are equivocal. With the completion of history, clinical presentation, imaging studies, and study of CSF, treatment is planned based on risk stratifications (Figure 2).

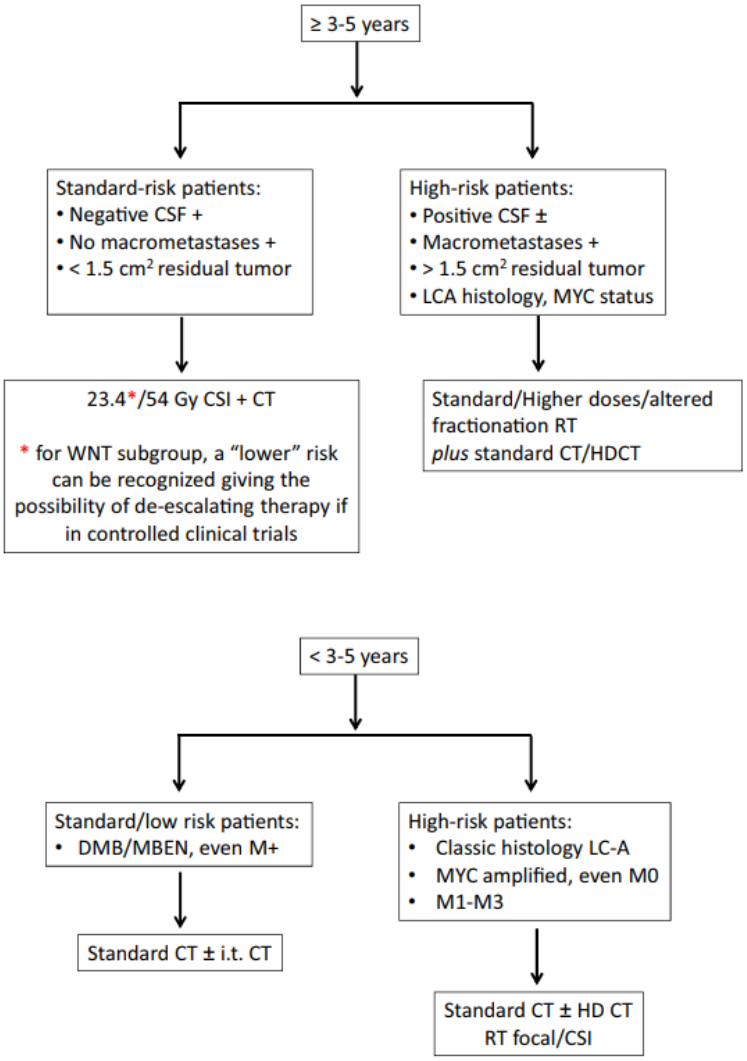


Figure 2: "Classification of patients by risk" (Reprinted from Massimino *et al*, 2016, with permission from Elsevier). CSF; cerebrospinal fluid, LCA; large cell anaplastic, WNT; wingless (one of the 4 molecular groups of medulloblastoma associated with high survival rate), CT; chemotherapy, HDCT; high-dose chemotherapy, DMB; desmoplastic, MBEN, medulloblastoma with extensive nodularity, M; metastases, M1-M3: metastases classification according to Chang et al, 1969.

1.6.2 Classification

Clinically, paediatric medulloblastoma patients are stratified into two risk groups (Ellison *et al*, 2005, Packer *et al*, 2003, Sakar *et al*, 2004):

1-Standard-risk: children older than three years, with post-op residual tumour measuring less than 1.5cm^2 and with no disease spread.

2-High-risk: children younger than three years, post-op residual tumour larger than 1.5 cm^2, and/or metastatic disease.

The stratification has since evolved (Figure 2, Massimino *et al*, 2016). This stratification does not account for all the variation in outcome observed, which also correlates with the histopathological variants of medulloblastoma. It has been shown, for example, that there was no significant difference in survival between M0 and M1 patients (patients without metastases and patients with positive CSF cytology, respectively), as illustrated by the Children's Cancer Group 921, and the German trial HIT'91 (Zeltzer *et al*, 1999, Kortmann *et al*, 2000).

Histopathology textbooks describe medulloblastoma according to the WHO classification as classic, desmoplastic/nodular or large cell. Two variants were added later: medulloblastoma with extensive nodularity, and the anaplastic type (Crawford *et al*, 2007). From a prognostic point of view, and although the histopathology is not fully a part of the risk stratification described above, patients with extensive nodularity have better prognosis than those with the desmoplastic variant, while patients with anaplastic type

tumours carry the least favourable prognosis (Packer *et al*, 2008, Rossi *et al*, 2008, Ellison DW, 2010, McManamy *et al*, 2007, Cogen *et al*, 1996).

Correlation of medulloblastoma with chromosomal or genetic abnormalities is an active area of research. Some of the abnormalities that have been identified are the loss of 17p and loss of isochromosome 17q; those being more frequent in anaplastic and classic subtypes (Cogen PH, 1996). 17p corresponds to the location of a tumour suppressor gene, and its deletion may lead to emergence of malignant phenotype. Another genetic factor undergoing study is the PTCH mutation, which is found in patients with Gorlin's syndrome (Raffel C, 2004). PTCH mutation is found in up to 15% of sporadic medulloblastoma. Anaplastic and large cell types of medulloblastoma, which are considered the more aggressive types, are usually associated with the amplification of the c-Myc and N-Myc genes (Rossi A, 2008, Ellison DW, 2010).

1.6.3 Treatment of medulloblastoma

Maximal surgical resection of the tumour, followed by cranio-spinal irradiation (CSI) and/or chemotherapy is considered to be the standard protocol for treatment. In patients less than 3 years-old, chemotherapy is given alone after surgery as it is recommended to omit radiation therapy in this age group. Chemotherapy is also given in combination with radiotherapy to patients who are labelled as high-risk for other reasons, such as incomplete resection of the tumour.

Maximal surgical resection is the preferred procedure whenever feasible. The location of the tumour may be an obstacle to completely or safely resect it, as it is usually located centrally near the vermis in younger children. Neurosurgeons have been able to perform improved medulloblastoma resections, due to recent advances in neurosurgery and surgical equipment, neurosurgeons have refined medulloblastoma resections and by doing so, have contributed to improved outcome. Chemotherapy forms a major component of treatment in this patient group. CSI with a posterior fossa boost has been shown to be effective in the standard-risk group, and in the high risk group in patient older than three years (Dahll G, 2009).

A common treatment protocol in standard risk patients is surgical resection followed by craniospinal irradiation to 23.4 Gy with a posterior fossa boost increasing the dose to 55.8 Gy, with concurrent vincristine, followed by vincristine, cisplatin plus either CCNU (lomustine) or cyclophosphamide (Packer *et al*,2006).

For high risk patients, surgical resection is typically followed by craniospinal irradiation to 36-39 Gy with a boost to the posterior fossa and metastases larger than 1 cm to 54 Gy along with concurrent vincristine, followed by intensive chemotherapy. In children younger than three years, radiotherapy is omitted and replaced with intensive chemotherapy (Bouffet E, 2010).

Radiotherapy for medulloblastoma is usually delivered in 1.8-2.0 Gy fractions, once a day, five days a week, and is usually well tolerated in children, with minimal acute side effects.

1.6.4 Outcome and prognosis

Treatment outcomes in medulloblastoma have significantly improved as a result of the advances in surgical technology and instrumentation, radiation therapy, and chemotherapy. Five-year-survival as high as 85% has been reported (Dahll G, 2009, Koeller *et al*, 2003, Packer *et al*, 2008). Five- and ten-year overall survival rates have been reported to be 72% and 55% respectively (Padovani *et al*, 2007). Other studies have reported lower numbers (44.1-55.7%) (Roldán *et al*, 2008). These figures should encourage radiation oncology teams to consider ways to decrease long-term side effects as patients are expected to live for many years after treatment and the avoidance of serious and debilitating side-effects is highly desirable. This can be achieved through highly precise radiation therapy delivery or the use of proton therapy to lower the risk of normal tissue complications and secondary cancer. The same approach should be applied to all paediatric patients with curable cancers who are expected to survive for more than 5 years. The burden is gradually shifting from curing cancer to curing cancer *and* ensuring quality of life.

1.6.5 Adult medulloblastoma

The literature describing the pathology and outcomes in paediatric medulloblastoma is larger than that of the adult medulloblastoma (Lai R, 2008). Medulloblastoma only accounts for 1-3% of all primary brain tumours in adults (Bloom and Bessell, 1990, Carrie *et al*,1994, Frost *et al*, 1995, Brandes *et al*, 2004) with an incidence of about 0.5 per million.

Patients with adult medulloblastoma are staged, classified, and treated in similar ways to children. Adults are able to tolerate a higher dose of radiation to the brain than children without serious neurocognitive sequelae, and are usually prescribed higher dose for craniospinal irradiation, up to 36-40 Gy (Carrie C, 1994, Kunschner *et al*, 2001, Brandes *et al*, 2007, Balducci *et al*, 2012). The treatment protocols for adults are usually adopted from the protocol designed for paediatric cases, as the experience with that age group is much more extensive.

The outcome of medulloblastoma treatment in adults varies widely. In adults, medulloblastoma is typically more aggressive than in paediatric cases. One reason behind this is that the dominant histological type in adult medulloblastoma is the anaplastic form, an aggressive variant of medulloblastoma that demands intensive chemotherapy, and higher doses of radiotherapy for control and which is also associated with a higher rate of spinal spread. Published studies mostly report an overall 5-year survival of 50-60% which is lower than that reported in the paediatric literature (Brandes *at al*, 1999). A paper by Rose Lai, which was a population-based study, reported 5, and 10-year relative survival of 64.9, and 52.1%, respectively (Lai R, 2008).

1.7 The role of radiotherapy in treatment of medulloblastoma

Radiotherapy is of great importance in the treatment of medulloblastoma, as it is essential in decreasing the chance of the survival of malignant cells, and hence decreases the risk of recurrence, by “sterilising” the neuroaxis (brain and spine).

Historically, photon therapy played a more prominent role than proton therapy, due to the availability of photon therapy equipment and its affordability when compared with the more sophisticated, complex, and more expensive particle therapy equipment. But since the emergence of hospital-based proton therapy facilities, and the increasing experience of treating with protons, and the decrease in cost of constructing proton therapy centres, more options of treatment for various cancers have become possible and are being studied, and more and more cancer types have been considered for proton therapy.

The precision of delivery techniques has improved significantly since the first generation of radiation therapy devices. Contouring, beam alignments, delivery time, positioning accuracy have all improved. Advanced computer facilities make it possible to store and file sophisticated treatment plans for future reference and studies. Cloud computing makes it feasible to store and recall detailed patient radiation therapy plan data without significant logistical difficulties in comparison to the late 1990s and early 2000s, when 3DCRT became the standard of care. The afore-mentioned improvements have also contributed to better quality particle therapy.

Some of the challenges associated with photon therapy can be overcome by using particle therapy. The utilisation of a range of different particles in cancer therapy was first considered, after Bragg's description of the behaviour of accelerated atoms and particles in the early 20th century, (Bragg *et al*, 1905, Wilson RR, 1946).

Figure 3's top panel shows the dose profile of a 140 MeV proton beam, an energy frequently used in medical-quality proton beams. In the region proximal to the target volume, the tissues receive a very low dose, the tissues distal to the target volume receives almost no dose at all. Tumour volumes can be completely covered by varying the energy of the proton beam to deliver a series of Bragg peaks at different depths within the body, summing to give a uniform dose across the tumour target volume (Figure 3, bottom panel). Proton therapy appears to have the potential to achieve the ultimate aim of radiation oncology: to deliver the maximum dose possible to the tumour volume, while delivering the minimal dose to the surrounding normal tissues. If this could be achieved, it would allow dose escalation to tumours that are surrounded by organs at risk, or dose-limiting organs, and so, proton therapy can, in theory, allow the radiation oncologist to increase local control rates and other survival indices.

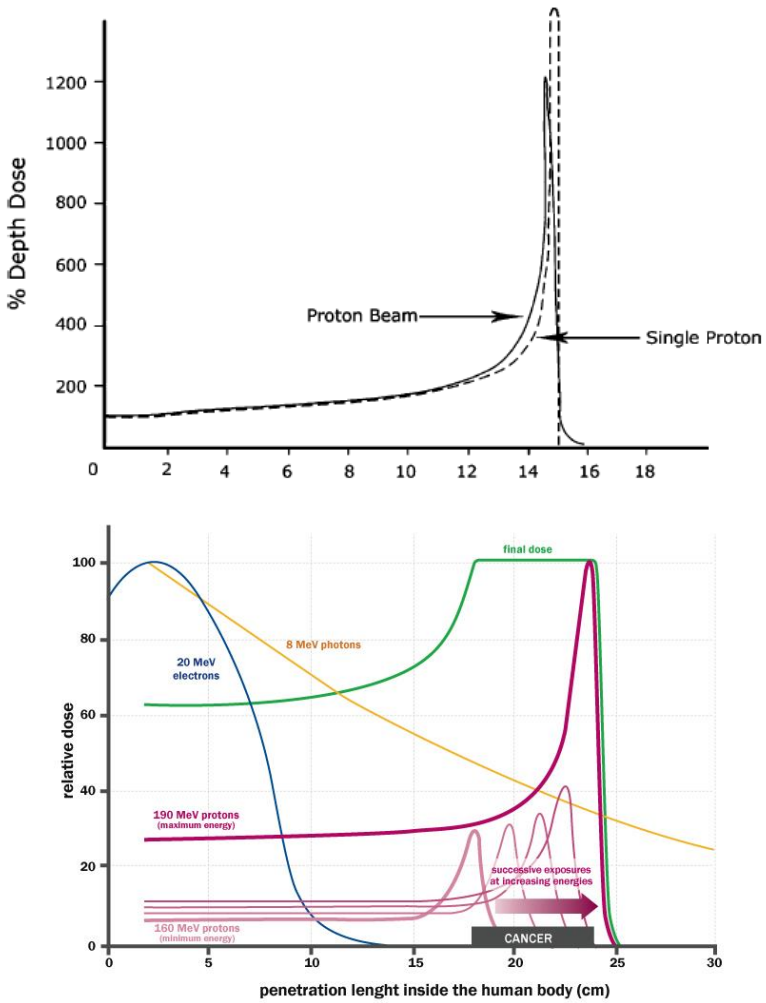


Figure 3: Top: the calculated path dose curve of a 140 MeV proton beam in tissue and single proton. Notice the relatively low dose before the Bragg peak, and the absence of any dose deposition beyond it (Reprinted from Wilson RR, 1946 with permission from Radiological Society of North America). Bottom: Depth dose distribution in tissues for a number of different particles and photons at given energies (INFN, 2008).

1.7.1 Differences between photon and proton therapy

When proton therapy and photon therapy are compared, it is important to consider certain physical and biological effect properties. Protons used in radiation oncology are of low linear energy transfer (LET), low radiobiological effectiveness (RBE), and high oxygen-enhancement ratio (OER). Published figures for RBE and OER values that are based on in-vitro studies if applied clinically, should be applied with caution. Nevertheless,

they do provide a general guide to assess the quality of the radiation therapy used, and its potential effect (Paganetti *et al*, 2002, Kanemoto *et al*, 2014).

RBE is a measure of relative effect of radiation. It is the ratio of doses required to reach the same endpoint or level of effect between two radiation modalities (photon and proton). It is defined by ICRP and ICRU as "A ratio of the absorbed dose of a reference radiation to the absorbed dose of a test radiation to produce the same level of biological effect, other conditions being equal". This definition assumes equal conditions, and is only applicable when the two radiations produce effects of the same extent and/or nature, otherwise RBE cannot be specified (ICRU, 2007). The general definition of RBE also assumes a homogeneous dose across the organ being studied, which in most cases may not be case.

Protons are considered to have LET, RBE, and OER values close to that of photons, but there are differences. The energy of protons changes in relation to the properties of the medium they pass through. Protons are scattered and stopped differently by atoms with different atomic numbers, and it is important to realise when planning proton therapy that a change in tumour volume and position mid-treatment can affect treatment delivery. Changes in the entry path of the beam may mean that the beam passes through tissues of different density and this would be expected to affect dose deposition due to change of the spread-out Bragg peak (SOBP) relative to the tumour volume. This makes treatment planning for proton therapy more challenging than that of photon therapy. Imprecise treatment planning or delivery could results in volumes outside the target receiving higher doses than they should,

possibly causing normal tissues complications, or in the tumour may receiving a lower than intended dose.

In clinical practice an RBE of 1.1 is used when planning proton therapy. The 1.1 value is thought to be the best uniform estimate of the difference between photon and proton therapy dose and it is what has been used in practice for years (ICRU, 2007). Although there is no direct clinical data to show that the using the value of 1.1 is not correct, concerns that use of this approximate value of RBE could lead to over- and/or under-dosing of organs have been raised (Paganetti *et al*, 2002, Paganetti, 2014, Jones B, 2014, Sethi *et al*, 2014). The variations in RBE were recognised early on as in vitro experiments showed that RBE can vary, as a function of dose, the biological endpoint studied, and radiation quality. In the case of proton therapy, the value of RBE varies in relation to the position of the SOBP. RBE could be ~1.1 in the proximal (entrance) region, ~1.15 in the centre, and ~1.35 at the distal end (Paganetti H, 2014, Cuaron *et al*, 2016). However these values are likely to depend on the incident energy and the size of SOBP (as this will affect the spectrum of proton energies at a given point). These variations, and particularly the increase in RBE toward the distal end of the proton beam, may have important clinical implications.

Knowledge of proton therapy implies that using a fixed RBE of 1.1 for all proton beams and dose ranges may lead to overdose of normal tissues near the distal edge of the target volume. This difference in dose may pose an increased risk of toxicity, and normal tissue complication probability (Jones B, 2014, Sethi *et al*, 2014). In case of medulloblastoma for example, Jones *et al*

argues that the RBE of the brain and spine is higher than 1.1 and that the RBE of medulloblastoma cells is lower than 1.1, as the fast growing and highly radiosensitive medulloblastoma has a high α/β value, which is more likely to be associated with a lower RBE (Jones *at al*, 2011). This means that the brain and spine may receive a higher than intended dose, while the tumour would receive a lower dose than planned. This would potentially result in higher toxicity and lower tumour control and higher chance of recurrence, especially for standard risk who are generally prescribed lower doses.

When dose maps for photon and proton therapy are compared, proton therapy plans may appear superior, as proton therapy has the potential to achieve enhanced dose conformity to structures of interest, when compared with conventional photon therapy (Figure 4). However, the outcomes are not always in favour of proton therapy. Timlin *et al* demonstrated that MIP can be higher when using proton therapy compared to photon therapy. This depends on the position of the tumour, arrangement of treatment beams, and the MIP model implemented (Timlin *et al*, 2011). The treatment technique, passive scattering or active scanning, also plays a role since these two different techniques generate neutrons in varying amounts and energies. Neutrons can produce high-LET damage, which may affect MIP and secondary cancer risk (Ullrich *et al*, 1977, Ullrich RL, 1983, Wolf *et al*, 2000).

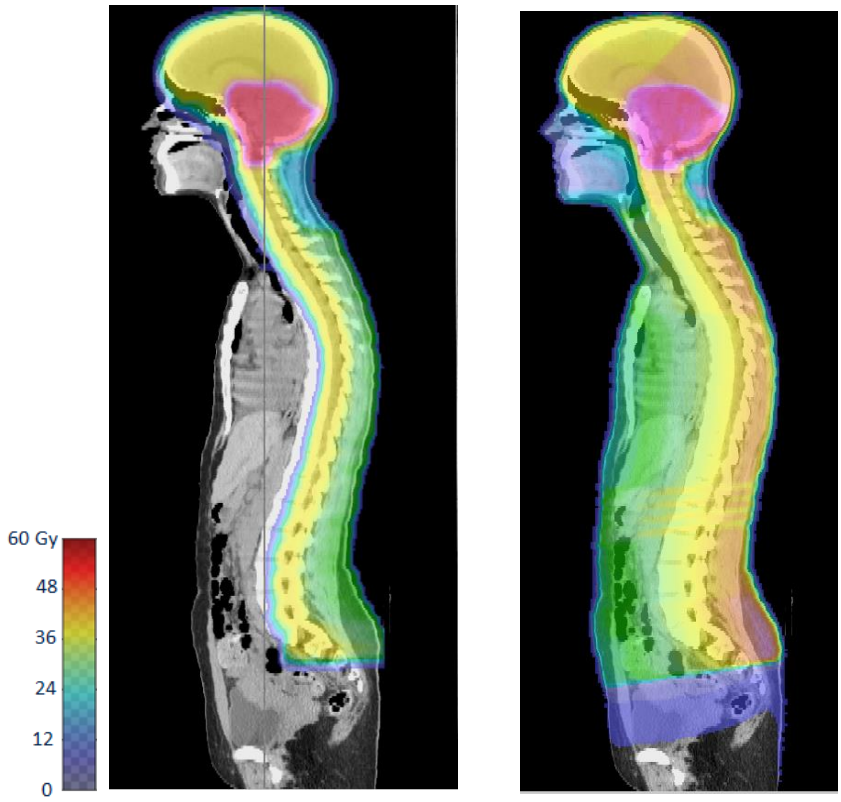


Figure 4: Dose map (sagittal section) of a female adult patient (Patient 1) with medulloblastoma. The left panel is from the proton treatment. When compared with the right panel (3DCRT), the dose sparing effect of protons can be observed, especially with respect to the lungs, liver, heart, kidneys, and other organs, which receive no or very low dose.

1.8 Proton beam delivery

If the cost of proton beam delivery was equal to that of the photon therapy, there would likely be a shift towards proton therapy facilities as superior treatment plans can be achieved. But as the cost of a proton treatment facility is currently approximately at 130 million USD compared to 3 million USD for a Linac machine, and the construction cost of a current two-gantry proton facility, complete with the equipment, was estimated to be about 4 times the cost of a two-linac X-ray facility (Goitein and Jermann, 2003) and with the logistics needed to deliver a proton therapy, a global move towards proton

therapy is far from being a reality. While more centres are acquiring proton therapy facilities, photon therapy is likely to remain a pivotal part of radiotherapy practice, and most likely the principle modality of treatment for the foreseeable future.

1.8.1 Proton beam

For proton delivery, protons are accelerated in a cyclotron or a synchrotron that is located in a dedicated facility next to the treatment rooms. The protons are fired through the relevant machinery and, depending on the type of the facility, is delivered to the patient who is on a special treatment bed in an adjacent treatment room.

Proton therapy beams can be categorised into two main types: passively scattered and actively scanned. Passively scattered consists of a single beam of protons that pass through modulators and compensators to deliver the desired dose to the tumour (Figure 5). The use of compensators and modulators leads to the generation of neutrons, which some consider can adversely affect treatment (Hall, E, 2006, Brenner *et al*, 2009). However, with current designs, it is thought that neutrons do not reach such high levels (Gottschalk B, 2006, Paganetti *et al*, 2006, Brenner and Hall, 2008).

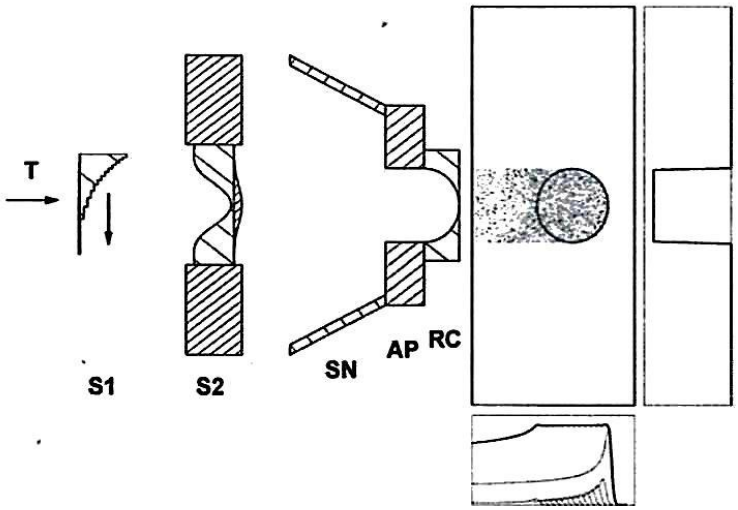


Figure 5: Schematic presentation of components in passively scattered proton system. T being the kinetic energy of the beam line, S1 is the range modulator and first scatterer, S2 is the second scatterer, while SN is the beam line snout which shields scattering protons, AP and RC are the patient-specific apertures and range compensator, respectively (Reprinted from DeLaney and Kooy, 2008 with permission from Wolters Kluwer Health).

The actively scanned proton therapy delivers a more precise and quicker treatment (Smith *et al*, 2009). The beam is delivered from a nozzle of a moving gantry that rotates around the treatment couch, while magnets deflect and steer the proton beams. Actively scanned proton therapy is thought to have lower neutron dose component than passively scattered. The most advanced techniques scan the tumour via a pencil beam, delivering treatment one volume unit at a time and moving across the tumour in slices to do so.

1.8.2 Spread-out Bragg Peak

Dose uniformity across the tumour volumes can be achieved by varying the energy of the proton beam (using a range modulator) to produce a SOBP, which is a series of Bragg peaks at different depths within the tumour, summing to give a uniform dose across its volume (Figure 6). Turning the

gantry to deliver beams from a number of different angles also aids optimisation of treatment delivery.

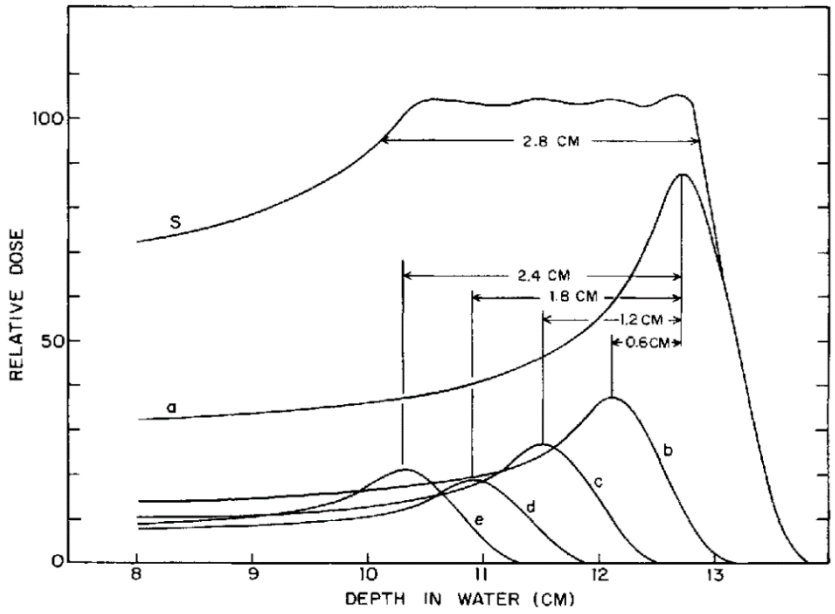


Figure 6: Spread-out Bragg peak (SOBP) covering a tumour of 2.8 cm in depth, using 5 different Bragg peaks (Reprinted from Koehler AM, Preston WM, 1972 with permission from Radiological Society of North America).

Wouters *et al* (Figure 7) illustrated the change in LET and RBE along the particle path, which implies a change of calculated dose (Wouters *et al*, 1996). Although this might carry significant ramifications for treatment planning, Gerweck *et al* (Figure 8) showed that an RBE value of 1.1 is an acceptable estimate of the mean RBE value for the middle of a typical spread-out region of the Bragg peak and for tissues with high α/β (Gerweck *et al*, 1999). For the distal end and for tissues with low α/β the RBE of 1.1 might not be the best estimate and this reinforces the need for accurate RBE estimation becomes vital, i.e. for normal tissues and exit dose areas/distal end of the Bragg peak.

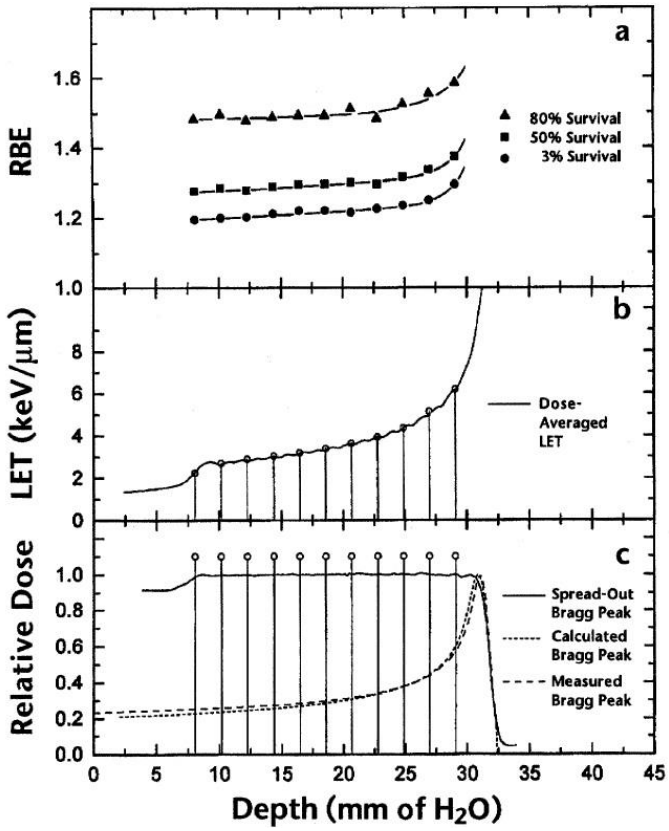


Figure 7: Panel a: RBE as a function of depth within the SOBP. Points plotted are RBE values determined from fits to survival data at different depths. The sharp rise at the end of the peak may be of concern when the treatment volume is near sensitive structures. Panel b shows the dose-averaged linear energy transfer (LET_d) determined from the weighted sum of range-shifted Monte Carlo-modelled raw Bragg peaks. Panel c shows the physical dose profile of the SOBP, along with the measured and Monte Carlo-calculated raw Bragg peaks (From Wouters *et al*, 1996) © 2018 Radiation Research Society. An RBE of 1.1 which used clinically is thought to be a reasonable estimate of the average RBE in the plateau region of the SOPB.

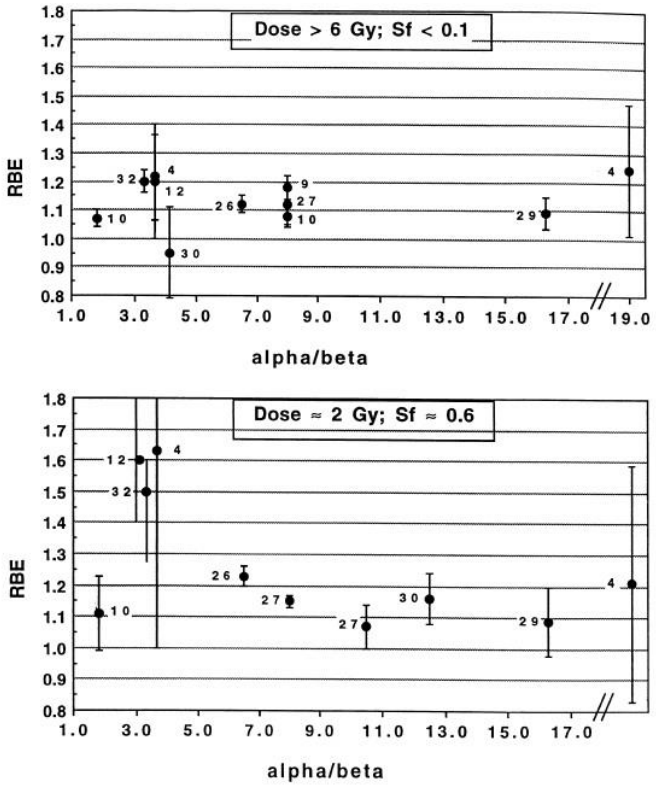


Figure 8: RBE values are plotted as a function of the estimated α/β values for the target cells or tissues. Confidence intervals are as stated in the source manuscript or interpolated from the information provided and represent one standard deviation or the 95% confidence interval. The mean RBE for all positions in the SOBP are shown. All other data pertain to the mid-SOBP protons. Numbers adjacent to data points are the source numbers as listed in the Gerweck *et al* original paper (1990) (Reprinted from Gerweck *et al*, 1999 with permission from Elsevier).

1.9 Scope of this work

To systematically study the difference between the radiation therapy modalities of photon and proton therapy, software that was developed in-house was extended and used, with parameters adopted and derived from the literature. This was done in order to compare the two treatment modalities and to take MIP modelling tools a step forward on the way to implementing them in future clinical practice. The hypothesis tested was that

even taking into account the uncertainties in the models used, parameters, how dose is incorporated into the models, and for proton therapy, RBE, in medulloblastoma 3DCRT treatment plans will have a higher probability of inducing malignancy or causing secondary cancer than proton plans. This work should also allow illustration of the effect of those uncertainties on MIP and $MIP_{Relative}$ and permit for a better understanding of how other clinical scenarios could possibly react when modelling is carried out.

The central questions that this work will be seeking to address include:

- What is the relative relation between MIP of photon and proton therapy for medulloblastoma?
- Does uncertainty in the radiobiological parameters used in the models affect the relative relationship between photon and proton therapy for medulloblastoma?
- How can MIP be calibrated and benchmarked against published data?
- Are the models and parameters, after calibration, able to predict the risk of secondary malignancy in agreement with existing literature?
- How does using mean dose versus voxel-by-voxel dose maps affect MIP calculations?
- How does the variation in RBE affect dose and MIP modelling results and how big is the difference in dose and MIP when using models for calculating RBE versus the standard RBE of 1.1?

2 Chapter 2: Theory

2.1 Modelling Malignant Induction Probability

In addition to cell killing, radiotherapy may also give rise to premalignant initiated cells (premalignant, tumour initiating cells) when DNA damage is misrepaired in those that survive, which can lead to genetic mutations. Part of this damage can contribute to malignancy over time, for example, if tumour suppressor genes were disrupted (Vineis *et al*, 2010). The process of transformation of a normal cell into a malignant one is complex. However, it has been widely accepted that the three main steps are initiation, promotion, and progression (Hennings *et al*, 1993, Vincent L, and Gatenby, R A, 2008). Initiation generally happens by a genetic mutation. Premalignant, tumour-initiating cells will not transform into tumour cells directly, but can gain some survival advantages when subsequently exposed to promoting risk factors. These cells may then progress into malignant ones, showing the core essentials of malignant growth, known as the hallmarks of cancer (Hanahan D and Weinberg R. A., 2000, Hanahan D and Weinberg R. A., 2011). Radiation can contribute to the initiation step, and hence, an assumption is made that secondary cancer risk calculation can be correlated with the initiation step, and that probability of secondary cancer will vary in a linear fashion with the number of initiated cells in the patient (Little *et al*, 2007, Sachs R K, and Brenner, D J, 2005).

As stated in Timlin et al, the constant of proportionality will be "a nontrivial function of many parameters such as patient age and general state of health, as well as exposure to environmental promoting factors, but is assumed to be

independent of any properties of the radiotherapy treatment" (Timlin *et al*, 2015). Clinical cases used in this work will compare plans for the same patient, and by doing so, separating the induction from promotion and progression (Schneider U, 2011), as comparing different patients may mean comparing cells at different stages of the transformation process, hence ensuring that any calculated differences in MIP relates to differences in the planned dose distributions and not variability between patients.

Although there is an established relationship between dose and cancer incidence in the dose range from ~ 0.05 Gy to 2.5 Gy (Hall E J, 2004), there is much debate about whether this dose-response relationship can be extended to predict secondary cancer following exposure to doses typically used in radiotherapy, especially as they are usually delivered over multiple fractions. Although some models have been suggested to describe the risk of various secondary cancers, the existing published literature provides insufficient statistical power to allow formulation of a dose-response curve in a robust manner (Timlin *et al*, 2015). Some evidence suggests that for thyroid, for example, a downturn in secondary thyroid cancer risk (Bhatti *et al*, 2010), while other suggest a linear relationship, as discussed earlier (see 1.3).

2.1.1 Models and Dose-response Curves

MATLAB code that was developed in-house (Timlin *et al*, 2015) was utilised to calculate MIP using a high-resolution dose matrix based on voxel-by-voxel data from radiotherapy treatment DICOM files. Three different models were used to calculate the MIP.

As there is no universal agreement on a model that best predicts malignant induction, a range of radiobiological models, possibly representing different mechanisms that lead to induction of malignancy, have been tested. The models used are the linear-quadratic malignant induction model (LQ), the linear malignant induction model (LIN), and the linear-no-threshold malignant induction model (LNT). Both the LQ and LIN models incorporate a reduction in induction at high doses due to cell killing, the LNT model does not.

For this thesis, MIP is calculated in a voxel-by-voxel fashion (VbV). Each voxel is assigned to a single organ or structure with an associated priority-based hierarchy (see 3.1.4). Each organ is assigned a cellular density per volume unit, which was set in this project to be uniform for all structures. The programme calculates the probability of a cell being "initiated". An initiated cell has the potential to transform into a malignant in the future should it undergo further progression. The MATLAB code integrates the MIP calculated on a voxel-by-voxel basis and generates an absolute MIP for each structure, and the MIP for the patient as a whole (whole body MIP). MIPs for individual patients, derived using the three models, are compared in order to assess the differences, if any, between the models.

2.1.2 MIP models used

2.1.2.1 The linear-quadratic malignant induction model (LQ):

It is widely accepted that the linear-quadratic model of tumour response to radiation is representative of the biological response of many cell lines to radiation (Roesch WC, 1978, Dale RG, 1985, Fowler JF, 1989). The model

applies to many cell lines for in vitro experiments and has also been widely applied to clinical data (Deacon *et al*, 1984, Webb *et al*, 1993). It is expressed by the formula:

$$SF = e^{-n(\alpha d+\beta d^2)} \quad (1)$$

Where SF is the surviving fraction of cells given dose per fraction (d) for (n) fractions. While α and β, also known as radiosensitivity parameters, describe the linear and quadratic component of the curve, respectively, and are dependent on tissue type. From this equation, a model was derived in which SF is included in the dose-response part for MIP in the following equation:

$$MIP_{LQ} = n(\gamma d + \delta d^2) e^{-n(\alpha d+\beta d^2)} \quad (2)$$

where γ and δ are the malignant induction coefficients. To reduce the number of free parameters, it is assumed that the ratio γ/δ is the same as α/β, arguing that the DNA damage and repair processes governing cell death or malignant induction are similar (UNSCEAR 1993, UNSCEAR 2000, Daşu *et al*, 2005, Timlin *et al*, 2015).

2.1.2.2 The linear malignant induction model (LIN):

This model is based in essence on the linear quadratic model, but instead of factoring in γ and δ, SF is multiplied by a single linear coefficient, λ, thus:

$$MIP_{LIN} = \lambda D e^{-n(\alpha d+\beta d^2)} \quad (3)$$

Where D is the total dose (nd), and d is the dose per fraction, and n is the number of fractions (ICRP, 2005). This model is called linear, as the dose-response relationship between dose and malignant induction is linear, but it is affected by the linear-quadratic nature of the surviving fraction component of the model.

2.1.2.3 Linear-no-threshold malignant induction model (LNT):

LNT model is usually used for low dose and low dose-rate malignant induction and risk predictions in the general population and in the occupational risk management setting, extrapolating the known risks at high doses to low doses related to typical human exposure.

In the linear-no-threshold model (LNT) it is assumed that there is no lower limit for induction of malignancy, regardless of how small the dose received by a tissue or organ. This means that there is a theoretical risk of developing cancer later in life as a result of low radiation dose exposure. Importantly, in this thesis, it was assumed that linear response also extends to high doses (i.e. the radiotherapy dose range) assuming no effect due to cell kill. According to this model, MIP can be calculated by using the following equation:

$$MIP_{LNT} = \lambda D \qquad (4)$$

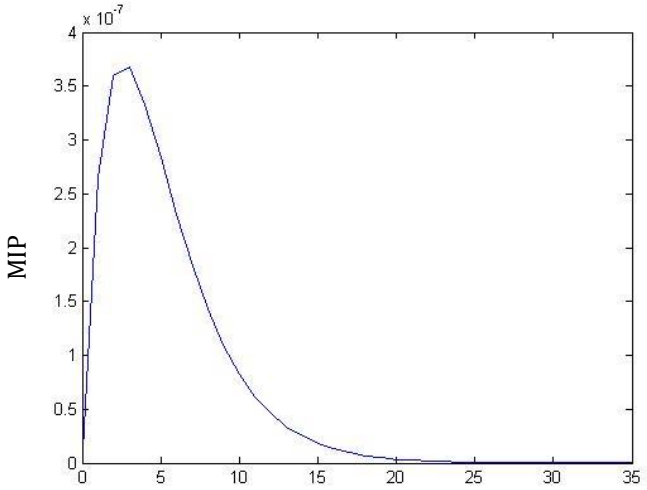
where λ is the linear coefficient and D is the total dose (BEIR VII Report, 2006).

2.1.3 Dose-response curves for MIP models

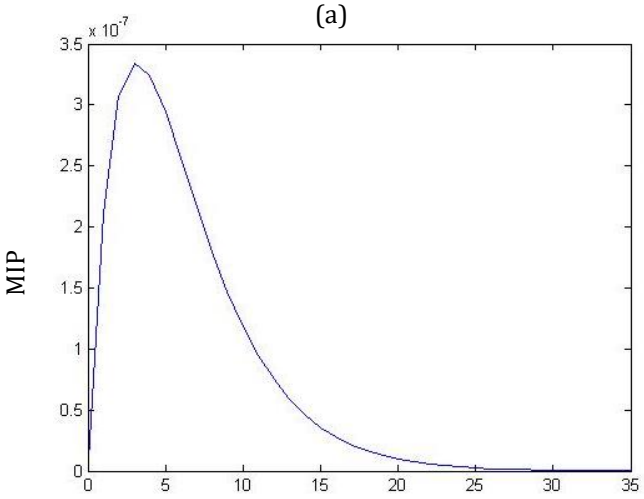
Visualisation of dose-response curves of the MIP models allows better understanding of the results to be obtained, and makes it easier to compare outcomes of modelling with what those models are expected to produce. Although the visualisation is made using an exemplary 'standard' single normal tissue as an example, the dose-response curve gives a relatively comprehensive over-view, of the behaviour of the models. Such a view allows an appreciation of what the outcome could be at different dose points for a certain organ or structure. This helps in the analysis and discussion of results and conclusions (Sachs and Brenner, 2005).

Figure 9 illustrates MIP after a single exposure for an exemplar model tissue. The effect of cell-kill and the incorporation of SF can be seen in Figure 9.a and 9.b. The difference in MIP between LIN and LQ is also evident. LNT, being a linear model, does not show a decline in risk after an exposure of 3-4 Gy, as the model does not include a cell-kill term. The dose-response curve for fractionated treatments (1.8 Gy/fraction) is similar in shape to that for single exposure (Figure 10), but the turn-over point and MIP values are different, and in the case of the LNT model, it is more clinically realistic, as a single exposure of a few Gy to the whole body can be lethal. The turn-over point illustrates an idea that links survival fraction and malignant induction, and may be of value when studying MIP and secondary cancer risk of IMRT plans for example, where large volumes receive low dose (Weber *et al*, 2004, Steneker *et al*, 2006, Diallo *et al*, 2009, Moskowitz *et al*, 2014, Moteabbed *et al*, 2014). The turn-over point is a manifestation of the sub-lethal damage in cells changing into lethal damage and causing subsequent cell death. This is a potential explanation of the observation

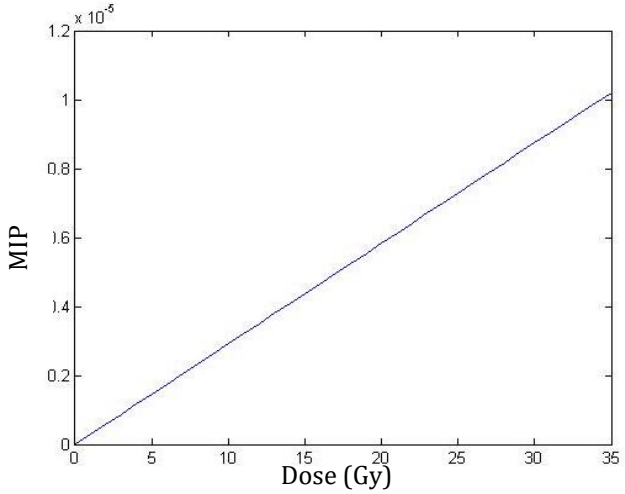
in some studies that the risk of secondary lung cancer is less than expected, an observation that could be explained by the that some of the sub-lethal damage progresses to lethal cell injury that causes cell death, which could decrease MIP and secondary cancer risk (Inskip *et al*, 1994, Little MP, 2001, Roncekrs *et al*, 2006).



(a)

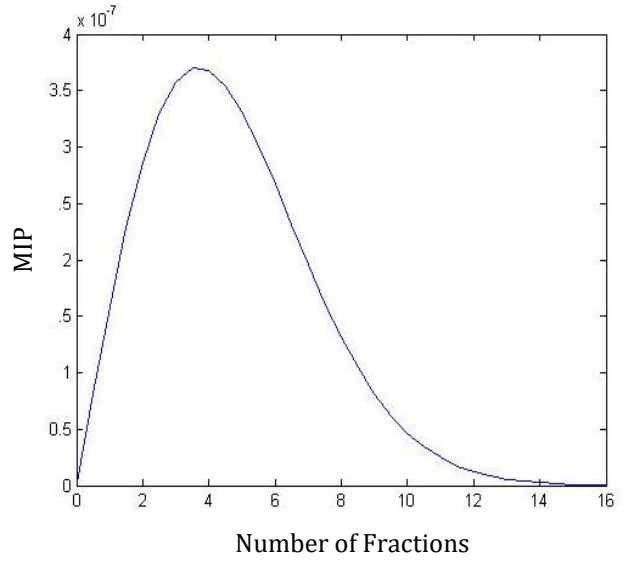


(b)

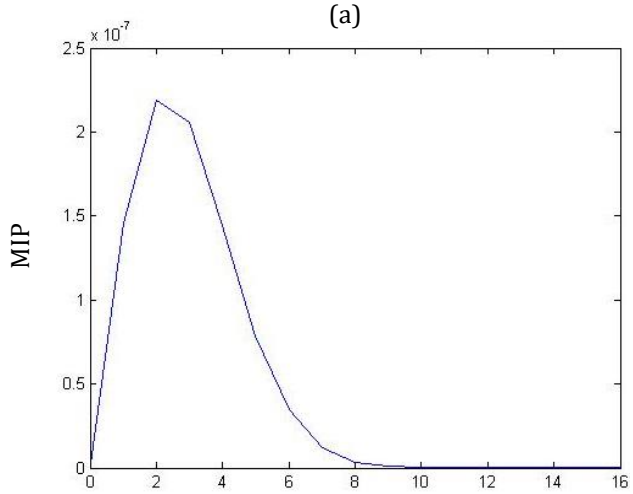


(c)

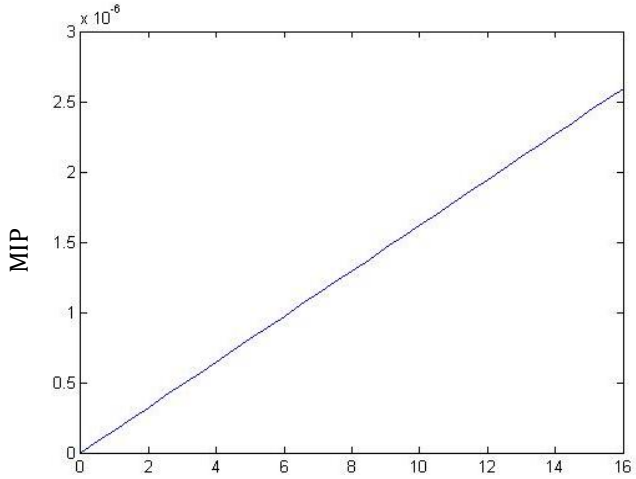
Figure 9: Dose-response curves for the LQ (a), LIN (b) and LNT (c) models for single exposure. Notice that the MIP axis is scaled differently for each of the models. (Parameters used α=0.16, β=0.09, γ=1.62x10^{-7}, δ=3x10^{-8}, λ=1.62x10-^{7}).



(a)



(b)



(c)

Figure 10: Dose-response curves for the LQ (a), LIN (b) and LNT (c) models for fractionated radiation exposures of 1.8 Gy per fraction. Notice that the MIP axis is scaled differently for each of the models. (Parameters used α=0.16, β=0.09, γ=1.62x10^{-7}, δ=3x10^{-8}, λ=1.62x10^{-7}).

2.2 Testing the sensitivity of MIP models towards the uncertainty of parameters

In modelling studies, there is always some uncertainty in the input parameter values. This uncertainty results from the method used to estimate the parameters, the endpoints they are intended to be associated with, and differences in tissues and experimental conditions, among a range of factors. Simulations were performed to calculate how those uncertainties affect the results, especially Relative MIP. This should help establish the degree of difference in predicted outcome with the uncertainties included in the simulations (see section 3.1.4 for how the parameters were selected).

2.2.1 Sensitivity testing over pre-set parameter space

Simulations were performed to investigate the magnitude of the differences in predicted outcomes that result from uncertainties in the input parameter. This was done by performing simulations using a range of values for each parameter. In the first set of experiments one parameter at a time was changed and then, in another set of experiments (2.2.2), all parameters were altered simultaneously. These simulations were performed to assess if the pattern of relative MIP values would change with variation in parameter values, and to understand the effect of this uncertainty on the results (see 3.2.1 for details).

2.2.2 Parameters sensitivity testing using randomly-generated parameter modifiers values

The experiment described in the previous section (2.2.1) was used to investigate the effect of varying a single parameter at a time by a pre-set

value, to assess sensitivity towards the uncertainty and to observe the behaviour of MIP under specific conditions. This was done to elucidate the importance of each parameter in the three MIP models. Next, a set of simulations was performed to investigate the effect of varying all parameters of a selected model simultaneously using randomly generated parameters-modifying factors. The purpose of this set is of simulations was to reflect a more realistic situation, because there is inherent uncertainty in all parameters to varying degrees (see 3.2.2 for details).

2.3 Benchmarking and calibration with BEIR VII report

The aim of the work described in this section and detailed later (3.3) was to bridge MIP output with published risk estimates. To start with, the risk for a single uniform exposure of 0.1 Gy was modelled and the resulting EAR and LAR were compared to data published in the BEIR VII report. The next step was to calibrate the model parameters so the 0.1 Gy exposure would produce results that matched the BEIR VII report results as closely as possible. The models and the calibrated parameters were then tested by modelling the risk for various doses against other data points for internal validation. Once these calibration and benchmarking tests were completed, modelling EAR and LAR for radiotherapy plans was performed. In order for this to be carried out, the first step was to introduce the mathematical terms needed to produce EAR and LAR values, rather than simply giving MIP. The derivation of the equations, origin of parameters and models are detailed in the methods chapter3.3.1).

3 Chapter 3: Methods and materials

3.1 Modelling MIP after proton and photon therapy

MATLAB is a high-level language and interactive environment for numerical computation, visualisation, and programming. Using MATLAB, users can analyse data, develop algorithms, and create models and applications (The Mathworks, Inc., 2012). A tool based on the Computational Environment for Radiotherapy Research (CERR) package (Deasy *et al*, 2003) was developed by Dr Claire Timlin in 2011 to model MIP for radiotherapy plans of patients with meningioma (Timlin *et al*, 2011). The code reads the DICOM radiotherapy treatment plans, accesses the required matrices (structures, dose maps and other features.), uses the three models, LQ, LIN, and LNT, to calculate the MIP for each organ and for the whole body, and produces detailed files with dose indices and MIP values. This code has been developed and extended as needed for this project to carry out the modelling tasks. The way the code works, as well as the significant modifications that were carried out before and during using the code for modelling, are described below.

3.1.1 Treatment plans details

A total of twenty-four radiation therapy plans for twelve different patients were utilised in this thesis. The plans were provided by collaborators from The Mayo Clinic (Rochester, MN, USA), The Haukeland University Hospital (Bergen, Norway), and Rigshospitalet (Copenhagen, Denmark) (summary of plans: Appendix 3).

In the case of the two patients from the Mayo Clinic (Patient 1 and Patient 2), the prescribed dose was 20 fractions (1.8 Gy/fraction) to the whole brain and spine (CSI) plus 11 fractions (totalling 19.8 Gy) as a boost to the posterior fossa. This gives a total dose of 36.0 Gy to the cranium and spine, and 55.8 Gy to the posterior fossa. The dose prescribed for all 10 remaining patients, was 23.4 Gy in 13 fractions (1.8 Gy/fraction) for CSI. No boost was included in this study for those plans. To confirm that not including boost data would have no significant effect on MIP calculation, the MIP was compared for plans with boost and without, and the difference was found to be negligible (Appendix 4). As the focus in this thesis was the *intra*-patient comparison of photon versus proton therapy, an assessment was made that the presence or absence of boost for a small subset of the patients was unlikely to have a significant impact on the outcome or overall conclusions.

The prescribed dose of the actively scanned proton therapy prescription was the same as the photon therapy one. All three institutions used an RBE of 1.1 for actively scanned protons.

The photon therapy and the proton therapy plans were generated using The Varian Eclipse planning systems (Varian Medical Systems, Palo Alto, CA, USA).

The plans were received in DICOM format. They were then processed using CERR. The processed plans were saved in a format compatible with the MATLAB code. Further processing was done using in-house built functions to interpolate the dose matrix of the radiotherapy plan on the same axes and

coordinates as that of the CT scan. After this step was completed, the MIP for a given treatment plan was modelled.

The code run-time on the local terminal computer was about 17 minutes on average using 16-GB RAM. After the modelling was completed, the files were saved in a designated output path. MIP was then plotted and analysed.
The cases were ordered and modelled in the order they were received in, by institution, to minimise any observational bias in regards of trends of MIP with age, for example.

3.1.2 Preparation of plans for MIP modelling

Radiotherapy treatment plans were provided by collaborators at The Mayo Clinic (Rochester, Minnesota, USA), The Haukeland University Hospital (Bergen, Norway), and Rigshospitalet (Copenhagen, Denmark). The files were downloaded and the data for each patient were placed in a separate folder. The plans were then imported using the import function built into CERR. CERR recognises the DICOM files and scans over the image files (the CT images), the structure files, and the dose files. All files relevant to those file classes are then merged into one MATLAB-compatible file (*.mat). The file is then further processed using a pre-process function, built in-house, with the main task of matching the coordinates of the CT images and the coordinates of the dose matrix so that each voxel is assigned both a CT value (HU) and a dose value. When the pre-process function is run, it asks the user to choose the modality for the plan, photon or proton. The case labelling with photon or proton is important for the simulation and MIP modelling, as the MIP code

takes RBE into account, based on the modality selected during the pre-processing step. The MIP modelling code applies a uniform RBE value of 1.1 for protons. Once the pre-processing is complete, the plan file is ready to be used for MIP modelling.

3.1.3 Step-wise analysis of the MATLAB code

Dr Claire Timlin made some changes that enables the code to handle the medulloblastoma radiotherapy plans. Those changes were carried out in discussion with, and in the presence of the author of this thesis.

The code runs in the following steps:

1-Reading the modelling job file. This includes the directory of the folder for the treatment plan(s) to be studied, the directory for the input radiobiological parameters, the MIP model to be used, and the number of fractions.

2-The interpolated dose matrix is accessed. The interpolated dose matrix is the dose matrix matched on the same coordinates (and resolution) as the CT scan matrix.

3-The structures, the structure arrays variables and voxel coordinates are read.

4-The modality parameters are then set, which includes the type of radiation (photon or proton), the input radiobiological parameters.

6-MIP model parameters arrays are created.

7-For analysis of the sensitivity of models to changes in model parameters, the input parameters are either spread out uniformly, or randomly perturbed depending on the aim of the simulation.

8- Three-dimensional structure matrices are labelled so each voxel is identified and prioritised so that each voxel is labelled as only belonging to the most radiobiologically relevant structure.

9-The voxel size is determined.

10- MIP, SF and the number of transformed/initiated cells per voxel are calculated.

11-The calculations are integrated over the volumes of the structures studied and the results, including dose indices (maximum, minimum, mean and median dose), and MIP, are generated and saved.

3.1.4 Parameters and parameters assignment

A range of organ-specific radiobiological parameters (α, β, γ, δ, and λ) were assigned before calculations were performed. Where possible, values were taken directly from published sources. Where no suitable published value could be found, values were assigned based on anatomical or structural considerations. For example, when a value for a structure with similar physiological or histological characteristics is quoted in the literature, this was used as a reasonable surrogate (Appendix Table 1). Most of the references researched provide values for α/β ratios for normal tissues and individual α and β values for tumour cell lines. Individual α and β values for

some normal tissues are not as readily available from the published literature as they generally are for tumour cell lines. In order to overcome this obstacle, α values were derived from the published α/β ratios using an assumed constant β value of 0.03 Gy^{-2} (Timlin *et al*, 2011, Timlin *et al*, 2015)(Appendix Table 1). As there are no data available on values for γ and δ, an estimate of these parameters was required. The cell kill mechanism and the mechanism of cell transformation were assumed to be similar in the processes they are governed by, and based on that assumption, γ/δ ratios were assumed to be the same as α/β ratios. The constant of scaling between α and γ was taken as $\alpha/\gamma = 10^6$ (Timlin *et al*, 2015).

For the MATLAB code to perform the calculations on a VbV basis, each voxel must be identified as being assigned to a single organ or structure. However, a voxel may be a part of more than one structure. To overcome this problem, the complete list of structures was rank-ordered so that any voxel labelled as belonging to more than a single structure was dealt with in accordance with the priority list, which was based on the relative importance of structures to MIP calculation. So, when the programme encounters a voxel that is labelled as involving two different structures for example, it checks the priority list and assigns this voxel to be a part of the organ with the highest priority, with "1" being the highest (Appendix 2). The highest priorities were given to normal tissues and organs, while lowest priorities were given to tumour volumes and planning-related volumes.

3.2 Sensitivity of MIP models to uncertainty in parameters

A system for modelling MIP using a modified version of the MATLAB code was utilised to test the sensitivity of models to the uncertainty of parameters. The system designed by Dr J Loken enables the user to choose the parameter they wish to vary. This system provides the option of either varying the parameter(s) using pre-assigned multiplication factors (0.2, 0.4, 0.6, 0.8, 1, 2, 4, 6, 8 and 10) or of using a randomly generated modifying factors sampled from a Gaussian distribution. The sensitivity testing was only done on two patients (4 plans: Patient 1 and Patient 2- see 3.2.1, 3.2.2 – results in 4.2.1 and 4.2.2) as it is extremely computer-intensive to be done for the entire 24 plans used in this thesis, as it would have taken nearly 10,240 hours (~430 days) of non-stop computational time, to carry those set of tests. Data related to section 3.2.2 presented in this thesis (see results section 4.2.2), which is the result of 4,800 runs took ~1,600 hours to compute.

3.2.1 Sensitivity testing over pre-set parameter modifier space

The first step in the sensitivity testing process was to run the simulations to model MIP while changing only one parameter at a time for each radiotherapy plan used in this section, using the pre-assigned values mentioned above.

The system was set up on a computer cluster within the Oxford University network (Department of Physics), and an access system was installed on a local terminal. The plans and the associated parameter files were uploaded into the system and appropriately labelled to avoid confusion, and reduce human error.

Cygwin interface (Cygnus Solutions, California, and United States) was used for access and operation of the system and the system directory. The system asks which action is needed. Examples include “new runs”, “back up”, “delete runs” and so on. The plan is then selected, followed by the associated parameter file. The simulation mode is then chosen: that is either variation over a pre-set parameter space or a randomly generated space. The parameter(s) to be varied are then selected. For the first sets of experiments, the selected number of runs was 10. The simulations were performed and the results placed in output files in the designated output directory file. Once simulations were complete, the results database was accessed and results of interest identified, extracted, tabulated, matched, plotted and analysed.

The absolute MIP for each pair of plans (3DCRT and proton) derived from each of the three models was plotted and the $MIP_{Relative}$ was plotted as well. This was done for all the parameters for all four of the radiotherapy plans for both Mayo Clinic patients (Patients1 and 2).

A total of 320 simulations were performed to generate the data used in the subsequent analyses. The total run time for this experiment was about 105 hours. The sensitivity testing for the adult patient (Patient 1) in this section, is a repeat of similar work carried out in the MSc dissertation submitted in 2012 (Madkhali A, 2012).

3.2.2 Sensitivity testing of parameters over randomly generated modifiers space

A Gaussian probability distribution function (PDF) was incorporated into the system mentioned earlier in the section by the system designer, Dr J Loken.

The system was operated using all four plans for Patient 1 and Patient 2, and all three models selected, while asking the system to vary the parameters simultaneously. The parameters modifying factors were generated using the PDF and a root-mean-square (RMS) of 0.25. RMS of 0.25 was selected as it showed it gave the most suitable range of modifiers not to overly skew results using LNT model, as higher values for modifying factors for λ would result in more MIP values trending towards 1, making the assessment of $MIP_{Relative}$ less meaningful. All parameters modifying factors were equal to or greater than 0, as input parameters values in the models can't be negative.

The system returned the results with an average run time of 20 minutes per run, and four hundred runs were performed for each plan and model combination, totalling 4,800 runs. The results of all these runtime for this experiment was about 1,600 hours. All these runs, for all patients, are unique for this DPhil. First, the parameters modifying factors were plotted as a histogram to visualise the distribution. The distribution and range of parameters are in shown in Table 1 and Figure 11.

	α	β	γ	δ	λ
Lower Limit	0.335	0.367	0.237	0.401	0.228
Upper Limit	1.709	1.829	1.842	1.716	1.722

Table 1: Range of modifying factors for the parameters α, β, γ, δ, and λ used.

For each one of the plans tested the absolute MIP values were plotted as frequency distributions. $MIP_{Relative}$ was plotted as well to demonstrate any changes in relative relation ($MIP_{Relative}$) between MIP_{Photon} and MIP_{Proton} if any (section 4.2.2).

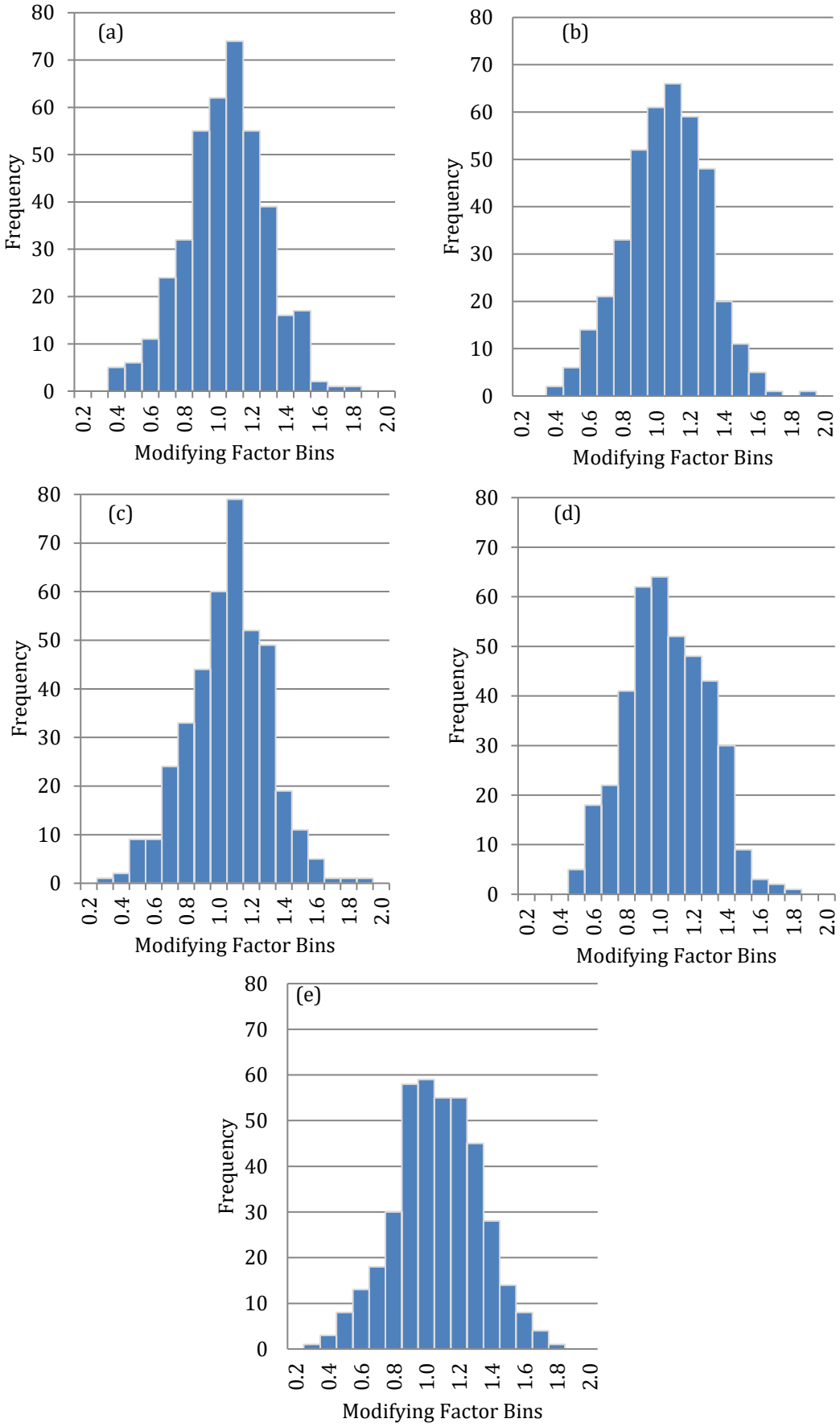


Figure 11: Frequency distribution of parameters modifying factors used in the sensitivity testing in this section: (a) α, (b) β, (c) γ, (d) δ, and (e) λ.

3.3 Calibration and benchmarking

3.3.1 Estimation of the Linear Coefficient value for the LNT model for calibration with the BEIR VII Report

One of the primary outputs of the patient-specific VbV calculation is induction of malignancy, the initial stages of cancer development. To translate the results of the models into clinically-applicable values, results were compared with data reported in the literature. These are typically expressed in terms of cancer incidence or mortality.

Brodin *et al* (Brodin *et al*, 2011) calculated the risk of developing secondary cancer after radiotherapy for medulloblastoma using the organ equivalent dose (Schneider *et al*, 2008). The excess absolute risk was calculated using the following model:

$$EAR = \boldsymbol{\beta}\, OED\, \mu \qquad (5)$$

Where **β** is the initial slope of the incidence curve (Schneider *et al*, 2008), OED is organ equivalent dose and μ is a population specific risk modification factor, which is a function of attained age (a), age at exposure (e) and sex (Schneider *et al*, 2008, Brodin *et al*, 2011):

$$\mu = \exp\left[\gamma_e(e-37) + \gamma_a \ln\left(\frac{a}{46}\right)\right].(1 \pm s)\ , +for\ females, -for\ males. \qquad (6)$$

Where γ_e and γ_a are constants related to the age at exposure and attained age, respectively, and were derived from fitting the original data (Schneider *et al*,

2008, Schneider and Walsh, 2008, Brodin *et al*, 2011). *a* and *e* are attained age and age at exposure respectively, and *s* is a sex-dependent variable.

To calibrate the outcome of the model, the output of the model is set as secondary cancer risk, a function of dose and secondary cancer risk parameters.

If it is assumed that secondary cancer risk (SCR) is linearly proportional to dose (for example, using the LNT model), it can be expressed as:

$$SCR\ \mu = EAR\ =\ \beta\ OED\ \mu \tag{7}$$

If it is assumed that SCR is proportional to the number of malignant cells (C_m), from Poisson statistics, the following can be obtained:

$$SCR\ \ =\ 1 - exp^{-C_m} \tag{8}$$

$$SCR \approx\ 1 - (1 - C_m) \approx\ C_m \tag{9}$$

the total number of malignant cells in a given organ can be expressed thus:

$$C_m\ =\ C_{org}\ P_m \tag{10}$$

where P_m is probability that a given cell is malignant and C_{org} is the number of cells per organ (cellular density (ρ) multiplied by the volume of the organ).The LNT model gives a probability of secondary cancer risk that is linearly related to dose and simply expressed as λD.

So, for a given structure, the total number of malignant cells is the sum over the voxel malignant cells (C_m):

$$C_m = C \cdot \lambda \sum_{i}^{N} D_i \tag{11}$$

Where C is cells per voxel, N is number of voxels in the organ studied, and D_i is dose at voxel i.

For calibration purposes, a uniform dose of 0.1 Gy over the whole patient was introduced. This dose was used for calibration, since cell killing is expected to be negligible at this level. Therefor for the organ studied:

$$D_i = D = 0.1\,Gy = OED \tag{12}$$

By now it can be seen that

$$SCR \approx C_m = N.C.\lambda.D \tag{13}$$

$$SCR\ \mu = \beta\ OED\ \mu \tag{14}$$

$$N.C.\lambda.D.\mu = \beta\ OED\ \mu \tag{15}$$

and for OED = D = 0.1 Gy

$$N.C.\lambda = \boldsymbol{\beta} \tag{16}$$

Hence:

$$\lambda = \frac{\boldsymbol{\beta}}{N \cdot C} \tag{17}$$

Introducing cell density ρ: cellular density (cells/cm^3) and defining C= ρ. Voxel Volume; N= Volume of the organ/Voxel Volume:

$$\lambda = \frac{\boldsymbol{\beta}}{\left(\frac{Volume}{Voxel\ Volume}\right).(\rho.Voxel\ Volume)} \tag{18}$$

$$\lambda = \frac{\boldsymbol{\beta}}{Volume \,.\, \rho} \tag{19}$$

And using the patient volume in cm^3 and a ρ of 10^8 cells/cm^3, and using a **β** value of 3.016 (Schneider and Walsh, 2008) the value of the linear coefficient can be calculated.

To further transform EAR into LAR, models from the BEIR VII Report and other published work (Kellerer et *al*, 2001, Arias E, 2014) that incorporate survival probability and cancer incidence, were used.

By using the λ value calculated using **β** and the number of cells assumed and the volume of the patient, EAR can be calculated by using SCR generated from the code and μ. The number generated can be then transformed into LAR by using:

$$LAR_{(D,e)} = \sum_{a=e+L}^{100} EAR_{(D,e,a)} \;\; S(a)/S(e) \tag{20}$$

Where the summation is from a=e+L to 100, where a is the attained age, and L is the risk-free period (5 years for solid cancers). S(a)/S(e) is the survival probability to age *a*, conditional on survival to age *e*.

As λ is volume-dependent in the derivation above, different patients may have different λ values. This also means that for patients of similar age, but who are of considerably different size, λ will differ and hence the LAR will also differ. But as will be explained in the calibration below (3.3.2 with results in 4.3.2), the value will be adjusted so the results would match LAR in the BEIR VII report, making the volume-dependency less of an issue.

The approach which was detailed earlier to initially estimate volume-based λ is used. The **β** (3.16) for Hodgkin's disease (Schneider and Walsh, 2008) was used, and by using the known volumes from the treatment plans, λ was estimated for each patient. The LNT model was selected, using λ, hence producing SCR.

The SCR produced was transformed into EAR by factoring in μ, and then into LAR by applying the survival function for the relevant age. The LAR is compared with the LAR values published in the BEIR VII Report (BEIR VII, Chapter 12, Table 12D).

λ was calibrated for each age point and the average of the mean and median calibration factors (as this value provided better matching results to BERI VII data) was used to re-calculate λ which was used for the additional EAR and LAR calculations.

3.3.2 Modelling and Calibration

To start with, to model SCR for 0.1 Gy the calculated λ derived from the adult patient volume (Patient 1) was used. The resulting SCR were then multiplied by the corresponding μ value (7.35), to calculate EAR. The EAR produced was then multiplied by S(a)/S(e), from e+5 until age attained of 100 years. The LAR produced was then compared with LAR in the BEIR VII Report. λ was calibrated based on the results attained and the modelling was done again, using the new values for λ. Modelling was done using the calibrated λ, while using the corresponding μ values for ages at exposure of 20, 30, 40, 50, 60, 70 and 80 years, assuming a constant volume for the adult patient. EAR and LAR were calculated and results are plotted for comparison. Calibration for LIN

model was done based on the assumption that SF was 1 at a low dose of radiation (0.1 Gy), and equating the linear coefficient of the LNT model with that of the LIN model.

For the LQ model, the assumption was made that at exposure of 0.1 Gy, effect on SF could be ignored and SF is made to be 1, so

$$\lambda d = \gamma\, d + \delta\, d^2 \tag{21}$$

By dividing by d

$$\lambda = \gamma + \delta\, d \tag{22}$$

At d = 0.1

$$\lambda = \gamma + 0.1\ \delta \tag{23}$$

With assuming $\alpha/\beta = \gamma/\ \delta$, as initially assumed for the model, and by replacing γ with δ (α/β),

$$\lambda = \delta\left(\frac{\alpha}{\beta}\right) + 0.1\ \delta \tag{24}$$

$$\lambda = \delta\left[\frac{\alpha}{\beta} + 0.1\right] \tag{25}$$

$$\delta = \frac{\lambda}{\left[\frac{\alpha}{\beta} + 0.1\right]} \tag{26}$$

γ and δ were then calculated based on the equations above. The results for a uniform single exposure to 0.1 Gy were plotted and analysed accordingly.

3.3.3 Validation

To validate the calibration results, a series of simulations was performed using the adult plan (Patient 1), with increasing total dose, delivered in a

uniform single exposure of 1, 2, 3, 4 and 6 Gy (Table 2). This exercise was carried out using the LQ, LIN and LNT models, using calibrated parameters. The results were compared with outcomes published in a paper published by Schneider and Walsh (Schneider and Walsh, 2008). The results were compared with the fit to the Hodgkin's disease cohorts in that paper. The authors plotted their results, which were generated using two different models (linear-exponential and plateau) for a range of doses and using different RBE values for the neutron component of 10, 35, 100 and dose-dependent. This validation was done against the data that it was calibrated against, which means that this step provides an internal validation rather than an external one.

Dose (Gy)	EAR
1	10.00
2	19.91
3	29.74
4	39.48
6	58.72

Table 2: EAR (per 10000 Person-Year, PY) for uniform single exposures at age of 37 years, and attained age of 46 years using LIN model. Numbers are compared with the plots in Figure 12.

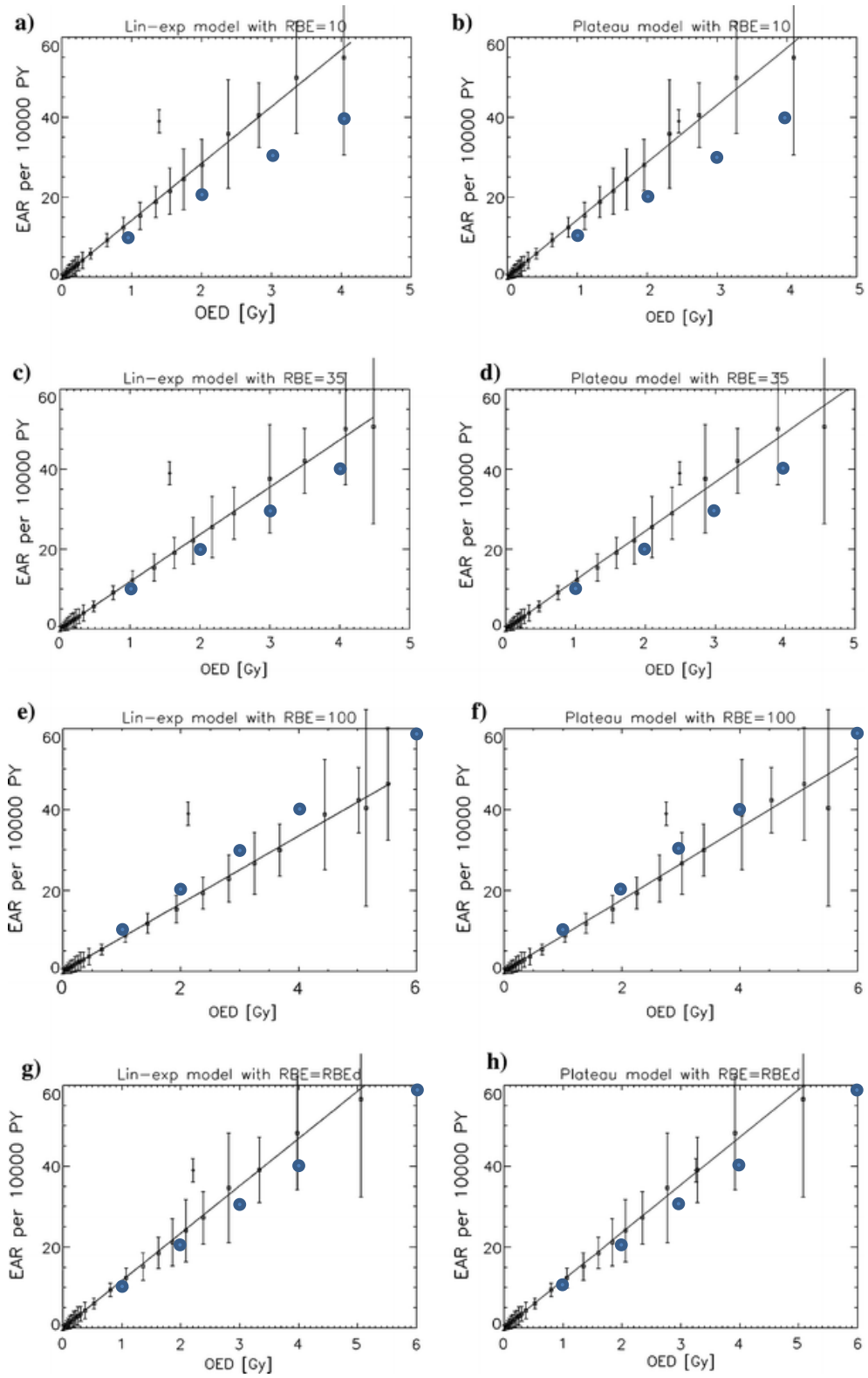


Figure 12: Plot (adapted from Schneider and Walsh, 2008) of cancer incidence per 10,000 persons per year as a function of organ equivalent dose (OED) of the atomic bomb survivors (as squares) and the Hodgkin's patients (as a diamond). a, c, e and g show the fit to the Hodgkin's patients using a linear-exponential model and b, d, f and h using a plateau-dose model. The data and fits are presented for four different neutron RBE models and for age at exposure of 37 years and attained age of 46 years. Blue dots are data points from Table 2.

3.4 The effect of spatial dose averaging on predicting malignant induction probability and secondary cancer risk

Dose delivered and dose heterogeneity are major uncertainties faced when studying secondary cancer risk estimates. Studies of historical cohorts typically have limited or no access to high-resolution dose maps and use DVHs or mean dose estimates from treatment records or reconstructed treatment plans to calculate risk. Some reports, such as BEIR VII, recommend using mean dose; since the majority of the historical data used to build and validate their models provide little or no detail about the spatial dose distribution. The shift towards CT-based planning systems in the 1990s and the ever-increasing computing capacity of radiation oncology departments, makes the use of high resolution dose maps feasible as the next step in the field of secondary cancer risk predictions. The use of high-resolution dose maps is made even more desirable by the need for verification and validation of dose-response curves, models, and parameters.

The MATLAB code used in this work was modified by Dr C Timlin so that it uses the mean dose to calculate MIP rather than using VbV dose maps in the MATLAB-compatible radiotherapy plan file. This was done by modifying the code lines so mean dose is calculated for each organ and then used as the single dose value over all voxels that constitute the organ/structure in question.

MIP was modelled for treatment plans using the LQ and LIN models utilising mean dose, and VbV dose maps. The whole body MIPs are compared and organ-specific results are analysed. Using the LNT model would produce

identical results, and so it was not included in this part of the analysis. This set of simulations was performed to demonstrate the extent of the differences in MIP values when modelled using two different methods to incorporate dose into the models. It was hypothesised that high-resolution maps would offer a more precise approach to calculating MIP, as using mean dose would most likely skew the results, and potentially dampens differences in MIP between photon and proton therapy, as using mean dose would probably increase MIP for both modalities disproportionately, and make their $MIP_{Relative}$ closer to 1.

3.5 Effect of radiobiological effectiveness on modelling malignant induction probability and dose calculation

As discussed in Chapter 1, the value of RBE is a subject of academic debate and scientific research. It has clinical implications that grow ever more important with the increasing number of proton therapy centres globally. An investigation of the effect of the variation in RBE as a function of proton energy and associated LET, would require detailed maps of the variation of LET across the patient, which are not currently available for the current study. However, in addition to the variation of RBE with proton energy, the RBE is also known to vary as a function of dose increasing to a maximum RBE_{max} at low dose. In this section, the dose-related RBE effect on MIP is investigated, and further, effect of RBE on dose calculation is explored.

The effect of RBE on MIP was investigated by comparing MIP modelled using a constant value of RBE for protons of 1.1, and MIP modelled using an RBE

that is calculated using the "MinMax" model described below. The effect on calculated MIP and/or dose produced by each of the different methods to define RBE is assessed. The Effect of LET on RBE, and how that can impact different tissues was explored using the Wedenberg model (on a selected range of input values – see 3.5.2.1 for details).

3.5.1 Effect of radiobiological effectiveness on modelling malignant induction probability

3.5.1.1 RBE of 1.1

In clinical practice, an RBE of 1.1 is used for protons. The proton therapy plans described in this thesis were originally created using an RBE of 1.1. The code can be instructed to use a uniform RBE of 1.1 or use an alternative method. RBE of 1.1 is thought to be a reasonable estimate of the average RBE in the plateau region of the spread-out Bragg peak, and there is no evidence that it is an incorrect estimate (Paganetti *et al*, 2002, Paganetti, 2014).

The MIP tool recognises that the plan being worked on is a proton therapy plan, and reads the instruction from the simulation job card. This part instructs the code to apply a uniform RBE of 1.1. The dose is then used for MIP calculations as described earlier. This approach is similar to the methodology followed in 3.1 and 3.1.3.

3.5.1.2 RBE_{MinMax}

A pre-set range of RBE is used to define RBE_{min} and RBE_{max}, the maximum and minimum plausible values for RBE (Paganetti H, 2014). Those values are

used along with α and β parameters in the following model to calculate RBE (Carabe-Fernandez *et al*, 2007):

$$RBE = \frac{-\alpha + \sqrt{\alpha^2 - 4\beta d(RBE_{max}\alpha + RBE_{min}^2\,\beta d)}}{2\beta d} \quad (27)$$

The RBE calculated from this model is incorporated into MIP modelling. The simulation is performed in a similar fashion to the standard modelling done in 3.1 and 3.1.3, with the following modification to the process.

RBE_{min} and RBE_{max} are defined in the parameter files to be used and the simulation job card is edited to instruct the MATLAB code to calculate RBE using the built-in RBE_{MinMax} model and not the constant, uniform1.1 RBE value.

MIP was calculated for the proton therapy plans using RBE of 1.1. The MIP is re-calculated here using the RBE_{MinMax} model, which is a function of dose (d), α and β and RBE_{min} and RBE_{max}. MIP and dose indices are compared between the two different methods (RBE1.1 and RBE_{MinMax}).

3.5.2 Effect of radiobiological effectiveness on dose calculation

3.5.2.1 Wedenberg model

To examine the impact of varying RBE on dose calculations, the RBE from the model by Wedenberg *et al,* 2013 was used. In that model, RBE is a function of LET, dose and α/β.

$$RBE(D, L, \left(\frac{\alpha}{\beta}\right)) = -\frac{1}{2D}\left(\frac{\alpha}{\beta}\right) + \frac{1}{D}\sqrt{\frac{1}{4}\left(\frac{\alpha}{\beta}\right)^2 + \left(qL + \left(\frac{\alpha}{\beta}\right)\right)D + D^2} \quad (28)$$

Where D is the dose, α/β is the ratio for the tissue or organ from photon therapy studies, L is linear energy transfer and q is a constant with the same value, regardless of the physical properties of the proton beam, The value of parameter q found by the authors to best fit the experimental data was 0.434 Gy mm/KeV (95% CI: 0.366 - 0.513) (Wedenberg *et al*, 2013). RBE was calculated using the Wedenberg model for a selected number of input parameters namely LET of 8.5 KeV/μm while varying α/β. This was performed to help illustrate how RBE would vary across a range of α/β values, and would visualise the impact of variation in tissues on RBE and dose calculation.

3.6 Statistical analysis

MIP and $MIP_{Relative}$ were analysed using the Wilcoxon signed rank test. Because some of the data studied were not normally distributed, based on Shapiro-Wilk Normality Test (Shapiro, S. S. and Wilk, M. B., 1965), the Wilcoxon signed rank test, which is a non-parametric test was selected to test the data statistically and to assess if the differences are significant. For relative relationships comparison ($MIP_{Relative}$), one sample Wilcoxon test was used, comparing the relevant data to 1.

To estimate variation in MIP values for the entire data set of the 12 available patients, changes in MIP values of Patients 1 and 2 were assessed and an F-test was performed, in which variances of different paired data points groups from 4.2.2 were compared (see4.2.3).

4 Chapter 4: Results

In this chapter, the results of the MIP modelling are divided into five sections. The first section compares the calculated MIP values for photon and proton therapy for 12 medulloblastoma patients using three different models (LQ, LIN and LNT), while the second section investigates the sensitivity of these models, and associated MIP values, to the uncertainty in the values used for the various model parameters. The third section covers the calibration and benchmarking assuming a 0.1 Gy whole body photon dose to compare the outcomes with absolute risk values obtained from BEIR VII report. The fourth section explores the effect of spatial dose averaging across organs and tissues on predicting MIP compared to values calculated on a voxel-by-voxel basis. Finally, the fifth section covers the effect of the variation in RBE of protons as a function of dose using the RBE_{MinMax} model, and presents an illustration of how RBE can vary with α/β ratios for a certain LET.

4.1 Modelling of MIP after Proton and Photon Therapy

In this section, results of MIP modelling are presented. MIP was calculated using three different models: LQ, LIN, and LNT. The uncertainty in the presented whole body MIP and $MIP_{Relative}$ values was determined from the analysis of the sensitivity of these values to the uncertainty in model parameter detailed in section 4.2.3. Statistical analyses of absolute and relative MIPs are also presented.

4.1.1 Whole Body MIP

A simulation was run individually on each patient plan, using each of the models described previously (LIN, LQ, and LNT). Each run produced two

results files. One file details outputs per organ (volume in cm^3, dose indices, MIP), and the other file gives the total (whole body) MIP.

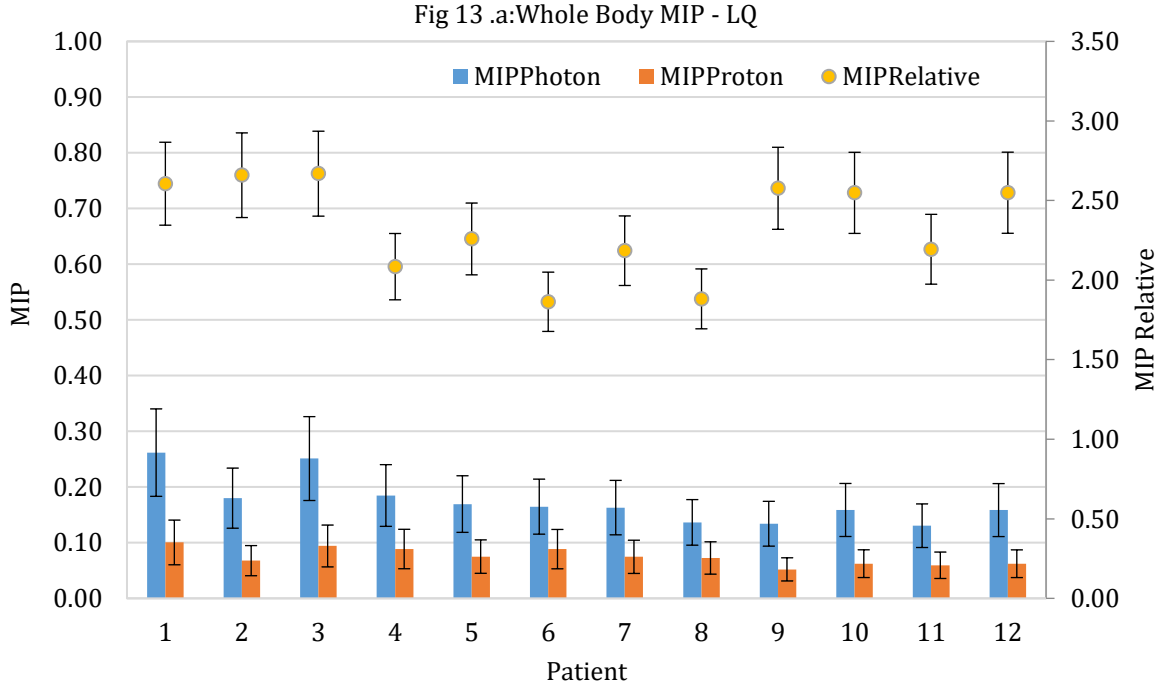
The outputs for the individual organs or structures were the volume (in cm3), mean, median, minimum, and maximum doses (Gy), MIP. The resulting whole body MIP values for the photon and proton plans for each of the 12 patients are illustrated in Figure 13, along with the ratio of these values (MIP_{Photon}:MIP_{Proton}) represented by $MIP_{Relative}$. The 3DCRT plan showed MIP values between 0.04 and 0.93. The smallest MIP (0.04) was calculated using the LIN model, while the MIP of 0.93 was calculated using the LNT model. The calculated MIP values for the corresponding proton plans were consistently less than those obtained for the photon plans in all cases.

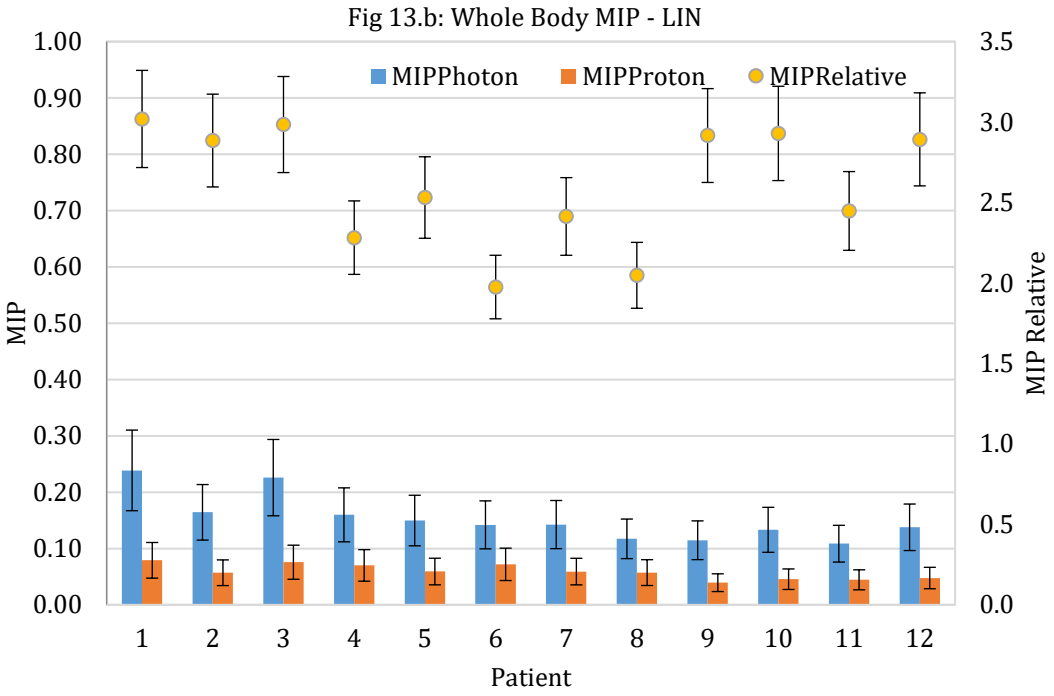
Wilcoxon signed rank tests were performed and there was a significant difference between MIP_{Photon} and MIP_{Proton} for all three models (LQ model: P = 0.001, LIN model: P = 0.001, LNT model: P = 0.001).

From these results, it can be seen that the three models generate different values of MIP, as expected from studying dose-response curves for the MIP models (as presented in 2.1.3). Although there is uncertainty in the absolute MIP values calculated (and therefore not directly clinically applicable) due to the inherent uncertainty in the model parameters used; these will likely affect both the photon and proton results in a similar fashion and therefore these uncertainties are expected to only have a small effect on the relative MIP values. When comparing proton and photon plans; it is the *relative* relations that are of importance.

The significance of the $MIP_{Relative}$ values compared to an $MIP_{Relative}$ of 1 was assessed (indicating an identical outcome from photon and proton therapy). The results shown in Figure 13 clearly show that the calculated $MIP_{Relative}$ values are consistently greater than 1. The results were significant for all three models (one sample Wilcoxon test: LQ model: $P = 0.003$, LIN model: $P = 0.0004$, LNT model: $P = 0.003$) and show that the MIP for photons is greater than that for protons for all cases studied.

Fig 13 .a:Whole Body MIP - LQ





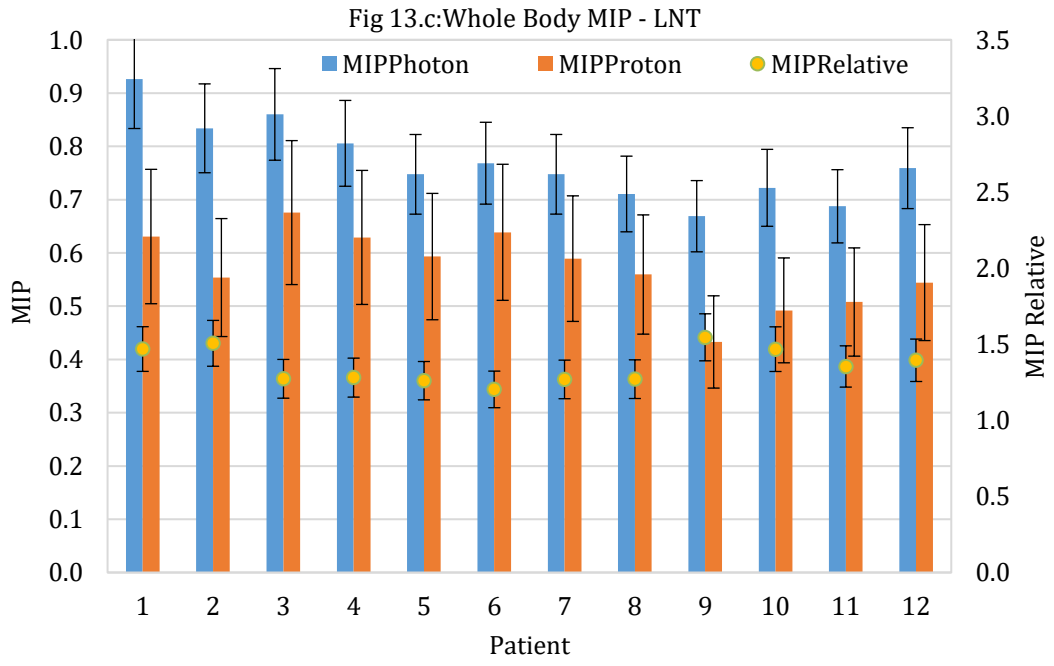


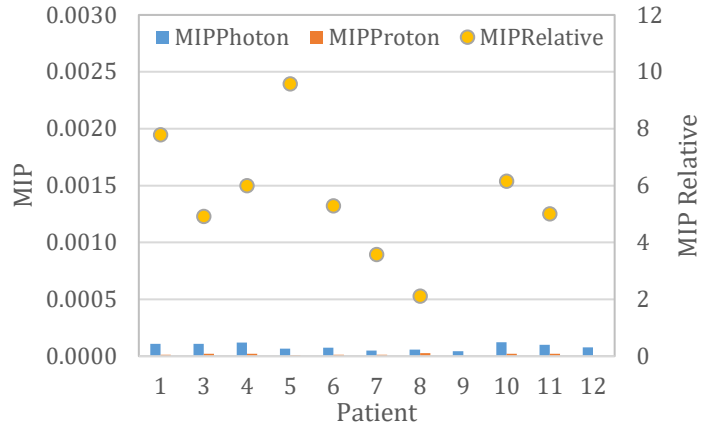
Figure 13: a-c The absolute and relative MIP values for the photon and proton treatment plans (12 patients) for each model. There is a consistent trend of MIP values being lower for protons than photons, regardless of the model used. The Relative MIP is plotted on the secondary vertical axis. Error bars represent 1 standard deviation.

4.1.2 Organ-specific MIP

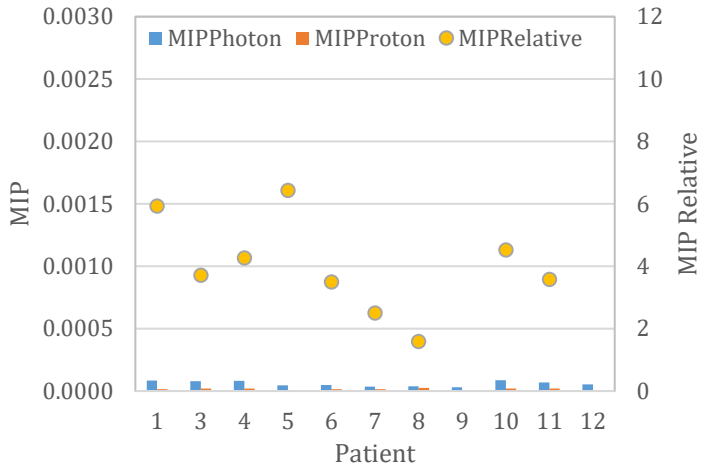
In many clinical settings, interest is focused on a limited number of organs rather than the whole body. The knowledge about secondary cancer development in some organs is more extensive in some than others. Whole body risk can mask the MIP values of some individual organs by being obscured by MIP values of other larger organs, for instance.

Studying organ-specific MIP can be a challenging task. But in this work the focus was on selected organs that were considered to be clinically relevant or showed interesting behaviour due to dosemetric characteristics.

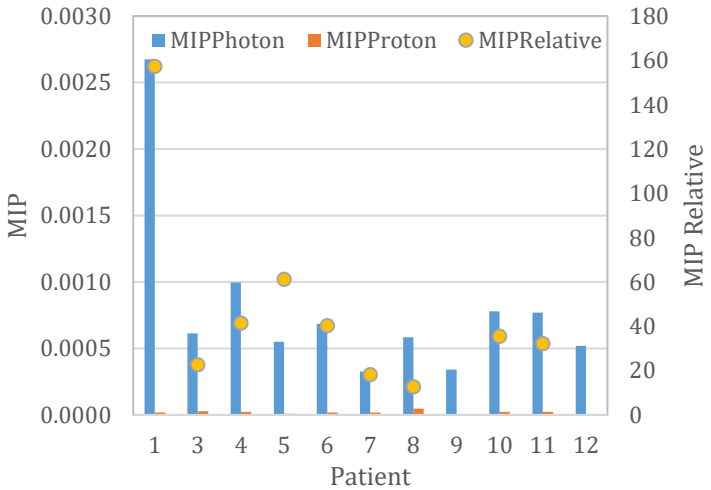
The organs that will be discussed are the thyroid and lung. MIP and $MIP_{Relative}$ values for the photon and proton plans for the aforementioned organs are illustrated in Figure 14 and Figure 15. Error bars derived from the uncertainty analysis could be only applied to whole body MIP, as the magnitude by which organ's MIP will vary is going to be different from one organ to another, as different organs may have different parameters and dose distribution, although it could be argued that the uncertainty for the individual organs is bound by the range of the uncertainty in the parameters used.



(a)

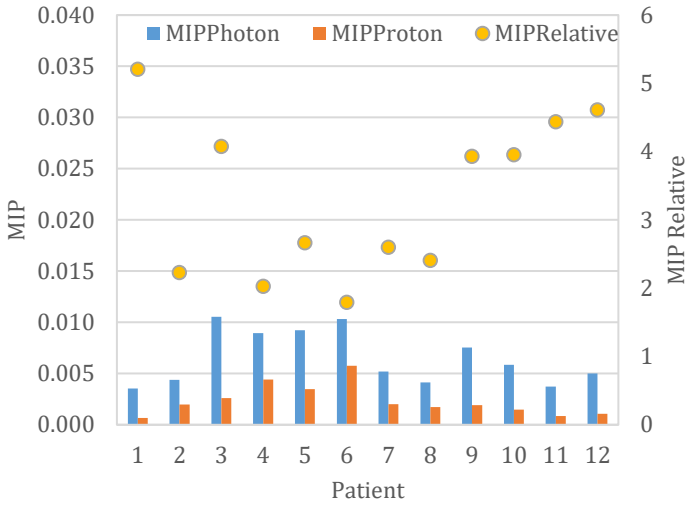


(b)

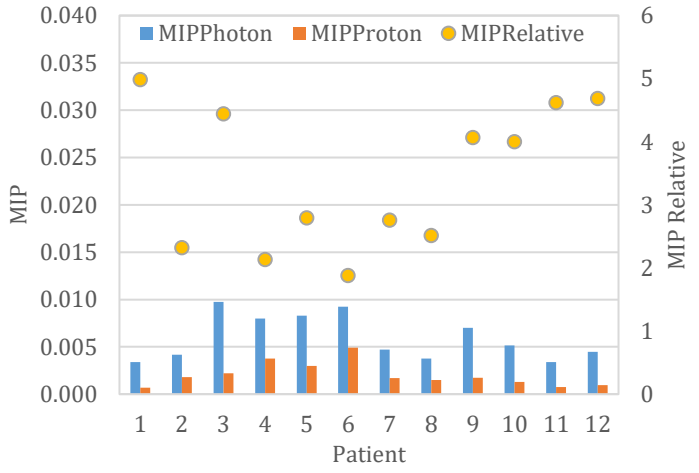


(c)

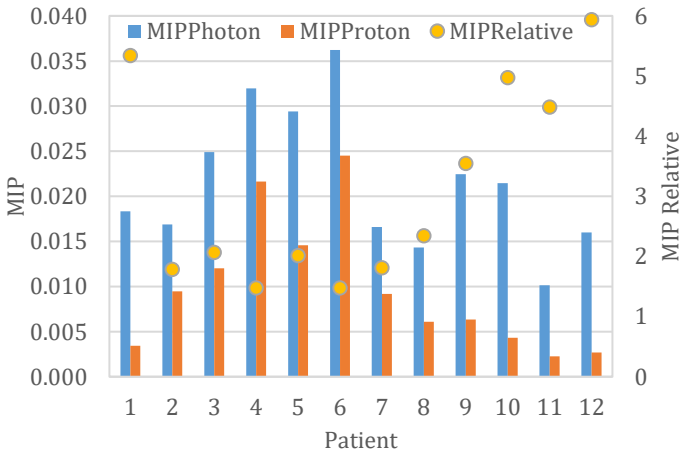
Figure 14: MIP and $MIP_{Relative}$ for thyroid, for (a) LQ, (b) LIN, and (c) LNT models. Patient 2 generated MIP of 0 for thyroid for all models and modalities and so is not included in this figure, and the proton plan of patients 9 and 12 delivered zero dose to the thyroid, giving a MIP value of 0.



(a)



(b)



(c)

Figure 15: MIP and $MIP_{Relative}$ for the lung, for (a) LQ, (b) LIN, and (c) LNT models.

MIP for thyroid varied widely and significantly depending on choice of model, with the $MIP_{Relative}$ the values obtained using LNT (12.7-157.3) being markedly higher than those obtained using the LQ and LIN models (1.5 – 9.6). Additionally the calculated MIP was also critically dependent on the dose to the thyroid, for patient 2 the calculated MIP was 0 for all models and modalities due to the thyroid not being irradiated (i.e. zero dose). This was also the case with the proton plan for patient 9 and 12. For the lung, the difference between photons and protons was generally upheld, as in it was clear that MIP for 3DCRT is higher than that of protons, but the magnitude in difference wasn't as large as seen with the thyroid ($MIP_{Relative}$: 1.8 – 5.2 for LQ and LIN models, 1.5-5.9 for LNT model). Wilcoxon signed rank tests were performed and there was a significant difference between MIP_{Photon} and MIP_{Proton} for all three models for both thyroid and lung (thyroid: LQ model: $P = 0.001$, LIN model: $P = 0.001$, LNT model: $P = 0.001$, lung: LQ model: $P = 0.0005$, LIN model: $P = 0.0005$, LNT model: $P = 0.0005$). $MIP_{Relative}$ was also shown to be statistically significant (one sample Wilcoxon test: thyroid: LQ model: $P = 0.004$, LIN model: $P = 0.004$, LNT model: $P = 0.004$, lung: LQ model: $P = 0.0005$, LIN model: $P = 0.0005$, LNT model: $P = 0.0005$).

4.2 Sensitivity of MIP models to uncertainty in parameters

There is uncertainty in the input parameter values used in the models. This uncertainty results from how those parameters are estimated, the different endpoints they are associated with, the differences between tissues, and the differences in experimental conditions. To establish the magnitude of the differences in predicted outcome due to these uncertainties, simulations

were performed to test their effect on the results. This was done by performing simulations using different values for each parameter, firstly one parameter at a time and in another set of experiments, all parameters were altered simultaneously. Parameter scans were performed to assess not only the uncertainty associated with the calculated absolute values of MIP for photon and protons, but more importantly the uncertainty on the relative MIP values.

4.2.1 Sensitivity testing over pre-set parameter modifier space

In this section, the results of MIP modelling while varying one parameter at a time are presented. The results are for Patients 1 and 2, for all three models. As described in section 3.2.1 each parameter was varied by applying a modifying factor that varied from 0.2 up to 10.

MIP was modelled varying one parameter at a time. Results showed (Figure 16 - Figure 20) relative relation between MIP_{Photon} and MIP_{Proton} remains broadly the same (MIP_{Photon} higher than MIP_{Proton}) for all the parameters studied over the range of modifying factors values tested. The general observation of MIP_{Photon} being higher than MIP_{Proton} holds true for all parameters across all models: even when a large range uncertainty is included in the calculations, MIP_{Photon} is likely to be higher than MIP_{Proton}.

For parameters α, β, γ, δ the calculated $MIP_{Relative}$ value is consistently greater than one for over the entire range of parameter values studied. While this is also true for the parameter λ using the LIN model, when the LNT model is used the $MIP_{Relative}$ values are greater than 1 for low values of λ, but trend to 1 as the assumed value increases; this is a result of the absolute MIP value

increasing to the maximum value of 1 (malignant induction) in all patients for both the photon and proton treatment plans with this model.

Those results emphasise the conclusion that uncertainty in parameters, although important and critical in absolute MIP estimates (as well as secondary cancer risk calculations), would have much of a less of an impact on the end-point decision when it comes to preference of one treatment modality over the other in medulloblastoma.

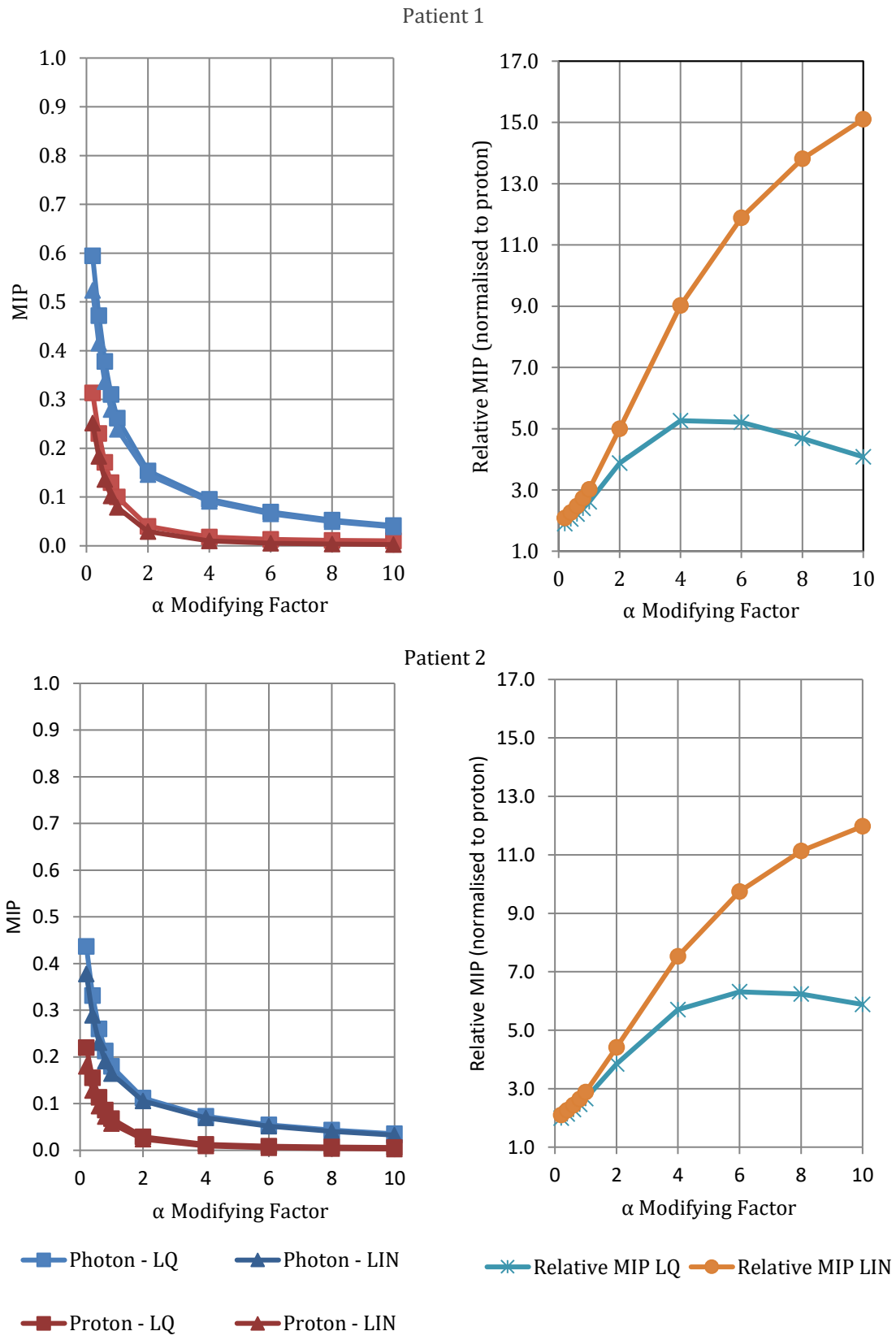


Figure 16: Whole body MIP and Relative MIP of adult patient (Patient 1- top panels) and teenage patient (Patient 2 – bottom panels) using single parameter variation approach for α. Note the consistent trend of $MIP_{Relative}$ greater than 1.

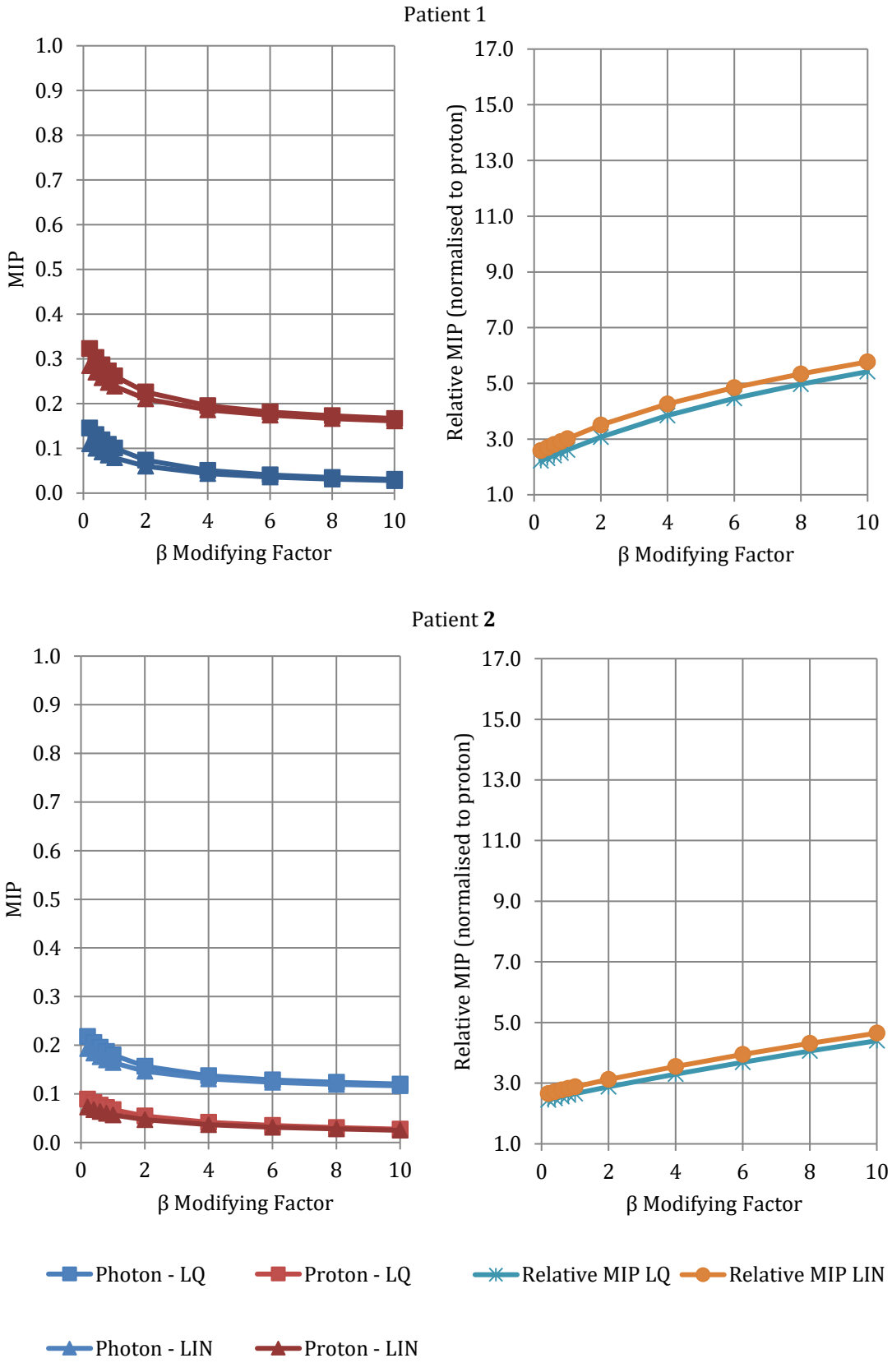


Figure 17: Whole body MIP and Relative MIP of adult patient (Patient 1- top panels) and teenage patient (Patient 2 – bottom panels) using single parameter variation approach for β . Note the consistent trend of $MIP_{Relative}$ greater than 1.

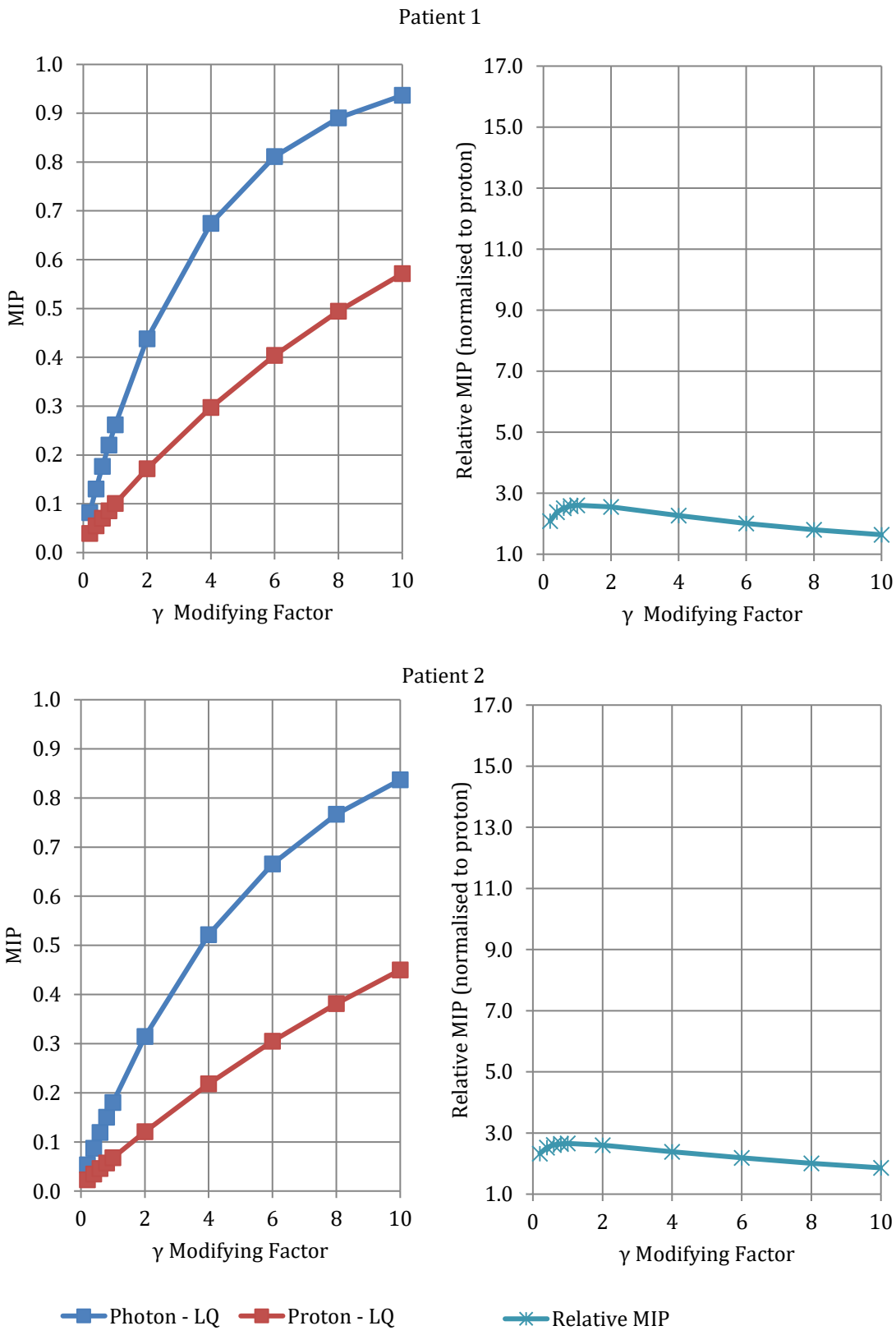


Figure 18: Whole body MIP and Relative MIP of adult patient (Patient 1- top panels) and teenage patient (Patient 2 – bottom panels) using single parameter variation approach for γ. Note the consistent trend of $MIP_{Relative}$ greater than 1.

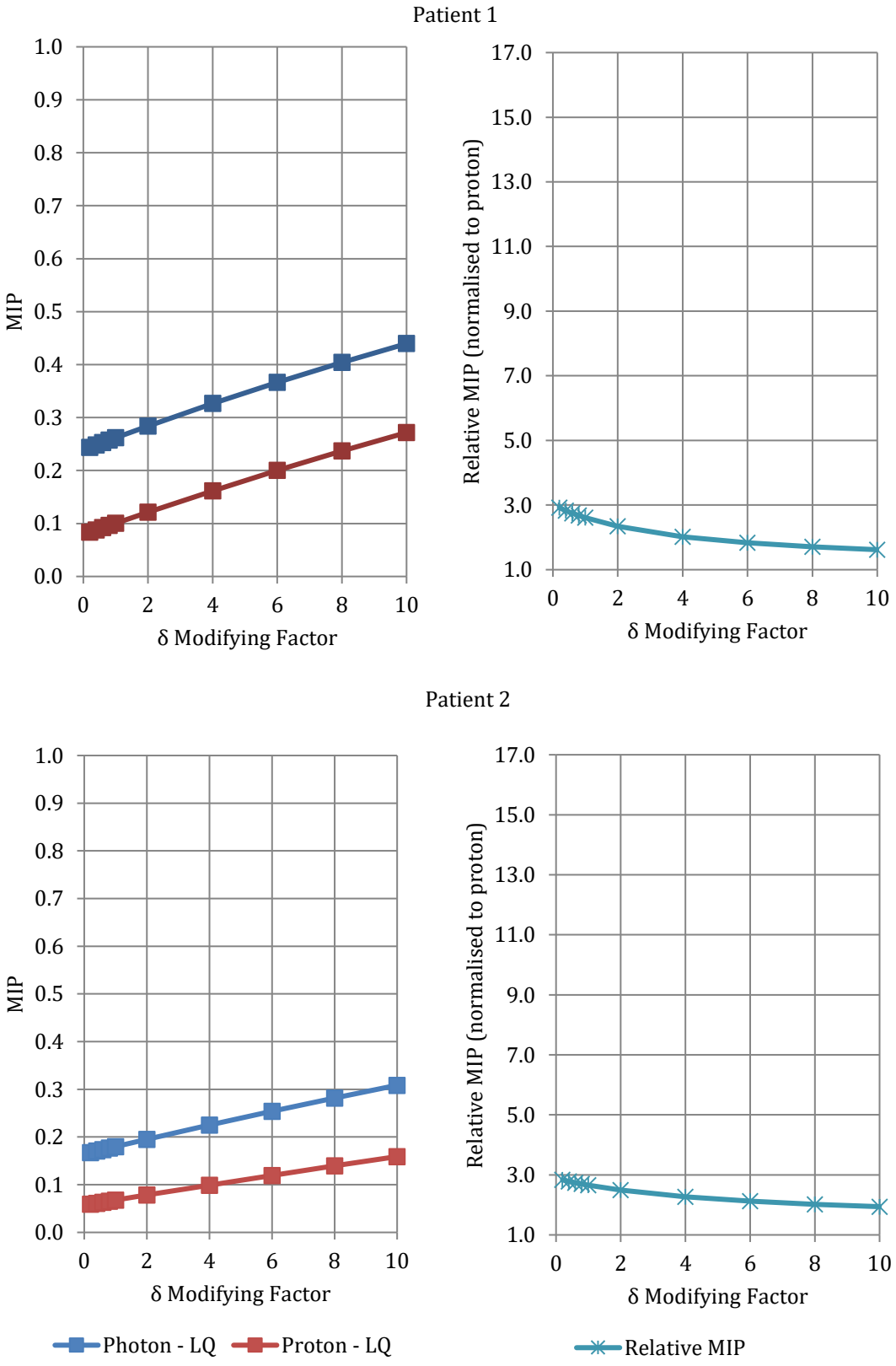


Figure 19: Whole body MIP and Relative MIP of adult patient (Patient 1- top panels) and teenage patient (Patient 2 – bottom panels) using single parameter variation approach for δ. Note the consistent trend of $MIP_{Relative}$ greater than 1.

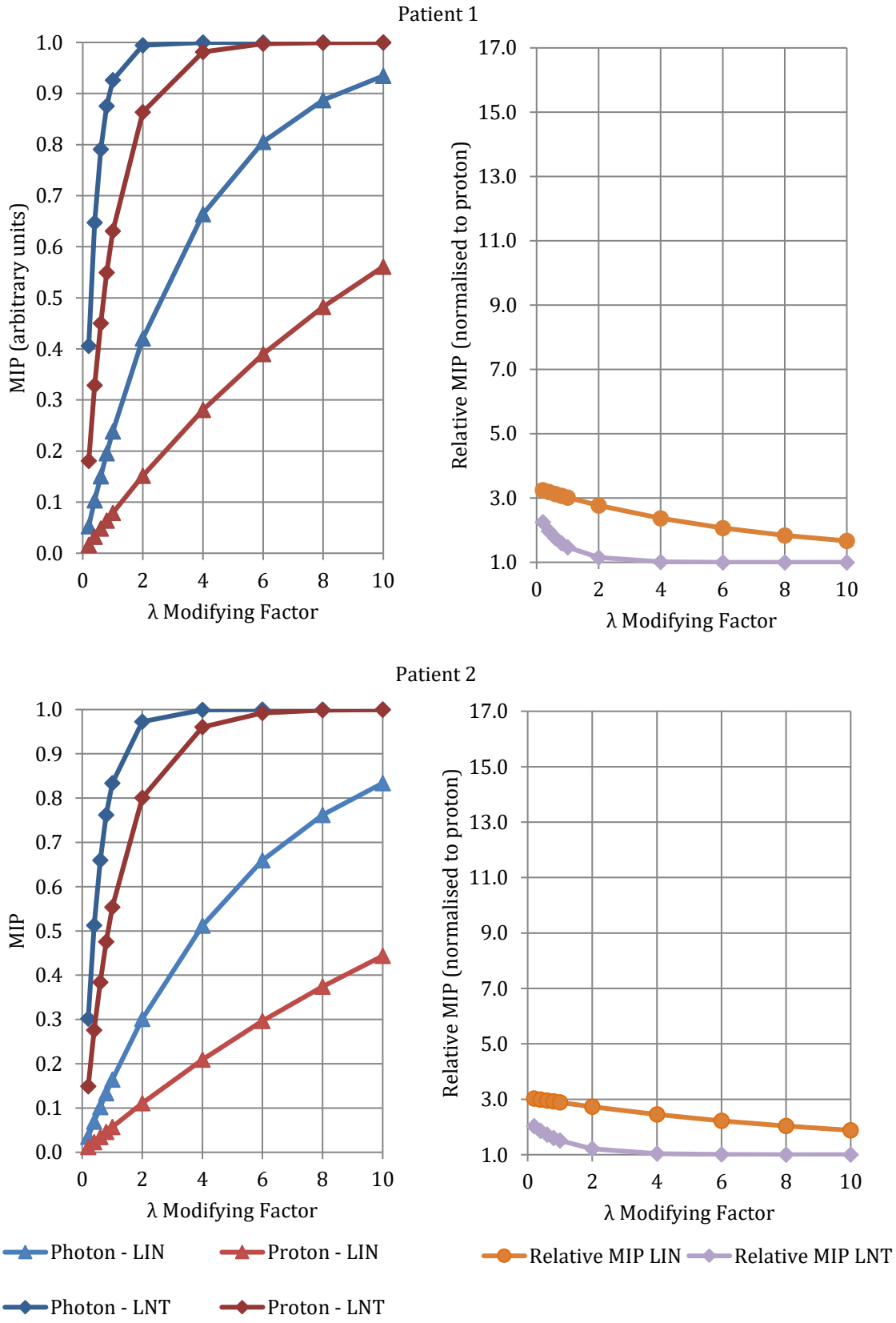


Figure 20: Whole body MIP and Relative MIP of adult patient (Patient 1- top panels) and teenage patient (Patient 2 – bottom panels) using single parameter variation approach for λ. Note the consistent trend of $MIP_{Relative}$ greater than 1. As MIP produced by LNT is linear with dose, increasing value of λ would increase MIP, making it trend to 1, and hence making $MIP_{Relative}$ trend to 1 as well.

4.2.2 Sensitivity testing of parameters over randomly generated modifiers space

The experiment above looked into the effect of varying one parameter at a time by a pre-set value, to assess sensitivity towards the parameter uncertainty and to give a better understanding of the importance of the parameters on the variation in MIP values in the three models in such a complex system. This section investigates the effect of varying all parameters of a selected model simultaneously using randomly generated parameters modifying factors. This is done in an attempt to introduce the inherent uncertainty in a more realistic setting, because the uncertainty is actually inherent to all parameters, in varying degrees.

In this section, the results of modelling MIP while varying all parameters in a model at the same time are presented for two patients. $MIP_{Relative}$ for those two patients is presented, and the effect (if any) of varying parameters is illustrated.

On plotting the MIP data, an MIP scale of 0.00-1.00, in increments of 0.05 was adopted. Each bin represents values of MIP that fell into that bin, with each bin's label representing the maximum value of that bin. So, for the bin labelled "0.20", it will have all MIP values between greater than the previous bin maximum value (0.15 in this example) and equal to or smaller than the maximum value of the bin itself, which is 0.20. For $MIP_{Relative}$, axis scale was set to be from smallest value bin of 1.00 to the right side bin of 5.50, in increments of 0.25.

4.2.2.1 Linear quadratic model:

α, β, γ and δ were varied randomly and simultaneously using RMS of 0.25. The values of modifying factors ranged between 0.237 and 1.842 for α, β, γ, and δ (Table 1). The 400 LQ model runs for the 3DCRT plans for Patients 1 and 2 were plotted as a frequency histogram. The same was done for the proton plans of Patients 1 and 2 (Figure 21 and Figure 22). The $MIP_{Relative}$ for MIP_{Photon} and MIP_{Proton} was calculated and a frequency histogram was generated, and the lower panels shows that the $MIP_{Relative}$ is always larger than 1, meaning that even with the inherent uncertainty in the parameters, and in this patient, the linear quadratic predicts a higher MIP_{Photon} than MIP_{Proton}.

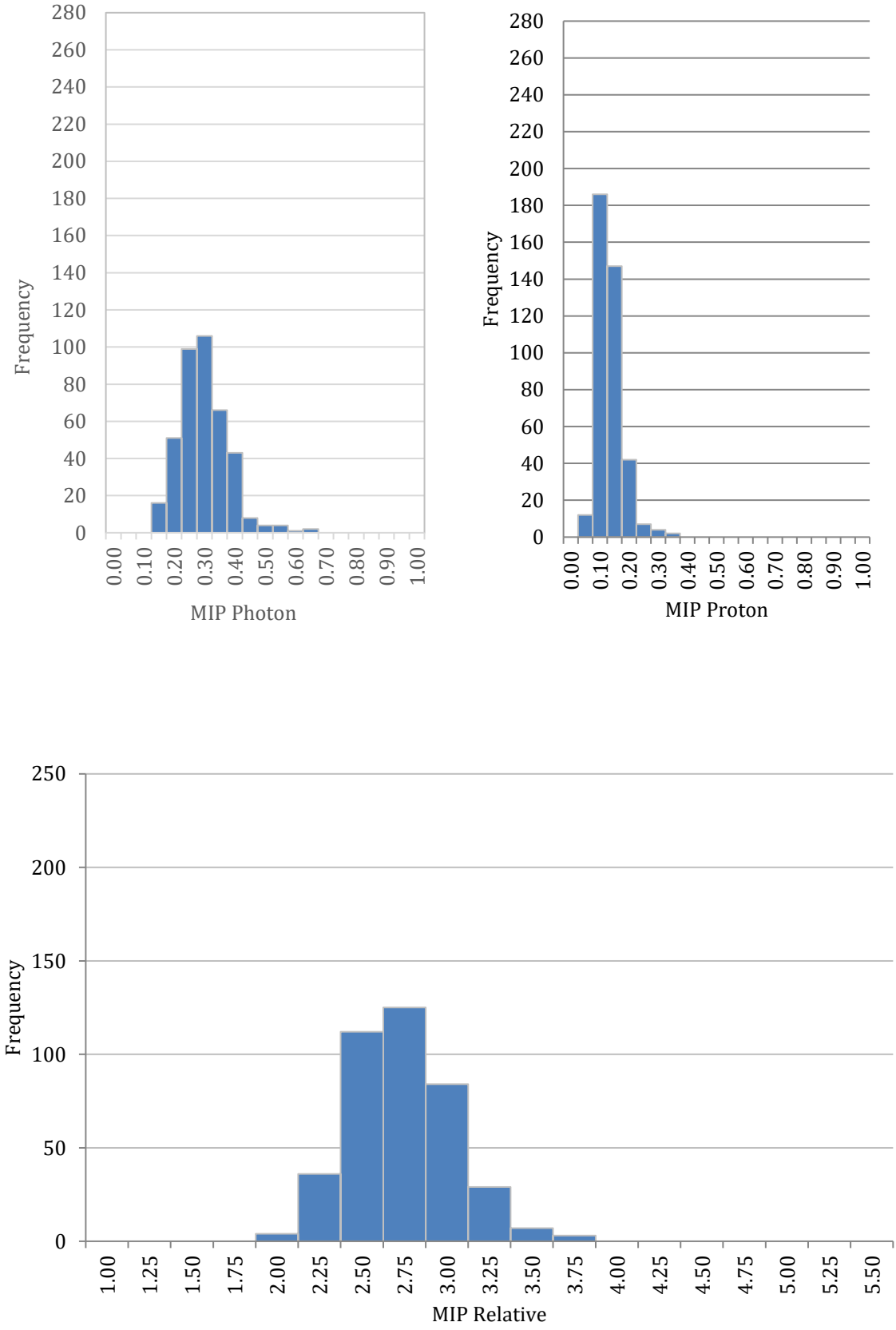


Figure 21: Frequency distribution of MIP_{Photon} and MIP_{Proton} for the adult patient (Patient 1) using LQ model, as well as distribution of $MIP_{Relative}$.

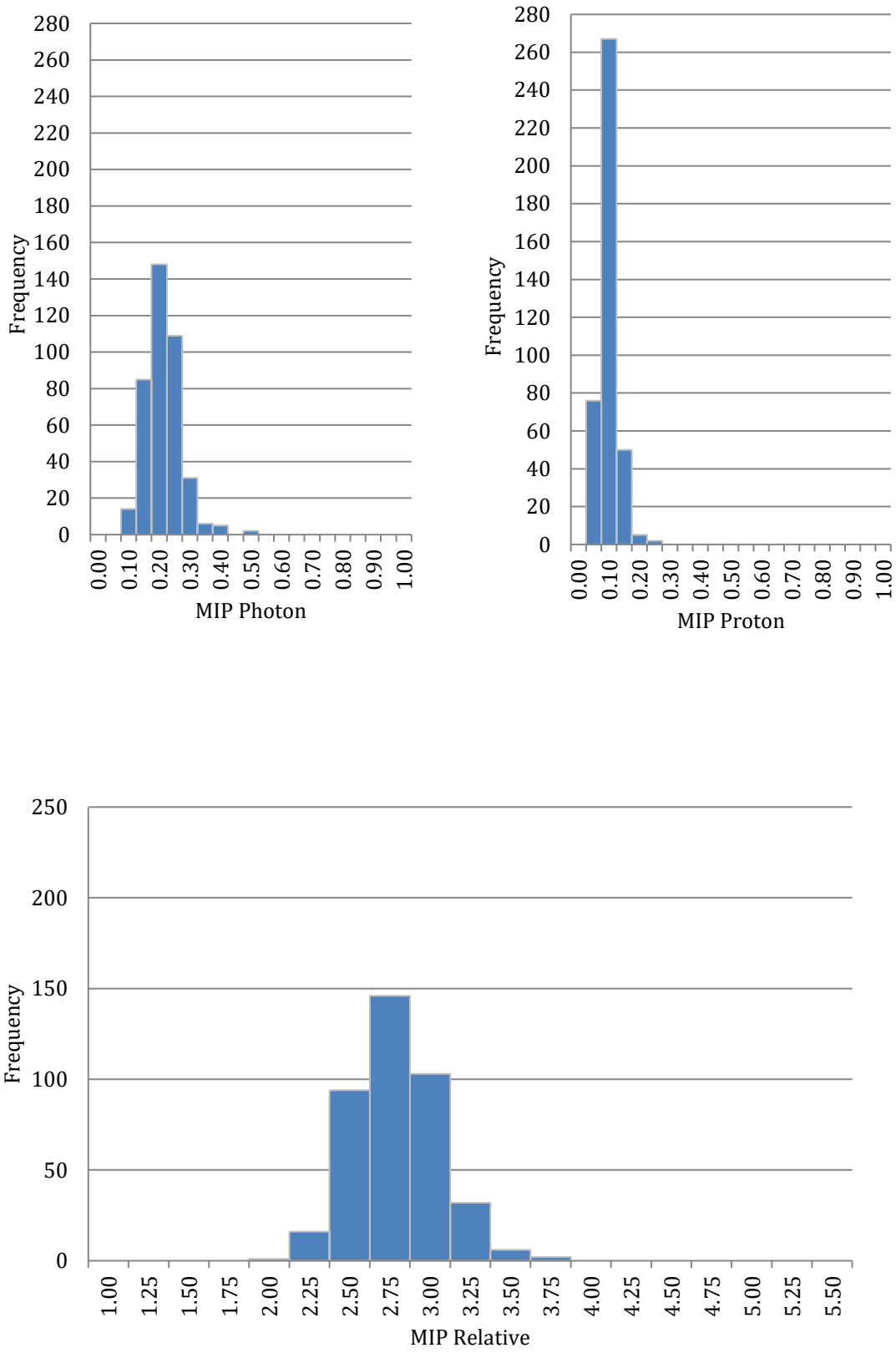


Figure 22: Frequency distribution of MIP_{Photon} and MIP_{Proton} for the teenage patient (Patient 2) using LQ model, as well as distribution of $MIP_{Relative}$.

4.2.2.2 Linear model:

α, β, and λ were varied randomly simultaneously using RMS of 0.25, with the values of modifying factors ranged between 0.228 and 1.829. The 400 LIN model runs for the photon plans were plotted in a frequency histogram. The same was done for the proton plans for Patients 1 and 2 (Figure 23 and Figure 24). The $MIP_{Relative}$ for MIP_{Photon} and MIP_{Proton} were calculated and the frequency distribution shows that the $MIP_{Relative}$ is always larger than 1, meaning that even with the inherent uncertainty in the parameters, the linear model predicts a higher MIP_{Photon} than MIP_{Proton}.

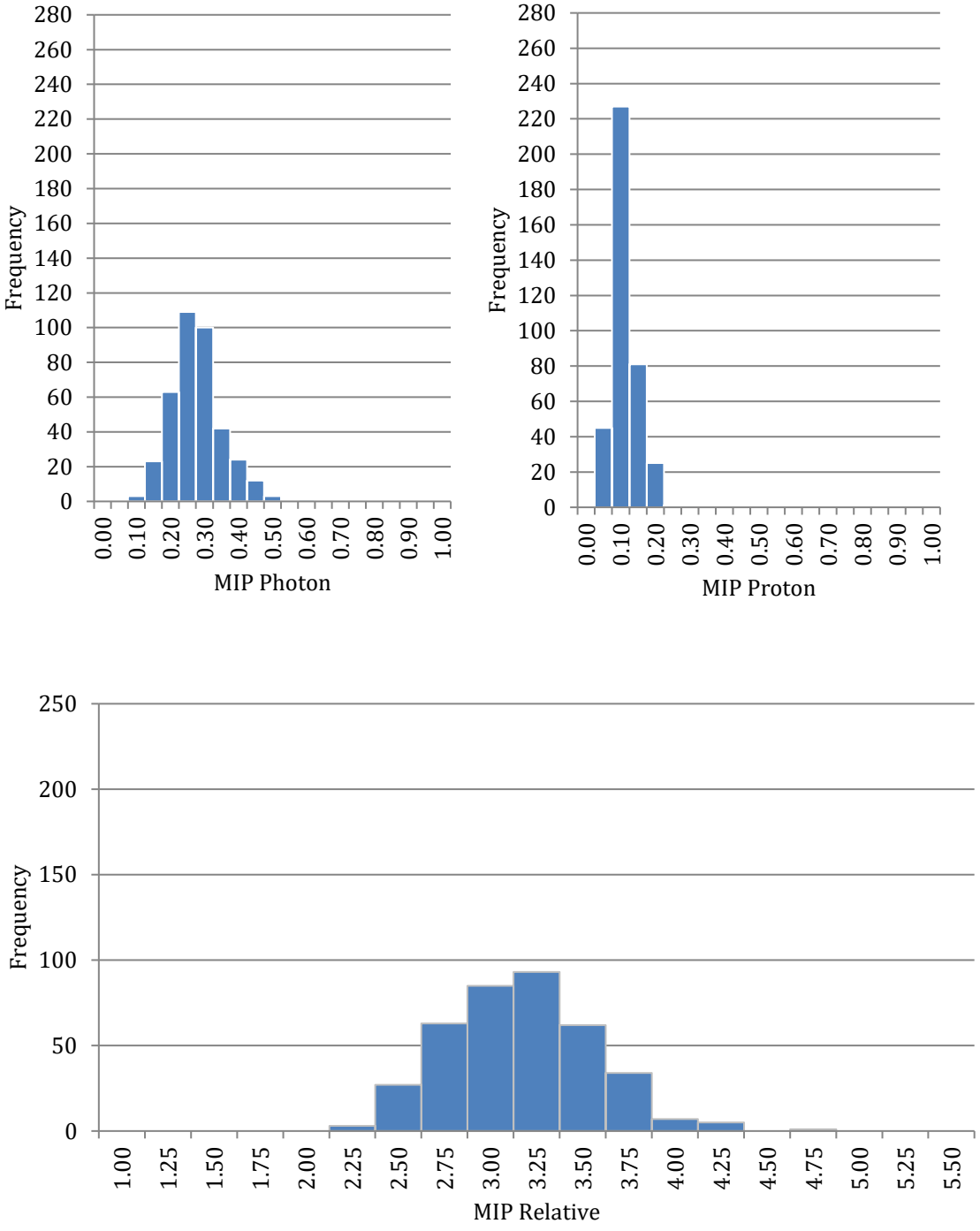


Figure 23: Frequency distribution of MIP_{Photon} and MIP_{Proton} for the adult patient (Patient 1) using LIN model, as well as distribution of $MIP_{Relative}$.

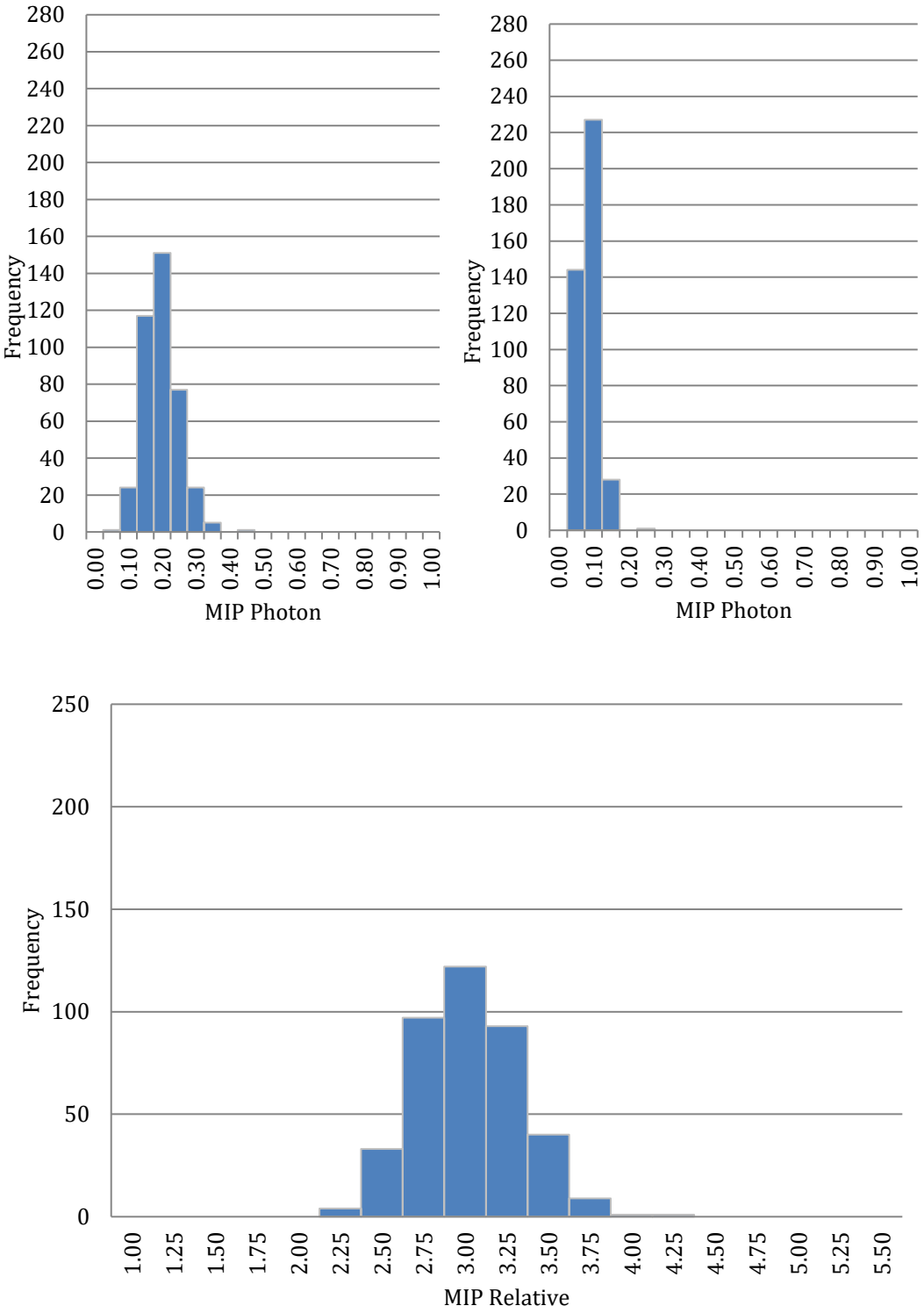


Figure 24: Frequency distribution of MIP_{Photon} and MIP_{Proton} for the teenage patient (Patient 2) using LIN model, as well as distribution of $MIP_{Relative}$.

4.2.2.3 Linear-no-threshold model:

λ was varied randomly, simultaneously using RMS of 0.25, with the values of modifying factors ranged between 0.228 and 1.722. The 400 LNT model runs for the photon plans for Patients 1 and 2 were plotted as a frequency distribution. The same was done for the proton plans (Figure 25 and Figure 26). The $MIP_{Relative}$ for MIP_{Photon} and MIP_{Proton} were calculated and the frequency distribution shows that the $MIP_{Relative}$ is always larger than 1, meaning that even with the inherent uncertainty in the parameters, the linear model predicts a higher MIP_{Photon} than MIP_{Proton}. Essentially these give the same general results as shown in Figure 20, and as the LNT model is only dependent on the parameter λ, it is presented to for comparison with the LQ and LIN results.

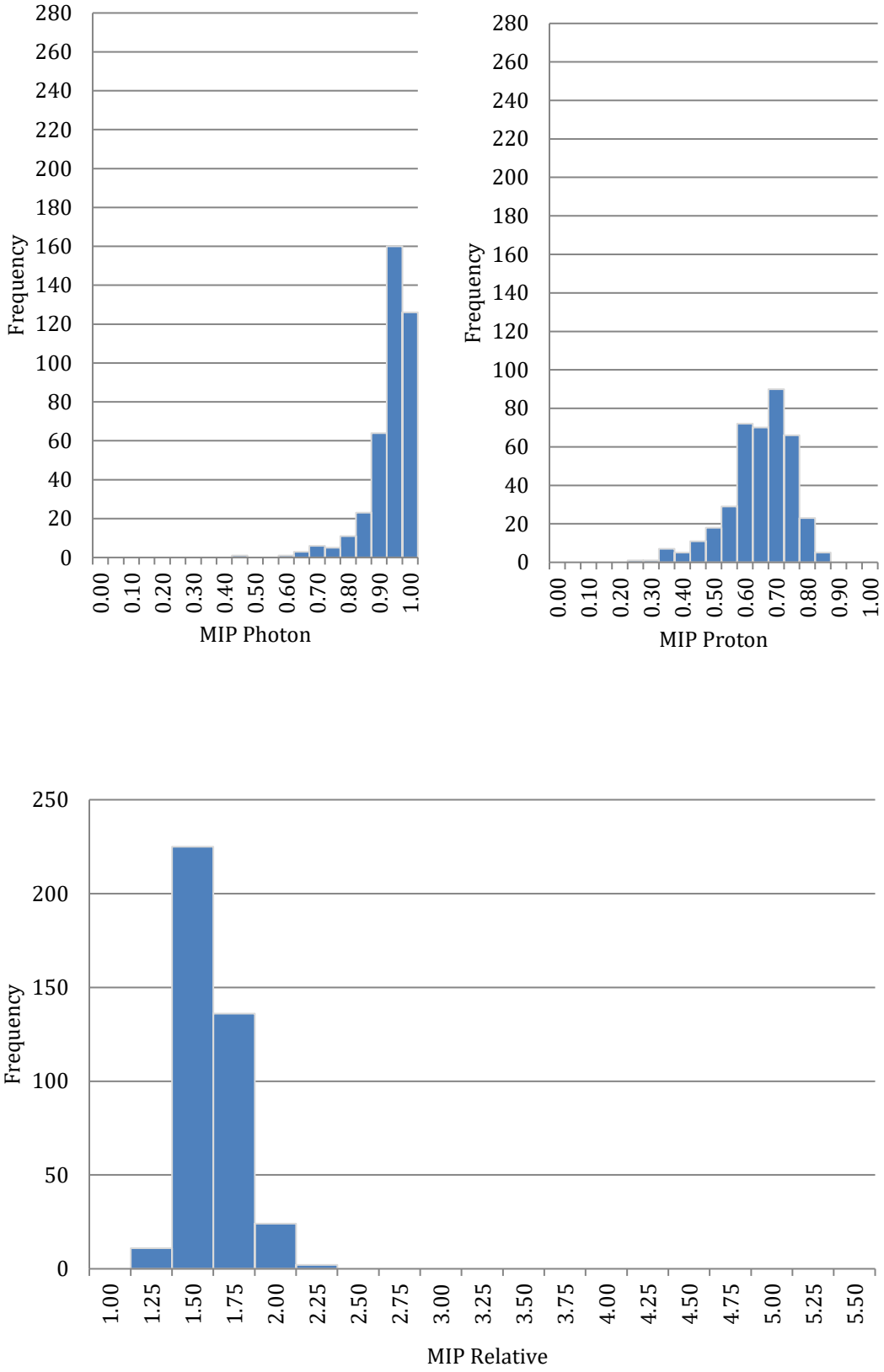


Figure 25: Frequency distribution of MIP_{Photon} and MIP_{Proton} for the adult patient (Patient 1) using LNT model, as well as distribution of $MIP_{Relative}$.

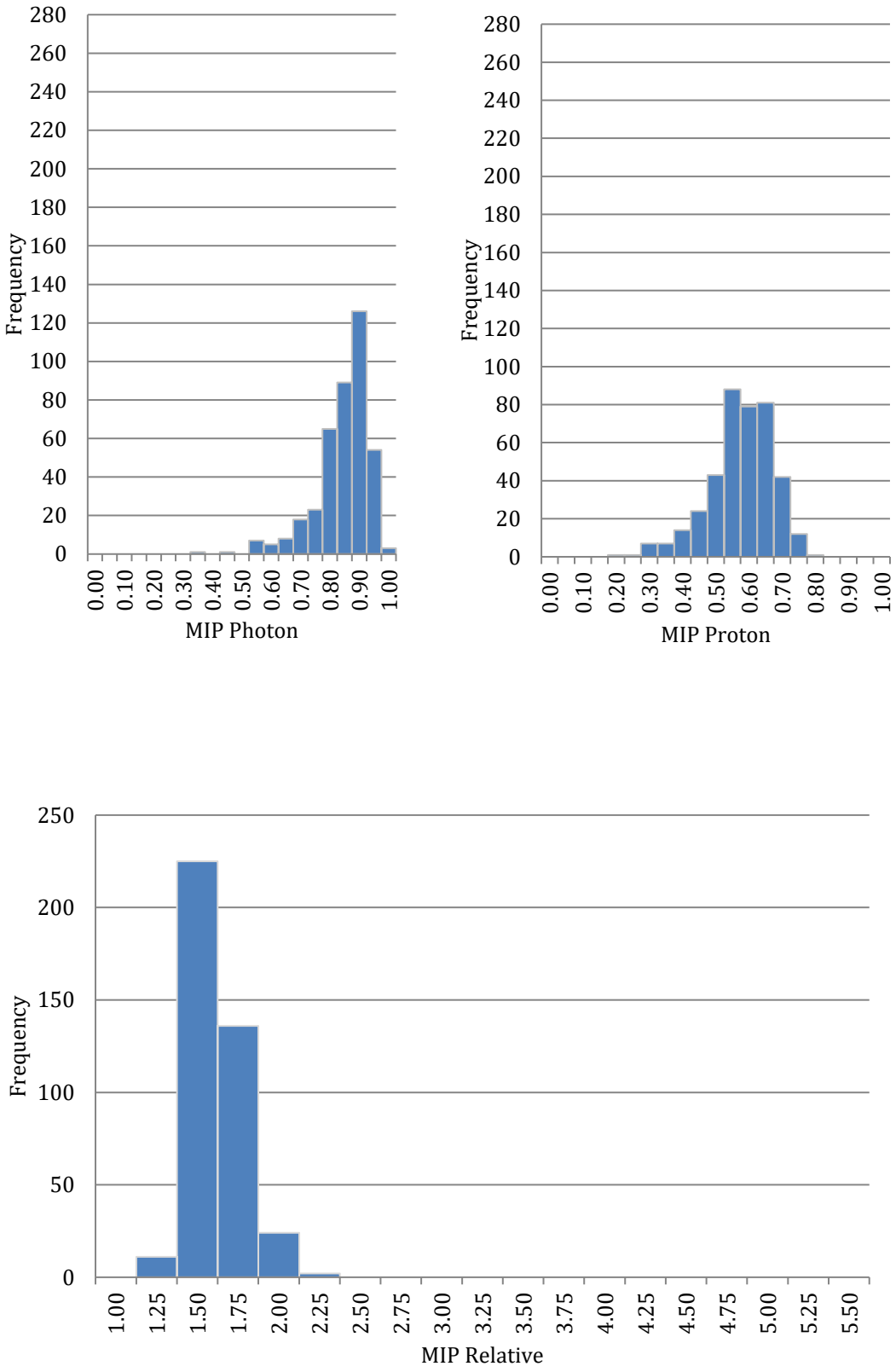


Figure 26: Frequency distribution of MIPPhoton and MIPProton for teenage patient (Patient 2) using LNT model, as well as distribution of $MIP_{Relative}$.

4.2.3 Assessment on of uncertainty in MIP and $MIP_{Relative}$ values

To estimate variation in MIP values for the entire data set of the 12 available patients, changes in MIP values of Patients 1 and 2 were assessed.

Data points from sensitivity testing of parameters over randomly generated modifiers space section (4.2.2) were used to calculate how the MIP of each patient's plans varied.

MIP variations are calculated by normalising the data in 4.2.2 to the relevant MIP values for the patient (i.e. Patient 1 or 2), treatment modality, and model (4.1.1). The standard deviation was then calculated from the data points for each plan and model combination for Patient 1. This was compared with the corresponding values for patient 2. Standard deviation values are shown in Table 3.

	Photon		Proton	
	Patient 1	Patient 2	Patient 1	Patient 2
LQ	0.3	0.3	0.4	0.4
LIN	0.3	0.3	0.5	0.4
LNT	0.1	0.1	0.2	0.2

	MIP Relative	
	Patient 1	Patient 2
LQ	0.1	0.1
LIN	0.1	0.1
LNT	0.1	0.1

Table 3: Standard deviation of normalised MIP for the treatment plans of Patients 1 and 2, and for $MIP_{Relative}$.

An F-test was performed, in which variances of different paired data points groups were compared. If the calculated F statistic was larger than the critical F value, then we conclude that the variances of the two groups are not equal (Table 4). For most comparisons, the variances were found not to be different. This could indicate that, regardless of the absolute MIP value itself, and regardless of the patient-specific relevant characteristics, overall variations in MIP are mostly influenced by the variation in the parameters. Based on the magnitude of variation of MIP, scaling up and down the MIP and $MIP_{Relative}$ data points was carried out to produce 1 standard deviation error bars for patients 3 through 12.

F-Test Two-Sample for Variances LQ Photon

	Variable 1	*Variable 2*
Mean	1.050	1.051
Variance	0.098	0.092
F	1.061	
P(F<=f) one-tail	0.278	0.557
F Critical one-tail	1.217	

alpha = 0.025

F-Test Two-Sample for Variances LQ Proton

	Variable 1	*Variable 2*
Mean	1.083	1.044
Variance	0.185	0.167
F	1.107	
P(F<=f) one-tail	0.156	0.312
F Critical one-tail	1.217	

alpha = 0.025

F-Test Two-Sample for Variances LIN Photon

	Variable 1	*Variable 2*
Mean	1.085	1.049
Variance	0.107	0.095
F	1.135	
P(F<=f) one-tail	0.109	0.218
F Critical one-tail	1.223	

alpha = 0.025

F-Test Two-Sample for Variances LIN Proton

	Variable 1	*Variable 2*
Mean	1.086	1.033
Variance	0.206	0.173
F	1.194	
P(F<=f) one-tail	0.043	0.085
F Critical one-tail	1.223	

alpha = 0.025

F-Test Two-Sample for Variances	LNT Photon	
	Variable 1	*Variable 2*
Mean	0.984	0.980
Variance	0.012	0.006
F	2.103	
P(F<=f) one-tail	1.1E-13	2.2E-13
F Critical one-tail	1.217	

alpha = 0.025

F-Test Two-Sample for Variances	LNT Proton	
	Variable 1	*Variable 2*
Mean	0.994	0.993
Variance	0.031	0.026
F	1.195	
P(F<=f) one-tail	0.038	0.076
F Critical one-tail	1.217	

alpha = 0.025

F-Test Two-Sample for Variances	MIP Relative LQ	
	Variable 1	*Variable 2*
Mean	1.00	1.00
Variance	0.01	0.01
F	1.44	
P(F<=f) one-tail	1.28E-04	
F Critical one-tail	1.22	

alpha = 0.025

F-Test Two-Sample for Variances	MIP Relative LIN	
	Variable 1	*Variable 2*
Mean	1.00	1.01
Variance	0.02	0.01
F	1.47	
P(F<=f) one-tail	6.95E-05	
F Critical one-tail	1.22	

alpha = 0.025

F-Test Two-Sample for Variances	MIP Relative LNT	
	Variable 1	*Variable 2*
Mean	1.01	1.00
Variance	0.01	0.01
F	1.81	
P(F<=f) one-tail	2.23E-09	
F Critical one-tail	1.22	

alpha = 0.025

Table 4: F-Test for variance for data from uncertainty testing performed according to 3.2.2 and illustrated in 4.2.2. For whole body MIP, only Photon's LNT variance was not equal, while the variances for $MIP_{Relative}$ between Patient 1 and Patient 2 were shown to be not equal, although the value of their variance is shown to be similar, and their SD is similar as well.

4.3 Calibration and benchmarking

In this section, different results of work involved in and leading to calibration and benchmarking are presented.

4.3.1 Comparison with Life Span Study

The rationale for conducting the 1.0 Gy simulation reported in this section was to compare the result with those from the LSS Report no. 14 (Ozasa *et al*, 2012).

In LSS Report 14, the value of the ERR/Gy for all solid cancers was 0.47/ Gy, while for MIP (1.0 Gy simulation; Table 5) ranged from 0.05 to 0. 57. As ERR and MIP are risk probabilities for two different endpoints, it is not appropriate to directly compare the numbers from the LSS report to the MIP values generated by the 1.0 Gy simulations. However, cautious assessment, that considers differences between the malignancy induction endpoint of the MIP modelling and the cancer-related death endpoint of the LSS, may potentially enable researchers to do so. This is where the steps mentioned earlier (3.3) to calibrate and benchmark parameters are potentially useful.

	MIP_{1Gy}	ERR (LSS 14)	Ratio
LQ	0.57	0.47	1.21
LIN	0.05	0.47	0.10
LNT	0.05	0.47	0.11

Table 5: MIP for a single uniform exposure of 1Gy using non-calibrated parameters for all three models, using the adult patient (Patient 1) plan contours, compared with the ERR from LSS.

4.3.2 Calibration and benchmarking to BEIR VII report

In the calibration and benchmarking process, the initial results of the 0.1 Gy uniform whole body single exposure using the LNT model are shown in Figure 27. The calibration results are shown in Figure 28. These figures illustrate the modelled variations in LAR using the LNT model compared to the BEIR VII report, with varying age following exposure to 0.1 Gy. Each of those plots (and the ones that follow in this section) is the result of a multi-step calculation, As this part of the work is focused on calibration and benchmarking, the method adopted to improve the fit was to calibrate the secondary risk input parameter(s) used in the models, rather than to modify other parameters as well, like μ, for instance.

The initial results of modelling LAR for a uniform single exposure of 0.1 Gy using the LIN and LQ are shown in Figure 29 and Figure 31. The improved fit following calibration and benchmarking is illustrated in Figure 30 and Figure 32 for the LIN and LQ models, respectively.

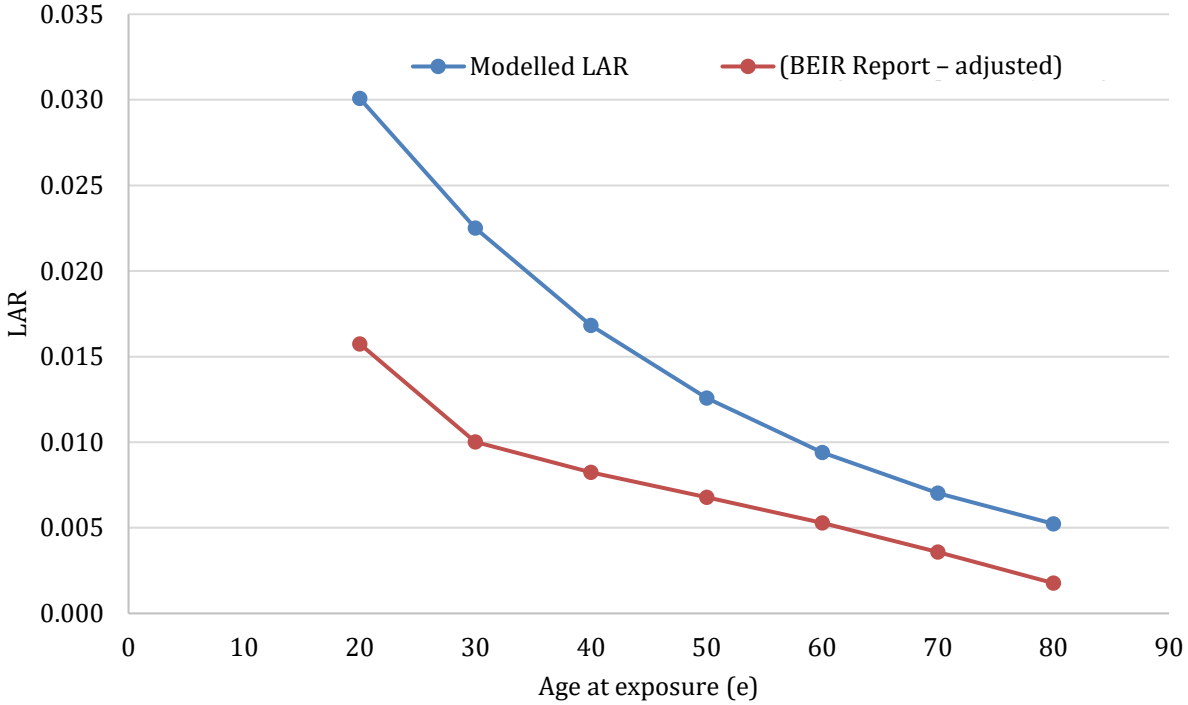


Figure 27: LAR after 0.1 Gy single exposure before calibration of λ, using the LNT model compared to the BEIR VII report values. Adjusted LAR refers to the adjustment made to LAR from cases per 100,000 (dividing by 100,000).

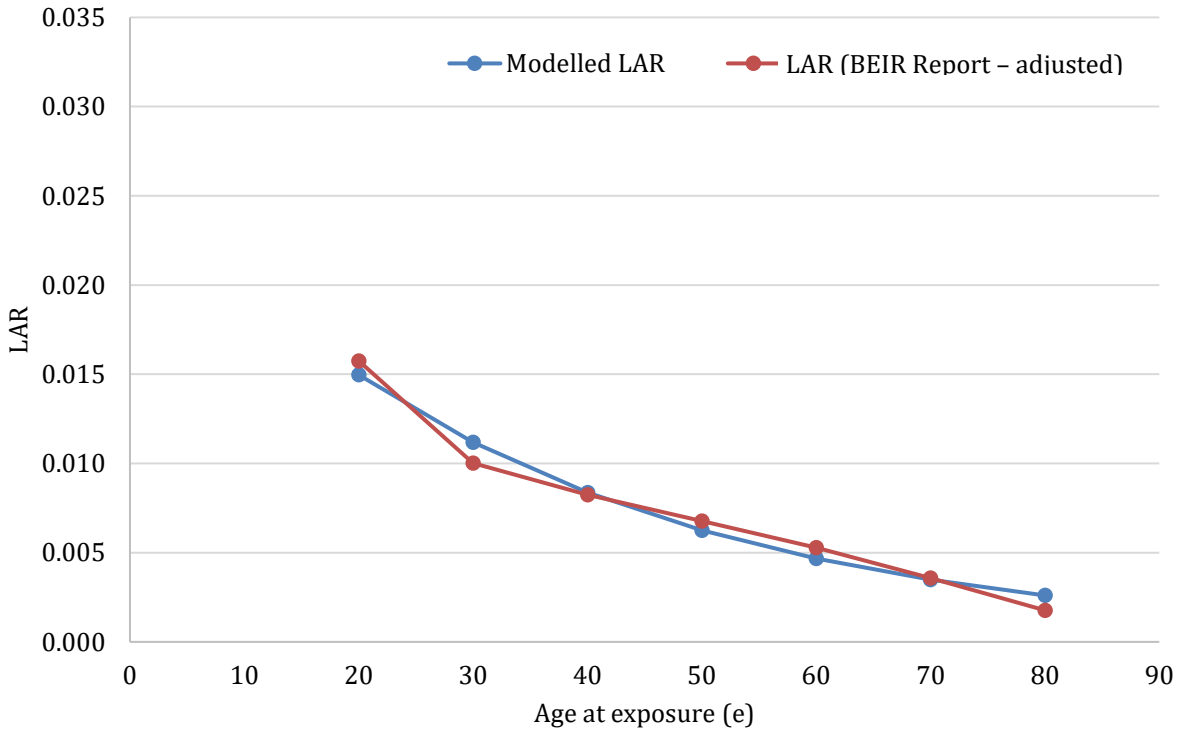


Figure 28: LAR for 0.1 Gy uniform single exposure, using LNT model (after calibration of λ.) and LAR from the BEIR VII report.

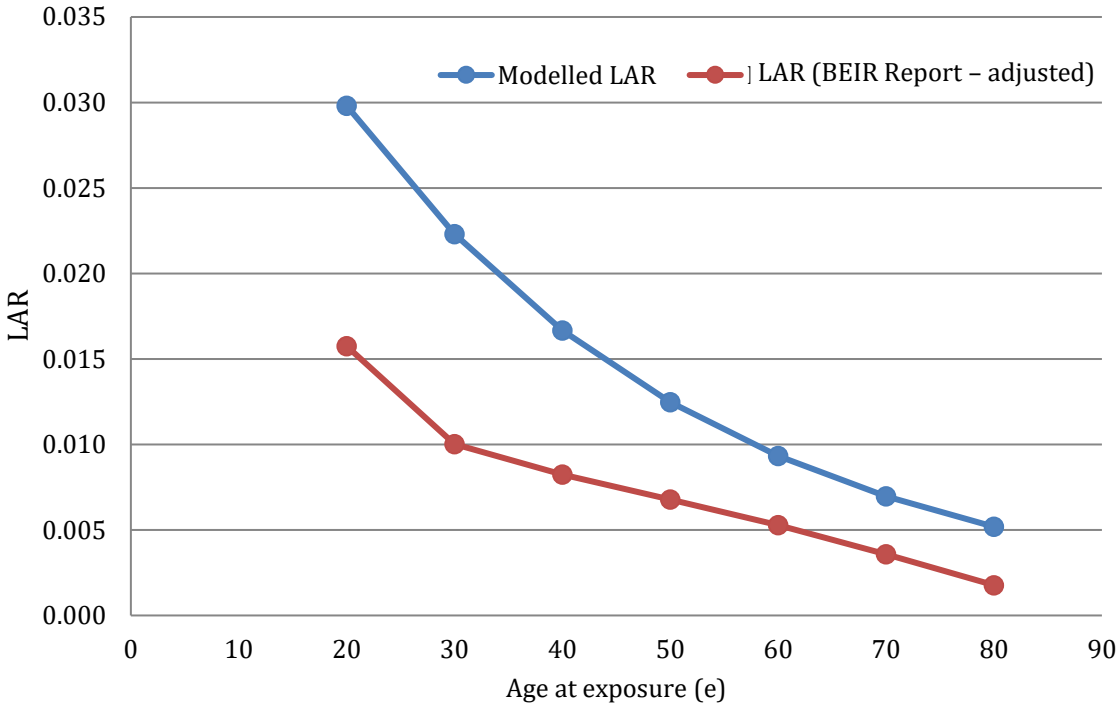


Figure 29: LAR after 0.1 Gy single exposure compared to the BEIR VII report values, before calibration of λ, using LIN model.

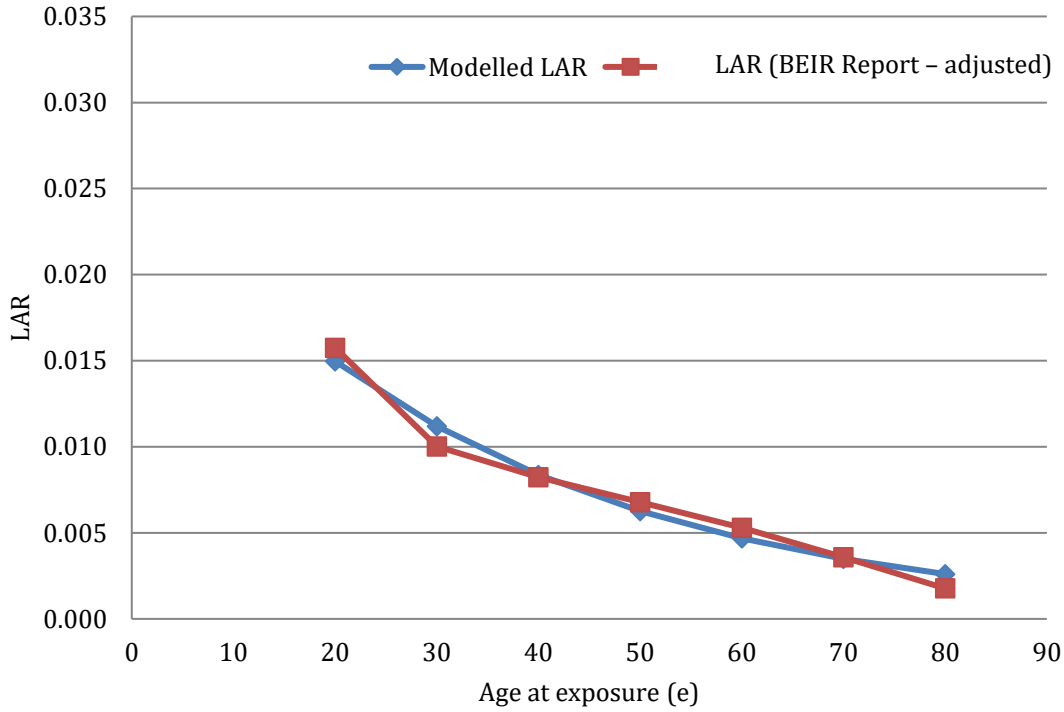


Figure 30: LAR for 0.1 Gy uniform single exposure, using LIN model, after calibration of λ, and LAR from BEIR VII report.

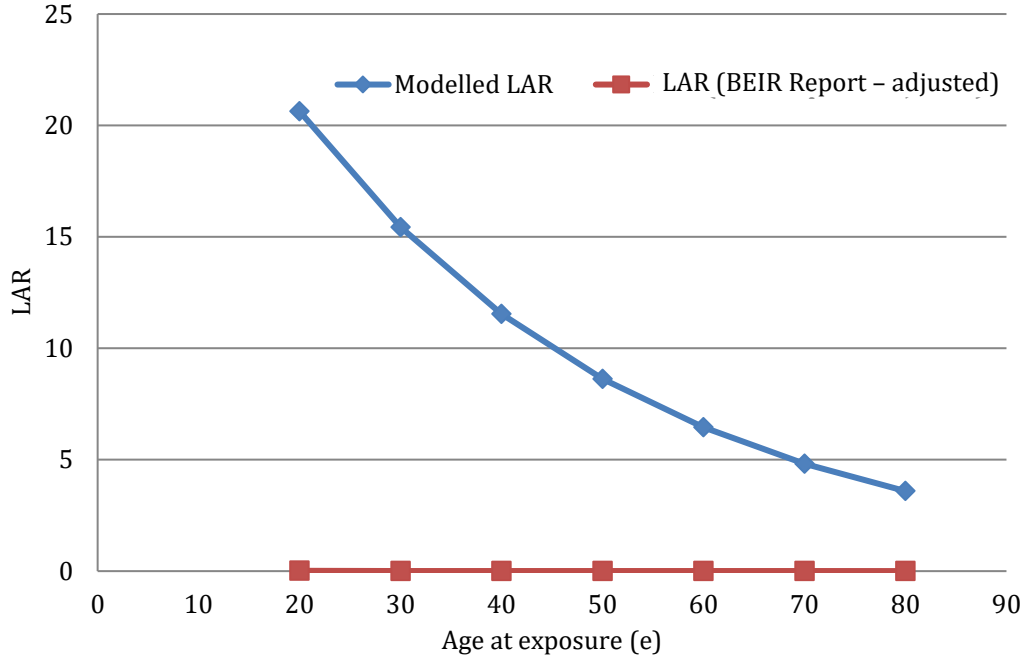


Figure 31: LAR after 0.1 Gy single exposure compared to the BEIR VII report values, before calibration of the model parameters of LQ model. LAR from the BEIR VII report is the same as shown in the above figures, but is not visible here is because the values generated by modelling LAR using non-calibrated parameters are large.

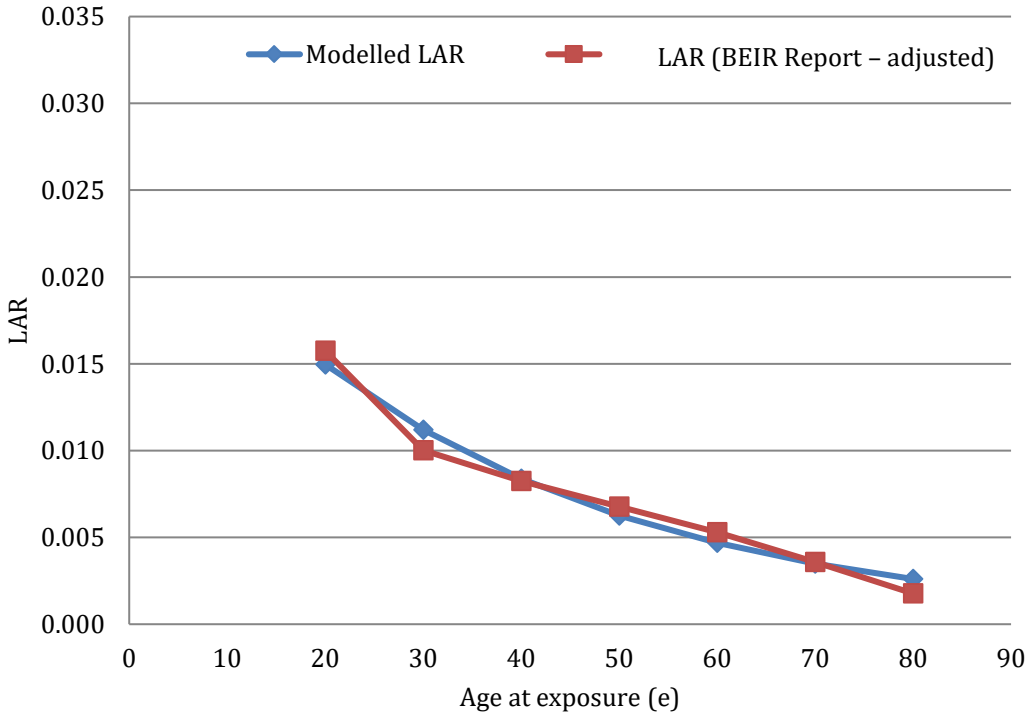


Figure 32: LAR for 0.1 Gy uniform single exposure, using LQ model, after calibration of LQ model parameters, and LAR from BEIR VII report.

The calibrated model parameters were subsequently used to the model EAR and LAR of the adult patient (Patient 1) following photon or proton treatment for all three models. The resulting EAR and LAR for the LQ, LIN and LNT models are shown in Figure 33- Figure 35.

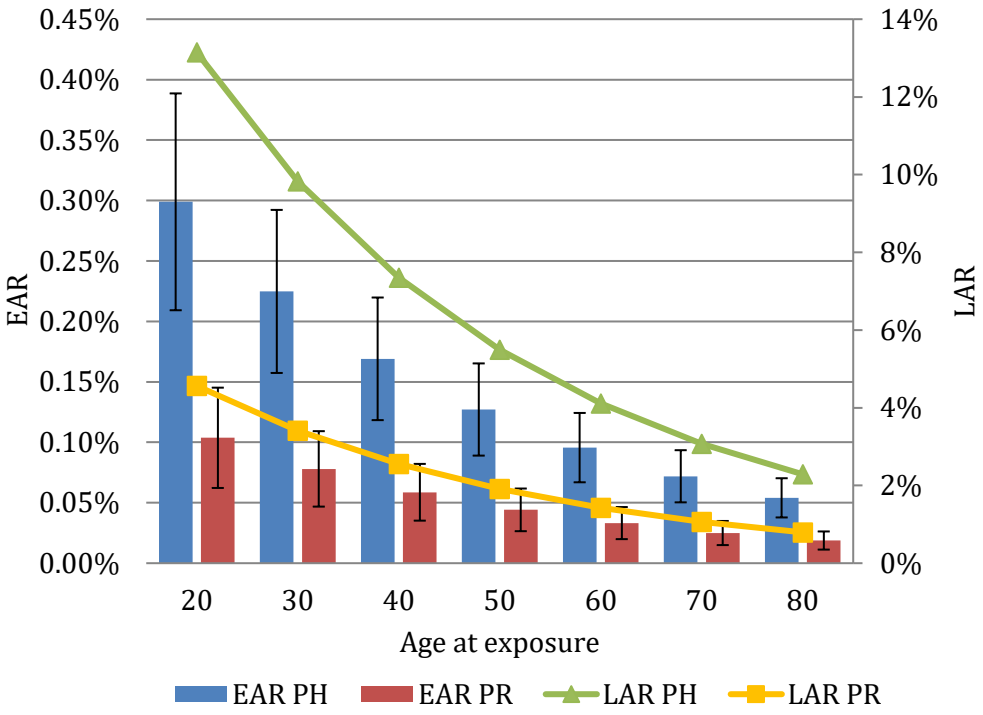


Figure 33: EAR and LAR for the adult (Patient 1) treatment plans (PH: photon plan, PR: proton plan) using LQ model, with varying age at exposure settings, using the calibrated model parameters. Error bars represent 1 standard deviation.

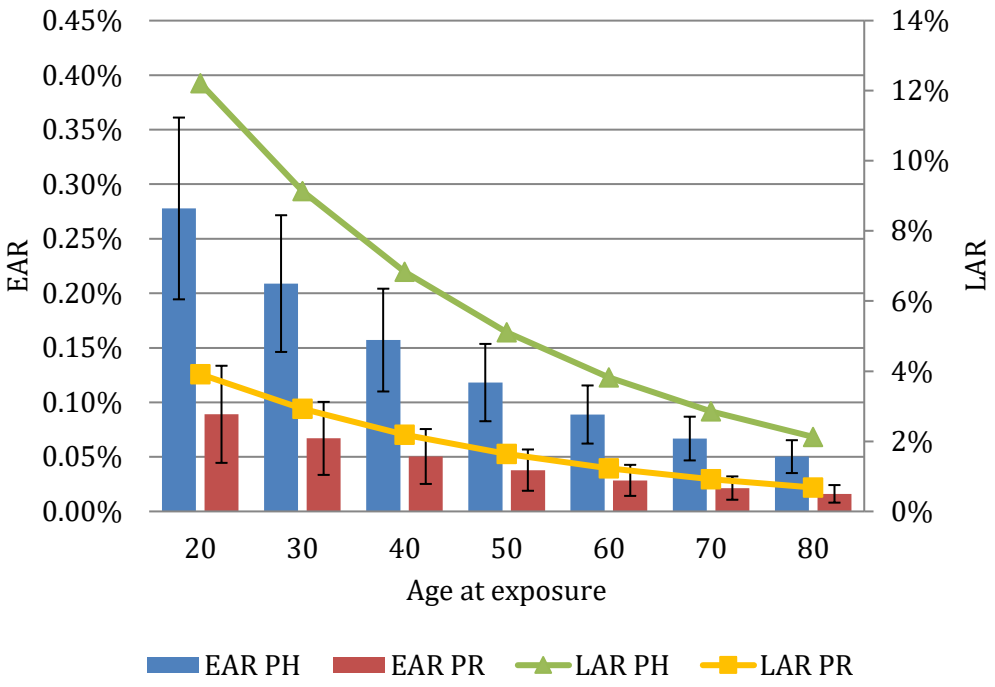


Figure 34: EAR and LAR for the adult (Patient 1) treatment plans (PH: photon plan, PR: proton plan) using LIN model, with varying age at exposure settings, using the calibrated model parameters. Error bars represent 1 standard deviation.

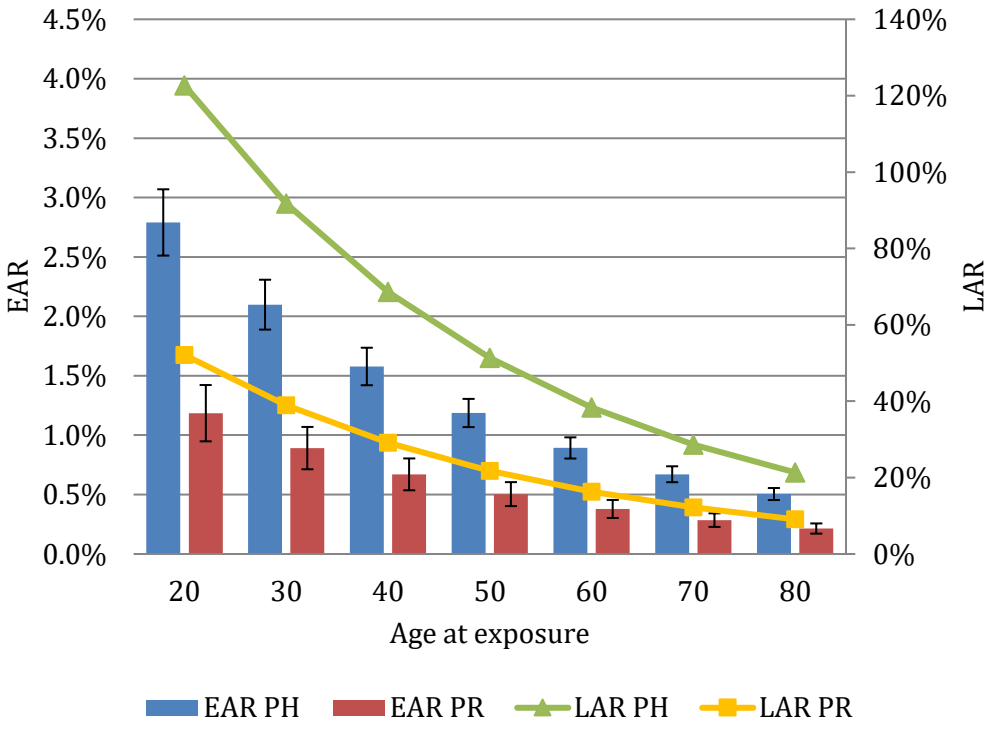


Figure 35: EAR and LAR for the adult (Patient 1) treatment plans (PH: photon plan, PR: proton plan) using LNT model, with varying age at exposure, using calibrated model parameter. Error bars represent 1 standard deviation.

The lower EAR and LAR (Figure 33 - Figure 35) associated with proton therapy further consolidates the initial conclusions from 4.1, namely that in medulloblastoma protons are superior than photons from secondary cancer risk point of view (Wilcoxon signed rank test: EAR PH vs EAR PR $P = 0.02$; LAR PH versus LAR PR $P = 0.02$, LIN: EAR PH vs EAR PR $P = 0.02$; LAR PH versus LAR PR $P = 0.02$, LNT: EAR PH vs EAR PR $P = 0.02$; LAR PH versus LAR PR $P = 0.02$). When similar methodology was applied to calculate EAR for younger patients (Patient 3-12) (Figure 36 and Figure 37), the difference in EAR between modalities is in agreement with that of Patient 1 which further reinforces the initial conclusions in sections 4.1 and 4.2 (Wilcoxon signed rank test: LQ model: $P = 0.002$, LIN model: $P = 0.002$). The relative relationship between EAR Photon and EAR Proton was also significant (one sample Wilcoxon test: LQ model: $P = 0.002$, LIN model: $P = 0.002$).

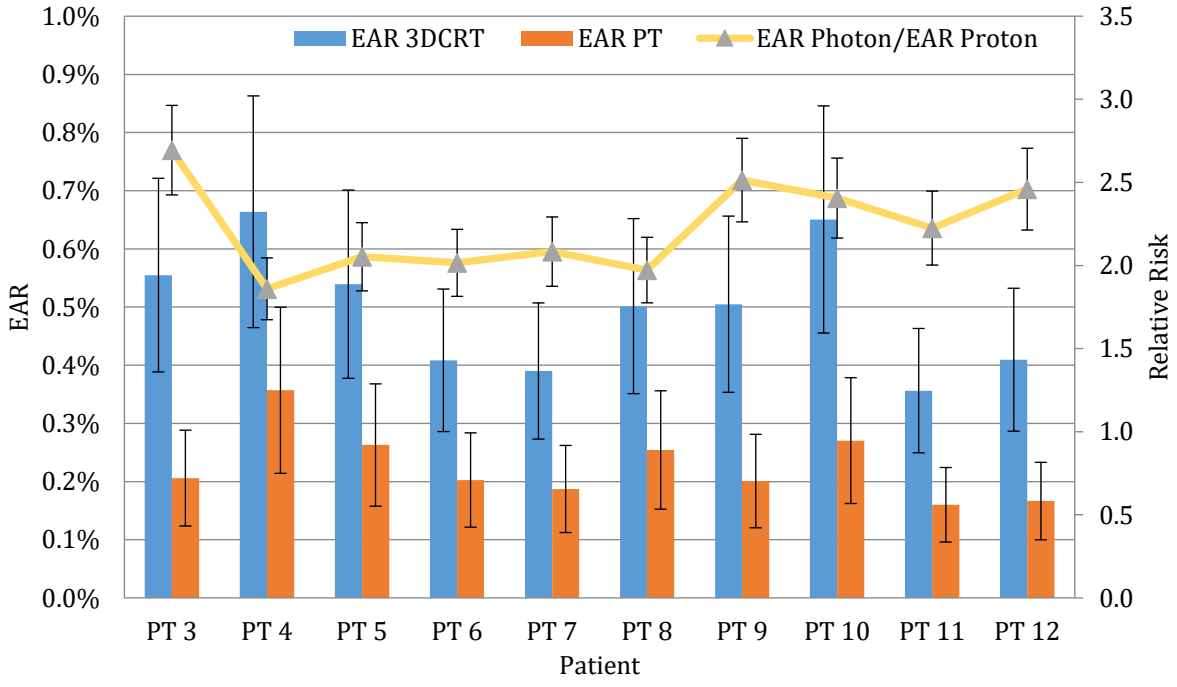


Figure 36: EAR for patients 3-12 radiotherapy plans calculated using LQ model with calibrated parameters. Error bars represent 1 standard deviation.

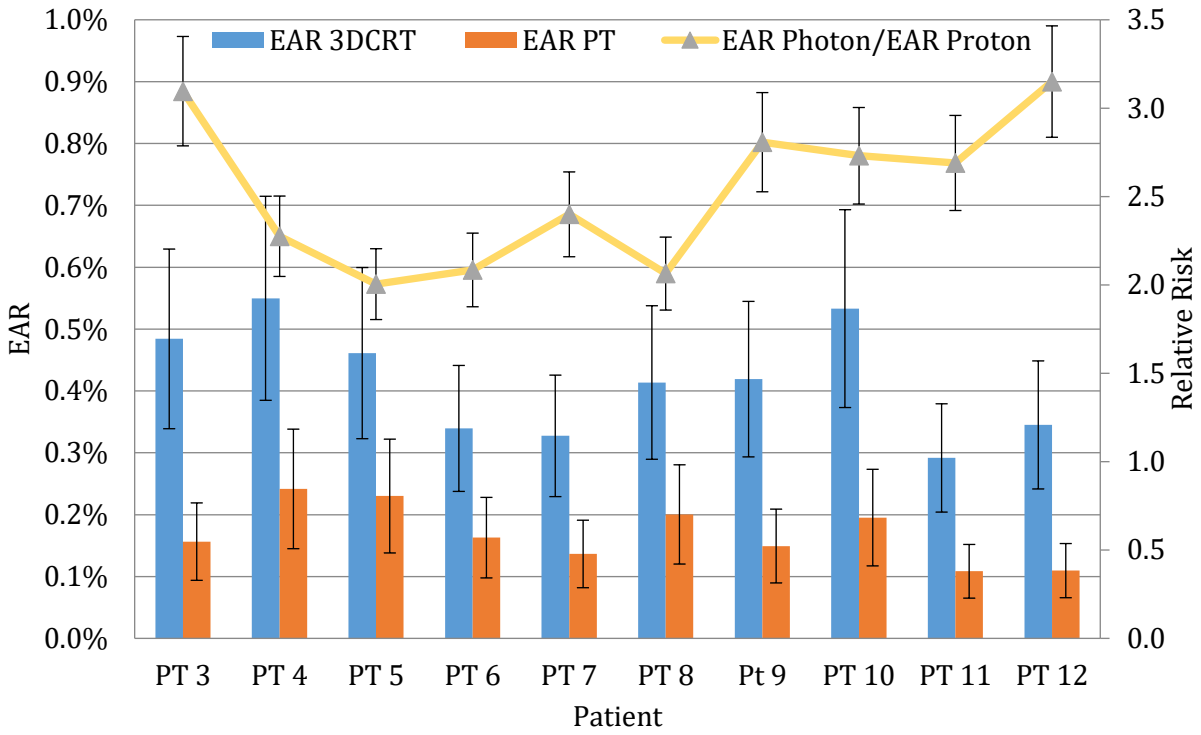


Figure 37: EAR for patients 3-12 radiotherapy plans calculated using LIN model with calibrated parameters. Error bars represent 1 standard deviation.

4.4 The effect of spatial dose averaging on prediction of malignant induction probability and secondary cancer risk

MIP calculated using mean dose for individual organs and structures is presented in this section and is compared to MIP calculated using VbV dose maps. The effect of using mean dose on $MIP_{Relative}$ is presented and described as well. As before, the uncertainty in the presented MIP and $MIP_{Relative}$ values was determined as detailed in section 4.2.3

4.4.1 Whole body

Figure 38 and Figure 39 show the MIPs obtained using the mean dose and VbV dose maps for the 3DCRT and proton plans using the LQ model, as well as the $MIP_{MeanDose}$:MIP_{VbV} ratio which is consistently greater than 1. Figure 40

shows the corresponding $MIP_{Relative}$ values for both the mean dose and VbV calculations, with these relative MIP values being consistently less when calculated using mean dose approach, but still all above 1. Figure 41 and Figure 42 show MIPs using LIN model, and Figure 43 shows MIP Relative for the plans using mean dose for individual organs and structures dose and using VbV maps.

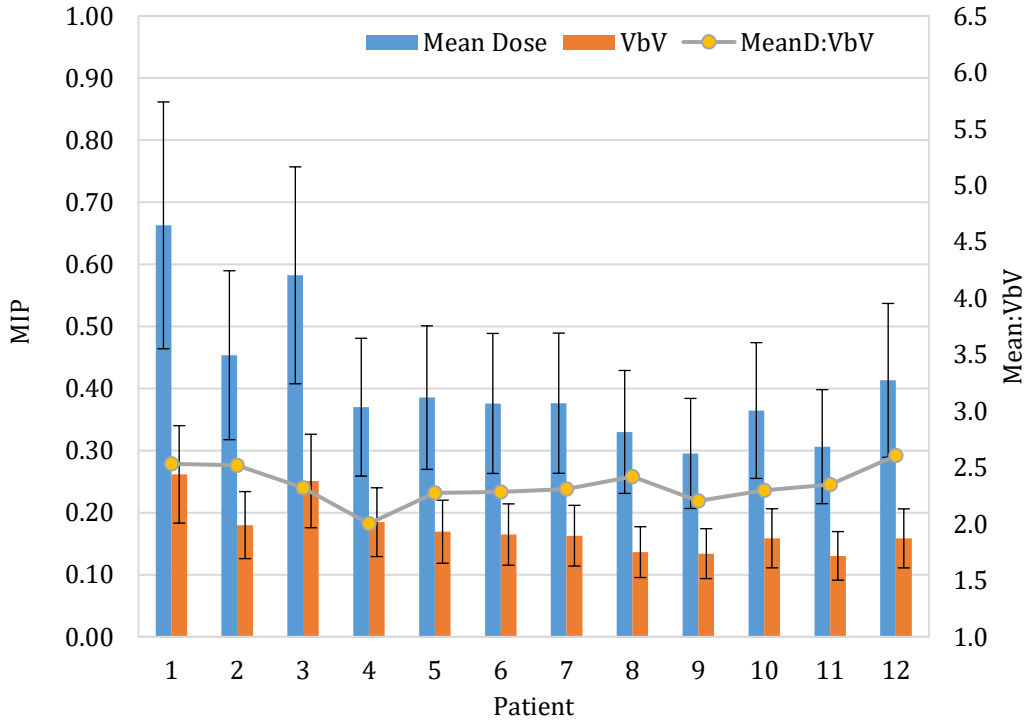


Figure 38: Whole body MIP for the 3DCRT plans using LQ model, calculated using mean dose and VbV dose maps.

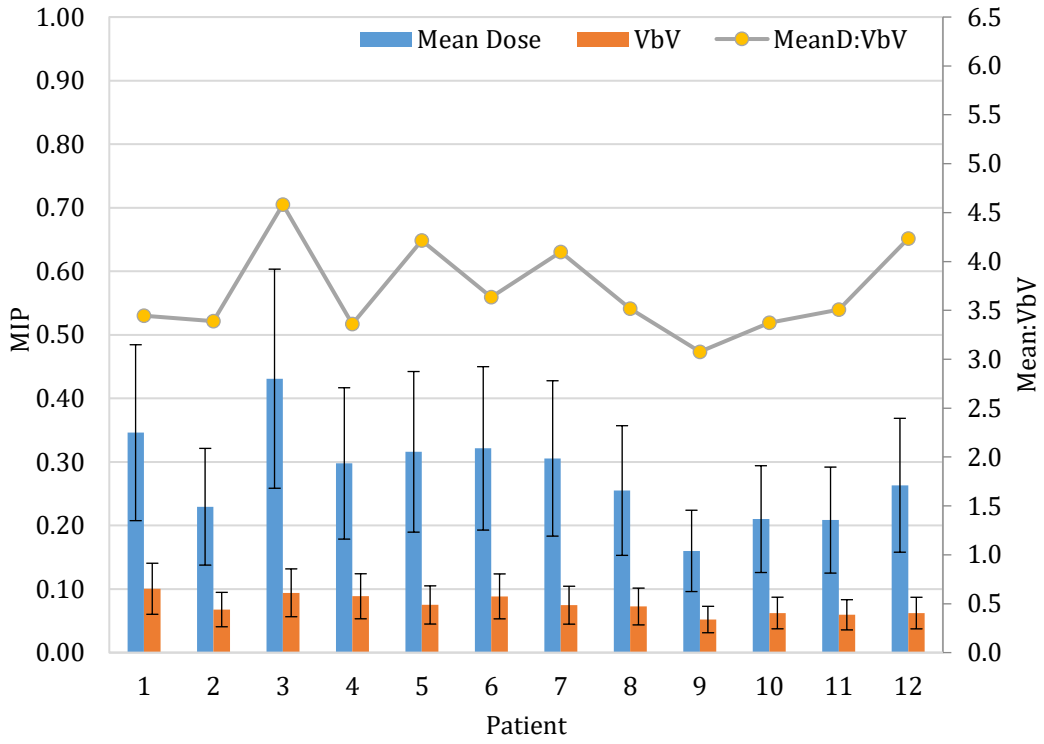


Figure 39: Whole body MIP for the Proton plans using LQ model, calculated using mean dose and VbV dose maps.

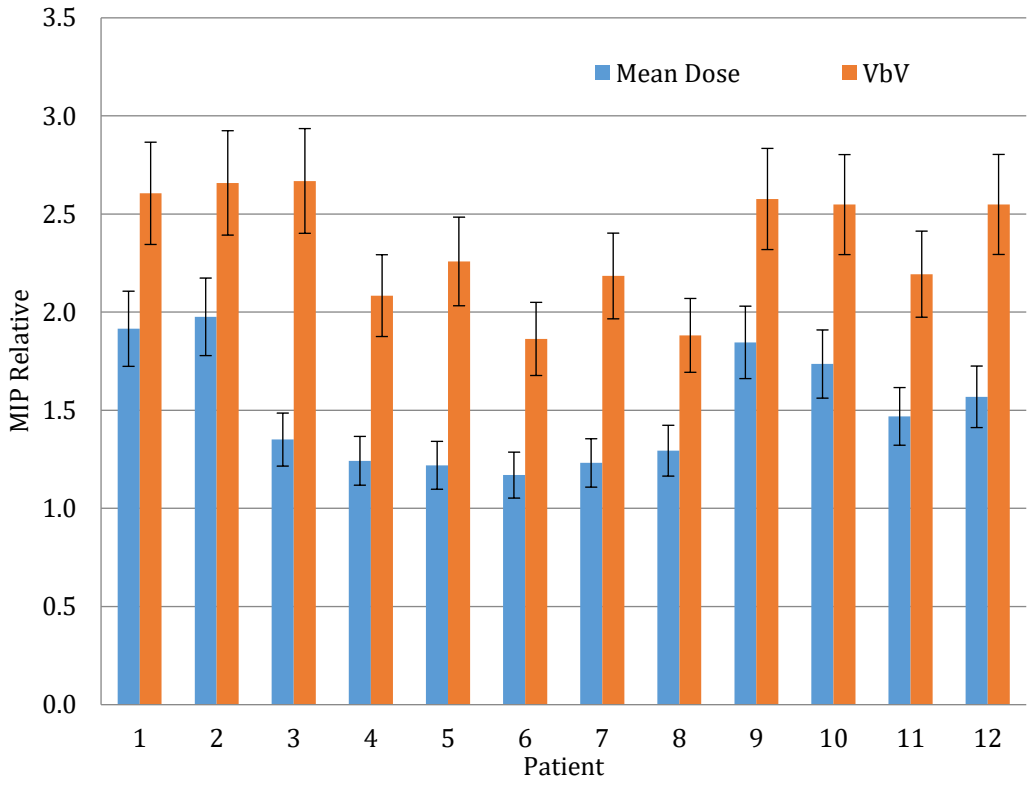


Figure 40: $MIP_{Relative}$ using LQ model for mean dose and VbV dose maps.

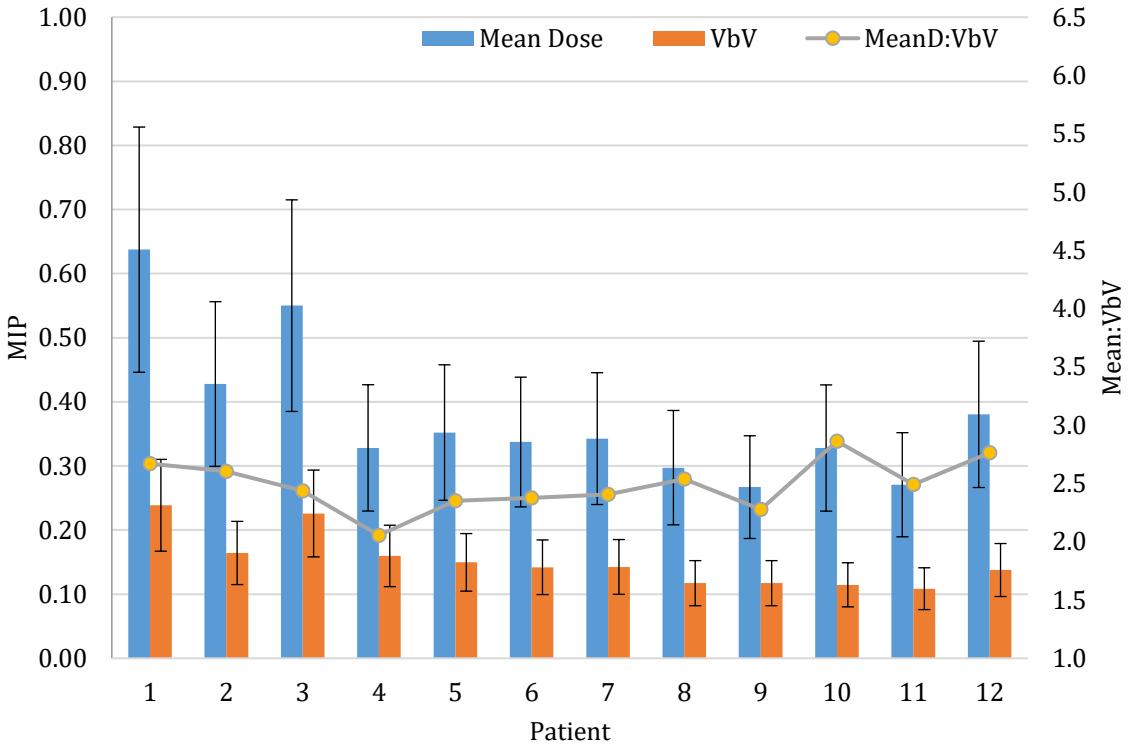


Figure 41: Whole body MIP for the 3DCRT plans using LIN model, calculated using mean dose and VbV dose maps.

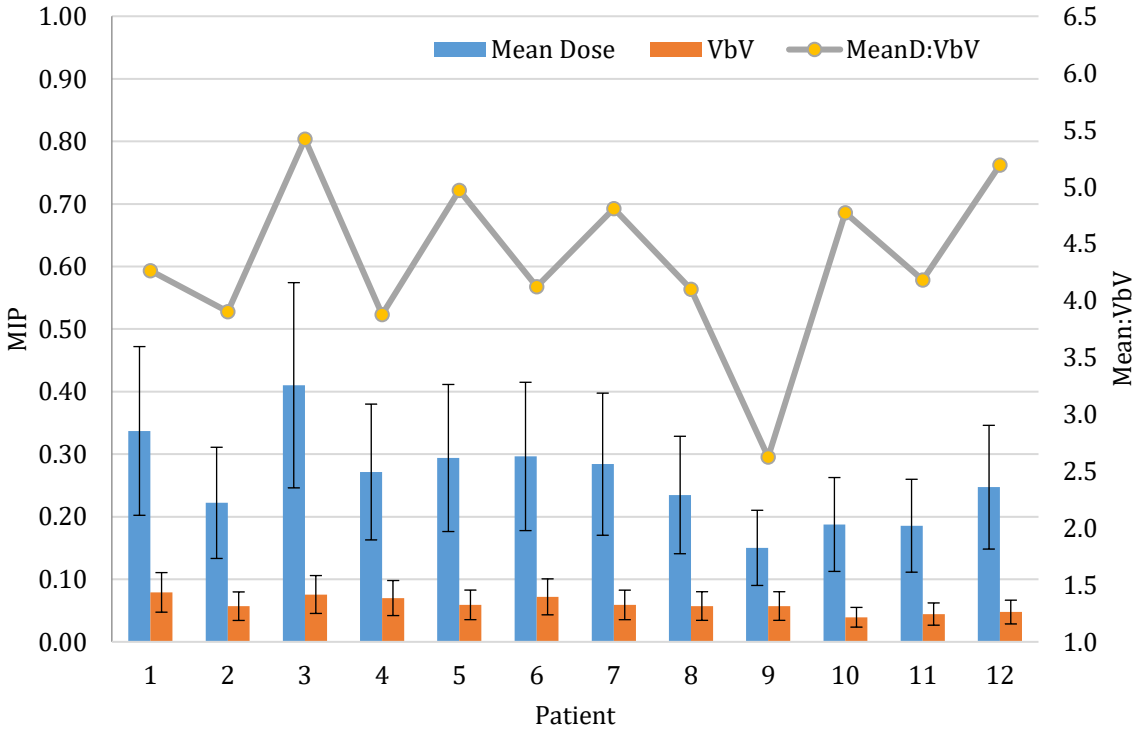


Figure 42: Whole body MIP for the Proton plans using LIN model, calculated using mean dose and VbV dose maps.

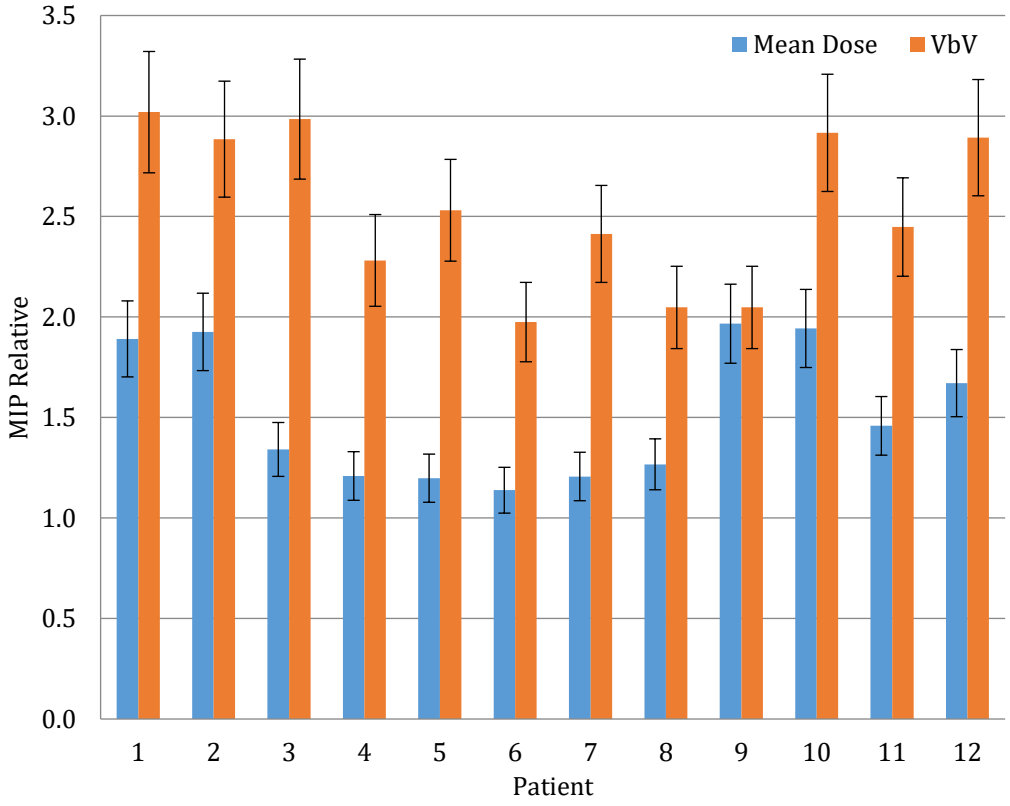


Figure 43: $MIP_{Relative}$ using LIN model for mean dose and VbV dose maps.

Use of mean dose resulted in a higher whole body MIP than the one modelled using VbV dose maps for the LQ model and the LIN model MIPs when used for the photon plans (LQ: $P = 0.002$, LIN: $P = 0.002$), due to underestimation of the effect of cell killing which would occur in the high dose regions.

Moving on to the proton plan, similar observations were made. Use of mean dose gave a higher MIP than using the VbV dose maps, with the differences being even larger than those observed for the 3DCRT plans (LQ: $P = 0.003$, LIN: $P = 0.002$). The higher MIP predicted by the use of the mean dose model calculation further illustrates the non-linear nature of MIP modelling using the LQ and LIN models.

Figure 40 and Figure 43 illustrate the $MIP_{Relative}$ when using mean dose in calculating MIP as well as that when using VbV dose maps. For whole body MIP, and for the models used here, and using mean dose, the photon plan will produce a higher MIP than the proton plan (LQ: $P = 0.002$, LIN: $P = 0.002$). The central observation noted in the earlier parts of this thesis still holds here: proton therapy is less likely to induce secondary malignancies than photon therapy, even with using mean dose to model MIP.

4.4.2 Organ Specific MIP

The variation in the calculated organ specific MIP values for 8 individual organs is shown in Figure 44 for both photon and proton plans of Patients 1 and 2. The figure compares the values calculated using the mean dose to the organ to those obtained using the VbV dose maps; the ratio between the two (MIP_{MD}:MIP_{VbV}) is also presented. The differences in absolute values between the two patients relate to difference in the individual treatment plans and associated dose to the organs.

The brain, an organ with homogenous high dose in both the photon and proton plan, and the bladder with homogeneous low dose, both show that the difference in MIP calculated using MD or VbV is not as large as the difference for the whole body (Figure 44). It is interesting that the MIP_{MD}:MIP_{VbV} ratio for the brain results in a value less than 1, this would suggest that the high average dose to brain results in a reduction in MIP due to a resulting lower SF as more voxels will be assigned a higher dose that what they are assigned in the VbV approach, which would include regions where the dose is such that the SF is higher.

The organs with high inhomogeneity, such as the lungs for example, show a distinct pattern. The lung in the photon plan receives a relatively high dose to a relatively small volume, the difference in MIP between the MD and VbV is more in line with that of the whole body. The difference across the organs below showed a significant overall difference (P = 0.003).

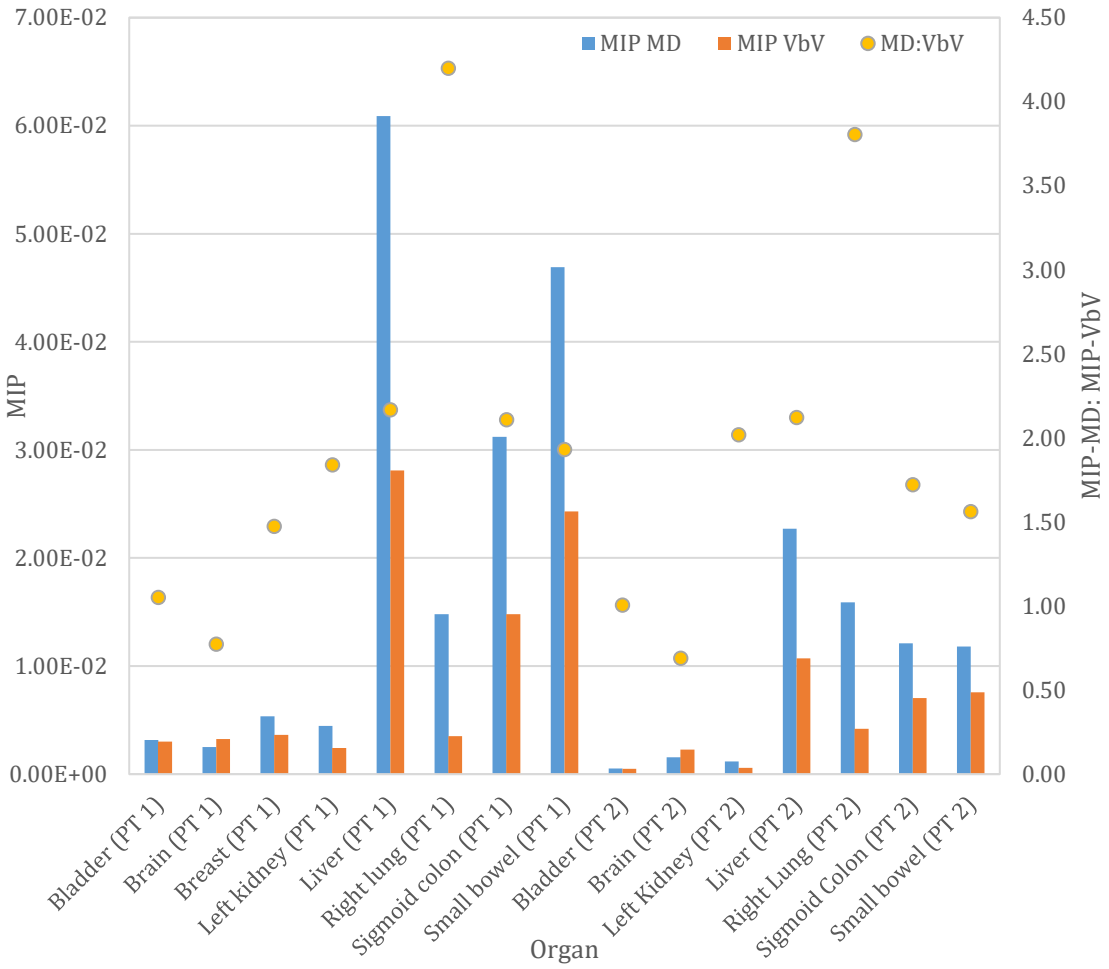
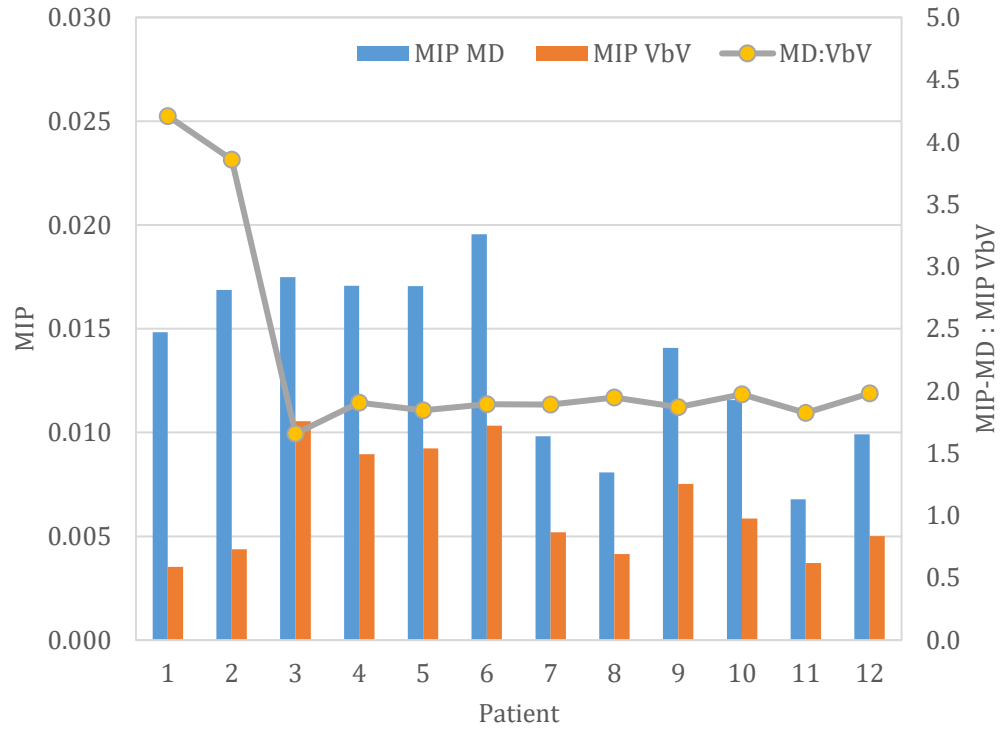


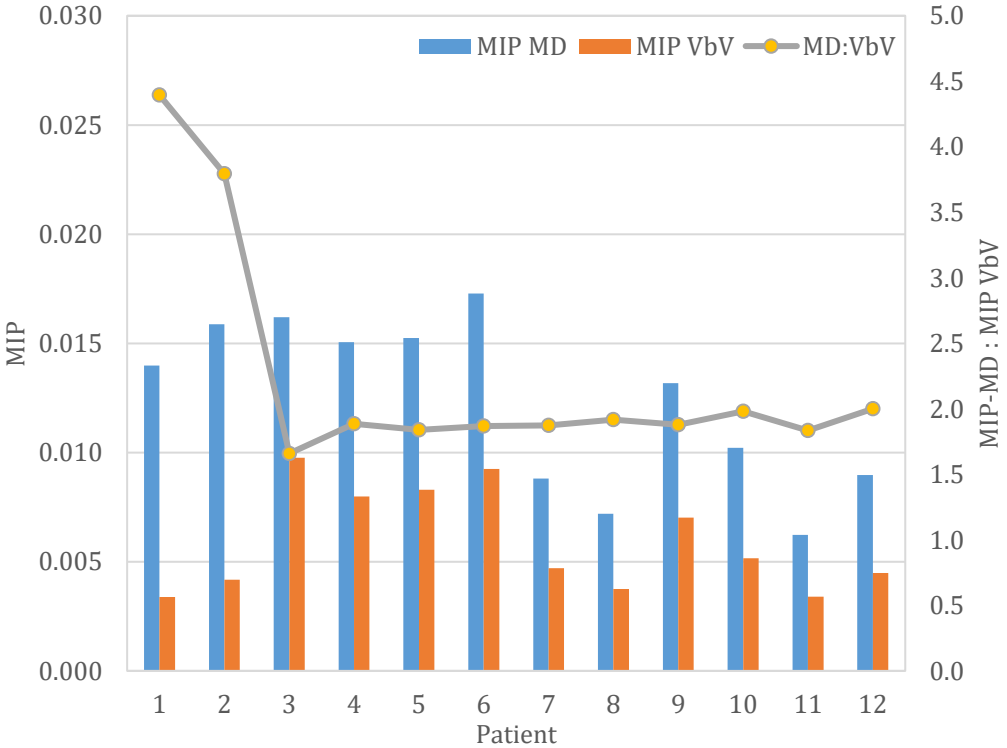
Figure 44: Organ-specific MIP for a number of selected organs from the 3DCRT plans of Patient 1 (PT 1), calculated using LQ model, and Patient 2 (PT 2) calculated using the LIN model with mean dose (MIP MD) and VbV dose maps (MIP VbV) for each organ.

Looking closer at two structures, the lung and the thyroid, the impact of the dose distribution in these selected organ becomes apparent. The right lung, a structure with a dose gradient in the 3DCRT plans would has an MIP that is significantly different when calculated using its mean dose (MIP MD) when

compared with the MIP calculated using VbV dose maps (MIP VbV) as shown in Figure 45 (LQ: $P = 0.002$, LIN: $P = 0.002$). In comparison, a closer look at the thyroid, a small organ, with nearly uniform dose, shows that there is no significant difference in MIP whether it is calculated using MD or VbV (Figure 46).

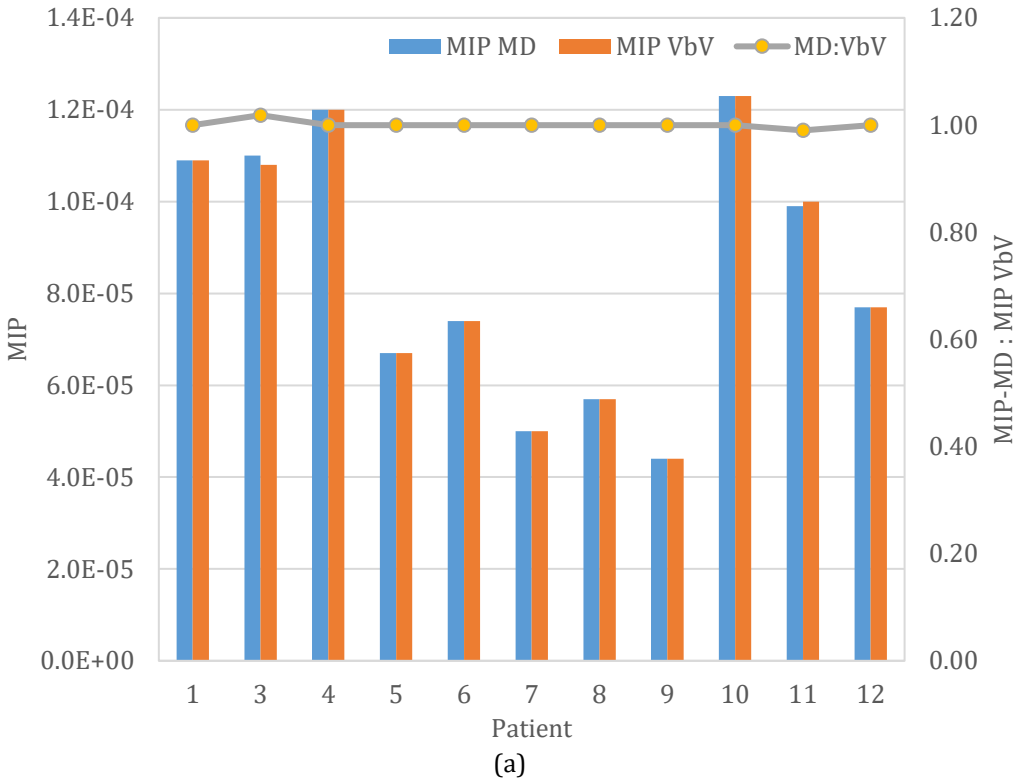


(a)

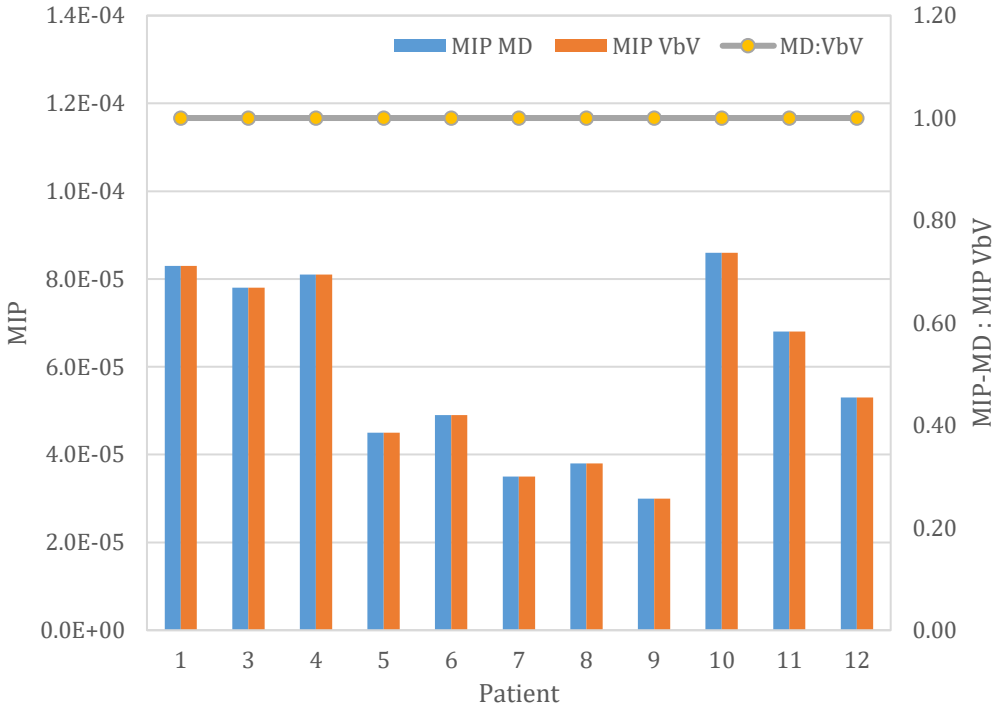


(b)

Figure 45: MIP for lung for the 3DCRT plans of the 12 patients, calculated using mean dose (MIP MD) and VbV dose maps (MIP VbV) for the LQ model (a), and LIN model (b).



(a)



(b)

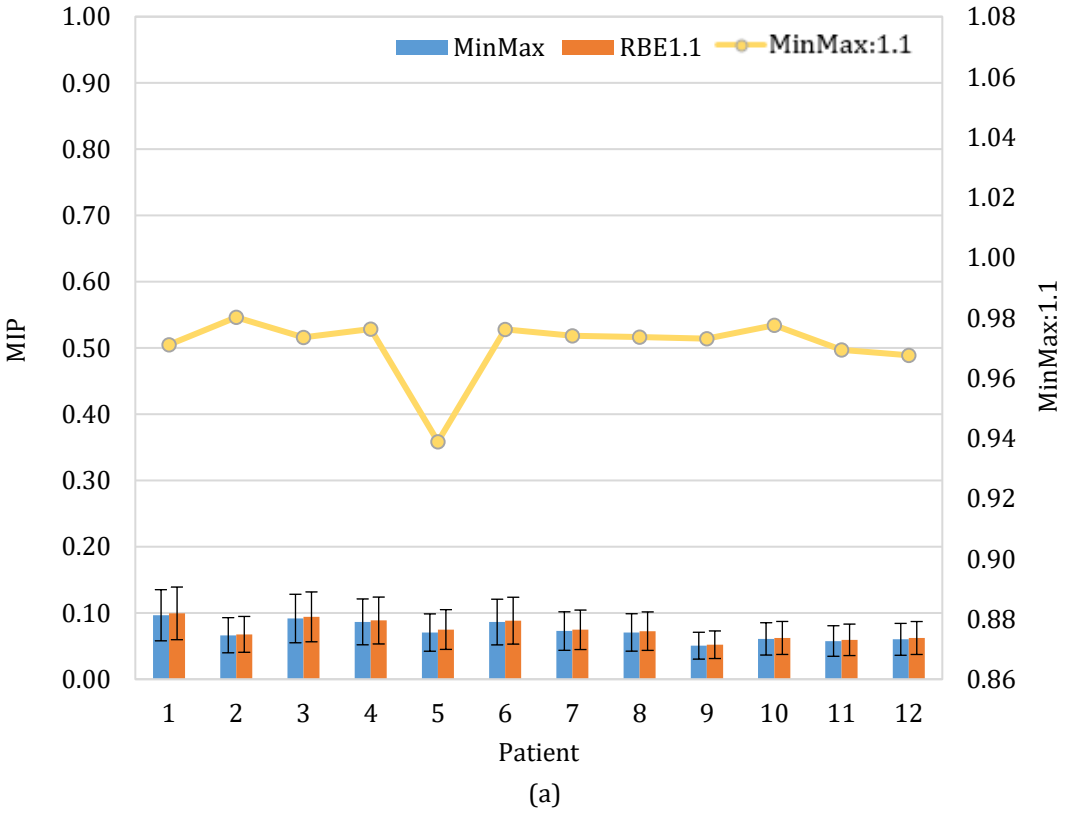
Figure 46: MIP for thyroid for the 3DCRT plans of the 12 patients, calculated using mean dose (MIP MD) and VbV dose maps (MIP VbV) for the LQ model (a), and LIN model (b)

4.5 Effect of radiobiological effectiveness on modelling malignant induction probability and dose calculation

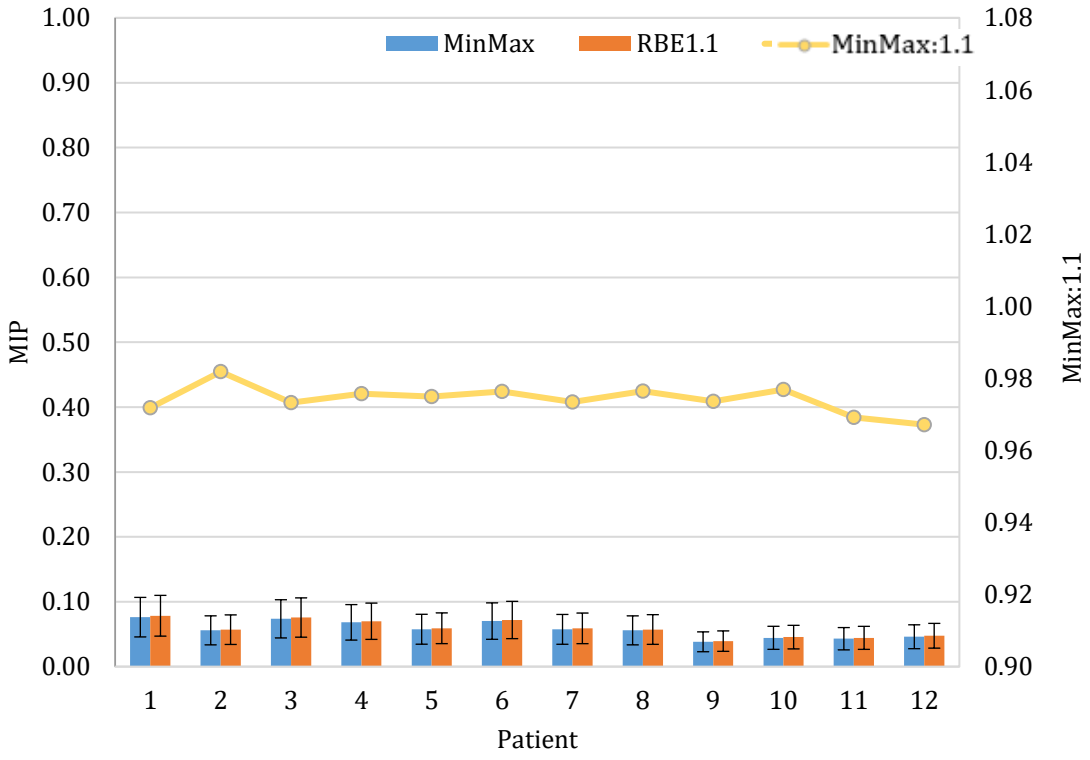
In this section, MIP for proton plans using an RBE of 1.1 are compared to MIP based on an RBE calculated using the RBE_{MinMax} model presented earlier (3.5.1.2), with the uncertainty in the presented MIP and $MIP_{Relative}$ values calculated as shown in section 4.2.3. The effect of including LET on RBE calculation and dose is also presented. The Wedenberg model is used to explore the potential effect of LET on RBE for tissues with different α/β ratio.

4.5.1 Modelling MIP for medulloblastoma cases

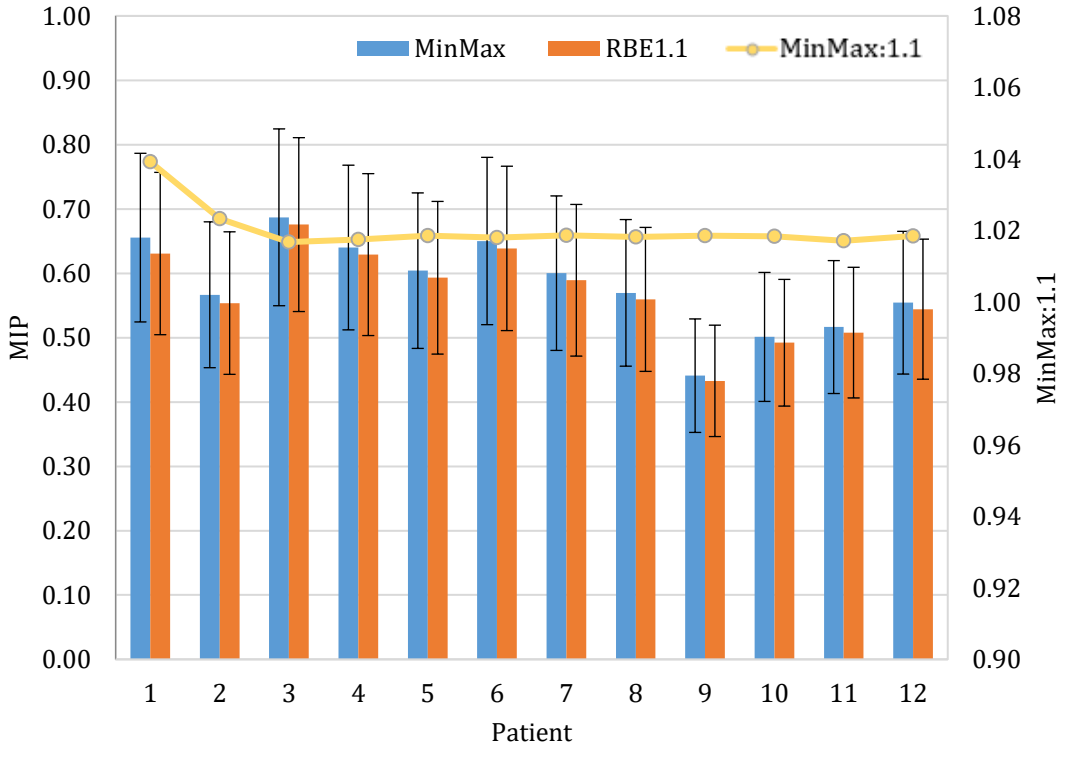
The MIP values generated through use of RBE_{MinMax} and $RBE_{1.1}$ are illustrated in Figure 47 for all 12 patients and the three different models. The difference in MIP when using $RBE_{1.1}$ versus RBE_{MinMax} is ~1-6%. The dose variations for selected structures are illustrated in Figure 48.



(a)

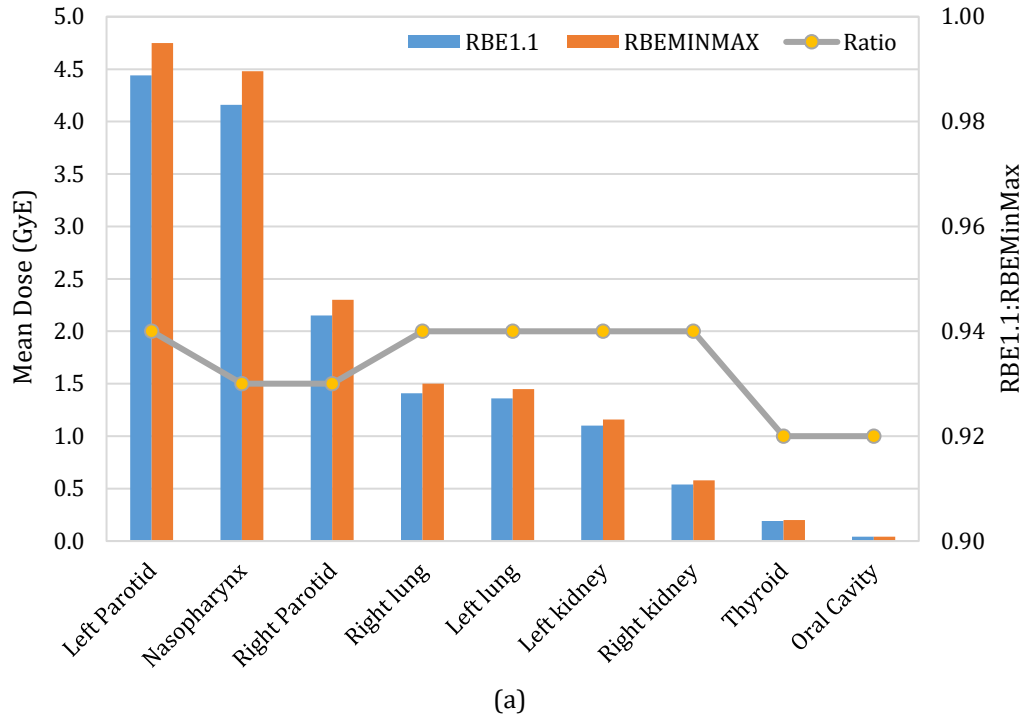


(b)

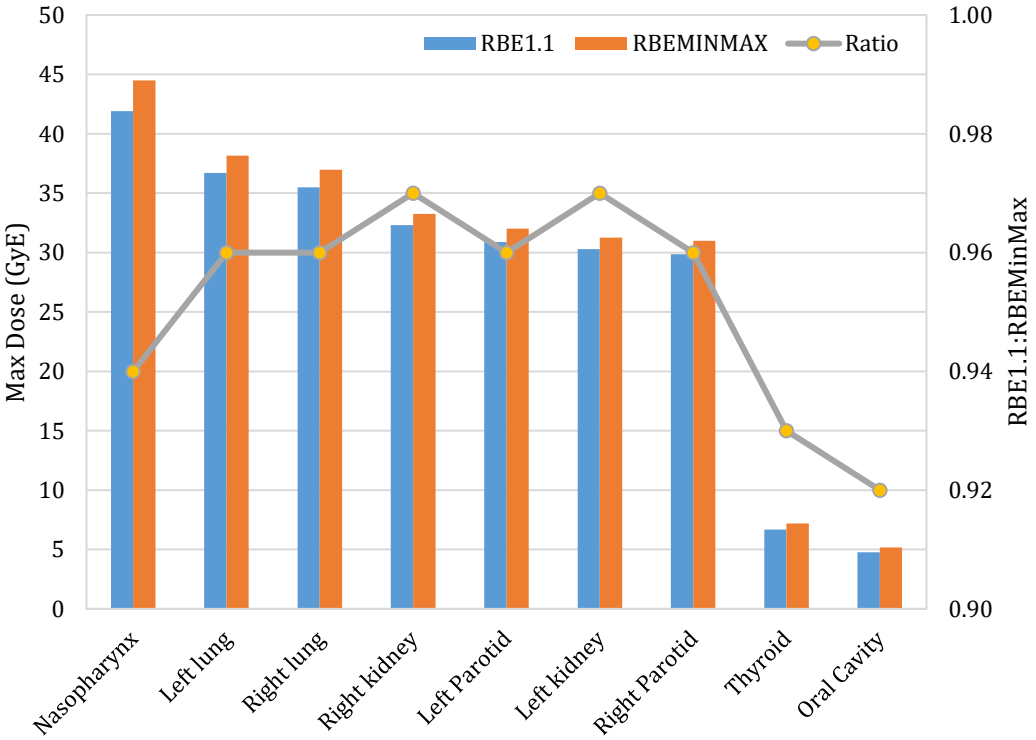


(c)

Figure 47: Whole body MIP for the patients calculated using RBE of 1.1 ($RBE_{1.1}$) or RBE_{MinMax} for the LQ model (a), LIN (b), and LNT (c). Error bars represent 1 standard deviation.



(a)



(b)

Figure 48: Mean dose (a) and maximum dose (b) for selected organs with using RBE of 1.1 and RBE using MinMax model.

In the case of medulloblastoma, and with the use of RBE_{min} of 1.05 and RBE_{max} of 1.20, the effect of RBE on absolute MIP values using this RBE model can be relatively small compared to the overall uncertainty in MIP estimates (LQ: $P = 0.003$, LIN: $P = 0.02$, LNT: $P = 0.002$).

Looking into some organ-specific MIP using the RBE_{MinMax} and $RBE_{1.1}$, patterns change according to the dose heterogeneity of the selected structure and its location in relation to the distal end of the proton beam.

The effect of using a fixed RBE of 1.1 or the RBE_{MinMax} model on mean dose varies between different organs and is between 5.5% and 8.2%. Clinical implications due to difference in RBE depend on beam characteristics, dose, structures concerned, and the volume irradiated. The difference in mean dose was significant ($P = 0.01$), as it was for the maximum ($P = 0.004$).

4.5.2 RBE modelling using Wedenberg model

The RBE was modelled using input parameters of LET of 8.5 KeV/µm, and a dose of 2.0 GyE, and range of α/β was used to demonstrate how different the dose would be. The results can be found in Figure 49. Tissues with low α/β ratios, mostly associated with some types of normal tissues, would be the tissues with highest RBE using this model. The opposite applies to tissues with high α/β ratios. Those tissues (tissues acutely reacting to radiation, and tumour tissues) would be the tissues with lowest RBE using this model.

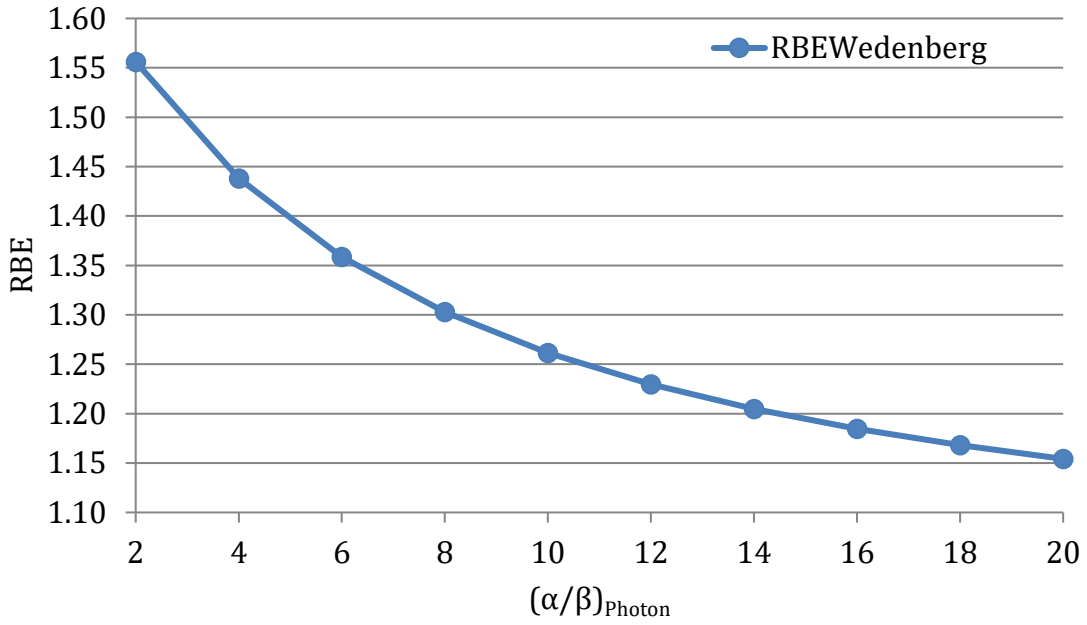


Figure 49: RBE calculated with the Wedenberg model using different $(\alpha/\beta)_{Photon}$ values.

5 Chapter 5: Discussion and Conclusions

Secondary cancer incidence and mortality are expected to continue to increase as advances in oncology result in prolongation of survival of many groups of cancer patients (Woodward *et al*, 2011). The clinical focus in many tumour sites, breast and prostate for instance, has therefore been shifting to the avoidance or elimination of long-term side effects, including secondary cancer. This is particularly relevant for younger patient cohorts with a good prognoses as they are expected to have a longer life expectancy and younger patients, especially children, are also known to be more sensitive to radiation-induced cancer. The advent of new treatment modalities, such as IMRT and particle therapy is helping to drive this increase in cure rates. While greater conformity of dose to the tumour can be achieved using techniques such as IMRT, this is at the expense of an increase in beam-on time resulting in an increase in overall volume of normal tissue receiving a modest dose (Hall E, 2006). In principle, Proton therapy can overcome this drawback since it can improves dose conformity to treatment volumes while reducing out-of-field dose to normal tissue and volume irradiated. It is this reduction in exposure of tissues outside the tumour volume that is the main driver behind the potential reduction in late effects and secondary cancer risk for proton therapy compared to photon therapy treatment.

The improved dose conformity to the tumour volumes and reduced normal tissue dose that proton therapy provides can also help in dose escalation, improve organ sparing, and can lower or eliminate dose to organs at risk. Proton therapy, however, carries some uncertainties including the question

of the associated RBE (Paganetti & Giantsoudi, 2018), the sensitivity of proton beam to variations in the density of the medium through which it passes resulting in range uncertainties (Paganetti H, 2012), positioning effects due to patient setup error, and the neutron dose in passive scattered proton therapy and, to a lesser degree, in actively scanned proton therapy (Hall E, 2006). Some argue that, in certain cases, proton therapy does not provide a sufficient dose reduction to justify its use. The capital cost of proton therapy facilities and treatment cost remains high. Hence different centres have different protocols and guidelines to facilitate clinical decision-making on the use of proton therapy (Langendijk *et al*, 2013).

The main focus of the work presented in this thesis is the variation in malignant induction probability and secondary cancer risk associated with the choice of treatment modality (photon vs proton) for a given patient. This represents the first step towards a system that could be used to inform the selection of proton therapy or photon therapy in a specific clinical situation. Specifically this has involved:

- Calculation of MIP using three different models (LQ, LNT and LNT) applied to photon and proton treatment plans for 12 medulloblastoma patients.
- Investigation of the robustness of these results with respect to the inherent uncertainty in the underlying parameters.
- Benchmarking and calibration of the results against BEIR VII report data to obtain lifetime absolute risk (LAR) and excess absolute risk (EAR).

- A comparison of the differences in calculated MIP when mean dose for individual organs is used versus the voxel-by-voxel dose map approach.
- Investigation of the effect of modelling the variation in RBE (compared to a constant value of 1.1) with dose using the RBE_{MinMax} model, along with the impact of differences in the α/β ratio for normal tissue on RBE.

The choice of which treatment modality or plan to select is informed by comparing risk estimates of secondary cancer risk associated with each modality (relative risk) and based on this information a treatment decision can be made.

The estimation of risk is based on a range of models that vary in robustness and whose dose-response curves differ in shape. Some of these models are based on the data provided from the LSS cohort; a large population that has been followed up for a long period of time after acute exposure to a range of doses (Ozasa *et al*, 2012) that are considered low compared to doses used in radiotherapy. Other models are based on follow-up of patients, including those with breast cancer, Hodgkin's disease, and prostate cancer (Travis *et al*, 2008, Gilbert E S, 2014, Dores *et al*, 2002 – see introduction chapter, section 1.3). The patients in these cohorts have generally been treated with what would now be considered to be outdated techniques that are now rarely used in clinical practice. These older treatment protocols are associated with markedly different dose profiles to some of organs of interest.

The relative relation between MIP of photon and proton therapy depends on the type of cancer being considered, and by association, the details of the treatment plan. The relative relationship between risk of induction of malignancy by photons versus protons for an individual patient depends mainly on the dose difference between the modalities.

The research conducted and presented in this thesis has resulted in several findings that are detailed in the following sections. Some of the findings are common across different sets of experiments and answer some of the questions laid out in section 1.9. Firstly, although the magnitude of the difference varies, MIP_{Photon} is always larger than MIP_{Proton}. The work also illustrated that $MIP_{Relative}$ is always larger than 1 even when large parameter uncertainties are included. The uncertainty in the radiobiological parameters used in the models has no impact on the relative relationship between photon and proton therapy for medulloblastoma, but can alter its magnitude. This is true except when both MIP_{Photon} and MIP_{Proton} trend to value of 1 if the assumed parameter value of λ is significantly increased. The different models produce different MIPs for same plan, due to the different underlying mathematical bases that represent different assumptions about the mechanisms of MIP. Additionally different patients have different MIP, mostly due to variation in size, which can be a result of age and sex. Finally, while it might be expected that protons would be better than photons with respect to malignant induction in the case of medulloblastoma, due to clearly superior proton dose distributions resulting in significant dose sparing in normal tissue. This is not necessarily the case for other sites and treatment

plans where dose sparing is not as obvious or not as significant, this could potentially lead to a different outcome with photons being better than protons, or at least as good.

5.1 Modelling of MIP after Proton and Photon Therapy

The results presented in section 4.1 clearly show that the calculated MIP values for the photon plans were consistently greater than the corresponding proton plans'. This was true for all 12 medulloblastoma patients, regardless of which of the three models was used (Figure 13), with the relative MIP value ($MIP_{Relative}$: 1.20-3.02) significantly greater than 1 across all models. Therefore in the case of medulloblastoma, proton therapy is consistently superior to photon therapy with respect to the risk of induction of malignancy. Similar observations where made when calculating specific organ-specific MIP values for the thyroid and lung (Figure 14 and Figure 15). Although based on only a relatively small group of patients, the outcome is robust because the use of different models and/or parameter values did not alter the risk ranking for any of the patients, and therefore gives confidence in the *relative* outcome value, which has a level of uncertainty substantially lower than that of absolute outcome values. As previously reported, relative values can decrease the uncertainty to about 10%, when compared to studying absolute values which can carry an uncertainty of 100% (Nguyen *et al*, 2015, Fontenot *et al*, 2010).

Looking at the MIP values presented in this thesis (Figure 13), the absolute values of MIP differ from one model to another for the same treatment modality by as much as a factor of 6, signifying how using different models

can markedly affect the MIP. The relative MIP values range between 1.26 and 3.02 (Figure 13). Having said that, the wide range of MIP values observed for each patient (using different models) makes it clear that further work is needed to produce useful absolute risk predictions by calibration and benchmarking, and to determine whether the mathematical form has any useful mechanistic interpretation. In order to do so, comparison with other sources of cancer-induction data is necessary, including the Life Span Study of the Japanese bomb survivors (Ozasa *et al*, 2012) and BEIR VII Report (BEIR VII, Chapter 12, Table 12D –see Section 4.3). Variation between patients is expected, as inter-patient differences in anatomy and dose deposition would be expected to cause a range in absolute values of MIP, and by association, $MIP_{Relative}$. However, inter-individual differences would not be expected to drastically affect the overall conclusion, and the work presented in this thesis confirms this prediction (Figure 13).

While in some of the cases presented the error bars associated between the absolute MIP values for photon and proton plans appear to overlap, the uncertainty is correlated, and as a result the uncertainty in $MIP_{Relative}$ is much smaller. This is in part is because the comparison between photon and proton plans are done in pairs on the same patient and therefore patient related uncertainties will be similar, but also that many of the uncertainties in the model parameters applying in a similar fashion (and in the same direction) to both the photon and proton plans (see sections 4.25.2). Additionally as this approach is devised to evaluate and compare multiple radiotherapy treatment options for an individual patient, then the

uncertainties associated with age, sex, or anatomy becomes less influential, as the comparison is intra-patient (Fontenot *et al*, 2010, Nguyen *et al*, 2015, Timlin *et al*, 2015). Different models were noted to produce different results, but most notably, the LNT model produced the highest MIPs for each plan/model/modality combination. This is due to the mathematical nature of the model which assumes a direct linear relationship between dose and risk, meaning that, for any given organ, the higher the dose, the higher the MIP. This assumption is less likely to hold true for the high dose range used in radiotherapy, as the LNT model implies an absence of cell killing and that the occurrence of malignant induction and secondary cancer is inevitable. In addition this model does not include cell killing which would be expected to result in a reduction in cells where a potential malignant induction event has taken place.

The general trend for the organs that were illustrated in section 4.1.2 follows a similar trend to that observed in the whole body MIP (4.1.1). Statistical analysis showed a significant difference between MIP_{Photon} and MIP_{Proton} for the thyroid and for all three models (P <0.001). This difference is expected for most other organs and structures, as in this treatment plan a lower does outside tumour volumes was achieved for the proton plans compared to the photon plans, resulting in some organs having a lower MIP in the proton therapy plan as well as a decrease in the whole body MIP. High resolution dose maps provide important information, as the presence of hot spots in some organs may dominate and shift the MIP in one direction or the other when mean dose is used. This factor is most important for relatively small organs or structures located near the distal end of the proton beam. When

organs site are particularly radiosensitive, then the risk of hotspots and its impact MIP should be taken into account during clinical decision making. The variation in values of MIP of a certain organ is expected between different patients, as the treatment plans are highly patient-specific, leading to differences in the resulting dose distribution to the various organs which ultimately will manifest in differences in MIP values, and in some cases, large differences in $MIP_{Relative}$ as well.

Finally, while it might be expected that protons would be better than photons with respect to malignant induction in the case of medulloblastoma, due to clearly superior proton dose distributions resulting in significant dose sparing in normal tissue. This may not always be the case for other clinical scenarios, where the arrangements of the proton beams is different and potentially closer to that of the corresponding photon plan the dose reduction effect is likely less than what is observed here, with a much smaller reduction in MIP, or potentially even a reversal of the preference towards 3DCRT (or other photon therapy techniques). Additionally not all tissues carry the same risk of carcinogenesis. Therefore, there may also be situations where proton therapy delivers a high dose to a sensitive tissue or a reduced dose to a less sensitive one compared to photons, making photon therapy the better option from a secondary cancer risk perspective. The work presented in this thesis provides a modelling framework that can be used to investigate these other cancer sites.

5.2 Sensitivity of MIP models to uncertainty in parameters

The results of the initial simulations gave some indication of the magnitude of MIP and, most importantly, its relative value for protons and photons, However, accounting for the uncertainty of parameters used in the models allows more firm conclusions to be made. The results presented in 4.2.1 provide an insight into the effect of each of the model parameters on the output of the models. From the whole body MIP plots (Figure 16- Figure 20) it is noticed that, while the absolute MIP values may vary significantly, the relative relationship between MIP_{Photon} and MIP_{Proton} remains largely the same. This reinforces the initial conclusion that in the case of medulloblastoma, proton therapy is less likely to induce secondary cancer than 3DCRT. This result remained true after varying all input parameters over almost 2 orders of magnitude. The LNT model results (Figure 20) showed a predictable outcome, which is that at higher values of a parameter, MIP trends towards 1, making $MIP_{Relative}$ trend towards 1 as well if the assumed parameter value of λ is significantly increased.

The linear factors, α in the LIN and LQ model and γ in the LQ model, are the parameters to which the models are most sensitive, changing the value of MIP by up to a factor of 7 (Figure 16 and Figure 18) from its originally calculated value in 4.1. In contrast, varying the quadratic components (β and δ) alters the outcome by up to a factor of 1.5 (Figure 17 and Figure 19). This indicates the greater importance of some parameters than others, as the uncertainty effect will be larger for α and γ for example. So, when working with models and model parameters, such exercises enable the researcher to

visualise the effect of the parameter uncertainty and clarify its effects on model outputs.

In section 4.2.2, the results for Patient 1 and Patient 2 for all the three models, showed that as the parameters were simultaneously varied over a randomly generated space, the relative MIP was always larger than 1 (Figure 21-Figure 26). This means that the trend noted in previous sections (4.1 and 4.2.1) holds true even with multi-variable uncertainty factored in, consolidating the observation made when the set of parameters was varied one parameter at a time. As expected, the magnitude of MIP is different between the two patients. This is attributable to the difference in volume and size of the patients which results in different doses being delivered to each organ. If the same set of simulations were to be performed on the other 10 patients, similar trends would be expected, as the difference between the photon and proton MIP is more dependent on differences in dose, and less on the size and shape of the individual patients.

As described, the model parameters are potentially a significant source of uncertainty due to the data and methods used to generate them and the endpoints they relate to. Therefore the most important aspect of this work is the *relative* relationship between photon and proton therapy. The uncertainty testing demonstrated the robustness of the trend and the superiority of the proton plan. So although the absolute values of MIP obtained are different between Patient 1 and Patient 2, the values of $MIP_{Relative}$ and associated errors for the two patients are very similar, and $MIP_{Relative}$ was larger than 1 for all models, for all patients. The F-test

conducted (4.3.2) demonstrated similar variance between most data sets, and almost identical standard deviation values. This indicates that the behaviour of MIP in relationship to the uncertainty in parameters is nearly the same for different patients, suggesting that even among different patients, MIP will behave in similar ways. This has enabled estimates of uncertainties to be made in patients 3 through 12 (see section 3.6).

5.3 Calibration and benchmarking

The results of 1 Gy whole body photon exposure (section 4.3.1 - Table 5), using the standard parameters for the three different models, was found to be out of line with the risk estimates set out in LSS Report 14 (Ozasa *et al*, 2012). This demonstrated the need to calibrate the parameters, if anything more than a relative (model-dependent) comparison is required, in order to generate absolute risk estimates, allowing a more valid comparison between models. While variation between the models is to be expected at high doses, the variation at a uniform single exposure of 0.1 Gy (to match the dose points in BEIR VII report), would be expected to be significantly smaller because the effects of cell killing, which are absent from some models, are negligible at this dose. Nonetheless it was observed that even at 1.0 Gy calibration of parameters is necessary as is for the 0.1 Gy level.

Results using calibrated parameters against BEIR VII report data showed agreement between models at the 0.1 Gy single exposure. Across different models, it was possible to calibrate parameters to come up with an outcome that resembles the data points in BEIR VII report Table 12D-1, giving the

variation in lifetime attributable risk (LAR) estimates for solid cancer incidence resulting from a single dose of 0.1 Gy at several specific ages (Figure 28, Figure 30, Figure 32).

The general agreement between all three models indicates their suitability, in principle, to model secondary cancer risks. The models are expected to show agreement in the low dose range, but potentially diverge at higher doses.

The calibrated models were used to calculate EAR and LAR resulting in a range of values for (Figure 33-Figure 37). This range is due to the inherent uncertainty of the models, as discussed earlier in this thesis. This variation is in agreement with the work of others in the field who have estimated risks using a variety of models and the difference between the models (Stokkevåg *et al*, 2014). As observed in previous sections, LNT produces results that are significantly higher than those obtained using the LQ and LNT models. Nevertheless, the absolute figures are more suitable for informing decisions during radiotherapy planning and delivery, and allow risk comparison with other late effects, such as heart disease, if desired.

The EAR was less than 1%, and yet the difference between EAR photon and proton can be large (Figure 36 - Figure 37). It was shown that proton therapy could reduce EAR by a factor of about 2 and this provides additional justification for recommending the use of proton therapy rather than photon 3DCRT in medulloblastoma. As for the calculation of absolute MIP values, the difference in EAR or LAR between the plans of different patients are patient and model-dependent. Calibration for age should be incorporated when modelling secondary cancer risk using suitable functions for the age range

desired. Importantly, the LAR decreases with older age at exposure, making young patients the most likely to benefit from the secondary cancer risk reduction of proton therapy (Schneider and Walsh, 2015).

The ability to provide absolute risk estimates of secondary cancer after radiotherapy is an important cornerstone in the field, and is critically important to a full understanding of the risks and benefits of radiotherapy. Validated methods for estimating absolute risk are more likely to be used and adopted clinically than non-benchmarked or calibrated methods.

The successful calibration of all the three models to the published data for the low dose and the general agreement between the models demonstrates the robustness of the method that was used for calculating the risk, calibration and benchmarking, and the mathematical approximation of models behind it.

5.4 The effect of spatial dose averaging on predicting malignant induction probability and secondary cancer risk

Using the LNT model, the calculated MIP value obtained using mean organ dose was identical to the MIP value obtained using the voxel-by-voxel (VbV) approach. This is as expected due to the direct linear relation of MIP with the dose. This also provides an internal check of the code modifications made for calculating MIP using mean dose of organs, and shows that it functions as expected.

Spatial information about dose distribution is an important element that contributes to the accuracy of dose-response models. The availability of

detailed dose maps allows for more precise correlations between radiation doses and effect. In practice the dose is very rarely uniform across individual organs and therefore for non-linear dose effect models it is unlikely that the mean dose to that organ will reflect the response across the organ. Individual organs are often complex systems made up of interdependent structures and tissues, which may have different sensitivity to radiation. For this reason it may be difficult to link the location of radiation dose deposited and the site of the secondary cancer (Schellong *et al*, 2014). In addition, factors such as patient-movement and the impact of fractionation on the dose distribution, make it even more difficult to accurately define the dose at the site of a secondary cancer origin (Schneider *et al*, 2017).Therefore it can be expected that using the most accurate and precise information about the dose distribution across individual organs is likely to add to the value of the models being studied.

The results presented in this thesis clearly show that the calculated whole body MIP_{MD} (obtained using the mean dose for individual organs) is 2-5 times larger than the MIP_{VbV} values (obtained using voxel-by-voxel dose maps- Figure 38 - Figure 43) and this results in a consistently lower $MIP_{Relative}$ value for photon vs proton plans calculated using mean dose. Therefore using mean organ dose for the calculations could result in the benefits of proton therapy with respect to secondary cancer being underestimated. The observation holds true for both the LQ and LIN models, with an expected difference in values.

Different organs are expected to behave differently depending on the dose distribution across them. Organs with a large dose gradient will have noticeable differences between MIP_{MD} and MIP_{VbV}. This is due to the change in dose that each voxel is assigned using mean dose prior to calculation of MIP_{MD} compared to the voxel-by-voxel method. The difference between MIP_{MD} and MIP_{VbV} will be less for organs with homogenous dose distributions and, in some cases, small volume, like the brain, bladder, and thyroid.

The use of mean dose assumes a direct linear relationship between dose and outcome for some models. This assumption generally holds true in epidemiological studies of A-bomb survives and accidental or occupational exposures, where the body and tissues are relatively uniformly irradiated. However, the assumption of a linear relationship between dose and risk of late side effects is not supported by evidence in the radiotherapy dose range. Many radiotherapy studies used mean dose as a surrogate for risk, but this does not take into consideration the mechanistic implications of a non-linear dose-response curve in the high dose region. That is not to say that the mean dose models are invalid, but that they are less applicable to cohorts that differ from the ones whose data were used to derive the model in the first place. It is also true that these models are likely to have been based on cohorts of patients who were treated using protocols that would now be considered outdated. Therefore the use of the mean dose should be avoided in modelling long-term side effects whenever possible. This is especially true for heterogeneous dose distributions, where the mean dose is unlikely to be

the optimal metric and so adds to the uncertainty of the calculated secondary cancer risk.

The use of high resolution dose maps adds precision to modelling the long-term side effects of radiotherapy. With increased computational power and advances in programming, it is possible for modelling of secondary cancer risk to be performed efficiently and effectively. Ultimately it may be possible to model risk in real time during the treatment planning process. With high resolution dose maps the modelling outcomes are likely to be more informative, as the more abundant input data available could lead to greater reliability of the output.

Another long-term advantage of VbV modelling over the use of mean dose to the individual organs, is that it potentially enables individual organs to be broken down further into substructures which may reflect variation in radiation sensitivity across individual organs.

5.5 The effect of radiobiological effectiveness on modelling malignant induction probability and dose calculation

Using an RBE of 1.1 has always been a topic of debate in the field of particle therapy, especially with protons, since they are more widely clinically available than other particle therapies. This controversy about RBE adds to the challenges in analysing long-term side effects of proton therapy. Assuming a uniform RBE of 1.1 does not account for changes in RBE in different tissues or account for the known increase in RBE with increasing LET that occurs at the distal end of the Bragg peak and for the tissues with low α/β. On the other hand, 1.1 is a reasonable value for the mean RBE of the

spread out region of the Bragg peak. Jones *et al* (Jones *et al*, 2012) have illustrated the risk of using a defined RBE on risk of local control and recurrence and the advantages of using LET to calculate RBE (Jones and Dale, 2000, Jones B, 2015). The increasing use of proton therapy with curative intent, especially in paediatric cases, provides a strong argument for the adoption of RBE modelling into proton therapy planning and dose calculation. Although historically there was no conclusive evidence that an RBE of 1.1 is an incorrect value (Paganetti *et al*, 2002, Paganetti H, 2014), there is increasing clinical evidence that variations in RBE are important clinically (Underwood *et al*, 2018). Radiobiology and physics research has resulted in a better understanding of RBE effects and mandates a move forward towards a beam-specific RBE modelling approach, although this still have to be fully validated for routine clinical use (Paganetti and Giantsoudi, 2018). Investigation of the effect of the variation in RBE as a function of proton energy and associated LET, would require detailed maps of the variation of LET across the patient, which are not available. However in addition to the variation of RBE with proton energy, the RBE is also known to vary as a function of dose, increasing to a maximum, RBE_{max}, at low dose. This phenomenon was modelled using the RBE_{MinMax} model, which showed a small decrease in MIP values (~3%) for the LQ and LIN models and a small increase (~2%) for the LNT model (Figure 47).

The effect of changing the value of RBE on dose is most pronounced for the maximum dose. The effect of the RBE value on dose translates into changes in in MIP and secondary cancer risk values. The effect of this difference is more

pronounced on the dose calculation than the secondary cancer risk. Although the main aim of this work was to address uncertainties associated with modelling MIP and secondary cancer risk, the implications of the RBE effect on dose calculation reaches beyond MIP and secondary cancer risk. Stokkevåg *et al* (Stokkevåg *et al*, 2016) have addressed the difference in secondary cancer risk and the influence that it may have on choosing between photon therapy and particle therapy. Although their work focuses on carbon ion therapy, a similar broad conclusion can be drawn: uncertainty in RBE can have very profound clinical implications and moving forward from a uniform RBE to beam-specific RBE is not an academic exercise, but a clinical necessity.

Additionally the use of the Wedenberg model demonstrated that tissues with the lowest α/β ratio (normal tissues, late reacting tissues) would have the highest RBE values for a given LET, making normal tissue complications more likely (Figure 49). While the tissues with high α/β (tumour tissues) would have the lowest RBE, making it less sensitive to inaccuracy of RBE.

As mentioned above, to fully understand the impact of proton RBE on MIP and other endpoints, it is essential that in addition to dose distribution through the patient, the 3D variation in proton LET is also determined. This not currently available via most commercial treatment planning software, but can be retrospectively determined using Monte Carlo simulations using beam and patient information from the planning system to create LET maps (Grassberg *et al,* 2011). This LET data can then be combined with the associated proton dose to generate 3D RBE maps through the patient

(Paganetti & Giantsoudi 2018). These maps could be used for biological optimisation of proton plans. Additionally, this approach has the potential to increase confidence in treatment planning and delivery for local control of disease and to achieve the desired clinical endpoint. Secondly, with more accurate RBE calculations, NTCP and secondary cancer risk can be modelled with greater accuracy and precision. One advantage of the modelling tool that has been presented in this thesis is its flexibility. If the LET maps were available for the current patients, then these values could also be updated to create a voxel-by-voxel variation in proton RBE across the patient and used for MIP calculations.

The impact that this is likely to have is the difference in effective dose calculations. Higher or lower doses can cause higher NTCPs or a decrease in tumour local control, respectively. For example, the difference in dose calculated here was found to be between 5% and 8% (Figure 48). In cases where patients with medulloblastoma were treated with a standard risk protocol (a regimen including radiotherapy with CSI doses of ~24 Gy), Jones et al have demonstrated that calculation of RBE correlates with cases of failure of local control in medulloblastoma (Jones *et al*, 2012, Jones, 2014). So, with the knowledge of the behaviour of particles, including protons, the observed local failure in some clinical cases, and the difference of 5-8% in dose, inclusion of RBE models is the next logical step.

One of the advantages of using a uniform $RBE_{1.1}$ is that it allows direct comparison of treatment plans between centres and patients. If RBE modelling is to be used, the flow of planning and dose calculation have to be

thoroughly thought out in order to make sure all correct measurements are made to avoid significant errors in dose calculations. It might also be useful to be able to produce dose difference maps, where dose calculated using modelled RBE is subtracted from dose calculated using RBE of 1.1 by subtracting dose matrices from each other and thus observing any hot or cold spots. This will aid in the transition between the current practices of a uniform RBE and the future of incorporation of RBE modelling into treatment planning.

5.6 General discussion and conclusions

One important issue with the vast majority of retrospective studies is the quality of data that is available. The author of this thesis was fortunate during the project to have access to original planning information (e.g. fully detailed treatment plan DICOM files). However, for other studies this has generally not been the case. In order to improve this situation, follow up protocols should be established, to capture data that allow subsequent analyses of end points of interest (such as clinical outcome, normal tissue toxicities, and secondary cancer) and parameters of interest. For example detailed information regarding the treatment plans, beam delivery, and patient geometry would be important for recreation of detailed dose maps if keeping DICOM files of those plans is not feasible. The candidates who it is most important to enrol in these studies relating to secondary cancer induction are younger patients, who have high probability of surviving beyond 5 years. As with all modelling studies, models are at first drawn up with simplified

assumptions, and after collection of data at periodic follow up, further iterations are made. And as more data and data points are collected and analysed, the understanding of secondary cancer risk is improved, and models are optimised. Such studies would improve dose-response models and would also improve parameters to enhance and improve the quality of the models. Some of the models may initially use parameters drawn from different end points that are not entirely suitable. The assessment of relevance of these parameters can be evaluated using methods similar to those used in section 4.2.

The modelling tools used in this project have the potential to improve the accuracy of the modelled output, through facile and convenient updating of parameters or the addition of new ones. The general applicability of this modelling tool makes it straightforward to perform modelling on data sets from different institutions with relatively little technical difficulty. MIP can be modelled with only short set up time even for sizable data sets of radiotherapy plans. However, these tools are not perfect. The present MATLAB code users need training and induction, making it less user-friendly and less intuitive. This could be overcome by removing any hard-coded parts that need modification, and by writing a clear and step-wise user instruction manual, along with library of the input parameters. The models used carry uncertainty as discussed, which makes the absolute values of the MIP or secondary cancer risk less reliable. In addition the code currently does not include the effect of repopulation, which could introduce a plateau in the dose-response curve for MIP at high doses (Sachs *et al*, 2007, Timlin et al,

2015). These deficiencies could be amended in future editions. Another problem is that the models take no account of the variability in cancer risk of different tissues, apart from differences in the parameters used for each organ and structure. However, the variation in cancer incidence and mortality have been estimated and used to establish weighting factors in calculations of effective dose for radiation protection purposes (ICRP Publication 60, 1991; BEIR VII Report, 2006; ICRP Publication 103, 2007). In the future, because the dose to individual organs is already derived from treatment plan file data, it will be relatively easy to incorporate this kind of information as weighting factor to reflect the differences in secondary cancer risk or mortality across different organs. This can be done directly by implementing weighting factors, or indirectly by calibrating the model parameters. Patient specific factors, such as age and sex, can be included (ICRP Publication 103, 2007). In addition, as the tool uses high resolution dose maps and carries out calculations on a voxel-by-voxel basis, it would be possible to conduct modelling that takes into account the variation in response of different sub-structures within an organ. The code could also benefit from the inclusion of organ equivalent dose models. This would aid comparison of different methods even further. Another challenge when working with this code is how computationally intensive it can be to run the models on a large sets of treatment plans data. Optimisation of the code, and use of a computer cluster suitable for this type of simulation could reduce the simulation run time.

The analyses performed for this thesis differ from those that have previously been published in the literature. For example, a high resolution dose map was used to calculate risk using three different models, which distinguishes it from related published studies. Brodin at el, using the plateau model of the organ equivalent dose (OED), compared treatment plans of 10 patients with medulloblastoma, with two different prescription CSI doses, 23.4 Gy and 36 Gy. The risk was calculated using an EAR model, which was assumed to be a function of OED adjusted for population-specific variables. They reached the conclusion that when comparing actively scanned proton therapy with 3DCRT, proton therapy has a lower secondary cancer risk, by about a factor of 6(Brodin *et al*, 2011). Their work, and work presented in this thesis is in agreement with conclusions from earlier work done by Mu et al, who used an ICRP recommended model, doses from DVH of organs studied, and parameters recommended by ICRP. Their results showed risk of secondary cancer after radiotherapy to be 7 folds higher for 3DCRT than that for protons in patients with medulloblastoma (Mu et al, 2005). The difference found between different studies in values of the relative relation between the different modalities would most likely be related to the choice of models and parameters used in each study. The models used for calculation of MIP during this doctorate differed from those used by Brodin and colleagues used, further establish the superiority of proton therapy to 3DCRT in medulloblastoma (Brodin *et al*, 2011). Brodin et al modelled EAR using the OED concept, and presented the results as the mean of the EAR values obtained from a group of patients. The approach taken in this thesis was to show results in a patient-by-patient fashion, to highlight inter-individual

variation in MIP and secondary cancer risk. Brodin's analysis included assessment of contemporary treatment methods, namely IMRT, while IMRT plans were not included in the current study. Stokkevåg *et al* used OED as well to estimate secondary cancer risk after radiotherapy for 6 patients with medulloblastoma using three different models (linear, bell-shaped, and plateau) for a number of different radiotherapy modalities including 3DCRT and proton therapy, and reached similar conclusions to the results here, estimating that the difference in secondary cancer risk can be up to 6 times greater for photon therapy compared to protons (Stokkevåg *et al,* 2014). The authors reached the conclusions reached earlier in this work that the statistics indicate that the predictions from the linear models overestimate the risk, in particular in regards to the structures receiving the highest doses. The authors also acknowledge that more work is needed to understand development of secondary cancer, they observe that the risk estimates obtained from the non-linear models are the most realistic. Both Brodin and Stokkevåg acknowledged the importance of relative comparison, rather than relying on absolute values of risk assessments. Zhang and colleagues approached the question of secondary cancer risk comparison by using models based on the BEIR report data (Zhang *et al*, 2014). They estimated the secondary cancer risk for 17 patients with medulloblastoma, comparing proton and photon therapy plans for each, at CSI dose of 23.4 Gy. They used LAR, defined in BEIR VII as the probability of cancer incidence or mortality during one's lifetime (living to 100 years) after exposure to a certain equivalent dose at age at exposure. The linearity of the model favours, by default, dose reduction plans, as the risk would increase linearly with dose,

so the smaller is the dose, the smaller is the secondary cancer risk. The estimated relative risks varied between about 5 and 10 times for LAR for secondary cancer incidence. In their analysis the investigators included the stray dose, which was not considered in the calculations performed for this thesis. It is not likely that neutron dose would impact MIP or secondary cancer risk linked to the radiotherapy treatment plans studied in this work to an extent that would overturn the general conclusion that proton therapy is associated with a lower MIP than photon therapy. The neutron dose might become relevant when a passively scattered proton plan is compared to an IMRT plan, but in actively scanned proton therapy, it is very unlikely that the neutron dose component would be high enough to alter the outcome, especially when anything but a completely linear model is used (Newhauser *et al*, 2009).

The work done here serves as an early step towards using patient specific dose distribution data to calculate MIP and secondary cancer risk in order to improve clinical decision-making. Work in the future should include studies to optimise and enhance dose-response models and parameters and the incorporation of other important end points in the modelling tool such as radiation-related cardiac morbidity and mortality. Future work should also specify the dose-response for each organ or structure, as it has been reported by others that different organs may have different dose-responses thus necessitating organ-specific modelling (Berrington de Gonzalez *et al*, 2013, Ng & Shuryak, 2015). Instead of applying the same MIP model to all organs

and structures, the MIP for each organ can be modelled using existing knowledge of their dose-response behaviour.

Future versions of the modelling tools should also strive to include tools to enable the code to use data from LET maps of proton therapy to calculate variable RBE so that this can be used to model MIP and other relevant end points. Modelling MIP and EAR for different photon therapy techniques such as IMRT and VMAT would also be a valuable piece of work, providing results for contemporary treatments that will be of relevance to medulloblastoma patients going forward, and enable comparisons with work done by other researchers discussed above. Extending the work done in this thesis to other tumour sites, like Hodgkin's disease or breast cancer would be of high clinical relevance, as these cancers are more common than medulloblastoma. There is also a rich literature concerning the long-term adverse effects, including cancer induction, for these groups of patients, which would facilitate the work.

In summary, a statistically significant reduction in the malignant induction probability was observed for proton medulloblastoma treatment plans compared to conventional photon plans. This was found to be a robust conclusion independent of model, patient and parameter uncertainty. Therefore the use of proton therapy in medulloblastoma would be expected to result in a significantly decreased risk of secondary cancer (current calculations indicate a reduction in EAR by a factor of about 2). The use of proton therapy should be considered in all clinical scenarios when considerable volumes of normal tissues receive radiation, especially in

younger patients who are predicted to survive for many years. The uncertainty of the parameters, RBE and dose delivery of proton therapy should be borne in mind in the clinical decision-making process but should not deter from utilising model-based approaches. Proton therapy is a powerful therapeutic option but it is not a magical one, nor the only one. Modelling can aid decision-making, and future clinical practice should be improved by utilising treatment plan data and by drawing upon follow-up data for the optimisation of long-term side effect prediction models.

Appendices

Appendix Table 1: Values for the parameters used for the organs and structures in the treatment plans.

Structure	α/β	α	β	γ/δ	γ	δ	Reference for α/β value	Note about the endpoint for the α/β
Bone	3	0.09	0.03	3	9.00E-08	3.00E-08		α/β Value averaged to 3.
Muscle fat	3	0.09	0.03	3	9.00E-08	3.00E-08		α/β Value averaged to 3.
Bladder	6	0.18	0.03	6	1.80E-07	3.00E-08	Marks *et al*, 1995	At least, grade 3 bladder toxicity.
Brain	2.9	0.09	0.03	2.9	8.70E-08	3.00E-08	Lee *et al*, 1998.	Radiation necrosis.
Brainstem	2.1	0.06	0.03	2.1	6.30E-08	3.00E-08	Bruman *et al*, 1991.	Cranial neuropathy.
Breast	3.5	0.11	0.03	3.5	1.05E-07	3.00E-08		α/β Value averaged to 3.
Cochlea	3	0.09	0.03	3	9.00E-08	3.00E-08		α/β Value estimated to be close to α/β of the brain.
Ear	3	0.09	0.03	3	9.00E-08	3.00E-08		α/β Value averaged to 3.
Eye	2.9	0.09	0.03	2.9	8.70E-08	3.00E-08		α/β Value estimated to be similar to the α/β of the brain.
Gallbladder	4	0.12	0.03	4	1.20E-07	3.00E-08		α/β Value estimated to be 4, note that α/β of the liver is 2.
Heart	2.5	0.08	0.03	2.5	7.50E-08	3.00E-08	Martel *et al*, 1998.	Pericarditis/pericardial effusion.
Lacrimal Gland	3	0.09	0.03	3	9.00E-08	3.00E-08		α/β Value averaged to 3.
Kidney	2.5	0.08	0.03	2.5	7.50E-08	3.00E-08		α/β Value estimated to be close to α/β of the liver.
Lung	3.5	0.11	0.03	3.5	1.05E-07	3.00E-08	Bentzen *et al*, 2000.	Pulmonary fibrosis.
Liver	2	0.06	0.03	2	6.00E-08	3.00E-08	Dawson *et al*, 2002.	RT-induced liver disease.
Nasopharynx	10	0.30	0.03	10	3.00E-07	3.00E-08		α/β Value estimated to be similar to α/β of the oesophagus.
Oesophagus	10	0.30	0.03	10	3.00E-07	3.00E-08	Werner-Wasik *et al*, 2010	At least grade 2 acute esophagitis.
Optic nerve	1.6	0.05	0.03	1.6	4.80E-08	3.00E-08	Jiang *et al*, 1994.	Radiation-induced optic neuropathy.
Oral cavity	10	0.30	0.03	10	3.00E-07	3.00E-08		α/β Value estimated to be similar to α/β of the oesophagus.
Ovaries	3	0.09	0.03	3	9.00E-08	3.00E-08		α/β Value averaged to 3.

Structure	α/β	α	β	γ/δ	γ	δ	Reference for α/β value	Note about the endpoint for the α/β
Pancreas	4	0.12	0.03	4	1.20E-07	3.00E-08		α/β Value estimated to be close to α/β of the liver and small bowel.
Parotid	20	0.60	0.03	20	6.00E-07	3.00E-08	Franzen *et al*, 1994	Xerostomia.
Rectum	5.4	0.16	0.03	5.4	1.62E-07	3.00E-08	Brenner D J, 2004.	At least, Grade 2 rectal toxicity.
Retina	2.9	0.09	0.03	2.9	8.70E-08	3.00E-08		α/β Value estimated to be similar to the α/β of the brain.
Sigmoid colon	5.4	0.16	0.03	5.4	1.62E-07	3.00E-08	Brenner D J, 2004.	Adopted using the α/β for rectum.
Skin	3	0.09	0.03	3	9.00E-08	3.00E-08		α/β Value averaged to 3.
Small bowel	3.5	0.11	0.03	3.5	1.05E-07	3.00E-08	Kavanagh, *et al*, 2010	α/β Value averaged to 3.
Spinal cord	0.87	0.026	0.03	0.87	2.61E-08	3.00E-08	Schultheiss, 2008.	Myelopathy.
Spleen	4	0.12	0.03	4	1.20E-07	3.00E-08		α/β Value averaged to 4.
Stomach	4	0.12	0.03	4	1.20E-07	3.00E-08		α/β Value estimated to be close to α/β of small bowel.
Thyroid	3	0.09	0.03	3	9.00E-08	3.00E-08		α/β Value averaged to 3.
Vaginouterus	3	0.09	0.03	3	9.00E-08	3.00E-08		α/β Value averaged to 3.

Values of α and β used for the LQ and LIN model, based on α/β values for different structures in the plans modelled. β = 0.03 was assumed to start with. For organs and structures without a clear reference, the α and β values was estimated from similar structures. For tumour volumes (CTVs and PTVs) α = 4.68 and β =0.75. Values of γ and δ used for the LQ and LIN model, based on α/β values for different structures in the plans modelled, assuming that the relation between γ and δ will be similar to the relation between α and β. δ = 3.00E-08 was assumed to start with. For organs and structures without a clear literature reference for an α/β values, the α and β values was estimated from similar structure. Those are the values of parameters prior to calibration done in chapter three.

Appendix Table 2.1: Priority list of organs in adult patient (Patient 1) plans.

Structure	Priority	Structure	Priority	Structure	Priority
brain	1	pituitary_gland	25	bone	49
eye_r	2	nasopharynx	26	All Air Cav BOX	50
eye_l	3	oral_cavity	27	spinal cord	51
len_r	4	thyroid	28	spinalcordPRV	52
lens_l	5	All Air Cavity	29	ts_plus_12	53
ear_r	6	Right lung	30	c1	54
ear_l	7	Left lung	31	structure06	55
coch_oss_r	8	heart	32	brain_plus_12	56
coch_oss_l	9	stomach	33	ptv_ts_new	57
cochlea_r	10	liver	34	Phantom	58
cochlea_l	11	spleen	35	All Bone	59
parotid_r	12	pancreas	36	Skin BOX	60
parotid_l	13	Right kidney	37	All Muscle Fat	61
lacrimal_r	14	Left kidney	38	body	62
lacrimal_l	15	bladder	39	ptv opitmize	63
White matter	16	vaginouterus	40	gtv_final	64
optNerveRt	17	Ovaries	41	ptv_5580	65
optNerveLt	18	ovary_l	42	ctv_5580	66
optChiasm	19	sigmoid-colon	43	ptv5580inc1+	67
opt nrv chismPRV	20	small bowel	44	ptv5580-c1+	68
parotid_rt	21	gallbladder	45	ctv_thecal_sac	69
parotid_lt	22	rectum	46	ptv_3600	70
brainstem	23	Breast tissue	47	Dose 1500[cGy]	71
brainstemPRV	24	skin	48		

Appendix Table 2.2: Priority list of organs in teenage patient (Patient 2) plans.

Structure	Priority	Structure	Priority	Structure	Priority
Brain	1	heart	21	All Muscle Fat	41
r_eye	2	stomach	22	ptvspine upper	42
l_eye	3	Liver	23	ptvspine lower	43
r_lens	4	Spleen	24	body	44
l_lens	5	pancreas	25	CTV PFossa TTS	45
r_cochlea	6	r_kidney	26	PTV PFossa TTS	46
l_cochlea	7	l_kidney	27	gtvplus3rdvent	47
rt parotid	8	bladder	28	gtv3rdvent10mm	48
lt parotid	9	Ovaries	29	gtv	49
r_opticnerv	10	sigmoid-colon	30	ctv3030	50
l_opticnerv	11	small intestine	31	thirdventricle	51
r_retina	12	Rectum	32	ptvspine	52
l_retina	13	thecal_sac	33	ptv3030	53
nasopharanx	14	CNS PTV	34	body-ptvspine	54
oropharynx	15	sub-ptv	35	ptvspine+5mm	55
Thyroid	16	thecal sac ptv	36	Dose 105[%]	56
Breast Tissue	17	All Bones	37	extra 105%	57
Lt Lung	18	A Skin BOX	38	Dose 105[%] xray	58
Rt Lung	19	All Air Cav BOX	39	Dose 105[%] post	59
total lung	20	All Air Cavity	40		

Appendix Table 2.3: Priority list of organs in Patient 3.

Patient 3					
Photon plan		Proton Plan			
Structure	Priority	Structure	Priority	Structure	Priority
EyeLeft	1	Bladder	1	PTVbrainIMPT	37
EyeRight	2	Bone	2	NormalTissueIMPT	38
Spinal_Cord1	3	Brain	3	Brain4mmMargines	39
Brain	4	Colon	4	PTVoverlapp	40
LensLeft	5	Colon+rectum	5	PTVimptCS	41
Heart	6	Cribriform plate	6	Brain5mmMargines	42
LungLeft	7	Eosophagus	7	PTVtotal5mmbrain	43
LungRight	8	EyeLeft	8	CTV95	44
LensRight	9	EyeRight	9	Dose 25[Gy]l	45
KidneyLeft	10	Heart	10	NonTargetVolume	46
KidneyRight	11	KidneyLeft	11		
Thyroid	12	KidneyRight	12		
Bone	13	LensLeft	13		
Colon	14	LensRight	14		
Eosophagus	15	Liver	15		
Liver	16	LungLeft	16		
Ovaries	17	LungRight	17		
Prostate	18	Ovaries	18		
Stomach	19	Prostate	19		
Uterus/Cervix	20	Spinal_Cord	20		
CribiformPlate	21	Stomach	21		
Eyes	22	Thyroid	22		
Lenses	23	Uterus/Cervix	23		
Lungs	24	Eyes	24		
Kidneys	25	Lenses	25		
Bladder	26	Kidneys	26		
Vertebrae	27	Lungs	27		
Trachea	28	Vertebrae	28		
BODY	29	Lungopt	29		
0.5 cm Bolus	30	BODY	30		
1 cm Bolus	31	CTVextended	31		
CTVphoton	32	CTVphoton	32		
NonTargetVolume	33	CTVproton	33		
CTV boost spinal	34	PTVpassivDS	34		
PTV boost spinal	35	Block	35		
CTVboost60Gy	36	PTVspineIMPT	36		

Appendix Table 2.4: Priority list of organs in Patient 4- Photon Plan.

Photon plan			
Structure	Priority	Structure	Priority
EyeLeft	1	PTVspineVMAT_5mm	37
EyeRight	2	PTVhelpbrainVMAT	38
Spinal_Cord	3	PTV_VMAT2	39
Brain	4	Dose 95[%]	40
LensLeft	5	opt	41
Heart	6	Breast	42
LungLeft	7	PTVvmatSpine7	43
LungRight	8	PTVvmathelp2mmSp	44
LensRight	9	PTVbrain3mm	45
KidneyLeft	10	PTVhelpBrain2mmV	46
KidneyRight	11		
Thyroid	12		
Bladder	13		
Bone	14		
Colon	15		
Eosophagus	16		
Liver	17		
Stomach	18		
CribiformPlate	19		
Lungs	20		
Kidneys	21		
Vertebrae	22		
Lenses	23		
Eyes	24		
BODY	25		
1/2 cm bolus	26		
CTVphoton	27		
Ovaries	28		
Uterus/Cervix	29		
NonTargetVolume	30		
CTVproton	31		
PTVspinVMAThelp2	32		
PTVbrainVMAT	33		
PTV_VMAT	34		
PTVhelpVMAT	35		
NormalTissueVMAT	36		

Appendix Table 2.5: Priority list of organs in Patient 4- Proton Plan.

Proton Plan			
Structure	Priority	Structure	Priority
CribriformPlate	1	PTVspineIMPT	37
Brain	2	CTVbrainExtCrib	38
EyeLeft	3	PTVbrainIMPT	39
EyeRight	4	PTV_IMPT	40
Spinal_Cord	5	NormalTissue	41
LensLeft	6	PTV_DS	42
LungRight	7	PTVbrain	43
LensRight	8	NonTargetVolume	44
KidneyRight	9	Dose 25.1[Gy]	45
Bladder	10	Dose 25.2[Gy]	46
Colon	11	CTVspineBoost	47
Liver	12	PTVspineBoost	48
Heart	13	PTVboost1cm	49
LungLeft	14	CTVprotonBoost	50
KidneyLeft	15	PTVprotonBoost	51
Thyroid	16		
Bone	17		
Eosophagus	18		
Ovaries	19		
Prostate	20		
Stomach	21		
Uterus/Cervix	22		
Eyes	23		
Lenses	24		
Lungs	25		
Kidneys	26		
Vertebrae	27		
LungOpt	28		
Breast	29		
SurroundTissue	30		
BODY	31		
CTVphoton	32		
CTVproton	33		
CTVageSpine	34		
CTVbrainExt	35		
PTVspineDS	36		

Appendix Table 2.6: Priority list of organs in Patient 5- Photon Plan.

Photon plan			
Structure	Priority	Structure	Priority
Bone	1	PTVspinVMAT	37
SpinalCord	2	PTVcranVMAT	38
Trachea	3	PTV_VMAT	39
Thyroid	4	PTVhelpVMAT	40
Heart	5	NormTissueVMAT	41
LungLeft	6	Dose 110[%]	42
LungRight	7		
Bladder	8		
Brain	9		
Colon	10		
CribriformPlate	11		
Uterus/Cervix	12		
Lungs	13		
EyeLeft	14		
EyeRight	15		
Ovaries	16		
Eyes	17		
LensLeft	18		
LensRight	19		
Lenses	20		
Eosophagus	21		
Liver	22		
KidneyLeft	23		
KidneyRight	24		
Kidneys	25		
Stomach	26		
Vertebrae	27		
BODY	28		
1/2 cm Bolus	29		
PTVcran	30		
PTVSpinal	31		
Normal Tissue	32		
PTV	33		
CTVphoton	34		
CTVproton	35		
NonTargetVolume	36		

Appendix Table 2.7: Priority list of organs in Patient 5- Proton Plan.

Proton Plan			
Structure	Priority	Structure	Priority
Bone	1	PTVbrain	37
SpinalCord	2	PTVbrainIMPT	38
Brain	3	PTVcranIMPT	39
Colon	4	PTV_IMPT	40
CribriformPlate	5	PTVspineDS	41
Uterus/Cervix	6	PTV_DS	42
Lungs	7	Dose 25.5[Gy]	43
EyeLeft	8	Dose 25.1[Gy]	44
EyeRight	9	Dose 25[Gy]	45
Ovaries	10	Dose 25.1[Gy]2	46
Eyes	11	Dose 25.1[Gy]22	47
LensLeft	12		
LensRight	13		
Lenses	14		
Eosophagus	15		
Liver	16		
KidneyLeft	17		
KidneyRight	18		
Kidneys	19		
Stomach	20		
Vertebrae	21		
Bladder	22		
Thyroid	23		
Trachea	24		
LungRight	25		
LungLeft	26		
Heart	27		
Lungopt	28		
BODY	29		
PTVcran	30		
PTVspineIMPT	31		
CTVproton	32		
NonTargetVolume	33		
CTVphoton	34		
Normal Tissue	35		
PTV	36		

Appendix Table 2.8: Priority list of organs in Patient 6.

Patient 6					
Photon plan		Proton Plan			
Structure	Priority	Structure	Priority	Structure	Priority
Bone	1	Bone	1	PTVspineIMPT	29
Bladder	2	Bladder	2	PTVbrain	30
Brain	3	Brain	3	PTVbrainIMPT	31
Colon	4	Colon	4	PTVcranIMPT	32
CribriformPlate	5	CribriformPlate	5	PTV_IMPT	33
Liver	6	Thyroid	6	NormalTissue	34
Stomach	7	Eosophagus	7	PTVspineDS	35
Lungs	8	Heart	8	PTV_DS	36
Eyes	9	Liver	9	CTVproton	37
Lenses	10	Stomach	10	NonTargetVolume	38
Kidneys	11	Lungs	11	Dose 25[Gy]	39
KidneyLeft	12	Eyes	12	Dose 25[Gy]2	40
KidneyRight	13	Lenses	13		
Thyroid	14	Kidneys	14		
Eosophagus	15	KidneyLeft	15		
Heart	16	KidneyRight	16		
LungLeft	17	LungLeft	17		
LungRight	18	LungRight	18		
Lens Right	19	Lens Right	19		
LensLeft	20	LensLeft	20		
EyeLeft	21	EyeLeft	21		
EyeRight	22	EyeRight	22		
Spinal_Cord	23	SpinInklVert	23		
Vertebrae	24	Vertebrae	24		
BODY	25	LungOpt	25		
1 cm Bolus	26	BODY	26		
CTVphoton	27	1 cm Bolus	27		
NonTargetVolume	28	CTVphoton	28		

Appendix Table 2.9: Priority list of organs in Patient 7.

Patient 7					
Photon plan		Proton Plan			
Structure	Priority	Structure	Priority	Structure	Priority
Bone	1	Bone	1	Dose 25[Gy]2	38
CribriformPlate	2	Brain	2		
Thyroid	3	CribriformPlate	3		
Brain	4	Eosophagus	4		
Eosophagus	5	Eyes	5		
Lungs	6	Kidneys	6		
Lenses	7	Lenses	7		
Heart	8	Lungs	8		
Eyes	9	SpinalCord	9		
SpinalCord	10	SpinInklVert	10		
Kidneys	11	Thyroid	11		
Vertebrae	12	Vertebrae	12		
Liver	13	Bladder	13		
Bladder	14	Liver	14		
Colon	15	Heart	15		
Stomach	16	Colon	16		
Prostate	17	Stomach	17		
BODY	18	LungOpt	18		
Bolus1	19	BODY	19		
Bolus2	20	CTVphoton	20		
Bolus3	21	NonTargetVolume	21		
CTVphoton	22	PTV_DS	22		
SpinInklVert	23	PTV_IMPT	23		
PTV_IMPT	24	PTVbrain	24		
PTVbrain	25	PTVbrainIMPT	25		
PTVcranIMPT	26	PTVcranIMPT	26		
PTVbrainIMPT	27	PTVspineDS	27		
PTVspineIMPT	28	PTVspineIMPT	28		
NonTargetVolume	29	Bolus1	29		
PTV_DS	30	Bolus2	30		
PTVspineDS	31	Bolus3	31		
PTV_VMATspine	32	NormalTissue	32		
PTV_VMATbrain	33	Dose 110[%]	33		
PTVvmatSpinHelp	34	Dose 107[%]	34		
PTVvmatBrainHelp	35	Dose 25[Gy]	35		
PTVhelpSpine2mm	36	Dose 25.1[Gy]	36		
normalvevVMAT	37	Dose 25[Gy]opt	37		

Appendix Table 2.10: Priority list of organs in Patient 8.

Patient 8					
Photon plan		Proton Plan			
Structure	Priority	Structure	Priority	Structure	Priority
Bone	1	Bone	1	NormTissueVMATex	38
Heart	2	Heart	2	Dose 107[%]	39
SpinalCord	3	SpinalCord	3	PTVspincroppIMPT	40
Trachea	4	SpinInklVertebra	4	PTVcrancroppIMPT	41
Brain	5	Trachea	5	CrancropIMPT2	42
Lungs	6	Brain	6	Dose 107[%]_2	43
Lenses	7	Lungs	7	PTVspineDS	44
Eyes	8	Lenses	8	PTV_DS	45
Kidneys	9	Eyes	9	PTVcroppSpineIMP	46
Thyroid	10	Kidneys	10	Dose 107[%]2	47
CribriformPlate	11	Thyroid	11	Dose 25[Gy]	48
Eosophagus	12	CribriformPlate	12		
Uterus/Cervix	13	Eosophagus	13		
Vertebrae	14	Uterus/Cervix	14		
Bladder	15	Vertebrae	15		
Liver	16	Liver	16		
Colon	17	Colon	17		
Stomach	18	Bladder	18		
SpinInklVertebra	19	Stomach	19		
BODY	20	LungOpt	20		
PTV spinalkanal	21	BODY	21		
PTV hjerne	22	NormalTissue	22		
Bolus_1.5cm	23	PTV spinalkanal	23		
NormalTissue	24	PTV hjerne	24		
CTVphoton	25	Bolus_1.5cm	25		
PTVspineIMPT	26	CTVphoton	26		
PTVbrain	27	PTVspineIMPT	27		
PTVbrainIMPT	28	PTVbrain	28		
PTVcranIMPT	29	PTVbrainIMPT	29		
PTV_IMPT	30	PTVcranIMPT	30		
NonTargetVolume	31	PTV_IMPT	31		
PTV_VMAT	32	NonTargetVolume	32		
PTVbrainVMAT	33	PTV_VMAT	33		
PTVspineVMAT	34	PTVbrainVMAT	34		
NormTissueVMAT	35	PTVspineVMAT	35		
PTV_VMAText	36	NormTissueVMAT	36		
NormTissueVMATex	37	PTV_VMAText	37		

Appendix Table 2.11: Priority list of organs in Patient 9's plans.

Patient 9					
Structure	Priority	Structure	Priority	Structure	Priority
Medulla	1	Rectum	28	Body_Optimizer	55
Hjerne	2	Pancreas	29	Neck avoidance	56
Liver	3	Ovaries	30	PTV_optimizer	57
Kidney dx	4	Testicles	31	PTV_opt_brain	58
Fossa posterior	5	Hippocampus sin	32	Bone tissue	59
Thyroid	6	Periven zone dx	33	Hippocampus dx	60
Heart	7	Periven zone sin	34	PTV_CSI	61
Spleen	8	Carotids	35	PTV_CSI_2	62
Kidney sin	9	Subman gland dx	36	PTV_Spin canal	63
Ventricle	10	Subman gland sin	37	Non-target bone	64
Esophagus	11	Skin	38	PTV_Fossa post	65
Pituitary gland	12	Temporal lobe	39	Boost_Optimizer	66
Chiasm	13	Sup tentor brain	40	Pelvis	67
Brainstem	14	Uterus	41	ThighHumerushead	68
Parotis dx	15	Optic Nerves	42	Bone marrow	69
Parotis sin	16	Eye dx	43	RA_junc1test	70
Mandible	17	Eye sin	44	RA_junc2test	71
Cochlea	18	Brain	45	PTV Heart	72
Eye lenses	19	Vertebral column	46	Tumor bed	73
Bladder	20	Vertebrae	47	SVZ	74
Oral Cavity	21	Spinal canal	48	Boost CTV 1.5cm	75
Mammary glands	22	Cranium	49	BoostPTV1.5+0.5	76
Larynx	23	ScapulaClavicle	50	Boost CTV 1.0cm	77
Cor. arteries	24	RibsSternum	51	Boost CTV 0.5cm	78
Lungs	25	GI tract	52	BoostPTV1.0+0.5	79
Small Intestine	26	BODY	53	BoostPTV0.5+0.5	80
Colon	27	N/A	54	ConfBoostAvoid	81

Appendix Table 2.12: Priority list of organs in Patient 10's plans.

Patient 10			
Structure	Priority	Structure	Priority
Pituitary gland	1	Skin	39
Cochlea	2	Fossa posterior	40
Oral Cavity	3	Temporal lobe	41
Mandible	4	Sup tentor brain	42
Parotid dx	5	Uterus	43
Parotid sin	6	Optic Nerves	44
Eye dx	7	Chiasm	45
Eye sin	8	Spinal canal	46
Thyroid	9	Vertebrae	47
Mammary glands	10	Vertebral column	48
Esophagus	11	Cranium	49
Larynx	12	ScapulaClavicle	50
Heart	13	RibsSternum	51
Cor. arteries	14	Pelvis	52
Lungs	15	ThighHumerushead	53
Liver	16	Bone marrow	54
Spleen	17	GI tract	55
Small Intestine	18	SVZ	56
Colon	19	Medulla_riktig	57
Rectum	20	BODY	58
Pancreas	21	PTV_Spinal canal	59
Kidney dx	22	PTV_Brain	60
Kidney sin	23	PTV_CSI_2	61
Bladder	24	Body_Optimizer	62
Ovaries	25	Neck avoidance	63
Testicles	26	PTV_Fossa Post	64
Hippocampus dx	27	Non-target bones	65
Hippocampus sin	28	PTV_Prot cran	66
Periven zone dx	29	Boost_Optimizer	67
Periven zone sin	30	Tumor bed	68
Carotids	31	Boost CTV 1.5cm	69
Subman gland dx	32	Boost CTV 1.0cm	70
Subman gland sin	33	Boost CTV 0.5cm	71
Bone tissue	34	Boost PTV1.5+0.5	72
Ventricle	35	Boost PTV1.0+0.5	73
Eye lenses	36	Boost PTV0.5+0.5	74
Brainstem	37	ConfBoostAvoid	75
Brain	38		

Appendix Table 2.13: Priority list of organs in Patient 11's plans.

Patient 11					
Structure	Priority	Structure	Priority	Structure	Priority
Brainstem	1	Skin	39	Boost PTV1.0+0.5	77
Pituitary gland	2	Fossa posterior	40	Boost PTV0.5+0.5	78
Cochlea	3	Sup tentor brain	41	ConfBoostAvoid	79
Oral Cavity	4	Uterus	42	BoostPTV0.5new	80
Mandible	5	Chiasm	43	BoostPTV1.0new	81
Parotid dx	6	Optic Nerves	44	BoostPTV1.5new	82
Parotid sin	7	Prostate	45	N/A	83
Eye dx	8	Spinal canal	46	N/A(1)	84
Eye sin	9	Non-target bone	47	PTV_Spinal canal	85
Thyroid	10	Vertebral column	48	Neck avoidance	86
Mammary glands	11	Cranium	49		
Esophagus	12	ScapulaClavicle	50		
Larynx	13	RibsSternum	51		
Heart	14	Vertebrae	52		
Cor. arteries	15	Pelvis	53		
Lungs	16	ThighHumerushead	54		
Liver	17	Bone marrow	55		
Spleen	18	GItract	56		
Small Intestine	19	SVZ	57		
Colon	20	BODY	58		
Rectum	21	Ovaries	59		
Pancreas	22	N/A(2)	60		
Kidney dx	23	N/A(3)	61		
Kidney sin	24	N/A(4)	62		
Bladder	25	Temporal lobe	63		
Testicles	26	PTV_Brain	64		
Hippocampus dx	27	PTV_CSI_2	65		
Hippocampus sin	28	PTV_Fossa post	66		
Periven zone dx	29	Boost_optimizer	67		
Periven zone sin	30	Body_Optimizer	68		
Carotids	31	PTV_CSI_Vert	69		
Subman gland dx	32	PTV_BrainDx	70		
Subman gland sin	33	PTV_BrainSin	71		
Bone tissue	34	Tumor bed	72		
Ventricle	35	Boost CTV 1.5cm	73		
Eye lenses	36	Boost CTV 1.0cm	74		
Medulla	37	Boost CTV 0.5cm	75		
Brain	38	Boost PTV1.5+0.5	76		

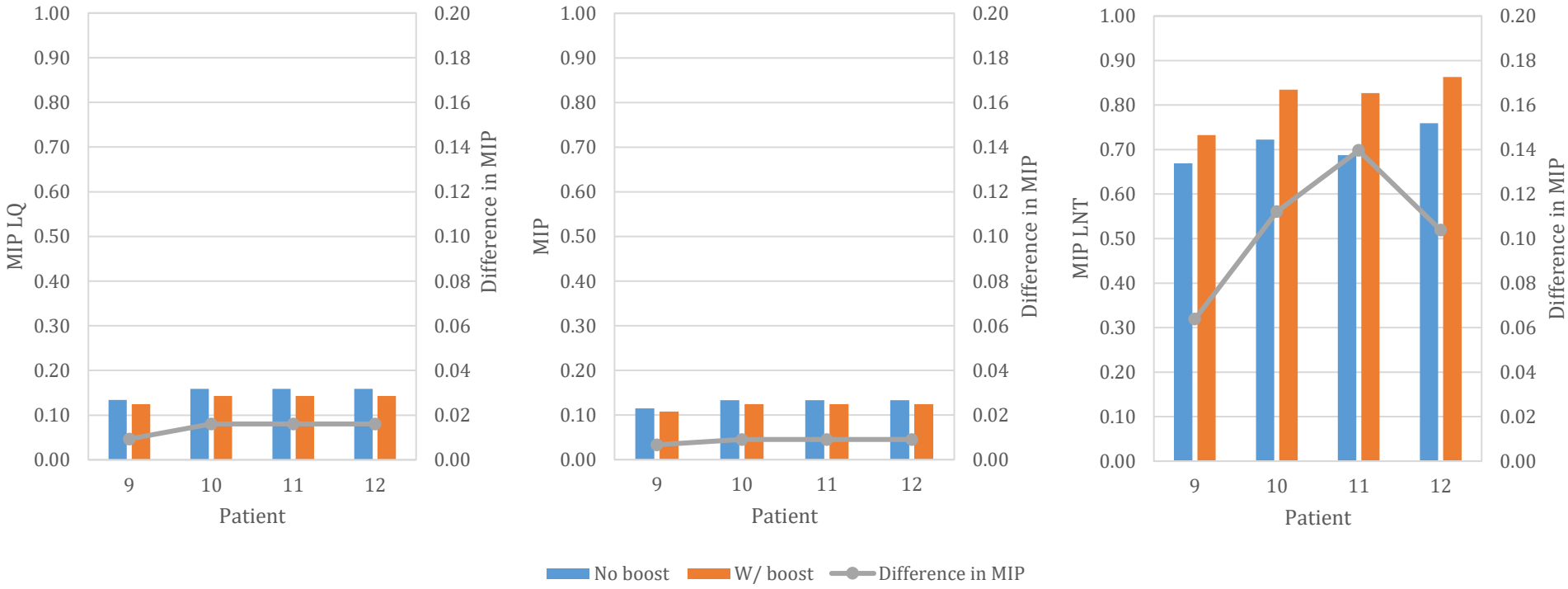
Appendix Table 2.14: Priority list of organs in Patient 12's plans.

Patient 12					
Structure	Priority	Structure	Priority	Structure	Priority
Oral Cavity	1	Prostate	39	N/A	77
Mammary glands	2	Medulla	40	N/A(1)	78
Cor. arteries	3	Brain	41	N/A(4)	79
Spleen	4	Lungs	42	Uterus	80
Small Intestine	5	Spinal canal	43	N/A(2)	81
Periven zone dx	6	Vertebrae	44	N/A(6)	82
Periven zone sin	7	Vertebral column	45	N/A(3)	83
Carotids	8	Chiasm	46	N/A(5)	84
Eye lenses	9	Cranium	47		
Testicles	10	ScapulaClavicle	48		
Ventricle	11	RibsSternum	49		
Hippocampus sin	12	Pelvis	50		
Pancreas	13	ThighHumerushead	51		
Pituitary gland	14	Bone marrow	52		
Rectum	15	GItract	53		
Thyroid	16	SVZ	54		
Temporal lobe	17	BODY	55		
Sup tentor brain	18	Ovaries	56		
Subman gland sin	19	Skin	57		
Subman gland dx	20	PTV_Spinal canal	58		
Parotid dx	21	PTV_Brain	59		
Parotid sin	22	PTV_CSI_2	60		
Esophagus	23	PTV_Fossa post	61		
Fossa posterior	24	Body_Optimizer	62		
Bladder	25	Boost_Optimizer	63		
Brainstem	26	Neck_Avoidance	64		
Hippocampus dx	27	PTV_Brain_prot	65		
Eye sin	28	TumorBed	66		
Eye dx	29	Boost CTV 1.5cm	67		
Kidney dx	30	Boost CTV 1.0cm	68		
Kidney sin	31	Boost CTV 0.5cm	69		
Mandible	32	Boost PTV1.5+0.5	70		
Liver	33	Boost PTV1.0+0.5	71		
Heart	34	Boost PTV0.5+0.5	72		
Larynx	35	ConfBoostAvoid	73		
Cochlea	36	Boost_PTV0.5new	74		
Bone tissue	37	Boost_PTV1.0new	75		
Colon	38	Boost_PTV1.5new	76		

Appendix 3: summary of plans and patients details.

Patient No	Providing Institution	Sex	Age	CSI Dose	Boost	Boost dose
1	Mayo Clinic	F	38	36	Y	19.8
2		F	14	36	Y	19.8
3	Haukeland University Hospital	M	11	23.4	N	NA
4		F	7	23.4	N	NA
5		F	8	23.4	N	NA
6		M	8	23.4	N	NA
7		M	8	23.4	N	NA
8		F	5	23.4	N	NA
9	Rigshospitalet	F	5	23.4	N	NA
10		F	5	23.4	N	NA
11		M	6	23.4	N	NA
12		M	5	23.4	N	NA

Appendix 4: Whole body MIP of photon plans of Patients 9 – 12 with and without boost.



Whole body MIP for Patients 9-12 without boost and with boost to the posterior fossa. The difference in MIP was found to be small, and was less likely to impact overall outcome in any significant degree. The difference in MIP across the three models for the patients presented in this appendix was found to be not statsically significant (p-value = 0.65)

Appendix 5: List of publication and conference papers

C. Timlin, D. R. Warren, B. Rowland, **A. Madkhali**, J. Loken, M. Partridge, B. Jones, J. Kruse, and R. Miller, "3D calculation of radiation-induced second cancer risk including dose and tissue response heterogeneities" *Medical Physics* 42, 866 (2015); doi: 10.1118/1.4905158

Contribution: as this was a parallel project to the DPhil in the team, tasks mainly revolved around assessing information in regards of data (how to compare and analyse risk), drafting and researching comments to reviewers comments (especially the clinically related ones), and overall input and commentary on the various drafts.

Z. D. Guss, **A. Madkhali**, Q. Chen, Y. Zhang, S. Dah, J. Moore and S. A. Terezakis "Intensity-modulated involved-site radiation therapy for non-Hodgkin'slymphoma of the head and neck" *Leukemia and Lymphoma* 58, - Issue 11 (2017); doi:10.1080/10428194.2017.1312388

Contribution: processing the data sets of the patients studied, performing modelling on them using a model to predict EAR (excess absolute risk), and compare different treatment modalities. Contribution also included writing needed for said work, and replying to reviewers comments on risk-analysis related parts.

Meeting	Year	Abstract Title	Authors	Journal (if applicable)
PTOCG	2013	Modelling Malignant Induction Probability in Medulloblastoma for Photon and Proton Therapy	A. M. Madkhali, C. L. Timlin, T. T. Sio, R. C. Miller, J. G. Loken, M. Partridge	International Journal of Particle Therapy 2014 1:1, 149
ESTRO	2014	Investigating Conversion Of Malignant Induction Probability To Cancer Mortality	A. M. Madkhali, C. L. Timlin, T. T. Sio, R. C. Miller, J. G. Loken, M. Partridge	Radiotherapy and Oncology , Volume 111 , S217
ESTRO	2015	The effect of mean dose or voxel-wise calculation in prediction of radiation-induced secondary cancers	A. M. Madkhali, C. L. Timlin, T. T. Sio, R. C. Miller, M. Partridge	Radiotherapy and Oncology , Volume 115 , S794 - S795
NCRI	2015	Calibrating and benchmarking absolute malignant induction probabilities	A. M. Madkhali, C. L. Timlin, M. Partridge	
PTCOG	2016	Radiobiological effectiveness and its role in modelling secondary cancer risk for proton therapy	A. M. Madkhali, C. L. Timlin, M. Partridge	International Journal of Particle Therapy: Summer 2016, Vol. 3, No. 1, pp. 113-114
ASTRO	2016	Radiobiological effectiveness and its role in modelling secondary cancer risk for proton therapy	A. M. Madkhali, C. L. Timlin, M. Partridge	International Journal of Radiation Oncology • Biology • Physics , Volume 96 , Issue 2 , E561
ESTRO	2016	Calibrating absolute malignant induction probabilities into life-time attributable risk	A. M. Madkhali, C. L. Timlin, M. Partridge	Radiotherapy and Oncology , Volume 119 , S395
ARS	2016	Intensity-Modulated Involved-Site Radiation Therapy for Non-Hodgkin's Lymphoma of the Head and Neck	Guss ZD, Madkhali A, Moore J, Zhang Y, Dah S, Terezakis SA	
ICCR	2016	Calibrating absolute malignant induction probabilities into life-time attributable risk	A. M. Madkhali, C. L. Timlin, M. Partridge	
NCRI	2016	Reducing Heart Toxicity In Medulloblastoma Using Proton Therapy	A Madkhali, M Partridge	

Meeting	Year	Abstract Title	Authors	Journal (if applicable)
PTCOG	2017	The effect of mean dose or voxel-wise calculation in prediction of radiation-induced secondary cancers	A. Madkhali, C. Timlin, M. Partridge	International Journal of Particle Therapy: Summer 2017, Vol. 4, No. 1, pp. 21
PTCOG	2017	Reducing Heart Toxicity In Medulloblastoma Using Proton Therapy	A. Madkhali, M. Partridge	International Journal of Particle Therapy: Summer 2017, Vol. 4, No. 1, pp. 28
ASTRO	2017	Relative biological effectiveness and its impact on dose calculation in proton therapy	A. Madkhali, M. Partridge, C. Hanquist Stokkevåg	International Journal of Radiation Oncology • Biology • Physics , Volume 99 , Issue 2 , E606 - E607
ESTRO	2017	Radiobiological effectiveness and its role in modelling secondary cancer risk for proton therapy	A. Madkhali, C. Timlin, M. Partridge	Radiotherapy and Oncology, Volume 123, S530-S531
ESTRO	2017	Reducing Heart Toxicity In Medulloblastoma Using Proton Therapy	A. Madkhali, M. Partridge	Radiotherapy and Oncology, Volume 123, S992
PTCOG	2017	Relative biological effectiveness and its impact on dose calculation in proton therapy	A. Madkhali, M. Partridge, C. Hanquist Stokkevåg	

Bibliography

Abdel-Wahab, M., I. M. Reis and K. Hamilton (2008). "Second primary cancer after radiotherapy for prostate cancer--a seer analysis of brachytherapy versus external beam radiotherapy." Int J Radiat Oncol Biol Phys 72(1): 58-68.

Aleman, B. M., A. W. van den Belt-Dusebout, W. J. Klokman, M. B. Van't Veer, H. Bartelink and F. E. van Leeuwen (2003). "Long-term cause-specific mortality of patients treated for Hodgkin's disease." J Clin Oncol 21(18): 3431-3439.

Aoki-Nakano, M., Y. Furusawa, A. Uzawa, Y. Matsumoto, R. Hirayama, C. Tsuruoka, T. Ogino, T. Nishio, K. Kagawa, M. Murakami, G. Kagiya, K. Kume, M. Hatashita, S. Fukuda, K. Yamamoto, H. Fuji, S. Murayama, M. Hata, T. Sakae and H. Matsumoto (2014). "Relative biological effectiveness of therapeutic proton beams for HSG cells at Japanese proton therapy facilities." J Radiat Res 55(4): 812-815.

Ardenfors, O., D. Josefsson and A. Daşu (2014). "Are IMRT treatments in the head and neck region increasing the risk of secondary cancers?" Acta Oncol 53(8): 1041-1047.

Arias, E. (2014). "United States life tables, 2009." Natl Vital Stat Rep 62(7): 1-63.

Balducci, M., S. Chiesa, D. Chieffo, S. Manfrida, N. Dinapoli, A. Fiorentino, F. Micciche, V. Frascino, C. Anile, V. Valentini and B. De Bari (2012). "The role of radiotherapy in adult medulloblastoma: long-term single-institution experience and a review of the literature." J Neurooncol 106(2): 315-323.

Barendsen, G.W. (1968) Responses of cultured cells, tumours and normal tissues to radiations of different linear energy transfer. Curr. Top. Radiat. Res. Q (4): 293–356.

Barendsen, G. W. (1982). "Dose fractionation, dose rate and iso-effect relationships for normal tissue responses." Int J Radiat Oncol Biol Phys 8(11): 1981-1997.

Bartkowiak, D., N. Humble, P. Suhr, J. Hagg, K. Mair, B. Polivka, U. Schneider, D. Bottke and T. Wiegel (2012). "Second cancer after radiotherapy, 1981-2007." Radiother Oncol 105(1): 122-126.

BEIR, Health Risks from Exposure to Low Levels of Ionizing Radiation: BEIR VII, Phase 2 (National Academy of Science, Washington, DC, 2006).

Belli, M., D. Bettega, P. Calzolari, F. Cera, R. Cherubini, M. Dalla Vecchia, M. Durante, S. Favaretto, G. Gialanella, G. Grossi, R. Marchesini, G. Moschini, A. Piazzola, G. Poli, M. Pugliese, O. Sapora, P. Scampoli, G. Simone, E. Sorrentino, M. A. Tabocchini, L. Tallone and P. Tiveron (2000). "Inactivation of human normal and tumour cells irradiated with low energy protons." Int J Radiat Biol 76(6): 831-839.

Bentzen, S. M., L. S. Constine, J. O. Deasy, A. Eisbruch, A. Jackson, L. B. Marks, R. K. Ten Haken and E. D. Yorke (2010). "Quantitative Analyses of Normal Tissue Effects in the Clinic (QUANTEC): an introduction to the scientific issues." Int J Radiat Oncol Biol Phys 76(3 Suppl): S3-9.

Bentzen, S. M., J. Z. Skoczylas and J. Bernier (2000). "Quantitative clinical radiobiology of early and late lung reactions." Int J Radiat Biol 76(4): 453-462.

Berrington de Gonzalez, A., E. Gilbert, R. Curtis, P. Inskip, R. Kleinerman, L. Morton, P. Rajaraman and M. P. Little (2013). "Second solid cancers after radiation therapy: a systematic review of the epidemiologic studies of the radiation dose-response relationship." Int J Radiat Oncol Biol Phys 86(2): 224-233.

Bhandare, N., A. Jackson, A. Eisbruch, C. C. Pan, J. C. Flickinger, P. Antonelli and W. M. Mendenhall (2010). "Radiation therapy and hearing loss." Int J Radiat Oncol Biol Phys 76(3 Suppl): S50-57.

Bhatia, S., L. L. Robison, O. Oberlin, M. Greenberg, G. Bunin, F. Fossati-Bellani and A. T. Meadows (1996). "Breast cancer and other second neoplasms after childhood Hodgkin's disease." N Engl J Med 334(12): 745-751.

Bhatia, S. and C. Sklar (2002). "Second cancers in survivors of childhood cancer." Nat Rev Cancer 2(2): 124-132.

Bhatti P, L. H. Veiga, C. M. Ronckers, A. J. Sigurdson, M. Stovall, S. A. Smith, R. Weathers, W. Leisenring, A. C. Mertens, S. Hammond, D. L. Friedman, J. P. Neglia, A. T. Meadows, S. S. Donaldson, C. A. Sklar, L. L. Robison, P. D. Inskip (2010). “Risk of second primary thyroidcancer after radiotherapy for a childhood cancer in a large cohort study: an update from the childhood cancer survivor study.” Radiat Res. 174(6):741-52.

Birdwell, S. H., S. L. Hancock, A. Varghese, R. S. Cox and R. T. Hoppe (1997). "Gastrointestinal cancer after treatment of Hodgkin's disease." Int J Radiat Oncol Biol Phys 37(1): 67-73.

Bloom, H. J. and E. M. Bessell (1990). "Medulloblastoma in adults: a review of 47 patients treated between 1952 and 1981." Int J Radiat Oncol Biol Phys 18(4): 763-772.

Boice, J. D. (2001). “Radiation and breast carcinogenesis.” Med. Pediatr. Oncol., 36(5): 508-513.

Boice, J. D., Jr., N. E. Day, A. Andersen, L. A. Brinton, R. Brown, N. W. Choi, E. A. Clarke, M. P. Coleman, R. E. Curtis, J. T. Flannery and et al. (1985). "Second cancers following radiation treatment for cervical cancer. An international collaboration among cancer registries." J Natl Cancer Inst 74(5): 955-975.

Boice, J. D., Jr., G. Engholm, R. A. Kleinerman, M. Blettner, M. Stovall, H. Lisco, W. C. Moloney, D. F. Austin, A. Bosch, D. L. Cookfair, E. T. Krementz, H. B. Latourette, J. A. Merrill, L. J. Peters, M. D. Schulz, H. H. Storm, E. Bjorkholm, F. Pettersson, C. M. Janine Bell, M. P. Coleman, P. Fraser, F. E. Neal, P. Prior, N. W. Choi, T. G. Hislop, M. Koch, N. Kreiger, D. Robb, D. Robson, D. H. Thomson, H. Lochmuller, D. von Fournier, R. Frischkorn, K. E. Kjorstad, A. Rimpela, M. H. Pejovic, V. P. Kirn, H. Stankusova, F. Berrino, K. Sigurdsson, G. B. Hutchison

and B. MacMahon (1988). "Radiation dose and second cancer risk in patients treated for cancer of the cervix." Radiat Res 116(1): 3-55.

Boivin, J. F., G. B. Hutchison, J. H. Lubin and P. Mauch (1992). "Coronary artery disease mortality in patients treated for Hodgkin's disease." Cancer 69(5): 1241-1247.

Borger, J. H., M. J. Hooning, L. J. Boersma, A. Snijders-Keilholz, B. M. Aleman, E. Lintzen, S. van Brussel, P. P. van der Toorn, M. Alwhouhayb and F. E. van Leeuwen (2007). "Cardiotoxic effects of tangential breast irradiation in early breast cancer patients: the role of irradiated heart volume." Int J Radiat Oncol Biol Phys 69(4): 1131-1138.

Bouffet, E. (2010). "Medulloblastoma in infants: the critical issues of the dilemma." Curr Oncol 17(3): 2-3.

Bragg, W. H. and R. Kleeman (1905). "XXXIX. On the α particles of radium, and their loss of range in passing through various atoms and molecules." Philosophical Magazine Series 6 10(57): 318-340.

Brandes, A. A., E. Franceschi, A. Tosoni, V. Blatt and M. Ermani (2007). "Long-term results of a prospective study on the treatment of medulloblastoma in adults." Cancer 110(9): 2035-2041.

Brandes, A. A. and M. K. Paris (2004). "Review of the prognostic factors in medulloblastoma of children and adults." Crit Rev Oncol Hematol 50(2): 121-128.

Brenner, D. J. (2004). "Fractionation and late rectal toxicity." Int J Radiat Oncol Biol Phys 60(4): 1013-1015.

Brenner, D. J. (2014). "What we know and what we don't know about cancer risks associated with radiation doses from radiological imaging." Br J Radiol 87(1035): 20130629.

Brenner, D. J., R. E. Curtis, E. J. Hall and E. Ron (2000). "Second malignancies in prostate carcinoma patients after radiotherapy compared with surgery." Cancer 88(2): 398-406.

Brenner, D. J., C. D. Elliston, E. J. Hall and H. Paganetti (2009). "Reduction of the secondary neutron dose in passively scattered proton radiotherapy, using an optimized pre-collimator/collimator." Phys Med Biol 54(20): 6065-6078.

Brenner, D. J. and E. J. Hall (2008). "Secondary neutrons in clinical proton radiotherapy: a charged issue." Radiother Oncol 86(2): 165-170.

Brenner, D. J. and I. Shuryak (2011). "Ten years of follow-up is not long enough to assess lifetime cancer risks caused by computed tomography scans in a young population." J Clin Oncol 29(30): 4062; author reply 4062.

Britten, R. A., V. Nazaryan, L. K. Davis, S. B. Klein, D. Nichiporov, M. S. Mendonca, M. Wolanski, X. Nie, J. George and C. Keppel (2013). "Variations in the RBE for cell killing along the depth-dose profile of a modulated proton therapy beam." Radiat Res 179(1): 21-28.

Brodin, N. P., P. Munck Af Rosenschold, M. C. Aznar, A. Kiil-Berthelsen, I. R. Vogelius, P. Nilsson, B. Lannering and T. Bjork-Eriksson (2011). "Radiobiological risk estimates of adverse events and secondary cancer for proton and photon radiation therapy of pediatric medulloblastoma." Acta Oncol 50(6): 806-816.

Brodin, N. P., I. R. Vogelius, M. V. Maraldo, P. Munck af Rosenschold, M. C. Aznar, A. Kiil-Berthelsen, P. Nilsson, T. Bjork-Eriksson, L. Specht and S. M. Bentzen (2012). "Life years lost--comparing potentially fatal late complications after radiotherapy for pediatric medulloblastoma on a common scale." Cancer 118(21): 5432-5440.

Buhring, U., M. Strayle-Batra, D. Freudenstein, H. G. Scheel-Walter and W. Kuker (2002). "MRI features of primary, secondary and metastatic medulloblastoma." Eur Radiol 12(6): 1342-1348.

Bull, K. S., H. A. Spoudeas, G. Yadegarfar and C. R. Kennedy (2007). "Reduction of health status 7 years after addition of chemotherapy to craniospinal irradiation for medulloblastoma: a follow-up study in PNET 3 trial survivors on behalf of the CCLG (formerly UKCCSG)." J Clin Oncol 25(27): 4239-4245.

Burman, C., G. J. Kutcher, B. Emami and M. Goitein (1991). "Fitting of normal tissue tolerance data to an analytic function." Int J Radiat Oncol Biol Phys 21(1): 123-135.

Cahan, W. G., H. Q. Woodard and et al. (1948). "Sarcoma arising in irradiated bone; report of 11 cases." Cancer 1(1): 3-29.

Cancer Research UK (2015), Breast cancer incidence (invasive) statistics, Cancer Research UK.

Carabe-Fernandez, A., R. G. Dale and B. Jones (2007). "The incorporation of the concept of minimum RBE (RbEmin) into the linear-quadratic model and the potential for improved radiobiological analysis of high-LET treatments." Int J Radiat Biol 83(1): 27-39.

Carmel, R. J. and H. S. Kaplan (1976). "Mantle irradiation in Hodgkin's disease. An analysis of technique, tumor eradication, and complications." Cancer 37(6): 2813-2825.

Carrie, C., C. Lasset, C. Alapetite, C. Haie-Meder, S. Hoffstetter, M. C. Demaille, C. Kerr, J. P. Wagner, J. L. Lagrange, J. P. Maire and et al. (1994). "Multivariate analysis of prognostic factors in adult patients with medulloblastoma. Retrospective study of 156 patients." Cancer 74(8): 2352-2360.

CBTRUS, (2004-2005). Primary Brain Tumors in the United States, Statistical Report, 1997–2001, Years Data Collected. Chicago, US, Chicago: Central BrainTumor Registry of the United States.

Chang, C. H., E. M. Housepian, and C. Herbert (1969). “An Operative Staging System and a Megavoltage Radiotherapeutic Technic for Cerebellar Medulloblastomas”. Radiology, 93(6): 1351-59.

Chargari, C., K. A. Goodman, I. Diallo, J. B. Guy, C. Rancoule, J. M. Cosset, E. Deutsch and N. Magne (2016). "Risk of second cancers in the era of modern radiation therapy: does the risk/benefit analysis overcome theoretical models?" Cancer Metastasis Rev 35(2): 277-288.

Chung, E., J. R. Corbett, J. M. Moran, K. A. Griffith, R. B. Marsh, M. Feng, R. Jagsi, M. L. Kessler, E. C. Ficaro and L. J. Pierce (2013). "Is there a dose-response relationship for heart disease with low-dose radiation therapy?" Int J Radiat Oncol Biol Phys 85(4): 959-964.

Clarke, M., R. Collins, S. Darby, C. Davies, P. Elphinstone, V. Evans, J. Godwin, R. Gray, C. Hicks, S. James, E. MacKinnon, P. McGale, T. McHugh, R. Peto, C. Taylor and Y. Wang (2005). "Effects of radiotherapy and of differences in the extent of surgery for early breast cancer on local recurrence and 15-year survival: an overview of the randomised trials." Lancet 366(9503): 2087-2106.

Cogen, P. H. and J. D. McDonald (1996). "Tumor suppressor genes and medulloblastoma." J Neurooncol 29(1): 103-112.

Correa, C. R., H. I. Litt, W. T. Hwang, V. A. Ferrari, L. J. Solin and E. E. Harris (2007). "Coronary artery findings after left-sided compared with right-sided radiation treatment for early-stage breast cancer." J Clin Oncol 25(21): 3031-3037.

Crawford, J. R., T. J. MacDonald and R. J. Packer (2007). "Medulloblastoma in childhood: new biological advances." Lancet Neurol 6(12): 1073-1085.

Cuaron, J. J., C. Chang, M. Lovelock, D. S. Higginson, D. Mah, O. Cahlon and S. Powell (2016). "Exponential Increase in Relative Biological Effectiveness Along Distal Edge of a Proton Bragg Peak as Measured by Deoxyribonucleic Acid Double-Strand Breaks." Int J Radiat Oncol Biol Phys 95(1): 62-69.

Cumberlin, R. L., K. H. Luk, W. M. Wara, G. E. Sheline and C. B. Wilson (1979). "Medulloblastoma: treatment results and effect on normal tissues." Cancer 43(3): 1014-1020.

Dale, E. and D. R. Olsen (1997). "Specification of the dose to organs at risk in external beam radiotherapy." Acta Oncol 36(2): 129-135.

Dale, R. G. (1985). "The application of the linear-quadratic dose-effect equation to fractionated and protracted radiotherapy." Br J Radiol 58(690): 515-528.

Dale, R. G. and B. Jones (1999). "The assessment of RBE effects using the concept of biologically effective dose." Int J Radiat Oncol Biol Phys 43(3): 639-645.

Dale, R. G., B. Jones and A. Carabe-Fernandez (2009). "Why more needs to be known about RBE effects in modern radiotherapy." Appl Radiat Isot 67(3): 387-392.

Darby, S. C., D. J. Cutter, M. Boerma, L. S. Constine, L. F. Fajardo, K. Kodama, K. Mabuchi, L. B. Marks, F. A. Mettler, L. J. Pierce, K. R. Trott, E. T. Yeh and R. E. Shore (2010). "Radiation-related heart disease: current knowledge and future prospects." Int J Radiat Oncol Biol Phys 76(3): 656-665.

Darby, S. C., M. Ewertz, P. McGale, A. M. Bennet, U. Blom-Goldman, D. Bronnum, C. Correa, D. Cutter, G. Gagliardi, B. Gigante, M. B. Jensen, A. Nisbet, R. Peto, K. Rahimi, C. Taylor and P. Hall (2013). "Risk of ischemic heart disease in women after radiotherapy for breast cancer." N Engl J Med 368(11): 987-998.

Darby, S. C., P. McGale, C. W. Taylor and R. Peto (2005). "Long-term mortality from heart disease and lung cancer after radiotherapy for early breast cancer: prospective cohort study of about 300,000 women in US SEER cancer registries." Lancet Oncol 6(8): 557-565.

Das, S. K., A. H. Baydush, S. Zhou, M. Miften, X. Yu, O. Craciunescu, M. Oldham, K. Light, T. Wong, M. Blazing, S. Borges-Neto, M. W. Dewhirst and L. B. Marks (2005). "Predicting radiotherapy-induced cardiac perfusion defects." Med Phys 32(1): 19-27.

Daşu, A., I. Toma-Daşu, L. Franzen, A. Widmark and P. Nilsson (2011). "Secondary malignancies from prostate cancer radiation treatment: a risk analysis of the influence of target margins and fractionation patterns." Int J Radiat Oncol Biol Phys 79(3): 738-746.

Daşu, A., I. Toma-Daşu, J. Olofsson and M. Karlsson (2005). "The use of risk estimation models for the induction of secondary cancers following radiotherapy." Acta Oncol 44(4): 339-347.

Dawson, L. A., B. D. Kavanagh, A. C. Paulino, S. K. Das, M. Miften, X. A. Li, C. Pan, R. K. Ten Haken and T. E. Schultheiss (2010). "Radiation-associated kidney injury." Int J Radiat Oncol Biol Phys 76(3 Suppl): S108-115.

Dawson, L. A., D. Normolle, J. M. Balter, C. J. McGinn, T. S. Lawrence and R. K. Ten Haken (2002). "Analysis of radiation-induced liver disease using the Lyman NTCP model." Int J Radiat Oncol Biol Phys 53(4): 810-821.

De Bruin, M. L., J. Sparidans, M. B. van't Veer, E. M. Noordijk, M. W. Louwman, J. M. Zijlstra, H. van den Berg, N. S. Russell, A. Broeks, M. H. Baaijens, B. M. Aleman and F. E. van Leeuwen (2009). "Breast cancer risk in female survivors of Hodgkin's lymphoma: lower risk after smaller radiation volumes." J Clin Oncol 27(26): 4239-4246.

de Vathaire, F., C. Hardiman, A. Shamsaldin, S. Campbell, E. Grimaud, M. Hawkins, M. Raquin, O. Oberlin, I. Diallo, J. M. Zucker, X. Panis, J. L. Lagrange, N. Daly-Schveitzer, J. Lemerle, J. Chavaudra, M. Schlumberger and C. Bonaiti (1999). "Thyroid carcinomas after irradiation for a first cancer during childhood." Arch Intern Med 159(22): 2713-2719.

Deacon, J., M. J. Peckham and G. G. Steel (1984). "The radioresponsiveness of human tumours and the initial slope of the cell survival curve." Radiother Oncol 2(4): 317-323.

Deasy, J. O., A. I. Blanco and V. H. Clark (2003). "CERR: a computational environment for radiotherapy research." Med Phys 30(5): 979-985.

Deasy, J. O., V. Moiseenko, L. Marks, K. S. Chao, J. Nam and A. Eisbruch (2010). "Radiotherapy dose-volume effects on salivary gland function." Int J Radiat Oncol Biol Phys 76(3 Suppl): S58-63.

Delaney, G., S. Jacob, C. Featherstone, and M. Barton (2005) “The role of radiotherapy in cancer treatment: estimating optimal utilization from a

review of evidence-based clinical guidelines." Cancer 15;104(6):1129-37. Erratum in: Cancer. 2006Aug 1;107(3):660.

DeLaney and Kooy [ed.], "Proton and charges particle therapy", Wolters Kluwer, ISBN 978-0-7817-6552-7 (2008)

Dhall, G. (2009). "Medulloblastoma." J Child Neurol 24(11): 1418-1430.

Diallo, I., N. Haddy, E. Adjadj, A. Samand, E. Quiniou, J. Chavaudra, I. Alziar, N. Perret, S. Guerin, D. Lefkopoulos and F. de Vathaire (2009). "Frequency distribution of second solid cancer locations in relation to the irradiated volume among 115 patients treated for childhood cancer." Int J Radiat Oncol Biol Phys 74(3): 876-883.

Donovan, E. M., H. James, M. Bonora, J. R. Yarnold and P. M. Evans (2012). "Second cancer incidence risk estimates using BEIR VII models for standard and complex external beam radiotherapy for early breast cancer." Med Phys 39(10): 5814-5824.

Dores, G. M., R. E. Curtis, F. E. van Leeuwen, M. Stovall, P. Hall, C. F. Lynch, S. A. Smith, R. E. Weathers, H. H. Storm, D. C. Hodgson, R. A. Kleinerman, H. Joensuu, T. B. Johannesen, M. Andersson, E. J. Holowaty, M. Kaijser, E. Pukkala, L. Vaalavirta, S. D. Fossa, F. Langmark, L. B. Travis, J. F. Fraumeni, Jr., B. M. Aleman, L. M. Morton and E. S. Gilbert (2014). "Pancreatic cancer risk after treatment of Hodgkin lymphoma." Ann Oncol 25(10): 2073-2079.

Dores, G. M., C. Metayer, R. E. Curtis, C. F. Lynch, E. A. Clarke, B. Glimelius, H. Storm, E. Pukkala, F. E. van Leeuwen, E. J. Holowaty, M. Andersson, T. Wiklund, T. Joensuu, M. B. van't Veer, M. Stovall, M. Gospodarowicz and L. B. Travis (2002). "Second malignant neoplasms among long-term survivors of Hodgkin's disease: a population-based evaluation over 25 years." J Clin Oncol 20(16): 3484-3494.

Dumas, A., C. Berger, P. Auquier, G. Michel, B. Fresneau, R. Setcheou Allodji, N. Haddy, C. Rubino, G. Vassal, D. Valteau-Couanet, S. Thouvenin-Doulet, L. Casagranda, H. Pacquement, C. El-Fayech, O. Oberlin, C. Guibout and F. de Vathaire (2016). "Educational and occupational outcomes of childhood

cancer survivors 30 years after diagnosis: a French cohort study." Br J Cancer 114(9): 1060-1068.

Ellison, D. W. (2010). "Childhood medulloblastoma: novel approaches to the classification of a heterogeneous disease." Acta Neuropathol 120(3): 305-316.

Ellison, D. W., O. E. Onilude, J. C. Lindsey, M. E. Lusher, C. L. Weston, R. E. Taylor, A. D. Pearson and S. C. Clifford (2005). "beta-Catenin status predicts a favorable outcome in childhood medulloblastoma: the United Kingdom Children's Cancer Study Group Brain Tumour Committee." J Clin Oncol 23(31): 7951-7957.

Emami, B., J. Lyman, A. Brown, L. Coia, M. Goitein, J. E. Munzenrider, B. Shank, L. J. Solin and M. Wesson (1991). "Tolerance of normal tissue to therapeutic irradiation." Int J Radiat Oncol Biol Phys 21(1): 109-122.

Eriksson, F., G. Gagliardi, A. Liedberg, I. Lax, C. Lee, S. Levitt, B. Lind and L. E. Rutqvist (2000). "Long-term cardiac mortality following radiation therapy for Hodgkin's disease: analysis with the relative seriality model." Radiother Oncol 55(2): 153-162.

Fontenot, J. D., Bloch, C., Followill, D., Titt, U., and Newhauser, W. D. (2010). “Estimate of the uncertainties in the relative risk of secondary malignant neoplasms following proton therapy and intensity-modulated photon therapy.” Physics in Medicine and Biology, 55(23), 6987–6998.

Fossati, P., U. Ricardi and R. Orecchia (2009). "Pediatric medulloblastoma: toxicity of current treatment and potential role of protontherapy." Cancer Treat Rev 35(1): 79-96.

Fowler, J. F. (1989). "The linear-quadratic formula and progress in fractionated radiotherapy." Br J Radiol 62(740): 679-694.

Fowler, J. F. (2010). "21 years of biologically effective dose." Br J Radiol 83(991): 554-568.

Friedman, D. L., J. Whitton, W. Leisenring, A. C. Mertens, S. Hammond, M. Stovall, S. S. Donaldson, A. T. Meadows, L. L. Robison and J. P. Neglia (2010). "Subsequent neoplasms in 5-year survivors of childhood cancer: the Childhood Cancer Survivor Study." J Natl Cancer Inst 102(14): 1083-1095.

Frost, P. J., N. J. Laperriere, C. S. Wong, M. F. Milosevic, W. J. Simpson and M. Pintilie (1995). "Medulloblastoma in adults." Int J Radiat Oncol Biol Phys 32(4): 951-957.

Fuji, H., U. Schneider, Y. Ishida, M. Konno, H. Yamashita, Y. Kase, S. Murayama, T. Onoe, H. Ogawa, H. Harada, H. Asakura and T. Nishimura (2013). "Assessment of organ dose reduction and secondary cancer risk associated with the use of proton beam therapy and intensity modulated radiation therapy in treatment of neuroblastomas." Radiat Oncol 8: 255.

Gagliardi, G., L. S. Constine, V. Moiseenko, C. Correa, L. J. Pierce, A. M. Allen and L. B. Marks (2010). "Radiation dose-volume effects in the heart." Int J Radiat Oncol Biol Phys 76(3 Suppl): S77-85.

Gaspar, L. E., D. J. Dawson, S. A. Tilley-Gulliford and P. Banerjee (1991). "Medulloblastoma: long-term follow-up of patients treated with electron irradiation of the spinal field." Radiology 180(3): 867-870.

Gerweck, L. E. and S. V. Kozin (1999). "Relative biological effectiveness of proton beams in clinical therapy." Radiother Oncol 50(2): 135-142.

Gilbert, E. S., M. Stovall, M. Gospodarowicz, F. E. Van Leeuwen, M. Andersson, B. Glimelius, T. Joensuu, C. F. Lynch, R. E. Curtis, E. Holowaty, H. Storm, E. Pukkala, M. B. van't Veer, J. F. Fraumeni, J. D. Boice, Jr., E. A. Clarke and L. B. Travis (2003). "Lung cancer after treatment for Hodgkin's disease: focus on radiation effects." Radiat Res 159(2): 161-173.

Gilbertson, R. J. and D. W. Ellison (2008). "The origins of medulloblastoma subtypes." Annu Rev Pathol 3: 341-365.

Giordana, M. T., D. Duo, S. Gasverde, E. Trevisan, A. Boghi, I. Morra, L. Pradotto, A. Mauro and A. Chio (2002). "MDM2 overexpression is associated

with short survival in adults with medulloblastoma." Neuro Oncol 4(2): 115-122.

Giordana, M. T., P. Schiffer, M. Lanotte, P. Girardi and A. Chio (1999). "Epidemiology of adult medulloblastoma." Int J Cancer 80(5): 689-692.

Goitein, M. and M. Jermann (2003). "The relative costs of proton and X-ray radiation therapy." Clin Oncol (R Coll Radiol) 15(1): S37-50.

Goldstein, A. M., J. Yuen and M. A. Tucker (1997). "Second cancers after medulloblastoma: population-based results from the United States and Sweden." Cancer Causes Control 8(6): 865-871.

Gottschalk, B. (2006). "Neutron dose in scattered and scanned proton beams: in regard to Eric J. Hall (Int J Radiat Oncol Biol Phys 2006;65:1-7)." Int J Radiat Oncol Biol Phys 66(5): 1594; author reply 1595.

Grahn, D., L. S. Lombard and B. A. Carnes (1992). "The comparative tumorigenic effects of fission neutrons and cobalt-60 gamma rays in the B6CF1 mouse." Radiat Res 129(1): 19-36.

Grantzau, T., L. Mellemkjaer and J. Overgaard (2013). "Second primary cancers after adjuvant radiotherapy in early breast cancer patients: a national population based study under the Danish Breast Cancer Cooperative Group (DBCG)." Radiother Oncol 106(1): 42-49.

Grassberger, C., A. Trofimov, A. Lomax, and H. Paganetti. (2011) “Variations in linear energy transfer within clinical proton therapy fields and the potential for biological treatment planning.” Int J Radiat Oncol Biol Phys, 80(5): 1559-66.

Guibout C., E. Adjadj, C. Rubino, A. Shamsaldin, E. Grimaud, M. Hawkins, M. C. Mathieu, O. Oberlin, J. M. Zucker, X. Panis, J. L. Lagrange, N. Daly-Schveitzer, J. Chavaudra, F. de Vathaire (2005). “Malignant breast tumors after radiotherapy for a first cancer during childhood.” J Clin Oncol 23(1):197-204.

Guss, Z. D. M., A. M. Madkhali, Y. Zhang, S. Dah and J. T. Moore, S. A. (2016). "(S041) Intensity-Modulated Involved-Site Radiation Therapy for Non-

Hodgkin Lymphoma of the Head and Neck." Oncology (Williston Park) 30 Suppl.

Gyenes, G., T. Fornander, P. Carlens and L. E. Rutqvist (1994). "Morbidity of ischemic heart disease in early breast cancer 15-20 years after adjuvant radiotherapy." Int J Radiat Oncol Biol Phys 28(5): 1235-1241.

Hall, E. J., and C. S. Wuu. (2003). ''Radiation-induced second cancers: the impact of 3D-CRT and IMRT'', Int J Radiat Oncol Biol Phys 56(1): 83-8.

Hall, E. J. (2004). "Henry S. Kaplan Distinguished Scientist Award 2003. The crooked shall be made straight; dose-response relationships for carcinogenesis." Int J Radiat Biol 80(5): 327-337.

Hall, E. J. (2006). "Intensity-modulated radiation therapy, protons, and the risk of second cancers." Int J Radiat Oncol Biol Phys 65(1): 1-7.

Hall, E. J. and D. J. Brenner (2012). "Cancer risks from diagnostic radiology: the impact of new epidemiological data." Br J Radiol 85(1020): e1316-1317.

Halperin, E. C. and H. S. Friedman (1996). "Is there a correlation between duration of presenting symptoms and stage of medulloblastoma at the time of diagnosis?" Cancer 78(4): 874-880.

Halperin, E. C., D. M. Watson and S. L. George (2001). "Duration of symptoms prior to diagnosis is related inversely to presenting disease stage in children with medulloblastoma." Cancer 91(8): 1444-1450.

Hanahan D, Weinberg RA (2000). “The hallmarks of cancer.” Cell 100(1):57-70.

Hanahan D, Weinberg RA (2011). “Hallmarks of cancer: the next generation.” Cell 144(5):646-74.

Hancock, S. L., S. S. Donaldson and R. T. Hoppe (1993). "Cardiac disease following treatment of Hodgkin's disease in children and adolescents." J Clin Oncol 11(7): 1208-1215.

Hancock, S. L., M. A. Tucker and R. T. Hoppe (1993). "Breast cancer after treatment of Hodgkin's disease." J Natl Cancer Inst 85(1): 25-31.

Hancock, S. L., M. A. Tucker and R. T. Hoppe (1993). "Factors affecting late mortality from heart disease after treatment of Hodgkin's disease." Jama 270(16): 1949-1955.

Harris, E. E., C. Correa, W. T. Hwang, J. Liao, H. I. Litt, V. A. Ferrari and L. J. Solin (2006). "Late cardiac mortality and morbidity in early-stage breast cancer patients after breast-conservation treatment." J Clin Oncol 24(25): 4100-4106.

Harrison, R. M. (2004). "Second cancers following radiotherapy: a suggested common dosimetry framework for therapeutic and concomitant exposures." Br J Radiol 77(924): 986-990.

Hartley, K. A., C. Li, F. H. Laningham, M. J. Krasin, X. Xiong and T. E. Merchant (2008). "Vertebral body growth after craniospinal irradiation." Int J Radiat Oncol Biol Phys 70(5): 1343-1349.

Hauptmann, M., T. Borge Johannesen, E. S. Gilbert, M. Stovall, F. E. van Leeuwen, P. Rajaraman, S. A. Smith, R. E. Weathers, B. M. Aleman, M. Andersson, R. E. Curtis, G. M. Dores, J. F. Fraumeni, Jr., P. Hall, E. J. Holowaty, H. Joensuu, M. Kaijser, R. A. Kleinerman, F. Langmark, C. F. Lynch, E. Pukkala, H. H. Storm, L. Vaalavirta, A. W. van den Belt-Dusebout, L. M. Morton, S. D. Fossa and L. B. Travis (2016). "Increased pancreatic cancer risk following radiotherapy for testicular cancer." Br J Cancer.

Hauptmann, M., S. D. Fossa, M. Stovall, F. E. van Leeuwen, T. B. Johannesen, P. Rajaraman, E. S. Gilbert, S. A. Smith, R. E. Weathers, B. M. Aleman, M. Andersson, R. E. Curtis, G. M. Dores, J. F. Fraumeni, P. Hall, E. J. Holowaty, H. Joensuu, M. Kaijser, R. A. Kleinerman, F. Langmark, C. F. Lynch, E. Pukkala, H. H. Storm, L. Vaalavirta, A. W. van den Belt-Dusebout, L. B. Travis and L. M. Morton (2015). "Increased stomach cancer risk following radiotherapy for testicular cancer." Br J Cancer 112(1): 44-51.

Hauri, P., R. A. Halg, J. Besserer and U. Schneider (2016). "A general model for stray dose calculation of static and intensity-modulated photon radiation." Med Phys 43(4): 1955.

Hazin, I., G. Dellatolas, D. Garcia, F. Pedrosa and A. Pedrosa (2011). "Intellectual impairment after treatment for medulloblastoma and astrocytoma in childhood: the Brazilian experience." J Pediatr Hematol Oncol 33(7): 506-515.

Hennings H, AB Glick, DA Greenhalgh, DL Morgan, JE Strickland, T Tennenbaum, and SH Yuspa SH. Critical aspects of initiation, promotion, and progression in multistage epidermal carcinogenesis. Proc Soc Exp Biol Med. 1993 Jan;202(1):1-8.

Hill, D. A., E. Gilbert, G. M. Dores, M. Gospodarowicz, F. E. van Leeuwen, E. Holowaty, B. Glimelius, M. Andersson, T. Wiklund, C. F. Lynch, M. Van't Veer, H. Storm, E. Pukkala, M. Stovall, R. E. Curtis, J. M. Allan, J. D. Boice and L. B. Travis (2005). "Breast cancer risk following radiotherapy for Hodgkin lymphoma: modification by other risk factors." Blood 106(10): 3358-3365.

Hojris, I., M. Overgaard, J. J. Christensen and J. Overgaard (1999). "Morbidity and mortality of ischaemic heart disease in high-risk breast-cancer patients after adjuvant postmastectomy systemic treatment with or without radiotherapy: analysis of DBCG 82b and 82c randomised trials. Radiotherapy Committee of the Danish Breast Cancer Cooperative Group." Lancet 354(9188): 1425-1430.

Hooning, M. J., A. Botma, B. M. Aleman, M. H. Baaijens, H. Bartelink, J. G. Klijn, C. W. Taylor and F. E. van Leeuwen (2007). "Long-term risk of cardiovascular disease in 10-year survivors of breast cancer." J Natl Cancer Inst 99(5): 365-375.

Hoppe-Hirsch, E., L. Brunet, F. Laroussinie, G. Cinalli, A. Pierre-Kahn, D. Renier, C. Sainte-Rose and J. F. Hirsch (1995). "Intellectual outcome in children with malignant tumors of the posterior fossa: influence of the field of

irradiation and quality of surgery." Childs Nerv Syst 11(6): 340-345; discussion 345-346.

ICRP, 1991. 1990 Recommendations of the International Commission on Radiological Protection. ICRP Publication 60. Ann. ICRP 21 (1-3).

ICRP, 2005. Low-dose Extrapolation of Radiation-related Cancer Risk. ICRP Publication 99. Ann. ICRP 35 (4).

ICRP, 2007. The 2007 Recommendations of the International Commission on Radiological Protection. ICRP Publication 103. Ann. ICRP 37 (2-4).

ICRU 2007 Prescribing, recording, and reporting proton-beam therapy Report No. 78 (Bethesda, MD: ICRU)

INFN (2008). Rivista dell'Istituto Nazionale di Fisica Nucleare. Asimmetrie 3(6):6.

Inskip, P. D., A. J. Sigurdson, L. Veiga, P. Bhatti, C. Ronckers, P. Rajaraman, H. Boukheris, M. Stovall, S. Smith, S. Hammond, T. O. Henderson, T. C. Watt, A. C. Mertens, W. Leisenring, K. Stratton, J. Whitton, S. S. Donaldson, G. T. Armstrong, L. L. Robison and J. P. Neglia (2016). "Radiation-Related New Primary Solid Cancers in the Childhood Cancer Survivor Study: Comparative Radiation Dose Response and Modification of Treatment Effects." Int J Radiat Oncol Biol Phys 94(4): 800-807.

Inskip, P. D., L. L. Robison, M. Stovall, S. A. Smith, S. Hammond, A. C. Mertens, J. A. Whitton, L. Diller, L. Kenney, S. S. Donaldson, A. T. Meadows, and J. P. Neglia. (2009) "Radiation Dose and Breast Cancer Risk in the Childhood Cancer Survivor Study" J Clin Oncol, 27: 3901-7.

Inskip, P. D., M. Stovall and J. T. Flannery (1994). "Lung cancer risk and radiation dose among women treated for breast cancer." J Natl Cancer Inst 86(13): 983-988.

Jakacki, R. I., J. W. Goldwein, R. L. Larsen, G. Barber and J. H. Silber (1993). "Cardiac dysfunction following spinal irradiation during childhood." J Clin Oncol 11(6): 1033-1038.

Jakacki, R. I., C. M. Schramm, B. R. Donahue, F. Haas and J. C. Allen (1995). "Restrictive lung disease following treatment for malignant brain tumors: a potential late effect of craniospinal irradiation." J Clin Oncol 13(6): 1478-1485.

Jiang, G. L., S. L. Tucker, R. Guttenberger, L. J. Peters, W. H. Morrison, A. S. Garden, C. S. Ha and K. K. Ang (1994). "Radiation-induced injury to the visual pathway." Radiother Oncol 30(1): 17-25.

Jones, B. (2014). "Patterns of failure after proton therapy in medulloblastoma." Int J Radiat Oncol Biol Phys 90(1): 25-26.

Jones, B. (2015). "Towards Achieving the Full Clinical Potential of Proton Therapy by Inclusion of LET and RBE Models." Cancers (Basel) 7(1): 460-480.

Jones, B. and R. G. Dale (2000). "Estimation of optimum dose per fraction for high LET radiations: implications for proton radiotherapy." Int J Radiat Oncol Biol Phys 48(5): 1549-1557.

Jones, B., T. S. Underwood, A. Carabe-Fernandez, C. Timlin, and R. G. Dale. (2011). “Fast neutron relative biological effects and implications for charged particle therapy.” Br J Radiol, 84 (Spec No 1): S11-8.

Jones, B., P. Wilson, A. Nagano, J. Fenwick and G. McKenna (2012). "Dilemmas concerning dose distribution and the influence of relative biological effect in proton beam therapy of medulloblastoma." Br J Radiol 85(1018): e912-918.

Kallman, P., A. Agren and A. Brahme (1992). "Tumour and normal tissue responses to fractionated non-uniform dose delivery." Int J Radiat Biol 62(2): 249-262.

Kavanagh, B. D., C. C. Pan, L. A. Dawson, S. K. Das, X. A. Li, R. K. Ten Haken and M. Miften (2010). "Radiation dose-volume effects in the stomach and small bowel." Int J Radiat Oncol Biol Phys 76(3 Suppl): S101-107.

Kellerer, A. M., E. A. Nekolla and L. Walsh (2001). "On the conversion of solid cancer excess relative risk into lifetime attributable risk." Radiat Environ Biophys 40(4): 249-257.

Kanemoto, A., R. Hirayama, T. Moritake, Y. Furusawa, L. Sun, T. Sakae, A. Kuno, T. Terunuma, K. Yasuoka, Y. Mori, K. Tsuboi, and H. Sakurai (2014). "RBE and OER within the spread-out Bragg peak for proton beam therapy: in vitro study at the Proton Medical Research Center at the University of Tsukuba." J Radiat Res 55(5): 1028-32.

Kerr, G. D. (2012). "DS86 and DS02 organ dose calculations." Radiat Prot Dosimetry 149(1): 15-20.

Kiltie A.E., Lashford L.S., and Gattamaneni H.R. (1997). "Survival and late effects in medulloblastoma patients treated with craniospinal irradiation under three years old." Med Pediatr Oncol 28 (5): 348-54.

Kirkpatrick, J. P., A. J. van der Kogel and T. E. Schultheiss (2010). "Radiation dose-volume effects in the spinal cord." Int J Radiat Oncol Biol Phys 76(3 Suppl): S42-49.

Koehler, A. M., and W. M. Preston (1972). "Protons in radiation therapy. Comparative dose distributions for protons, photons, and electrons", Radiology, 104(1): 191-195.

Koeller, K. K. and E. J. Rushing (2003). "From the archives of the AFIP: medulloblastoma: a comprehensive review with radiologic-pathologic correlation." Radiographics 23(6): 1613-1637.

Kortmann, R. D., J. Kuhl, B. Timmermann, U. Mittler, C. Urban, V. Budach, E. Richter, N. Willich, M. Flentje, F. Berthold, I. Slavc, J. Wolff, C. Meisner, O. Wiestler, N. Sorensen, M. Warmuth-Metz and M. Bamberg (2000). "Postoperative neoadjuvant chemotherapy before radiotherapy as compared to immediate radiotherapy followed by maintenance chemotherapy in the treatment of medulloblastoma in childhood: results of the German prospective randomized trial HIT '91." Int J Radiat Oncol Biol Phys 46(2): 269-279.

Kumar, R., G. Achari, D. Banerjee and D. K. Chhabra (2001). "Uncommon presentation of medulloblastoma." Childs Nerv Syst 17(9): 538-542; discussion 543.

Kunschner, L. J., J. Kuttesch, K. Hess and W. K. Yung (2001). "Survival and recurrence factors in adult medulloblastoma: the M.D. Anderson Cancer Center experience from 1978 to 1998." Neuro Oncol 3(3): 167-173.

Kutcher, G. J. and C. Burman (1989). "Calculation of complication probability factors for non-uniform normal tissue irradiation: the effective volume method." Int J Radiat Oncol Biol Phys 16(6): 1623-1630.

Lai R. “Survival of patients with adult medulloblastoma: a population-based study.” Cancer . 2008;112(7):1568–1574

Langendijk, J. A., P. Lambin, D. De Ruysscher, J. Widder, M. Bos and M. Verheij (2013). "Selection of patients for radiotherapy with protons aiming at reduction of side effects: the model-based approach." Radiother Oncol 107(3): 267-273.

Lawrence, Y. R., X. A. Li, I. el Naqa, C. A. Hahn, L. B. Marks, T. E. Merchant and A. P. Dicker (2010). "Radiation dose-volume effects in the brain." Int J Radiat Oncol Biol Phys 76(3 Suppl): S20-27.

Lee, A. W., W. Foo, R. Chappell, J. F. Fowler, W. M. Sze, Y. F. Poon, S. C. Law, S. H. Ng, S. K. O, S. Y. Tung, W. H. Lau and J. H. Ho (1998). "Effect of time, dose, and fractionation on temporal lobe necrosis following radiotherapy for nasopharyngeal carcinoma." Int J Radiat Oncol Biol Phys 40(1): 35-42.

Li, F. P., J. R. Cassady and N. Jaffe (1975). "Risk of second tumors in survivors of childhood cancer." Cancer 35(4): 1230-1235.

Ligot, L., I. Diallo, A. Shamsaldin, J. Chavaudra, C. BonaIti-Pellie and F. de Vathaire (1998). "Individualized phantom based on CT slices and auxological data (ICTA) for dose estimations following radiotherapy for skin haemangioma in childhood." Radiother Oncol 49(3): 279-285.

Little, M. P. (2001). "Comparison of the risks of cancer incidence and mortality following radiation therapy for benign and malignant disease with the cancer risks observed in the Japanese A-bomb survivors." Int J Radiat Biol 77(4): 431-464.

Little, M. P., W. F. Heidenreich, S. H. Moolgavkar, H. Schöllnberger, and D. C. Thomas (2007). “Systems biological and mechanistic modelling of radiation induced cancer.” Radiat. Environ. Biophys. 47, 39–47.

Lyman, J. T. (1985). "Complication probability as assessed from dose-volume histograms." Radiat Res Suppl 8: S13-19.

Madkhali, A M. (2012). “Modelling Malignancy Induction Probability in Medulloblastoma for Photon Therapy and Proton Therapy” Unpublished master’s thesis, University of Oxford, Oxford, United Kingdom.

Malheiros, S. M., H. Carrete, Jr., J. N. Stavale, A. J. Santos, L. R. Borges, I. F. Guimaraes, M. P. Pelaez, C. M. Franco and A. A. Gabbai (2003). "MRI of medulloblastoma in adults." Neuroradiology 45(7): 463-467.

Manolio, T. A., F. S. Collins, N. J. Cox, D. B. Goldstein, L. A. Hindorff, D. J. Hunter, M. I. McCarthy, E. M. Ramos, L. R. Cardon, A. Chakravarti, J. H. Cho, A. E. Guttmacher, A. Kong, L. Kruglyak, E. Mardis, C. N. Rotimi, M. Slatkin, D. Valle, A. S. Whittemore, M. Boehnke, A. G. Clark, E. E. Eichler, G. Gibson, J. L. Haines, T. F. Mackay, S. A. McCarroll and P. M. Visscher (2009). "Finding the missing heritability of complex diseases." Nature 461(7265): 747-753.

MATLAB version R2012b, The Mathworks, Inc., Natick, MA, 2012

Mariotto, A. B., J. H. Rowland, K. R. Yabroff, S. Scoppa, M. Hachey, L. Ries and E. J. Feuer (2009). "Long-term survivors of childhood cancers in the United States." Cancer Epidemiol Biomarkers Prev 18(4): 1033-1040.

Marks, L. B., S. M. Bentzen, J. O. Deasy, F. M. Kong, J. D. Bradley, I. S. Vogelius, I. El Naqa, J. L. Hubbs, J. V. Lebesque, R. D. Timmerman, M. K. Martel and A. Jackson (2010). "Radiation dose-volume effects in the lung." Int J Radiat Oncol Biol Phys 76(3 Suppl): S70-76.

Marks, L. B., P. R. Carroll, T. C. Dugan and M. S. Anscher (1995). "The response of the urinary bladder, urethra, and ureter to radiation and chemotherapy." Int J Radiat Oncol Biol Phys 31(5): 1257-1280.

Martel, M. K., W. M. Sahijdak, R. K. Ten Haken, M. L. Kessler and A. T. Turrisi (1998). "Fraction size and dose parameters related to the incidence of pericardial effusions." Int J Radiat Oncol Biol Phys 40(1): 155-161.

Martinez Leon, M. I. (2011). "[Review and update about medulloblastoma in children]." Radiologia 53(2): 134-145.

Massimino, M., V. Biassoni, L. Gandola, M. L. Garrè, G. Gatta, F. Giangaspero, G. Poggi, and S. Rutkowski. (2016). “Childhood medulloblastoma” Critical Reviews in Oncology / Hematology 105: 35-51.

Mayo, C., M. K. Martel, L. B. Marks, J. Flickinger, J. Nam and J. Kirkpatrick (2010). "Radiation dose-volume effects of optic nerves and chiasm." Int J Radiat Oncol Biol Phys 76(3 Suppl): S28-35.

Mayo, C., E. Yorke and T. E. Merchant (2010). "Radiation associated brainstem injury." Int J Radiat Oncol Biol Phys 76(3 Suppl): S36-41.

McManamy, C. S., J. Pears, C. L. Weston, Z. Hanzely, J. W. Ironside, R. E. Taylor, R. G. Grundy, S. C. Clifford and D. W. Ellison (2007). "Nodule formation and desmoplasia in medulloblastomas-defining the nodular/desmoplastic variant and its biological behavior." Brain Pathol 17(2): 151-164.

Merchant, T. E. (2013). "Clinical controversies: proton therapy for pediatric tumors." Semin Radiat Oncol 23(2): 97-108.

Michalski, J. M., H. Gay, A. Jackson, S. L. Tucker and J. O. Deasy (2010). "Radiation dose-volume effects in radiation-induced rectal injury." Int J Radiat Oncol Biol Phys 76(3 Suppl): S123-129.

Miralbell, R., A. Lomax, L. Cella and U. Schneider (2002). "Potential reduction of the incidence of radiation-induced second cancers by using proton beams in the treatment of pediatric tumors." Int J Radiat Oncol Biol Phys 54(3): 824-829.

Mody, R., S. Li, D. C. Dover, S. Sallan, W. Leisenring, K. C. Oeffinger, Y. Yasui, L. L. Robison and J. P. Neglia (2008). "Twenty-five-year follow-up among survivors of childhood acute lymphoblastic leukemia: a report from the Childhood Cancer Survivor Study." Blood 111(12): 5515-5523.

Morton, L. M., G. M. Dores, R. E. Curtis, C. F. Lynch, M. Stovall, P. Hall, E. S. Gilbert, D. C. Hodgson, H. H. Storm, T. B. Johannesen, S. A. Smith, R. E. Weathers, M. Andersson, S. D. Fossa, M. Hauptmann, E. J. Holowaty, H. Joensuu, M. Kaijser, R. A. Kleinerman, F. Langmark, E. Pukkala, L. Vaalavirta, A. W. van den Belt-Dusebout, J. F. Fraumeni, Jr., L. B. Travis, B. M. Aleman and F. E. van Leeuwen (2013). "Stomach cancer risk after treatment for hodgkin lymphoma." J Clin Oncol 31(27): 3369-3377.

Moskowitz, C. S., J. F. Chou, S. L. Wolden, J. L. Bernstein, J. Malhotra, D. Novetsky Friedman, N. Z. Mubdi, W. M. Leisenring, M. Stovall, S. Hammond, S. A. Smith, T. O. Henderson, J. D. Boice, M. M. Hudson, L. R. Diller, S. Bhatia, L. B. Kenney, J. P. Neglia, C. B. Begg, L. L. Robison and K. C. Oeffinger (2014). "Breast cancer after chest radiation therapy for childhood cancer." J Clin Oncol 32(21): 2217-2223.

Moteabbed, M., T. I. Yock and H. Paganetti (2014). "The risk of radiation-induced second cancers in the high to medium dose region: a comparison between passive and scanned proton therapy, IMRT and VMAT for pediatric patients with brain tumors." Phys Med Biol 59(12): 2883-2899.

Mu, X., T. Bjork-Eriksson, S. Nill, U. Oelfke, K. A. Johansson, G. Gagliardi, L. Johansson, M. Karlsson and D. B. Zackrisson (2005). "Does electron and proton therapy reduce the risk of radiation induced cancer after spinal irradiation for childhood medulloblastoma? A comparative treatment planning study." Acta Oncol 44(6): 554-562.

Mulhern, R. K., S. L. Palmer, T. E. Merchant, D. Wallace, M. Kocak, P. Brouwers, K. Krull, M. Chintagumpala, R. Stargatt, D. M. Ashley, V. L. Tyc, L. Kun, J. Boyett and A. Gajjar (2005). "Neurocognitive consequences of risk-adapted therapy for childhood medulloblastoma." J Clin Oncol 23(24): 5511-5519.

Murray, L., A. Henry, P. Hoskin, F. A. Siebert and J. Venselaar (2013). "Second primary cancers after radiation for prostate cancer: a review of data from planning studies." Radiat Oncol 8: 172.

National Research Council. (2006). Health Risks from Exposure to Low Levels of Ionizing Radiation: BEIR VII Phase 2. Washington, DC, The National Academies Press.

Neglia, J. P., D. L. Friedman, Y. Yasui, A. C. Mertens, S. Hammond, M. Stovall, S. S. Donaldson, A. T. Meadows and L. L. Robison (2001). "Second malignant neoplasms in five-year survivors of childhood cancer: childhood cancer survivor study." J Natl Cancer Inst 93(8): 618-629.

Newhauser, W. D., J. D. Fontenot, A. Mahajan, D. Kornguth, M. Stovall, Y. Zheng, P. J. Taddei, D. Mirkovic, R. Mohan, J. D. Cox, and S. Woo (2009). “The risk of developing a second cancer after receiving craniospinal proton irradiation.” Phys Med Biol 54(8): 2277-91.

Neglia, J. P., L. L. Robison, M. Stovall, Y. Liu, R. J. Packer, S. Hammond, Y. Yasui, C. E. Kasper, A. C. Mertens, S. S. Donaldson, A. T. Meadows and P. D. Inskip (2006). "New primary neoplasms of the central nervous system in survivors of childhood cancer: a report from the Childhood Cancer Survivor Study." J Natl Cancer Inst 98(21): 1528-1537.

Nguyen, J., M. Moteabbed and H. Paganetti (2015). "Assessment of uncertainties in radiation-induced cancer risk predictions at clinically relevant doses." Med Phys 42(1): 81-89.

O'Malley, S., D. Weitman, M. Olding and L. Sekhar (1997). "Multiple neoplasms following craniospinal irradiation for medulloblastoma in a patient with nevoid basal cell carcinoma syndrome. Case report." J Neurosurg 86(2): 286-288.

Ozasa, K., Y. Shimizu, A. Suyama, F. Kasagi, M. Soda, E. J. Grant, R. Sakata, H. Sugiyama and K. Kodama (2012). "Studies of the mortality of atomic bomb survivors, Report 14, 1950-2003: an overview of cancer and noncancer diseases." Radiat Res 177(3): 229-243.

Packer, R. J. (2011). "Risk stratification of medulloblastoma: a paradigm for future childhood brain tumor management strategies." Curr Neurol Neurosci Rep 11(2): 124-126.

Packer, R. J., A. Gajjar, G. Vezina, L. Rorke-Adams, P. C. Burger, P. L. Robertson, L. Bayer, D. LaFond, B. R. Donahue, M. H. Marymont, K. Muraszko, J. Langston and R. Sposto (2006). "Phase III study of craniospinal radiation therapy followed by adjuvant chemotherapy for newly diagnosed average-risk medulloblastoma." J Clin Oncol 24(25): 4202-4208.

Packer, R. J., B. R. Rood and T. J. MacDonald (2003). "Medulloblastoma: present concepts of stratification into risk groups." Pediatr Neurosurg 39(2): 60-67.

Packer, R. J. and G. Vezina (2008). "Management of and prognosis with medulloblastoma: therapy at a crossroads." Arch Neurol 65(11): 1419-1424.

Padovani, L., M. P. Sunyach, D. Perol, C. Mercier, C. Alapetite, C. Haie-Meder, S. Hoffstetter, X. Muracciole, C. Kerr, J. P. Wagner, J. L. Lagrange, J. P. Maire, D. Cowen, D. Frappaz and C. Carrie (2007). "Common strategy for adult and pediatric medulloblastoma: a multicenter series of 253 adults." Int J Radiat Oncol Biol Phys 68(2): 433-440.

Paganetti, H. (2014). "Relative biological effectiveness (RBE) values for proton beam therapy. Variations as a function of biological endpoint, dose, and linear energy transfer." Phys Med Biol 59(22): R419-472.

Paganetti, H., T. Bortfeld and T. F. Delaney (2006). "Neutron dose in proton radiation therapy: In regard to Eric J. Hall " Int J Radiat Oncol Biol Phys 66(5): 1594-1595.

Paganetti, H. and D. Giantsoudi. (2018) “Relative Biological Effectiveness Uncertainties and Implications for Beam Arrangements and Dose Constraints in Proton Therapy.” Semin Radiat Oncol, 28(3): 256-63.

Paganetti, H., A. Niemierko, M. Ancukiewicz, L. E. Gerweck, M. Goitein, J. S. Loeffler and H. D. Suit (2002). "Relative biological effectiveness (RBE) values for proton beam therapy." Int J Radiat Oncol Biol Phys 53(2): 407-421.

Paganetti, H. and P. van Luijk (2013). "Biological considerations when comparing proton therapy with photon therapy." Semin Radiat Oncol 23(2): 77-87.

Pan, C. C., B. D. Kavanagh, L. A. Dawson, X. A. Li, S. K. Das, M. Miften and R. K. Ten Haken (2010). "Radiation-associated liver injury." Int J Radiat Oncol Biol Phys 76(3 Suppl): S94-100.

Parry, C., E. E. Kent, A. B. Mariotto, C. M. Alfano and J. H. Rowland (2011). "Cancer survivors: a booming population." Cancer Epidemiol Biomarkers Prev 20(10): 1996-2005.

Paszat, L. F., W. J. Mackillop, P. A. Groome, K. Schulze and E. Holowaty (1999). "Mortality from myocardial infarction following postlumpectomy radiotherapy for breast cancer: a population-based study in Ontario, Canada." Int J Radiat Oncol Biol Phys 43(4): 755-762.

Paszat, L. F., K. A. Vallis, V. M. Benk, P. A. Groome, W. J. Mackillop and A. Wielgosz (2007). "A population-based case-cohort study of the risk of myocardial infarction following radiation therapy for breast cancer." Radiother Oncol 82(3): 294-300.

Pearce, M. S., J. A. Salotti, M. P. Little, K. McHugh, C. Lee, K. P. Kim, N. L. Howe, C. M. Ronckers, P. Rajaraman, A. W. Sir Craft, L. Parker and A. Berrington de Gonzalez (2012). "Radiation exposure from CT scans in childhood and subsequent risk of leukaemia and brain tumours: a retrospective cohort study." Lancet 380(9840): 499-505.

Pera, M., A. Cardesa, J. A. Bombi, H. Ernst, C. Pera and U. Mohr (1989). "Influence of esophagojejunostomy on the induction of adenocarcinoma of the distal esophagus in Sprague-Dawley rats by subcutaneous injection of 2,6-dimethylnitrosomorpholine." Cancer Res 49(23): 6803-6808.

Pizer, B. and S. Clifford (2008). "Medulloblastoma: new insights into biology and treatment." Arch Dis Child Educ Pract Ed 93(5): 137-144.

Preston, D. L., E. Ron, S. Tokuoka, S. Funamoto, N. Nishi, M. Soda, K. Mabuchi and K. Kodama (2007). "Solid cancer incidence in atomic bomb survivors: 1958-1998." Radiat Res 168(1): 1-64.

Prosnitz, R. G., J. L. Hubbs, E. S. Evans, S. M. Zhou, X. Yu, M. A. Blazing, D. R. Hollis, A. Tisch, T. Z. Wong, S. Borges-Neto, P. H. Hardenbergh and L. B. Marks (2007). "Prospective assessment of radiotherapy-associated cardiac toxicity in breast cancer patients: analysis of data 3 to 6 years after treatment." Cancer 110(8): 1840-1850.

Radcliffe, J., G. R. Bunin, L. N. Sutton, J. W. Goldwein and P. C. Phillips (1994). "Cognitive deficits in long-term survivors of childhood medulloblastoma and other noncortical tumors: age-dependent effects of whole brain radiation." Int J Dev Neurosci 12(4): 327-334.

Raffel, C. (2004). "Medulloblastoma: molecular genetics and animal models." Neoplasia 6(4): 310-322.

Ramaswamy V, Remke M, Bouffet E, Bailey S, Clifford SC, Doz F, Kool M, Dufour C, Vassal G, Milde T, Witt O, von Hoff K, Pietsch T, Northcott PA, Gajjar A, Robinson GW, Padovani L, André N, Massimino M, Pizer B, Packer R, Rutkowski S, Pfister SM, Taylor MD, Pomeroy SL. "Risk stratification of childhood medulloblastoma in the molecular era: the current consensus." Acta Neuropathol. 2016 Jun;131(6):821-31.

Rancati, T., M. Schwarz, A. M. Allen, F. Feng, A. Popovtzer, B. Mittal and A. Eisbruch (2010). "Radiation dose-volume effects in the larynx and pharynx." Int J Radiat Oncol Biol Phys 76(3 Suppl): S64-69.

Robison, L. L. and M. M. Hudson (2014). "Survivors of childhood and adolescent cancer: life-long risks and responsibilities." Nat Rev Cancer 14(1): 61-70.

Rodriguez, A. M., Y. F. Kuo and J. S. Goodwin (2014). "Risk of colorectal cancer among long-term cervical cancer survivors." Med Oncol 31(5): 943.

Roesch W C (1978). Third Symposium on Neutron Dosimetry in Biology and Medicine. (Commission of the European Communities, Luxembourg).

Roldan, G., P. Brasher, G. Vecil, D. Senger, B. Rewcastle, G. Cairncross, P. Forsyth and M. Hamilton (2008). "Population-based study of medulloblastoma: outcomes in Alberta from 1975 to 1996." Can J Neurol Sci 35(2): 210-215.

Ronckers, C. M., A. J. Sigurdson, M. Stovall, S. A. Smith, A. C. Mertens, Y. Liu, S. Hammond, C. E. Land, J. P. Neglia, S. S. Donaldson, A. T. Meadows, C. A. Sklar, L. L. Robison and P. D. Inskip (2006). "Thyroid cancer in childhood cancer survivors: a detailed evaluation of radiation dose response and its modifiers." Radiat Res 166(4): 618-628.

Rossi, A., V. Caracciolo, G. Russo, K. Reiss and A. Giordano (2008). "Medulloblastoma: from molecular pathology to therapy." Clin Cancer Res 14(4): 971-976.

Rubino, C., A. Shamsaldin, M. G. Le, M. Labbe, J. M. Guinebretiere, J. Chavaudra and F. de Vathaire (2005). "Radiation dose and risk of soft tissue and bone sarcoma after breast cancer treatment." Breast Cancer Res Treat 89(3): 277-288.

Sachs, R. K. and D. J. Brenner (2005). "Solid tumor risks after high doses of ionizing radiation." Proc Natl Acad Sci U S A 102(37): 13040-13045.

Sachs, R. K., I. Shuryak, D. Brenner, H. Fakir, L. Hlatky, and P. Hahnfeldt. (2007). “Second cancers after fractionated radiotherapy: stochastic population dynamics effects.” J Theor Biol 249: 518-31.

Sasajima, K., T. Kawachi, T. Sano, T. Sugimura and Y. Shimosato (1977). "Esophageal and gastric cancers with metastases induced in dogs by N-ethyl-N'-nitro-N-nitrosoguanidine." J Natl Cancer Inst 58(6): 1789-1794.

Schellong, G., M. Riepenhausen, K. Ehlert, J. Bramswig, W. Dorffel, R. K. Schmutzler, K. Rhiem and U. Bick (2014). "Breast cancer in young women after treatment for Hodgkin's disease during childhood or adolescence--an observational study with up to 33-year follow-up." Dtsch Arztebl Int 111(1-2): 3-9.

Schneider, U. (2011). "Modeling the risk of secondary malignancies after radiotherapy." Genes (Basel) 2(4): 1033-1049.

Schneider, U., S. Agosteo, E. Pedroni and J. Besserer (2002). "Secondary neutron dose during proton therapy using spot scanning." Int J Radiat Oncol Biol Phys 53(1): 244-251.

Schneider, U., A. Lomax and N. Lombriser (2000). "Comparative risk assessment of secondary cancer incidence after treatment of Hodgkin's disease with photon and proton radiation." Radiat Res 154(4): 382-388.

Schneider, U., A. Lomax and B. Timmermann (2008). "Second cancers in children treated with modern radiotherapy techniques." Radiother Oncol 89(2): 135-140.

Schneider, U., M. Sumila, J. Robotka, G. Gruber, A. Mack and J. Besserer (2011). "Dose-response relationship for breast cancer induction at radiotherapy dose." Radiat Oncol 6: 67.

Schneider, U. and L. Walsh (2008). "Cancer risk estimates from the combined Japanese A-bomb and Hodgkin cohorts for doses relevant to radiotherapy." Radiat Environ Biophys 47(2): 253-263.

Schneider, U. and L. Walsh (2015). "Age at exposure and attained age variations of cancer risk in the Japanese A-bomb and radiotherapy cohorts." Med Phys 42(8): 4755-4761.

Schneider, U., and L. Walsh. (2017). “Risk of secondary cancers: Bridging epidemiology and modelling”, Phys Med, 42: 228-31.

Schneider, U., D. Zwahlen, D. Ross and B. Kaser-Hotz (2005). "Estimation of radiation-induced cancer from three-dimensional dose distributions: Concept of organ equivalent dose." Int J Radiat Oncol Biol Phys 61(5): 1510-1515.

Schultheiss, T. E. (2008). "The radiation dose-response of the human spinal cord." Int J Radiat Oncol Biol Phys 71(5): 1455-1459.

Sethi, R. V., D. Giantsoudi, M. Raiford, I. Malhi, A. Niemierko, O. Rapalino, P. Caruso, T. I. Yock, N. J. Tarbell, H. Paganetti and S. M. MacDonald (2014). "Patterns of failure after proton therapy in medulloblastoma; linear energy transfer distributions and relative biological effectiveness associations for relapses." Int J Radiat Oncol Biol Phys 88(3): 655-663.

Shah, D. J., R. K. Sachs and D. J. Wilson (2012). "Radiation-induced cancer: a modern view." Br J Radiol 85(1020): e1166-1173.

Shapiro, S., S. and M. B. Wilk (1965). “An Analysis of Variance Test for Normality (Complete Samples).” Biometrika, 52(3 and 4), 591-611.

Shuryak, I., R. K. Sachs and D. J. Brenner (2010). "Cancer risks after radiation exposure in middle age." J Natl Cancer Inst 102(21): 1628-1636.

Sklar, C., J. Whitton, A. Mertens, M. Stovall, D. Green, N. Marina, B. Greffe, S. Wolden and L. Robison (2000). "Abnormalities of the thyroid in survivors of Hodgkin's disease: data from the Childhood Cancer Survivor Study." J Clin Endocrinol Metab 85(9): 3227-3232.

Smith, A., M. Gillin, M. Bues, X. R. Zhu, K. Suzuki, R. Mohan, S. Woo, A. Lee, R. Komaki, J. Cox, K. Hiramoto, H. Akiyama, T. Ishida, T. Sasaki and K. Matsuda (2009). "The M. D. Anderson proton therapy system." Medical Physics 36(9): 4068-4083.

Smoll, N. R. and K. J. Drummond (2012). "The incidence of medulloblastomas and primitive neurectodermal tumours in adults and children." J Clin Neurosci 19(11): 1541-1544.

St Clair, W. H., J. A. Adams, M. Bues, B. C. Fullerton, S. La Shell, H. M. Kooy, J. S. Loeffler and N. J. Tarbell (2004). "Advantage of protons compared to

conventional X-ray or IMRT in the treatment of a pediatric patient with medulloblastoma." Int J Radiat Oncol Biol Phys 58(3): 727-734.

Steneker, M., A. Lomax and U. Schneider (2006). "Intensity modulated photon and proton therapy for the treatment of head and neck tumors." Radiother Oncol 80(2): 263-267.

Stokkevåg, C. H., G. M. Engeseth, K. S. Ytre-Hauge, D. Rohrich, O. H. Odland, L. P. Muren, M. Brydoy, L. B. Hysing, A. Szostak, M. B. Palmer and J. B. Petersen (2014). "Estimated risk of radiation-induced cancer following paediatric cranio-spinal irradiation with electron, photon and proton therapy." Acta Oncol 53(8): 1048-1057.

Stokkevåg, C. H., M. Fukahori, T. Nomiya, N. Matsufuji, G. M. Engeseth, L. B. Hysing, K. S. Ytre-Hauge, E. Rorvik, A. Szostak and L. P. Muren (2016). "Modelling of organ-specific radiation-induced secondary cancer risks following particle therapy." Radiother Oncol.

Swerdlow, A. J., J. A. Barber, G. V. Hudson, D. Cunningham, R. K. Gupta, B. W. Hancock, A. Horwich, T. A. Lister and D. C. Linch (2000). "Risk of second malignancy after Hodgkin's disease in a collaborative British cohort: the relation to age at treatment." J Clin Oncol 18(3): 498-509.

Swerdlow, A. J., C. D. Higgins, P. Smith, D. Cunningham, B. W. Hancock, A. Horwich, P. J. Hoskin, T. A. Lister, J. A. Radford, A. Z.S. Rohatiner, and D. C. Linch (2011). “Second Cancer Risk After Chemotherapy for Hodgkin's Lymphoma: A Collaborative British Cohort Study.” Journal of Clinical Oncology, 29 (31): 4096-104.

Swerdlow, A. J., C. D. Higgins, P. Smith, D. Cunningham, B. W. Hancock, A. Horwich, P. J. Hoskin, A. Lister, J. A. Radford, A. Z. Rohatiner and D. C. Linch (2007). "Myocardial infarction mortality risk after treatment for Hodgkin disease: a collaborative British cohort study." J Natl Cancer Inst 99(3): 206-214.

Taylor, C., C. Correa, F. K. Duane, M. C. Aznar, S. J. Anderson, J. Bergh, D. Dodwell, M. Ewertz, R. Gray, R. Jagsi, L. Pierce, K. I. Pritchard, S. Swain, Z.

Wang, Y. Wang, T. Whelan, R. Peto, and P. McGale (2017). “Estimating the Risks of Breast Cancer Radiotherapy: Evidence From Modern Radiation Doses to the Lungs and Heart and From Previous Randomized Trials.” J Clin Oncol, 35 (15): 1641-9.

Timlin, C., M. Houston and B. Jones (2011). "Malignant induction probability maps for radiotherapy using X-ray and proton beams." Br J Radiol 84 Spec No 1: S70-78.

Timlin, C., D. R. Warren, B. Rowland, A. Madkhali, J. Loken, M. Partridge, B. Jones, J. Kruse and R. Miller (2015). "3D calculation of radiation-induced second cancer risk including dose and tissue response heterogeneities." Med Phys 42(2): 866-876.

Travis, L. B., D. Hill, G. M. Dores, M. Gospodarowicz, F. E. van Leeuwen, E. Holowaty, B. Glimelius, M. Andersson, E. Pukkala, C. F. Lynch, D. Pee, S. A. Smith, M. B. Van't Veer, T. Joensuu, H. Storm, M. Stovall, J. D. Boice, Jr., E. Gilbert and M. H. Gail (2005). "Cumulative absolute breast cancer risk for young women treated for Hodgkin lymphoma." J Natl Cancer Inst 97(19): 1428-1437.

Travis, L. B., D. A. Hill, G. M. Dores, M. Gospodarowicz, F. E. van Leeuwen, E. Holowaty, B. Glimelius, M. Andersson, T. Wiklund, C. F. Lynch, M. B. Van't Veer, I. Glimelius, H. Storm, E. Pukkala, M. Stovall, R. Curtis, J. D. Boice, Jr. and E. Gilbert (2003). "Breast cancer following radiotherapy and chemotherapy among young women with Hodgkin disease." Jama 290(4): 465-475.

Travis, L. B., A. K. Ng, J. M. Allan, C. H. Pui, A. R. Kennedy, X. G. Xu, J. A. Purdy, K. Applegate, J. Yahalom, L. S. Constine, E. S. Gilbert and J. D. Boice, Jr. (2014). "Second malignant neoplasms and cardiovascular disease following radiotherapy." Health Phys 106(2): 229-246.

Travis, L. B., D. Hodgson, J. M. Allan, F. E. van Leeuwen. (2008) “Second cancers.” In: Devita, V. T., Lawrence, T.S., Rosenberg S. A., editors. “Cancer: Principles and Practice of Oncology.” 8th. Philadelphia: Lippincott Williams and Wilkins; 2008. p. 2718-2743.

Tsuchida, T., R. Tanaka, M. Fukuda, N. Takeda, J. Ito and H. Honda (1984). "CT findings of medulloblastoma." Childs Brain 11(1): 60-68.

Tucker, M. A., G. J. D'Angio, J. D. Boice, Jr., L. C. Strong, F. P. Li, M. Stovall, B. J. Stone, D. M. Green, F. Lombardi, W. Newton and et al. (1987). "Bone sarcomas linked to radiotherapy and chemotherapy in children." N Engl J Med 317(10): 588-593.

Ullrich, R. L. (1983). "Tumor induction in BALB/c female mice after fission neutron or gamma irradiation." Radiat Res 93(3): 506-515.

Ullrich, R. L., M. C. Jernigan and J. B. Storer (1977). "Neutron carcinogenesis. Dose and dose-rate effects in BALB/c mice." Radiat Res 72(3): 487-498.

Underwood, T. S. A., C. Grassberger, R. Bass, S. M. MacDonald, N. M. Meyersohn, B. Y. Yeap, R. B. Jimenez, and H. Paganetti. (2018) “Asymptomatic Late-phase Radiographic Changes Among Chest-Wall Patients Are Associated With a Proton RBE Exceeding 1.1.” Int J Radiat Oncol Biol Phys, 101(4): 809-19.

UNSCEAR (1993). Sources and effects of ionising radiation. 1993 report to the General Assembly. New York: United Nations.

UNSCEAR (2000). Sources and Effects Of Ionizing Radiation. UNSCEAR 2000 report to the General Assembly with Scientific Annexes. New York: United Nations.

UNSCEAR (2012). Sources, Effects and Risks of Ionizing Radiation. UNSCEAR Report 2013 to the General Assembly with Scientific Annexes. New York United Nations.

UNSCEAR (2013). Sources, Effects and Risks of Ionizing Radiation. UNSCEAR Report 2013 to the General Assembly with Scientific Annexes. Volume II, Scientific Annex B: Effects of Radiation Exposure of Children. New York United Nations.

Vincent TL, and RA Gatenby. “An evolutionary model for initiation, promotion, and progression in carcinogenesis.” Int J Oncol. 2008 Apr;32(4):729-37.

Vineis, P., Schatzkin, A., & Potter, J. D. (2010). “Models of carcinogenesis: an overview.” Carcinogenesis, 31(10): 1703–1709.

van Leeuwen, F. E., W. J. Klokman, M. Stovall, E. C. Dahler, M. B. van't Veer, E. M. Noordijk, M. A. Crommelin, B. M. Aleman, A. Broeks, M. Gospodarowicz, L. B. Travis and N. S. Russell (2003). "Roles of radiation dose, chemotherapy, and hormonal factors in breast cancer following Hodgkin's disease." J Natl Cancer Inst 95(13): 971-980.

Viswanathan, A. N., E. D. Yorke, L. B. Marks, P. J. Eifel and W. U. Shipley (2010). "Radiation dose-volume effects of the urinary bladder." Int J Radiat Oncol Biol Phys 76(3 Suppl): S116-122.

Webb, S. and A. E. Nahum (1993). "A model for calculating tumour control probability in radiotherapy including the effects of inhomogeneous distributions of dose and clonogenic cell density." Phys Med Biol 38(6): 653-666.

Weber, D. C., A. V. Trofimov, T. F. Delaney and T. Bortfeld (2004). "A treatment planning comparison of intensity modulated photon and proton therapy for paraspinal sarcomas." Int J Radiat Oncol Biol Phys 58(5): 1596-1606.

Wedenberg, M., B. K. Lind and B. Hardemark (2013). "A model for the relative biological effectiveness of protons: the tissue specific parameter alpha/beta of photons is a predictor for the sensitivity to LET changes." Acta Oncol 52(3): 580-588.

Wedenberg, M., B. K. Lind, I. Toma-Dașu, H. Rehbinder and A. Brahme (2010). "Analytical description of the LET dependence of cell survival using the repairable-conditionally repairable damage model." Radiat Res 174(4): 517-525.

Wedenberg, M. and I. Toma-Daşu (2014). "Disregarding RBE variation in treatment plan comparison may lead to bias in favor of proton plans." Med Phys 41(9): 091706.

Werner-Wasik, M., E. Yorke, J. Deasy, J. Nam and L. B. Marks (2010). "Radiation dose-volume effects in the esophagus." Int J Radiat Oncol Biol Phys 76(3 Suppl): S86-93.

Weyrather, W. K., S. Ritter, M. Scholz and G. Kraft (1999). "RBE for carbon track-segment irradiation in cell lines of differing repair capacity." Int J Radiat Biol 75(11): 1357-1364.

Williams, M. V., J. Denekamp and J. F. Fowler (1985). "A review of alpha/beta ratios for experimental tumors: implications for clinical studies of altered fractionation." Int J Radiat Oncol Biol Phys 11(1): 87-96.

Wilson, R. R. (1946). "Radiological use of fast protons." Radiology 47(5): 487-491.

Wolf, C., J. Lafuma, R. Masse, M. Morin and A. M. Kellerer (2000). "Neutron RBE for induction of tumors with high lethality in Sprague-Dawley rats." Radiat Res 154(4): 412-420.

Woodward, E., M. Jessop, A. Glaser, and D. Stark. 2011. “Late effects in survivors of teenage and young adult cancer: does age matter?” Ann Oncol 22(12): 2561-8.

Wouters, B. G., G. K. Y. Lam, U. Oelfke, K. Gardey, R. E. Durand, and L. D. Skarsgard.(1996). "Measurements of Relative Biological Effectiveness of the 70 MeV Proton Beam at TRIUMF Using Chinese Hamster V79 Cells and the High-Precision Cell Sorter Assay." Radiation Research 146(2): 159-70.

Yoon, M., S. H. Ahn, J. Kim, D. H. Shin, S. Y. Park, S. B. Lee, K. H. Shin and K. H. Cho (2010). "Radiation-induced cancers from modern radiotherapy techniques: intensity-modulated radiotherapy versus proton therapy." Int J Radiat Oncol Biol Phys 77(5): 1477-1485.

Zeltzer, P. M., J. M. Boyett, J. L. Finlay, A. L. Albright, L. B. Rorke, J. M. Milstein, J. C. Allen, K. R. Stevens, P. Stanley, H. Li, J. H. Wisoff, J. R. Geyer, P. McGuire-Cullen, J. A. Stehbens, S. B. Shurin and R. J. Packer (1999). "Metastasis stage, adjuvant treatment, and residual tumor are prognostic factors for medulloblastoma in children: conclusions from the Children's Cancer Group 921 randomized phase III study." J Clin Oncol 17(3): 832-845.

Zhang, R., R. M. Howell, P. J. Taddei, A. Giebeler, A. Mahajan and W. D. Newhauser (2014). "A comparative study on the risks of radiogenic second cancers and cardiac mortality in a set of pediatric medulloblastoma patients treated with photon or proton craniospinal irradiation." Radiother Oncol 113(1): 84-88.

Copyrights permissions:

Figure 2: Reprinted from Critical Reviews in Oncology / Hematology, (105), Massimino, M., V. Biassoni, L. Gandola, M. L. Garrè, G. Gatta, F. Giangaspero, G. Poggi, and S. Rutkowski, “Childhood medulloblastoma”, 35-51, © Elsevier 2016, with permission from Elsevier.

Figure 3: Reprinted from Radiology, (47), Wilson RR, "Radiological use of fast protons”, 487-491, © RSNA 1946, with permission from Radiological Society of North America.

Figure 5: Reprinted from Proton and charged particle radiotherapy, DeLaney and Kooy [ed.], p. 37, © Wolters Kluwer 2008, with permission from Wolters Kluwer Health.

Figure 6: Reprinted from Radiology, 104(1), Koehler AM, W M Preston, "Protons in radiation therapy. Comparative dose distributions for protons, photons, and electrons”, 191-195, © RSNA 1972, with permission from Radiological Society of North America. Radiology.

Figure 7: Reprinted from Radiation Research, 146(2), Wouters, B. G., G. K. Y. Lam, U. Oelfke, K. Gardey, R. E. Durand, and L. D. Skarsgard, "Measurements of Relative Biological Effectiveness of the 70 MeV Proton Beam at TRIUMF Using Chinese Hamster V79 Cells and the High-Precision Cell Sorter Assay", 159-70, © 2018 Radiation Research Society

Figure 8: Reprinted from Radiother Oncol, 50(2), Gerweck, L. E. and S. V. Kozin, "Relative biological effectiveness of proton beams in clinical therapy", 135-142, © Elsevier 1999, with permission from Elsevier.

Figure 12: Reprinted by permission from Springer Nature Customer Service Centre GmbH: Springer-Verlag, Radiation and Environmental Biophysics, “Cancer risk estimates from the combined Japanese A-bomb and Hodgkin cohorts for doses relevant to radiotherapy”, Schneider, U. and L. Walsh. © Springer-Verlag 2007.